

AD-A195 972

INVESTIGATIONS OF MAGNETOSPHERE-IONOSPHERE COUPLING
RELEVANT TO OPERATION (U) JOHNS HOPKINS UNIV LAUREL MD
APPLIED PHYSICS LAB C 1 MEMO ET AL. FEB 88

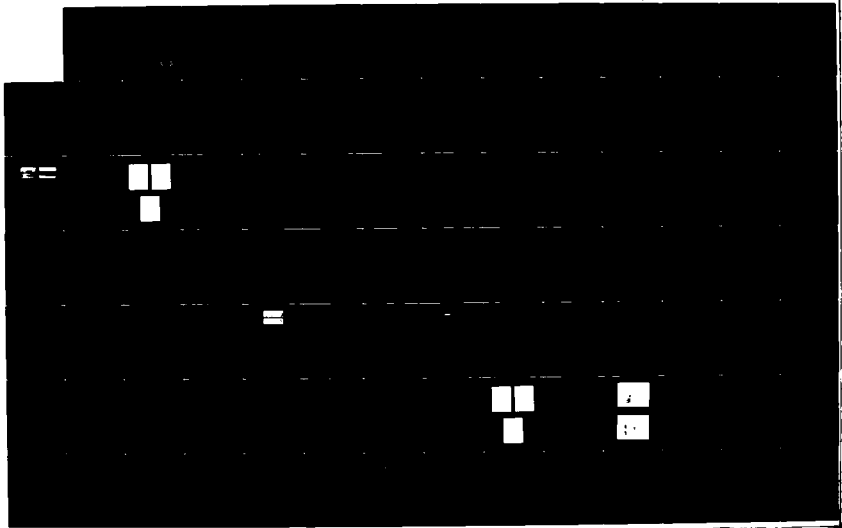
1/2

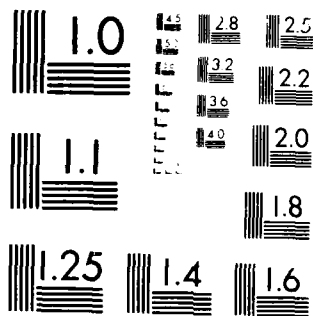
UNCLASSIFIED

AFOSR-TR-88-0622 AFOSR-84-0049

F/G 4/1

NL





MICROCOPY RESOLUTION TEST CHART
NATIONAL BUREAU OF STANDARDS-1963-A

AD-A195 972

AFOSR-TR. 88-0622

2

Final Scientific Report

on

Investigations of Magnetosphere-Ionosphere Coupling

Relevant to Operational Systems

AFOSR Grant 84-0049

by

C.-I. Meng, Principal Investigator

The Johns Hopkins University Applied Physics Laboratory

Laurel, Maryland, 20707

DTIC FILE COPY

DTIC
ELECTE
S JUN 30 1988 D
H

DISTRIBUTION STATEMENT A

Approved for public release;
Distribution Unlimited

*Original contains color
plates: All DTIC reproductions
will be in black and
white*

000

UNCLASSIFIED

SECURITY CLASSIFICATION OF THIS PAGE

REPORT DOCUMENTATION PAGE

Form Approved OMB No. 0704-0188

1a. REPORT SECURITY CLASSIFICATION Unclassified		1b. RESTRICTIVE MARKINGS Unclassified	
2a. SECURITY CLASSIFICATION AUTHORITY		3. DISTRIBUTION / AVAILABILITY OF REPORT Approved for public release; distribution unlimited.	
2b. DECLASSIFICATION / DOWNGRADING SCHEDULE			
4. PERFORMING ORGANIZATION REPORT NUMBER(S)		5. MONITORING ORGANIZATION REPORT NUMBER(S) AFOSR-TR-88-0622	
6a. NAME OF PERFORMING ORGANIZATION The Johns Hopkins University Applied Physics Laboratory	6b. OFFICE SYMBOL (if applicable)	7a. NAME OF MONITORING ORGANIZATION Air Force Office of Scientific Research	
6c. ADDRESS (City, State, and ZIP Code) Johns Hopkins Road Laurel, Maryland 20707		7b. ADDRESS (City, State, and ZIP Code) Building 410 Bolling Air Force Base Washington, DC 20332	
8a. NAME OF FUNDING / SPONSORING ORGANIZATION AFOSR 86 NP	8b. OFFICE SYMBOL (if applicable)	9. PROCUREMENT INSTRUMENT IDENTIFICATION NUMBER AFOSR-84-0049	
8c. ADDRESS (City, State, and ZIP Code) Building 410 Bolling Air Force Base Washington, DC 20332		10. SOURCE OF FUNDING NUMBERS	
		PROGRAM ELEMENT NO. 61102F	PROJECT NO. 2311
		TASK NO. AI	WORK UNIT ACCESSION NO.
11. TITLE (Include Security Classification) Investigations of Magnetosphere-Ionosphere Coupline Relevant to Operational Systems (71)			
12. PERSONAL AUTHOR(S) C. I. Meng and P. T. Newell			
13a. TYPE OF REPORT Final Scientific Report	13b. TIME COVERED FROM 1984 TO 1987	14. DATE OF REPORT (Year, Month, Day) 1988, February	15. PAGE COUNT 105
16. SUPPLEMENTARY NOTATION			
17. COSATI CODES		18. SUBJECT TERMS (Continue on reverse if necessary and identify by block number)	
FIELD	GROUP	Magnetosphere, Ionosphere, Aurora, Cusp, Storm, Particle Precipitation	
19. ABSTRACT (Continue on reverse if necessary and identify by block number) The scientific results of the research effort supported by AFOSR grant 84-0049 are reported. Important advances were made in understanding the dynamics of the magnetosphere and its coupling to the ionosphere. Significant progress was made in the areas of polar cusp precipitation and dynamics; dayside auroral morphology and auroral boundary dynamics; polar rain; the quiescent polar cap; the physics of impulsive injection phenomena; and problems of global magnetospheric plasma transport.			
20. DISTRIBUTION / AVAILABILITY OF ABSTRACT <input checked="" type="checkbox"/> UNCLASSIFIED/UNLIMITED <input type="checkbox"/> SAME AS RPT. <input type="checkbox"/> DTIC USERS		21. ABSTRACT SECURITY CLASSIFICATION Unclassified	
22a. NAME OF RESPONSIBLE INDIVIDUAL Dr. Henry R. Radoski		22b. TELEPHONE (Include Area Code) (202) 767-4906	22c. OFFICE SYMBOL NP

UNCLASSIFIED

Final Scientific Report on AFOSR grant 84-0049

The research supported by the Air Force Office of Scientific Research grant 84-0049 to the Johns Hopkins University Applied Physics Laboratory allowed us to carry out a number of studies concerning the dynamics of the magnetosphere and its coupling with the ionosphere. In this report, we summarized the results in 6 categories: (1) Polar cusp precipitation and related auroral morphology; (2) Polar rain studies; (3) Auroral oval, polar cap and cusp boundary dynamics; (4) The quiescent polar cap; (5) The physics of impulsive plasma injection phenomena; and (6) Global magnetospheric plasma transport.

1. Cusp precipitation and related auroral morphology

As the schematic in Figure 1 indicates, the topology of the polar cusps suggests that the cusps allow the direct connection between the upper ionosphere and the interplanetary environment. With research supported by this grant, we have studied the characteristics of the cusp particle precipitations. For instance, such precipitations show strong modulations in flux value. This problem has been tackled and a strong correlation has been shown to exist between this intensity and the density of solar wind plasma (Candidi and Meng, 1984a). The correlation is not unexpected since the cusp electrons are believed to be of solar wind origin; but no previous research was performed on this subject due to its complexity. It is found, however, that the cusp flux is linearly correlated to the square root of the solar wind

For

 on



Availability Codes	
Dist	Avail and/or Special
A-1	

density. This relationship can be interpreted as an effect of the interaction between the solar wind and the magnetosphere. For instance, in the magnetic field merging model, the maximum allowable velocity of penetration of plasma into the merging region is theoretically proportional to the local Alfvén velocity, which in turn is proportional to the square root of the plasma density. Simultaneously the influence of the IMF B_z component on the polar cusp electron flux has been shown to be present, with the flux statistically twice as high for B_z negative as for B_z positive.

We have also addressed the question of conjugacy of polar cusp precipitations. Given the results described above, which shows the solar wind-magnetosphere coupling exercises some control over solar wind access to the cusps, exact conjugacy is not necessarily expected. Using two DMSP satellites that nearly simultaneously traverse the conjugate cusps, we have studied a few cases, finding the conjugacy at times to be exact, and at other times finding large differences (Candidi and Meng, 1984b). A follow up study using a much larger data base was recently completed; the results should appear in the February, 1988 issue of the Journal of Geophysical Research.

Finally, in a study that has turned out to be related to our studies of cusp precipitations, we have addressed the auroral optical emission morphology of the midday auroral oval using the DMSP imaging capabilities during the austral winters. We have found 5 distinct types of spatial patterns whose occurrences depend on geomagnetic activity and the IMF B_z component (see Figure 2). Most important is the fact that there is a clear disconnection between the noon side and nightside discrete auroras. Also, there is a lack of correlation between the concurrent nightside substorm activity and the midday discrete auroral activity. The midday aurora is interpreted as representing

the occurrences of local injection of the magnetosheath plasma into the dayside boundary layer in the region of the dayside cusps. These observations are consistent with the existence of 2 separated major injection regions along the auroral oval: the dayside cusp and the nightside plasmashet (Meng and Lundin, 1986).

2. Polar rain studies

Several studies have been performed during the present grant period concerning the polar rain phenomenon. Greenspan et al. (1986) showed, using simultaneous DMSP and ISEE-1 electron distributions measurements, that electron distributions within the lobes of the magnetotail (10 to 23 R_e) provide a direct (unaccelerated) source for the polar rain. Coupling this finding with a previous suggestion (Fairfield and Scudder, 1985) that the field-aligned electron distributions within the lobes of the magnetotail result from direct access by the solar wind "strahl" electrons (a very narrow field-aligned component distinct from the bulk solar wind component) has resulted in the confirmation of the Fairfield and Scudder suggestion that the strahl solar wind component is the source of the polar rain at energies above ~ 100 eV.

Makita and Meng (1986) studied the long term variation of the polar rain including the simultaneous observations in opposite hemispheres. A lack of correlation found between the polar rain variation and solar wind densities is consistent with the "strahl" electron component explanation given above. Also, the pole-to-pole asymmetric enhancement is shown to be strongly

controlled by the sector structure of the IMF magnetic field. However, that control is binary in nature (the solar wind either has access or it does not). The variations in the flux, once access is gained, is not controlled by the IMF. Pole-to-pole symmetric polar rain flux enhancements (which were unknown prior to the work of Makita and Meng, 1986) are also occasionally observed in association with IMF sector structure transition periods.

3. Relations of Cusp and Auroral Boundaries Dynamics to Internal and External Processes

The polar cusp is not a static entity. It responds to changing conditions in interplanetary space, in the magnetosphere, and in the ionosphere. The movement of the cusp boundary to low latitudes during storms and substorms provides a good example of the dynamic variation of the cusp (e.g., Burch, 1976; Meng, 1982; 1983).

Recently, a question has arisen over whether the interplanetary field or the magnetospheric current in the polar ionosphere exerts primary control over the location of the cusp. Several investigators have asserted that the current system of which the auroral electrojet is a component mainly controls the cusp location (e.g., Eather et al., 1979; Eather 1985). Our understanding of the global configuration of the magnetosphere (and, hence, the cusp) assumes implicitly that external factors such as field merging play a key role (e.g., Crooker, 1979). Does this assumption break down when applied to the cusp?

In an effort to answer the question of prime controller, our cusp research

has concentrated on the use of charged particles to mark the polar cusps. Particle observations from the DMSP spacecraft have provided several years' worth of usable cusp data. These data have been combined with interplanetary data from IMP-8 and ISEE-3 satellites and with ground-based data in the form of Kp or AE indices.

Two strategies were adopted to test whether cusp location depended on external conditions or internal conditions. First, cusp data were combined with IMF data (representing external factors) and AE index data (representing internal factors) during very quiet times or during times when AE varied in a manner opposite that expected from the IMF variation effect. The data were examined on a case by case basis to find examples of cusp motion that were unambiguously associated with either the IMF or with the AE index. The second strategy involved the correlation of a full year's worth of cusp, IMF B_z , and AE measurements to quantitatively reveal whether an external factor or an internal factor provided a better predictor of cusp location. Of course, the close connection of B_z and AE necessitated very careful examination of the correlations.

The application of the first strategy proved inconclusive (Carbary and Meng, 1986a). The study of seven month's worth of combined data revealed that during quiescent auroral conditions the IMF B_z , AE index, and cusp latitude tended to act coherently. During some very quiet periods, the cusp location exhibited variability unassociated with either B_z or AE. From the case by case study, then, one could not conclude that either the IMF or AE exhibited a dominant influence on the position of the polar cusps.

The second strategy proved more fruitful. In this study, eleven months of IMF B_z , AE, and cusp latitude observations were linearly correlated to yield a

quantitative measure of cusp control (Carbary and Meng, 1986b). No special selection criteria were employed in the correlation, except for the requirement that the daily average of AE had to exceed 200 nT (i.e., non-quiet conditions). The study also explored the effects of a time delay between the cusp motion and both AE and B_z . The strongest correlations ($R=0.75-0.77$) occurred between the 30-minute delayed B_z and the cusp latitude. The best correlations between cusp latitude and AE were generally less ($R=0.68-0.71$) and involved no time delay. Figure 3 shows examples of the kinds of correlations obtained, while Figure 4 indicates the effect of time delays on the correlations. The study also suggested that the equatorward and poleward cusp boundaries may respond differently to B_z . The paper represented the first time that a full year's worth of cusp data were quantitatively examined.

The results of the second paper favor external factors as the principal controllers of cusp location. However, one could further ask whether the cusp size depends on internal or external factors and if a time delay is again involved. A recent manuscript in the publication process has explored the dependence of cusp latitude size on B_z and AE (Carbary and Meng, 1988). The cusp latitudinal width generally correlates poorly with both AE ($R=0.44$) and B_z ($R=0.59$) but always tended to increase for smaller negative B_z or larger northward B_z .

The above studies used only electron data to investigate the cusp position. With the new detectors on DMSP F6 and F7, both precipitating electrons and ions can be measured. This proves to allow a far more reliable determination of cusp boundaries. A new study (Newell and Meng, 1987c) examined the cusp boundaries as determined by both species for 10 instances of IMF B_z southward turning. It was found that in all instances the cusp width dramatically

narrowed as B_z turned southward. A simple conceptual model was also presented to explain this narrowing. Essentially the enhanced tailward rate of magnetospheric convection during southward B_z could lead to fewer open lines mapping to the slow flow region of the magnetosheath in which it is possible for plasma to gain entry to low altitude.

Of substantial interest in diagnosing other aspects of the magnetospheric state are the poleward and equatorward boundaries of the auroral oval, particularly away from the noon position. The poleward boundary locations indicate the size of the polar cap which in turn provides an indication of the magnetic flux within, and therefore the state of, the magnetotail. The equatorward boundary should yield an indication of the internal state (on closed field lines) of the magnetosphere.

We performed several studies during the present grant period concerning the auroral oval dynamics. Meng (1984) showed that the position of the nightside equatorward boundary is much more closely correlated with the dayside cusp region than one might have thought, given the different regions involved. The correlation is close during the initial phases of a magnetic storm, and both boundaries appear to be controlled by external parameters (i.e., IMF B_z) rather than the internal Dst parameter. Differences are manifested during the recovery phase, where the equatorward boundary recovery lags the cusp recovery, indicating some internal magnetospheric influences on the auroral boundary. The close control of the equatorward boundary by external parameters is not explained by existing models.

Our second study (Makita et al., 1985) is concerned more with the poleward boundary of the auroral oval and its correlation with the external B_z component and the internal AE index. Of substantial consequence to models of

substorm activity was the finding that the maximum dimension of the polar cap occurred in the maximum phase of the AE enhancement (within the limitation of the discrete timing measurements). This finding may be at variance with the substorm model which requires energy storage in the tail lobe and subsequent unloading.

Many other details of the variation of auroral oval dynamics with the internal and external parameters is discussed in the papers cited here.

4. The Quiescent Polar Cap

The emphasis of our research is on magnetospheric dynamics. However that dynamics cannot be fully understood unless it is placed in the context of magnetospheric statics. Most relevant to this discussion is the question of what constitutes the ground state of the magnetosphere.

This question has become of very substantial interest to the magnetospheric physics community with the discovery of considerable structure in the high latitude polar cap during periods of northward IMF. The so-called Theta Aurora (Frank et al., 1986) is one manifestation of this structure. Controversies have arisen concerning whether certain high latitude features exist on open or closed field lines. For instance Frank et al (1985) suggest that the transpolar arc region exists on closed field lines with the regions on either side connecting directly to the interplanetary regions.

We have recently addressed the configuration of the "quiescent" polar cap in the context of the global precipitation patterns and the visual aurora. Under positive IMF B_z conditions, we have found that the polar region precipitation consists of two distinct types that differ from those found in

active times (Makita and Meng, 1984). The high latitude part has bursty but continuous spatial structures with average energies below 0.5 keV, while the low latitude part has smoother spatial structures and average energies above 0.5 keV. We have indentified a "transition boundary" between these two regions. We have documented the statistical properties of the boundary positions (low latitude, high latitude, and transition) and other characteristics. We have found that the "auroral" regions are unusually wide and extend typically to geomagnetic latitudes of 81 to 84 degrees depending on local time. Also there are not many discrete aurora in the high latitude zone, only in the low latitude, hard precipitation zone. The low latitude transition boundary positions appear to be controlled by internal magnetospheric processes. We believe that the polar cap exists only poleward of the very high latitude soft precipitation zone, and, as a result, there is only a very minimal interconnection with the interplanetary medium during quiescent conditions. Under this assumption, and combining the works of Makita and Meng (1984) together with that of Meng and Lundin (1986), the pattern of open and closed field lines suggested by Frank et al. (1982) for the Theta Aurora has not emerged from our work as a general condition.

5. The Physics of Impulsive Injection Phenomena

The fundamental issue involved here is the manner in which particles are transported to the middle and inner regions of the magnetosphere during active periods. During previous grant periods we provided evidence that: a) everyday characteristics of certain geosynchronous particle features (observed during quiet to active periods) have characteristics that are inconsistent

with the commonly invoked global, curl-free (even time dependent) plasma convection from the tail regions (Mauk and Meng, 1983b), and b) all of the many types of commonly observed particle energy dispersion features in the geosynchronous orbit can be explained by invoking the so-called injection boundary model. During the present grant period we have strengthened our arguments by examining data from the highly elliptical orbit ISEE-1 satellite (Greenspan et al., 1985), by critically reexamining the evidence in favor of the previous global convection picture, and by clarifying the evidence in favor of the injection boundary model (Mauk and Meng, 1986a). The evidence appears to be clear that transport to the middle (near geosynchronous) regions of the Earth's magnetosphere always occurs in association with localized, impulsive, inductively driven transport processes that work together with the global, curl-free convective processes in causing particles to be transported to the middle magnetosphere. This view is consistent with some recent theoretical work on particle transport within the tail regions (Erickson and Wolf, 1980; Schindler and Birn, 1982).

Having helped establish the important role of localized, impulsive processes in moderating the particle transport, our attentions have turned to understanding the basic physics of such processes. Our efforts have been motivated initially by a suggestion from Quinn and Southwood (1982). In order to explain what they called "bounce-phase-bunched" ion distributions observed within the near-geosynchronous region these authors discussed the impulsive motion or "convection surge" of field lines toward the Earth in association with transient, east-to-west electric fields.

Our efforts have involved putting these suggestions onto a quantitative footing by constructing computer models of the process and by incorporating

realistic observational characteristics of the events. Our model (Mauk, 1986) easily generates the bounce-phased-bunched ion distributions, but more significantly it can generate dramatically field-aligned ion distributions at energies less than 1 to 20 keV (species dependent) due to the violation of the second adiabatic invariants and the strong field-aligned acceleration.

The substorm injection boundary model implies that at substorm onset both electron and ions of all energies share a common Earthward boundary. Such an injection should leave a clear signature in the auroral precipitation data. We used the DMSF F6 and F7 satellites to search for such signatures in the \leq 30 keV auroral electron and ion data. Clear examples of an equatorward leap of the previously energy dependent equatorward cutoffs in auroral precipitation to a cutoff boundary common to ions of all energies measured (i.e., dispersionless up to 30 keV) and electrons up to several keV (usually less than 10 keV) were observed in the near-midnight sector at a time corresponding to substorm onset. A collection of 10 such events occurring over a 1-month interval was studied, providing unusually direct confirmation that the phenomenological model of an initially dispersionless boundary accurately describes at least some injections. The DMSF data show the injection boundary to be dispersionless over a wide longitudinal range, but often only a dispersive injection is seen at dawn. These results are reported in detail in (Newell and Meng, 1987b).

6. Global Magnetospheric Transport

Recently we have begun applying the DMSF data set to problems involving

transport of plasmas within the magnetosphere. The low altitude (840 km) polar orbits of these satellites provide a "projection screen" view of the magnetosphere, and is thus a form of global imaging. Most relevant to questions of global transport are the sensitive ion detectors on F6, F7 and all later DMSPs, which allows us to investigate the high latitude ion precipitations. We had previously found that it is the dispersion features of ions that are most discriminating in making distinctions between transport processes (Mauk and Meng, 1986a).

Our first transport phenomenon study using the DMSP data set lead to a finding that low energy ions (up to about 1 keV) are injected deep into the plasmaspheric regions during intense prolonged substorm activity ($K_p = 4,5,6$ or more for several hours). These injections occur in the postmidnight region to about 0830 MLT sector, and by comparison with previous observations can be inferred to have an enhanced oxygen content. It is therefore likely that these ions are primarily of ionospheric origin; and are injected into the magnetosphere at high latitudes. Our observations show in detail the subsequent convection of these particles to lower latitudes, and indeed, into the plasmasphere. Results of this study (Newell and Meng, 1986) gives support to the low energy plasma convection patterns during substorm activity deduced by Carpenter et al. (1979) from whistler observations.

The second topic we have investigated in the area of global magnetospheric transport made use of the energy dependence in the equatorward edges of diffuse auroral precipitation. By using both DMSP satellites now in operation (F6 and F7), we were able to establish the latitudinal dispersion in

equatorward edges as a function of the particle energy in the diffuse auroral oval for both electrons and ions, and in various local time zones. Figure 6 shows an example of the dynamical behavior as a function of time and magnetic activity. Note that the energy dispersion is smallest during intervals of prolonged quiet. Also, our results provide further evidence against the assumption that steady state, global convective transport (i.e., forming Alfvén layers) determines the morphology of the diffuse auroral oval; and hence presumably the plasma sheet inner edge. Plate 1, a color spectrogram of DMS F7 particle data, shows an example. Note that the energy dispersion in Plate 1 (c) has a concave appearance, with intermediate energy ions cutting off at higher latitudes than do either the low or high energy ions. The global convective transport giving rise to Alfvén layers would have a convex appearance. These results are discussed in detail by (Newell and Meng, 1987b).

7. Concluding Remarks

We have carried out a vigorous research program involved in the study of various aspects of the earth's magnetospheric dynamics. As evidenced by the attached citation list, we have made basic contributions to the understanding of processes involved in the cusps, polar rain, magnetospheric plasma transport, and impulsive injection phenomena. A few representative samples of the resulting publications are included; they represent only a small portion of the scientific work supported by AFOSR grant 84-0049 and appearing in the literature.

Bibliography of Publications Supported by AFOSR 84-0049

1. Akasofu, S.-I., and C.-I. Meng, Effects of the IMF on the plasma sheet, Planet. Space Sci., (in press).
2. Bythrow, P. F. M. A. Doyle, T. A. Potemra, L. J. Zanetti, R. E. Huffman, C.-I. Meng, D. A. Hardy, F. J. Rich and R. A. Heelis, Multiple auroral arcs and Birkeland currents: Evidence for plasma sheet boundary waves, Geophys. Res., Lett., 13, 805, 1986.
3. Bythrow, P. F., T. A. Potemra, L. J. Zanetti, C.-I. Meng, R. E. Huffman, F. J. Rich, D. A. Hardy, W. B. Hanson and R. A. Heelis, Earthward directed high density Birkeland currents observed by HILAT, J. Geophys. Res., 89, 9114, 1984.
4. Candidi, M., and C.-I. Meng, The relation of the cusp precipitating electron flux to the solar wind and interplanetary magnetic field, J. Geophys. Res., 89, 9741, 1984a.
5. Candidi, M. and C.-I. Meng, Near simultaneous observations of the conjugate polar cusp regions Planet. Space Sci., 32, 41, 1984b.
6. Carbary, J. F., and C.-I. Meng, Relations between the interplanetary magnetic field B_z , AE index, and cusp latitude, J. Geophys. Res., 91, 1549, 1986a.

7. Carbary, J. F., and C.-I. Meng, Correlation of cusp latitude with B_z and AE (12) using nearly one year's data, *J. Geophys. Res.*, 91, 10047, 1986b.
8. Carbary, J. F., and C.-I. Meng, Correlation of cusp width with AE(12) and B_z , (in press) *Planet. Space Sci.*, 1988.
9. Engebretson, M. J., C.-I. Meng, R. L. Arnoldy and L. J. Cahill, Pc3 pulsations observed near the south polar cusp, *J. Geophys. Res.*, 91, 8909, 1986.
10. Greenspan, M. E., D. J. Williams, B. H. Mauk, and C.-I. Meng, Ion and electron energy dispersion features detected by ISEE-1. *J. Geophys. Res.*, 90, 4079, 1985.
11. Greenspan, M. E., C.-I. Meng, and D. H. Fairfield, Simultaneous polar cap and magnetotail observations of intense polar rain, *J. Geophys. Res.*, 91, 11123, 1986.
12. Holzworth, R. H., and C.-I. Meng, Auroral boundary variations and the interplanetary magnetic field, *Planet. Space. Sci.*, 32, 25, 1984.
13. Lassen, K., C. Danielsen and C.-I. Meng, Average configuration of quiet auroral oval, *J. Geophys. Res.*, (submitted) 1986.
14. Lin, C. S. and C.-I. Meng, Observations of quiet-time Pc5 wave in the outer magnetosphere, *Planet. Space. Sci.*, 32, 551, 1984.

15. Makita, K., and C.-I. Meng, Average electron precipitation patterns and visual auroral characteristics during geomagnetic quiescence, *J. Geophys. Res.*, 2861, 1984.
16. Makita, K., C.-I. Meng, and S.-I. Akasofu, Temporal and spatical variations of the polar cap dimension inferred from the precipitation boundaries, *J. Geophys. Res.*, 90, 2744, 1985.
17. Makita, K. and C.-I. Meng Polar cusp electron during quiet and disturbed period, *Memoirs of National Institute of Polar research, Japan*, 42, 103- 1986.
18. Makita, K. and C.-I. Meng, Long-period polar rain variations, solar wind and hemispherically symmetric polar rain, *J. Geophys. Res.*, 92, 7381-7393, 1987.
19. Mauk, B. H., Comment on "Heating of thermal helium in the equatorial magnetosphere: A simulation study", by Y. Omura, M. Ashour-Abdalla, R. Gendrin, and K. Quest, *J. Geophys. Res.*, 91, 4590, 1986.
20. Mauk, B. H., Quantitative modeling of the convection surge mechanism of ion acceleration, *J. Geophys. Res.*, 91, 13423, 1986.
21. Mauk, B. H., The convection surge mechanism of ion acceleration during substorms, in *Magnetotail Physics*, edited by A. T. Y. Lui, The Johns Hopkins University Press, Baltimore, Maryland, 1986.

22. Mauk, B. H., Contribution to dialog session: Injection boundary versus Alfvén layer models, *Magnetotail Physics*, edited by A. T. Y. Lui, 1986.
23. Mauk, B. H., and C.-I. Meng, Macroscopic ion acceleration associated with the formation of the ring current in the Earth's magnetosphere, *Ion Acceleration in the Magnetosphere and Ionosphere*, Geophysical Monograph, 38, edited by T. Chang, p. 351, American Geophysical Union, 1986a.
24. Mauk, B. H., and C.-I. Meng, Plasma injection during substorms, *Physica Scripta*, (in press) 1986.
25. Mauk, B. H., and L. J. Zanetti, IUGG Quadrennial Report on: Magnetospheric Electric Fields and Currents, *Rev. Geophys.*, 541, 1987.
26. Meng, C.-I., Dynamic variations of the auroral oval during intense magnetic storms, *J. Geophys. Res.*, 89, 227, 1984.
27. Meng, C.-I., Dynamic variations of the auroral precipitation and the polar cap, in *Results of the ARCADE Project and of the Recent Programmes in Magnetospheric and Ionospheric Physics*, French National Center of Space Research Collection, 289, 1985.
28. Meng, C.-I., and M. Candidi, Some polar cusp features observed by DMSP Satellites, in *The Polar Cusp*, 177, ed. by J. A. Holtet and A. Egeland, D. Reidel Publ., Dordrecht, Holland, 1985.

29. Meng, C.-I., and J. F. Carbary, Effects of interplanetary magnetic field and magnetospheric substorm on polar cusp position, submitted to *Physica Scripta*, and to the Proceedings of the Sixth International Symposium on Solar Terrestrial Physics (Toulouse, France, July, 1986), 1986.
30. Meng, C.-I. and S. Chakrabarti, The extreme ultraviolet emissions for monitoring auroras in dark and daylight hemispheres, *J. Geophys. Res.*, 90, 4261, 1985.
31. Meng, C.-I., and R. E. Huffman, Ultraviolet imaging from space of the aurora under full sunlight, *Geophys. Res., Lett.*, 11, 315, 1984.
32. Meng, C.-I., and R. Lundin, Auroral morphology of the midday oval, *J. Geophys. Res.*, 91, 1572, 1986.
33. Meng, C.-I., and K. Makita, Dynamic variations of the polar cap, *Solar Magnetosphere Coupling*, D. Reidel Publishing, 1986.
34. Monchick, L., M. J. Linevsky, C.-I. Meng, S. Favin, S. Chakrabarti, and F. Paresce, Some auroral properties from far ultraviolet observations, *Planet. Space Sci.*, 33, 175, 1985.
35. Murphree, J. S., C. D. Anger, C.-I. Meng, and S.-I. Akasofu, Large-scale auroral distribution and the open field line region, *Planet. Space Sci.*, 32, 105, 1984.

36. Newell, P. T., and C.-I. Meng. Substorm introduction of ≤ 1 keV magnetospheric ions into the inner plasmasphere, *J. Geophys. Res.*, 91, 11133, 1986.
37. Newell, P. T., and C.-I. Meng. Energy dependence of the equatorward cutoffs in auroral electron and ion precipitation, *J. Geophys. Res.*, 92, 7519-7530, 1987a.
38. Newell, P. T., and C.-I. Meng. Low altitude observations of dispersionless substorm plasma injections, *J. Geophys. Res.*, 92, 10063-10072, 1987b.
39. Newell, P. T., and C.-I. Meng. Cusp width and B_z : Observations and a conceptual model. *J. Geophys. Res.*, 92, 13673-13678, 1987c.
40. Oliver, W. L., J. C. Foster, J. M. Holt, G. B. Lariot, V. B. Wickwar, J. D. Kelley, D. de la Beaujardiere, P. F. Bythrow, C.-I. Meng, F. J. Rich, and R. E. Huffman. Initial Millstone Hill, Sondrestrom, and HILAT observations of thermospheric temperatures and frictional heating, *Geophys. Res. Lett.*, 9, 911, 1984.
41. Varga, L., D. Venkatesan, and C.-I. Meng. Low altitude observations of the energetic electrons in the outer radiation belt during isolated substorms, *Planet. Space Sci.*, 33, 1259, 1985.

References (excepting publications supported by AFOSR grant 84-0049)

Carpenter, D. L., C. G. Park, and T. R. Miller, A model of substorm electric fields in the plasmasphere based on whistler data, J. Geophys. Res., 84, 6559-6563, 1979.

Crooker, N. U., Dayside merging and cusp geometry, J. Geophys. Res., 84, 951-959, 1978.

Eather, R. H., Polar cusp dynamics, J. Geophys. Res., 90, 1569, 1985.

Eather, R. H., S. B. Mende, and E. J. Weber, Dayside aurora and relevance to substorm current systems and dayside merging, J. Geophys. Res., 84, 3339, 1979.

Erickson, G. M., and R. A. Wolf, Is steady state convection possible in the earth's magnetotail?, Geophys. Res. Lett., 7, 897-900, 1980.

Fairfield, D. H., and J. D. Scudder, Polar rain: solar coronal electrons in the earth's magnetosphere, J. Geophys. Res., 90, 4055-4068, 1985.

Quinn, J. M., and D. J. Southwood, Observations of parallel ion energization in the equatorial region, J. Geophys. Res., 87, 10536, 1982.

Schindler, K., and J. Birn, Self-consistent theory of time-dependent convection in the earth's magnetotail, J. Geophys. Res., 87, 2263-2275, 1982.

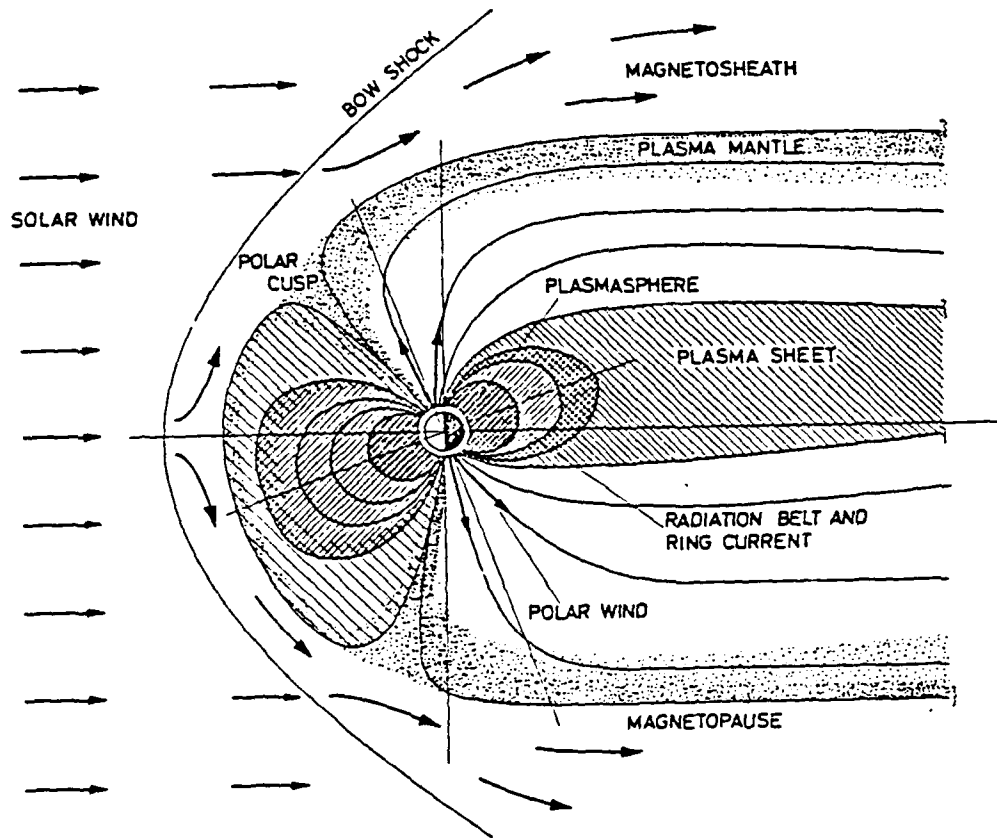


Fig. 1. Schematic of the earth's magnetosphere showing, among other things, the positions of the polar cusps.

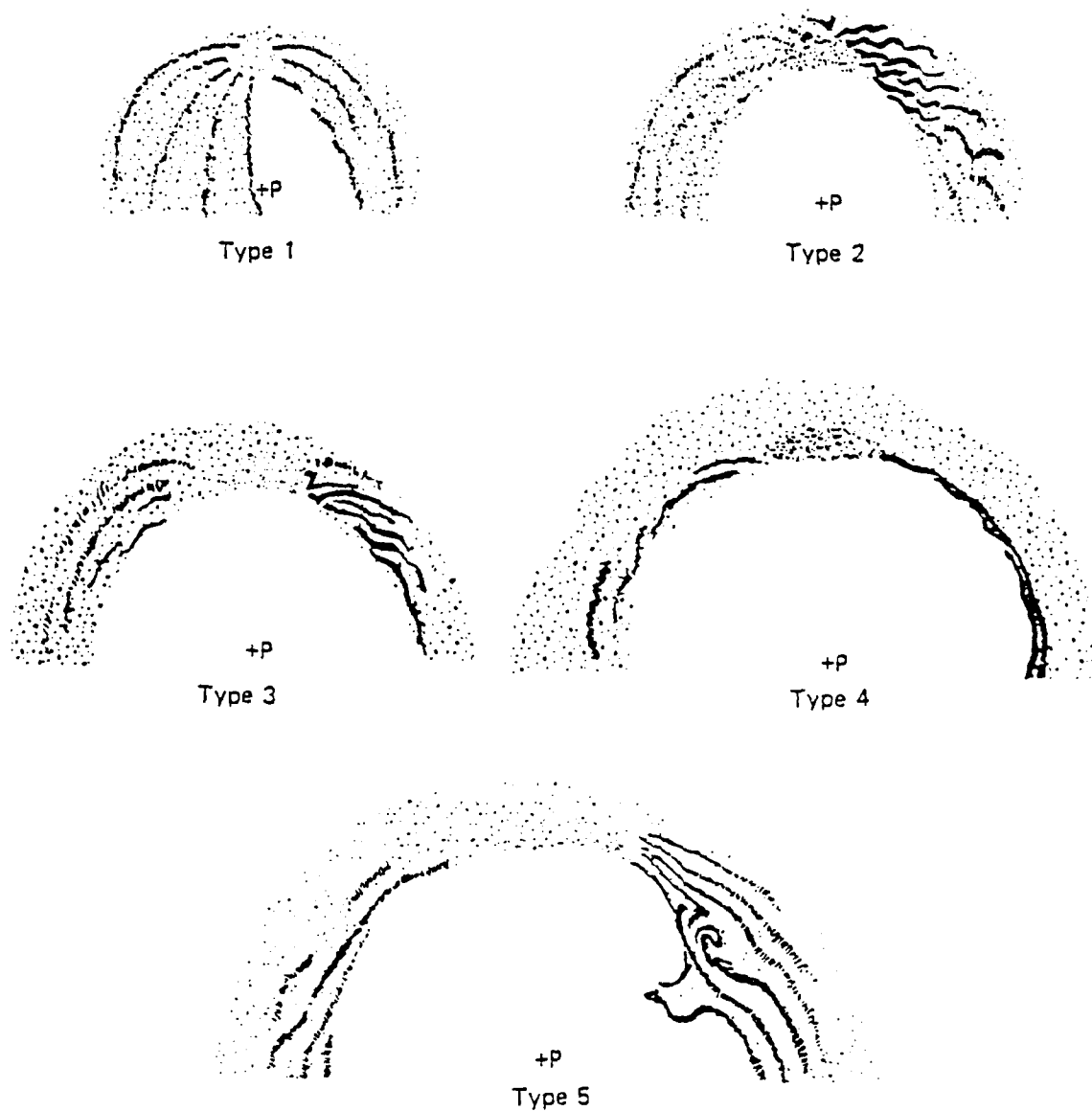


Fig. 2. Schematics of newly categorized auroral oval dayside displays at the southern polar region. Types 1 through 5 represent the average conditions as the IMF B_z component changes from strongly northward to strongly southward. The discrete features are detached and uncorrelated from the nightside features and are attributed to injections in the vicinity of the cusps (from Meng and Lundin, 1986).

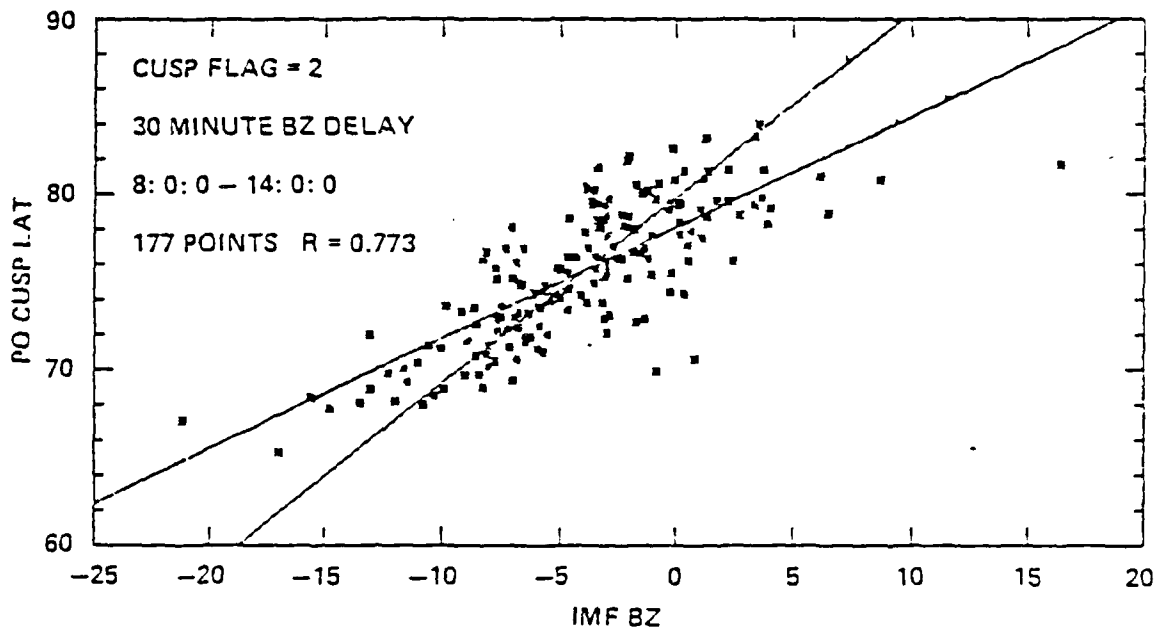
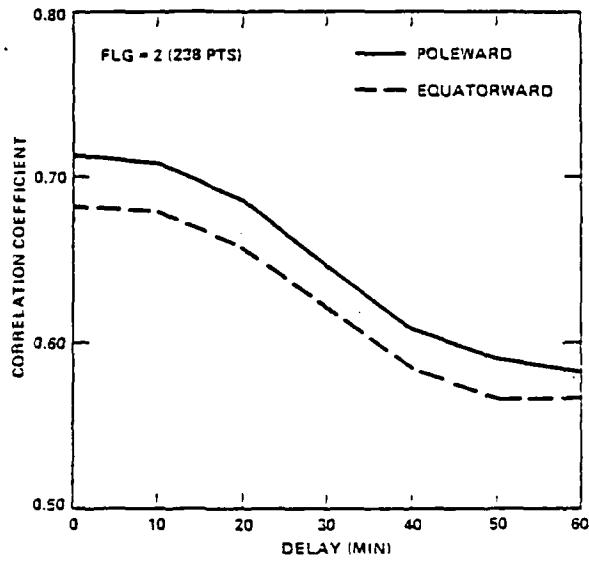


Fig. 3. Example of linear correlation between the polar cusp magnetic latitude and the IMF B_z component measured 30 minutes prior to the cusp position measurement time (from Carbary and Meng, (1986b)).

CUSP BOUNDARY VERSUS AE (12)



CUSP BOUNDARY VERSUS ALL BZ

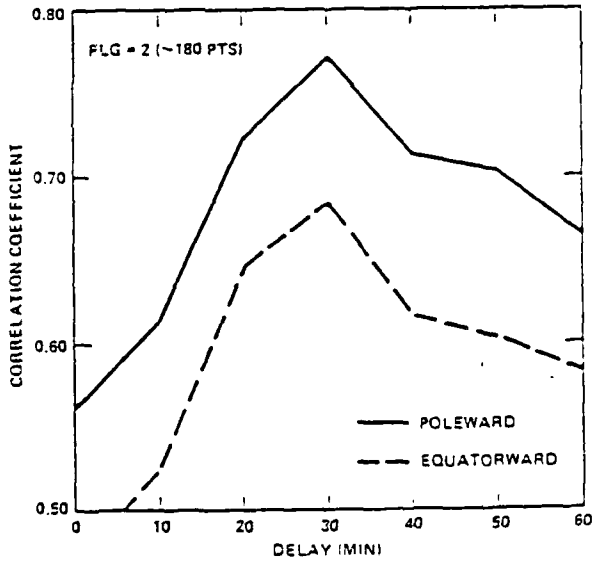
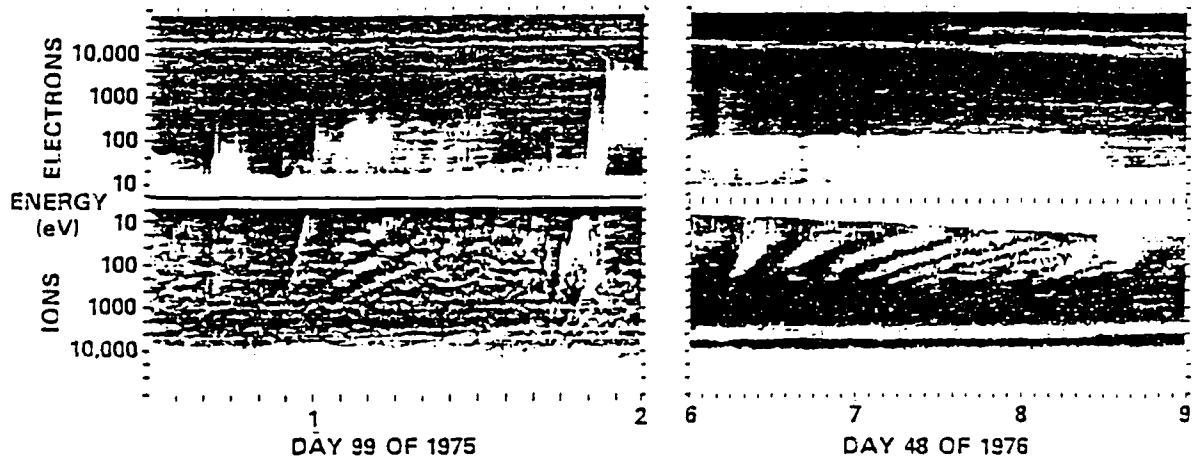
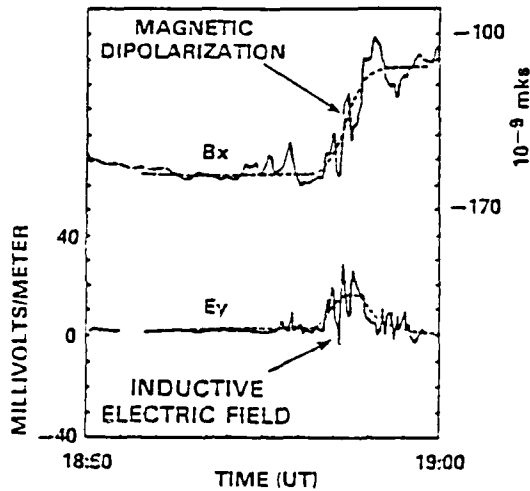


Fig. 4. The effect of time delays on the correlation coefficients for cusp position versus AE (top) and cusp position versus IMF B_z (bottom) correlations (from Carbary and Meng, 1986b)).

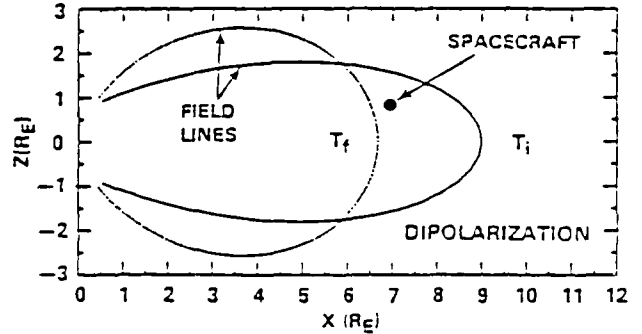
MODELING OF IMPULSIVE (SUBSTORM) PARTICLE TRANSPORT WITHIN SPACE OPERATIONAL ENVIRONMENTS



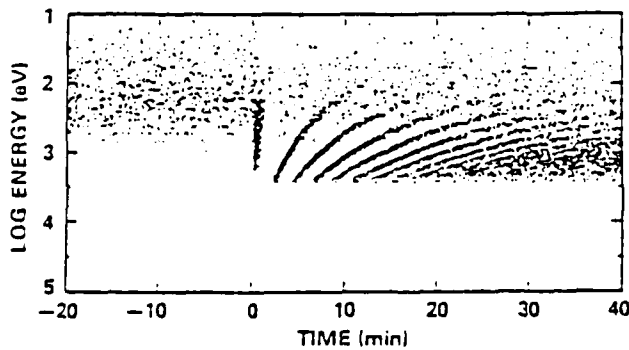
A. OBSERVED GEOSYNCHRONOUS ORBIT PARTICLE SIGNATURES



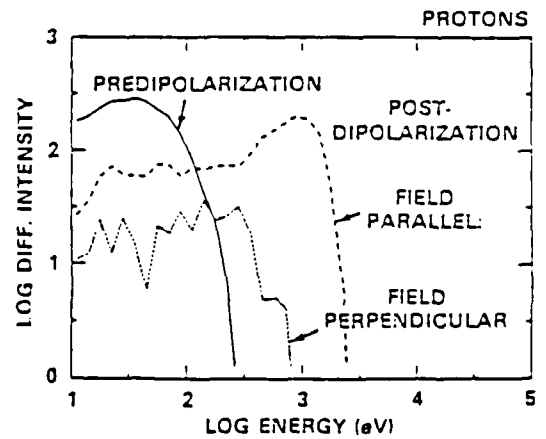
B. ASSOCIATED ELECTRIC AND MAGNETIC SIGNATURES (AGGSON et al., 1983)



C. CONFIGURATION FOR COMPUTER MODELING



D. MODELED PARTICLE SIGNATURES



E. PREDICTED PARTICLE SPECTRA

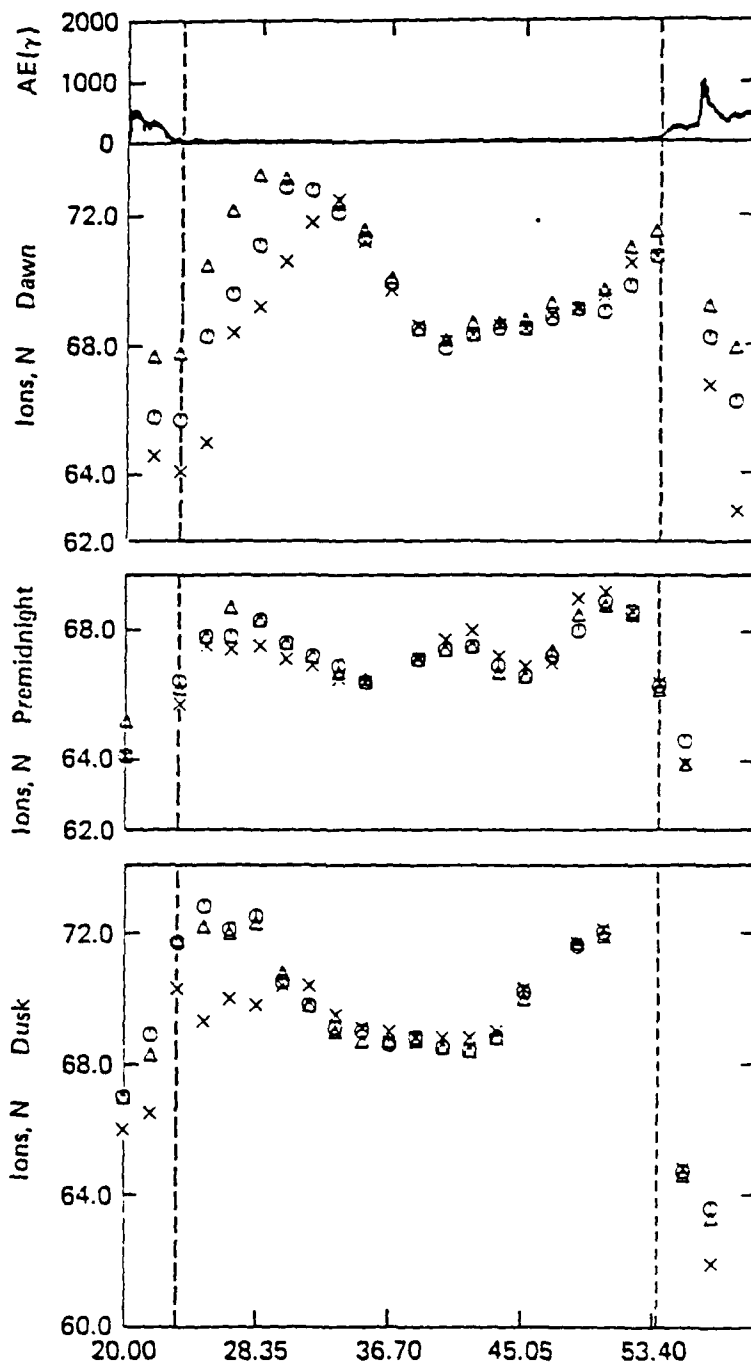


Fig. 6. Example of dynamical variations of the energy dispersion of the equatorward edges of precipitated ions at dawn (second panel), premidnight (third panel), and dusk (bottom panel). The top panel shows the AE index.

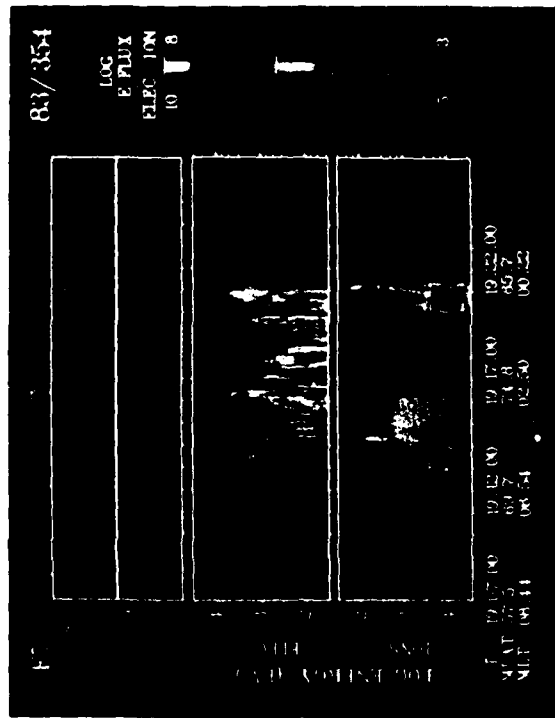


Plate 1a. A spectrogram of the DMSP F7 particle data for the very quiet time period immediately preceding the December 20 injection. Notice that the ion energy scale is inverted with higher energies downward, so that the low-energy particles of both species appear in the center of the figure. The color scale axes differential energy flux in units of $(eV cm^{-2} s^{-1})$ and the average energy is in eV. The energies covered for both electrons and ions are 30 eV to 30 keV.

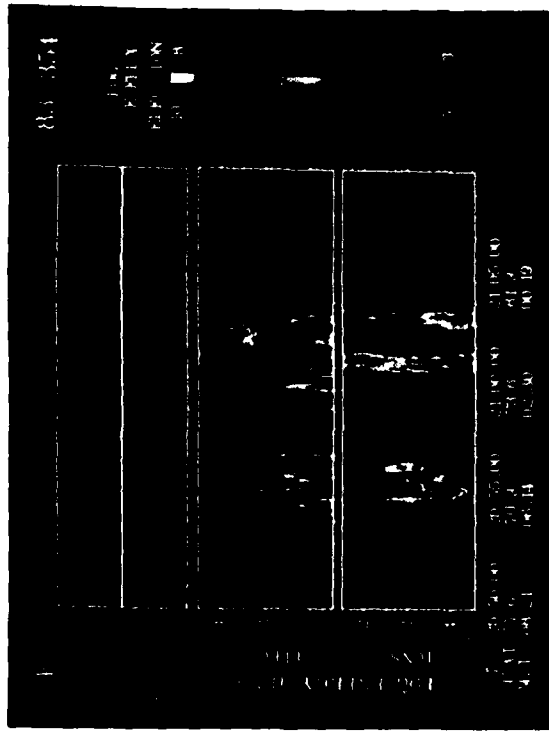


Plate 1b. A spectrogram for the DMSP F7 pass which observed the injection. Notice how the ion cutoffs at all energies and the electron cutoffs below several keV coincide in the midnight region.

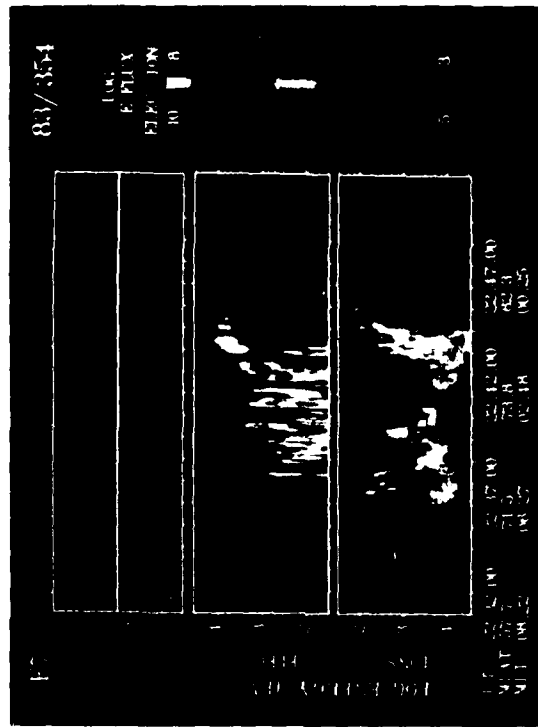


Plate 1c. The DMSP F7 northern hemisphere data on the next pass after the injection. Notice the strong dispersion that has already developed, particularly for the ions. The color scale axes differential energy flux is in units of $(eV cm^{-2} s^{-1})$ and the average energy is in eV.

Appendix: Selected reprints from refereed publications

Dynamic Variations of the Polar Cap

Ching-I. MENG and Kazuo MAKITA*

Applied Physics Laboratory, The Johns Hopkins University, Laurel, Maryland 20707, U.S.A.

The morphology and dynamics of the polar cap, defined as the region poleward of auroral electron precipitations, are discussed, based on observations made by the low-altitude polar-orbiting satellites of the U.S. Defense Meteorological Satellite Program (DMSP). Particular attention is given to polar cap variations with the interplanetary magnetic field (IMF) and substorm activity. Their implications on the magnetospheric configuration and the solar-terrestrial interaction will also be presented.

It is found that during geomagnetically quiet times the average location of the electron precipitation poleward boundary is at particularly high geomagnetic latitudes: about 82° to 84° in the morning, noon, and evening sectors and at about 81° to 82° in the midnight sector. This indicates a very small polar cap. The equatorward edge of the auroral oval is at about 70° in the morning, noon, and evening sectors and at about 69° in the midnight sector. The latitudinal width of the region of auroral electron precipitation is unusually large, indicating a widening of the auroral oval in periods of geomagnetic quiescence. Faint, stable auroral arcs sometimes are seen in the precipitation region, associated with the so-called polar cap arcs. The location of the poleward boundary (i.e., the polar cap size) is affected by the magnitude of the northward interplanetary magnetic field (IMF) component; however, the location of the auroral precipitation equatorward boundary is not related to the positive IMF B_z magnitude. These results indicate that the unusually high latitude of the auroral oval poleward boundary is the consequence of a very small number of geomagnetic flux lines interconnected with the IMF during a northward IMF condition. They also imply that the size of the polar cap is inversely controlled by the magnitude of the northward B_z component. The insensitivity of the equatorward auroral precipitation boundary to the northward IMF B_z can be used to infer that its dynamics is dominated by internal magnetospheric processes and not by direct solar-magnetospheric interactions.

It is also found that both the dawn-dusk and noon-midnight dimensions of the polar cap tend to vary in harmony with the AE index. The increase of the polar cap size begins after the southward turning of the IMF with an increase of the energy input ϵ parameters but prior to the corresponding increase of the AE index. The period of the maximum dimension of the polar cap approximately coincides with the period of the maximum AE value. The polar cap size decrease begins at about the same time that the substorm activity begins to subside, but it continues well after the AE index is reduced to very small values. If the size of the polar cap is considered as a measure of the open geomagnetic flux and thus of the magnetic energy stored in the magnetotail, these results suggest that the magnetic energy in the magnetotail increases and decreases in harmony with the growth and decay of substorm activity, respectively.

*Permanent Address: Takushoku University, Tokyo, Japan.

1. Introduction

In the past 20 years, various types of satellite observations have revealed that the earth's magnetosphere is open: namely, that geomagnetic field lines from the polar cap regions extend into interplanetary space and connect with the magnetic field lines of solar origin. Variations of the solar wind and the interplanetary magnetic field (IMF) will undoubtedly affect the configuration of the terrestrial magnetosphere. Associated with an increase of the solar wind dynamic pressure, compression of the dayside magnetosphere and the magnetotail has been detected. The location of the magnetopause can be accurately determined from magnetohydrodynamics by balancing the solar wind dynamic pressure in the interplanetary space with the magnetic pressure of the geomagnetic field inside the magnetosphere. However, responses of the terrestrial magnetosphere to variations of the IMF are far from clear, and the importance of the IMF in the solar-terrestrial interaction, especially in the energy coupling, has been recognized.

One of the possible processes of the energy transfer from the solar wind into the magnetosphere to produce the magnetospheric substorm is the field line merging between the IMF and the geomagnetic field. The dayside northward-directed closed geomagnetic field lines near the magnetopause can be eroded away by a southward-directed IMF (i.e., the geomagnetic field lines are opened by and connected with the interplanetary field lines); consequently, the dayside magnetopause moves earthward. Due to the "frozen-in" condition between the interplanetary field and the solar wind, the antisunward motion of the solar wind carries the newly merged geomagnetic field lines from the dayside magnetosphere (or the magnetosheath) across the polar cap into the magnetotail. Associated with this so-called "magnetic flux transfer" process, one of the expected configurational responses of the magnetosphere is the change in the polar cap size, which is controlled by the flux of open geomagnetic field lines. The polar cap is defined as the area bounded by the auroral oval, and the bundle of the geomagnetic field lines originating in the polar cap is connected (i.e., open) to the IMF of the solar origin. The purpose of this paper is to report progress in the observation and understanding of the polar cap size variation with changes of the IMF; some new results on configurational changes of the auroral oval (i.e., the polar cap) with the different orientation of the IMF are also discussed based on the Defense Meteorological Satellite Program (DMSP) observations. The polar cap size is defined here by using the poleward boundary of the instantaneous auroral electron precipitations.

Usual observations of the auroral electron precipitations have corresponded generally to moderately active geomagnetic conditions (during magnetospheric substorms) when the auroral optical display and electron precipitations are intense and dynamic. Therefore, previous studies of auroral electron precipitations primarily represent the active or moderately active magnetosphere. During periods of relative magnetic quiescence, the global auroral display observed by imagers onboard ISIS-2 and DMSP satellites showed that quiet auroral arcs extend along the contracted poleward edge of the auroral oval and, at times, the luminosity of the auroral oval is even below the detector threshold of these satellites (AKASOFU, 1974). Due to the rarity of extremely quiet magnetospheric conditions and the nondynamic nature of

the auroral display, the morphology of the very quiet auroral oval has not yet drawn much of the attention of magnetospheric and auroral physicists (HOFFMAN and BURCH, 1973; WINNINGHAM *et al.*, 1975; LUI *et al.*, 1976; MENG, 1981a, b; MURPHREE *et al.*, 1982). The purpose of this paper is to examine the dynamics of the polar cap inferred from the auroral electron precipitations observed by polar-orbiting USAF DMSP satellites. The main questions of importance are: (1) what is the electron precipitation at very quiet conditions, (2) how small is the polar cap, and (3) what are the distinct variations of the polar cap region from quiet to disturbed geomagnetic conditions?

The DMSP is a continuous U.S. Department of Defense operational system for global weather monitoring. Normally, the program has two satellites in ~ 840 -km sun-synchronous circular polar orbits with a period of 101 min and 98.75° inclination (PIKE, 1975). One satellite is in the dawn-dusk meridian orbit, and the other is in the noon-midnight meridian orbit. Depending on launch dates and system lifetimes, there can be as many as three satellites or as few as one satellite in operation at a given time. Radiometers onboard DMSP satellites produce the familiar images of the global auroral display in the dark hemisphere. In addition to the principal meteorological instruments, since 1974 some of the satellites have carried low-energy electron detectors to monitor auroral electron precipitation. These DMSP satellites provide continual soft electron ($E \leq 20$ keV) measurements from both northern and southern polar regions, without any systematic data gaps, except from 1980 to 1982. Improvements of particle detectors were made initially from only 8-channel electron measurement between 200 and 20 keV to the present 20-channel measurements of both electrons and ions from 30 eV to 30 keV.

In the following, the auroral electron precipitation and the polar cap size of the quiet magnetosphere will be discussed first, followed by an investigation of dynamic variation of the polar cap with substorm development and IMF. Detailed reports of these results are published elsewhere (MAKITA and MENG, 1984; MAKITA *et al.*, 1983; 1985).

2. Polar Cap of Geomagnetic Quiescence

A typical example of the polar-region domains inferred from electron precipitations observed by a dawn-dusk satellite during the quiet condition is shown in Fig. 1 (October 6, 1978). The top panel illustrates the auroral electron integral number flux, energy flux, and the electron average energy. The bottom left diagram shows the satellite trajectory, given at the top of this diagram, in corrected geomagnetic-latitude local-time coordinates. As the satellite traveled from the evening to the morning sector, it passed through the approximate center of the polar cap, at about 85° geomagnetic latitude along the midnight meridian (HOLZWORTH and MENG, 1975). The bottom right panel shows 24 hours of AE index, with arrows indicating this and three other passes used in the later statistical analysis to demonstrate the data selection and the condition of the defined geomagnetic quiescence. In this event, the hourly value of the AE index was less than 50 nT from 2000 UT on October 5 to 0300 UT on October 6. A moderate magnetic disturbance (~ 300 nT) occurred at about

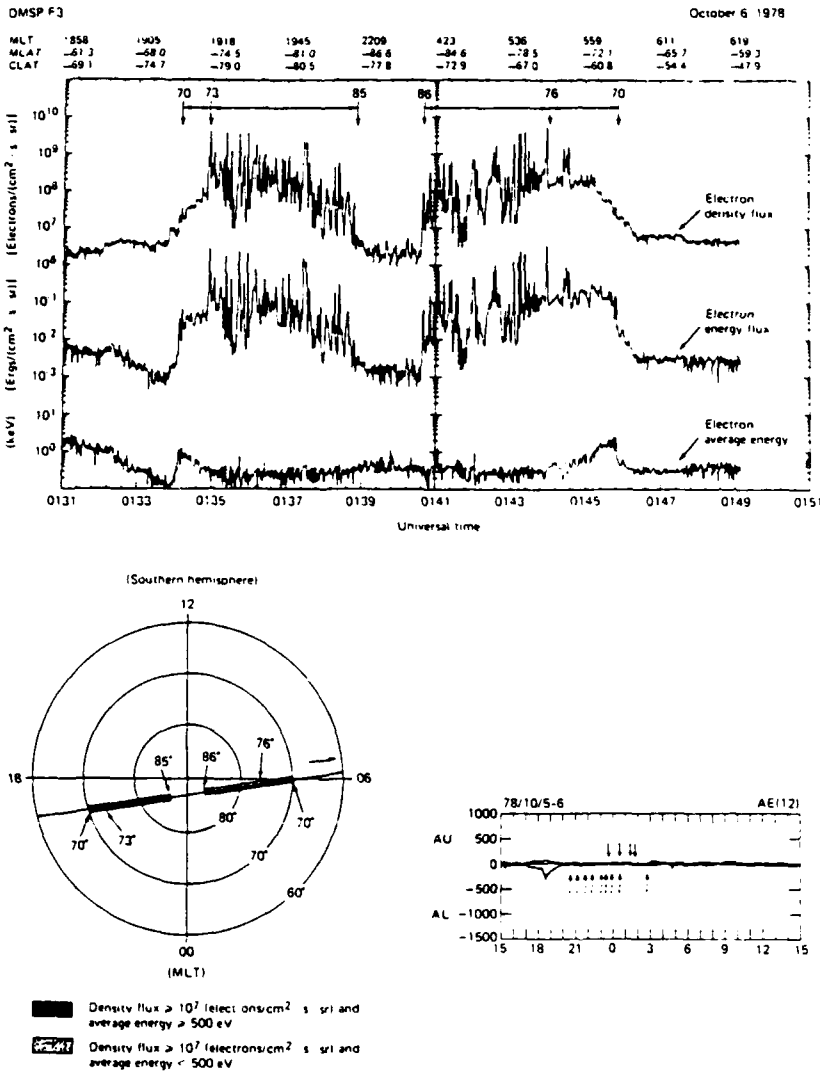


Fig. 1. An example of the auroral electron precipitation in the dawn-dusk sector during a quiet period. Top panel consists of the electron total number flux, energy flux, and average energy observed by the DMSP-F3 satellite. Bottom left panel shows the satellite trajectory in the corrected geomagnetic latitude-local time coordinates as given at the top of the figure. The solid and dotted regions indicate the hard and soft electron precipitation regions, respectively, as defined in the text. The bottom right panel shows 24 hours of AE index with the solid arrows indicating this and three other passes used in the statistical analysis of the study. Dashed arrows indicate available DMSP passes that do not satisfy the quiescence and trajectory selection criteria and that are deleted from this analysis.

1830 UT on October 5 and ended at about 2000 UT. Four orbits of DMSP made observations of electron precipitation that were within 3 hours after the activity (shown by dashed arrows) from 2000 UT to 2300 UT were deleted from the data base. Between 2300 UT and 0300 UT, there were nine DMSP polar passes, but the maximum geomagnetic latitudes of two passes were below 80° and may not traverse the polar cap region. Three others were partial polar-crossing observations. Therefore, out of 13 DMSP passes in this interval, we can use only the four passes shown by solid arrows to study the polar cap morphology in quiet condition. Figure 1 represents one of the four good passes within the time span indicated by the *AE* plot. The enhanced auroral electron number flux and energy flux were detected over most of the polar region above 70° geomagnetic latitude. The equatorward and poleward boundaries of the region of auroral electron precipitation were determined at the edge of the region extended precipitation, where the electron number flux and energy flux rise and/or drop noticeably with respect to the background level. In this example, the region of enhanced electron precipitation extends from 70° to 85° geomagnetic latitude in the dusk sector and 70° to 86° in the dawn sector. Thus, the polar cap extends only to $\sim 85^\circ$ gm latitude in the evening side and to $\sim 86^\circ$ gm latitude in the morningside; the dawn-dusk diameter of the polar cap is only $\sim 10^\circ$ wide. Based on characteristics of electron precipitations, two distinctly different precipitation regions over the auroral oval can be recognized on both the dawn and the dusk sectors. The average energy in the lower latitude part is generally higher than 500 eV, corresponding to a region of hard electron precipitation that maps to the central plasma sheet. The poleward part of the precipitation region has an average electron energy lower than 500 eV, corresponding to a region of soft precipitation or the boundary plasma sheet as defined by WINNINGHAM *et al.* (1975). The boundary between these hard and soft regions is defined here as the transition boundary. The selection of 500 eV is somewhat arbitrary since it merely represent as change in precipitation characteristics and is used in this analysis for the sake of consistency. The latitudinal characteristics of the precipitation also change near the transition boundary from somewhat smooth and continuous in the lower latitude to highly fluctuating burst type in the higher latitude. In this example, the region of high-average-energy electron precipitation is rather narrow, about 3° in the dusk sector and about 6° in the dawn sector, compared with the width of the entire auroral oval. The region of low-average-energy electron precipitation is very wide, with widths of about 12° in the dusk sector and about 10° in the dawn sector.

The electron precipitations in the noon and midnight sectors are illustrated by the next example (Fig. 2). The geomagnetic condition is again quiet as shown by the *AE* index. The hourly value of the *AE* index was continuously low from 0000 UT to 2400 UT on December 25. From high-resolution *AE* data, a disturbance of ~ 200 nT occurred between 2100 UT and 2300 UT on December 24. Thus, the electron precipitation observations from 0000 UT to 0200 UT shown by dashed arrows are not included in the statistical analysis, which will be discussed in the next section. From 0200 UT to 2400 UT, there were 43 DMSP polar passes from two DMSP satellites, of which 18 passes were the low-latitude polar passes below 80° gm latitude and the other 14 passes were only partial polar crossings. Therefore, only 11 passes, shown by

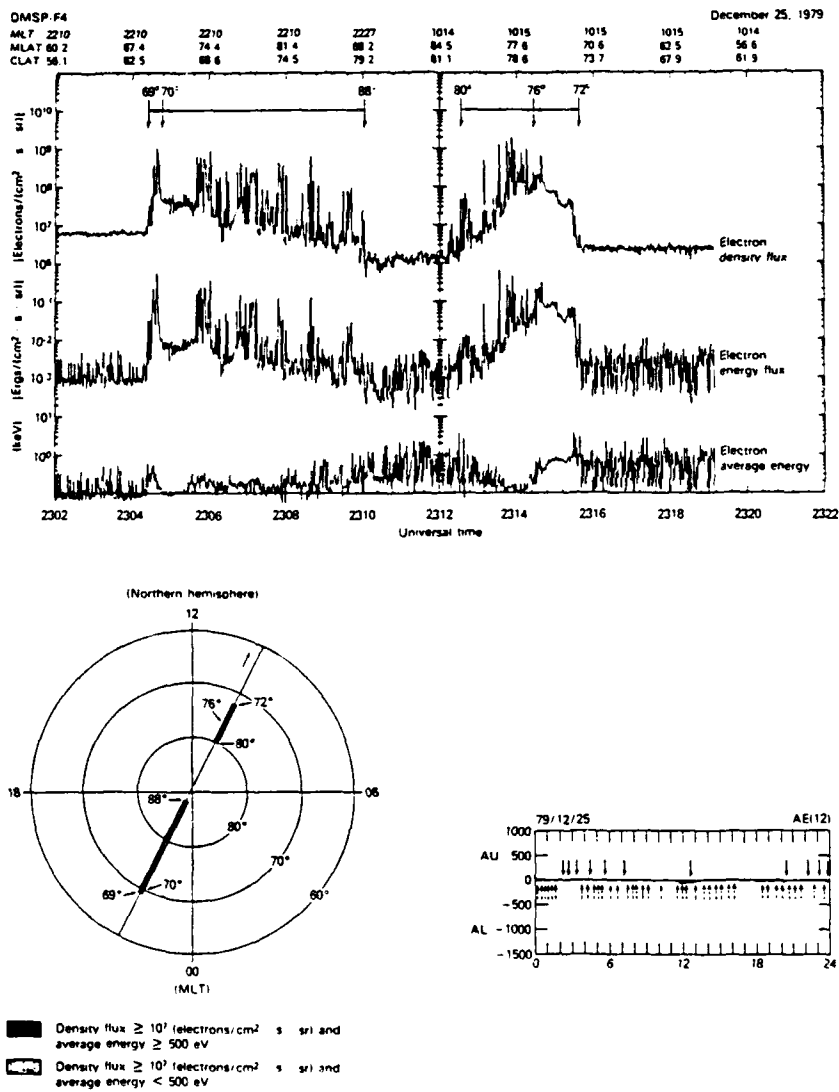


Fig. 2. An example of the auroral electron precipitation in the noon-midnight sectors during quiet periods observed by the DMSP-F4 satellite. The format of the presentation is the same as that of Fig. 1 but for December 25, 1979, ~2310 UT.

solid arrows, out of 49 passes in this interval are used in understanding the morphology of quiet-time auroral precipitations. Figure 2 is one of the selected passes observed from 2302 UT to 2322 UT along the noon-midnight meridian. In this example, the region of high-average-energy electron precipitation extends from 69° to 70° gm latitude in the midnight sector and 72° to 76° in the noon sector. The region of low-average-energy electron precipitation extends from 70° to 88° in the midnight sector and 76° to 80° in the noon sector. The polar cap is only ~12° in dimension in the noon-midnight orientation. It again indicates a very small polar cap in the quiet times as shown by the trajectory plot at lower left.

It is important to know whether the polar cap region defined by using the poleward boundary of the soft extended auroral electron precipitations is a reasonable one. One way to check is to examine the polar cap locations over both the northern and southern hemispheres. Based on the definition of the polar cap as the area of opened geomagnetic field lines, a near symmetry is expected. Figure 3 is an example of nearly simultaneous conjugate observations made by DMSP-F2 and -F3 satellites at ~0930 UT on August 14, 1978. The boundary of the polar cap was at ~82°-83° in the dusk sector and at ~84°-85° in the dawn sector over both polar regions. Therefore, the polar cap dimension as determined is a reasonable one; a small polar cap region was detected over both the northern and southern hemispheres, similar to previous results reported in MENG (1981b).

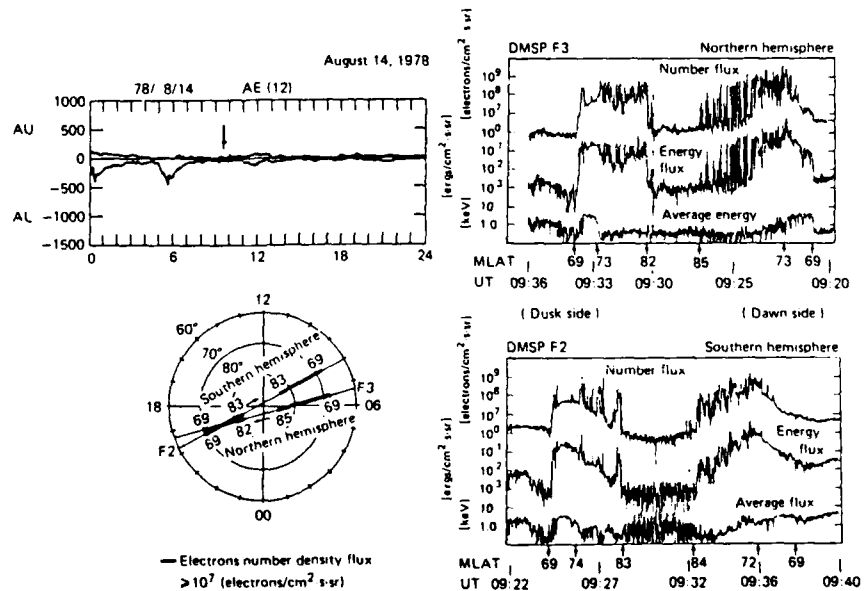


Fig. 3. Auroral electron precipitations observed at both northern and southern polar regions, near simultaneously at about 0930 UT on August 14, 1978, by two DMSP satellites. Note the similarity between two hemispheres, especially in the defined polar cap configuration.

3. Average Location of Quiet-Time Polar Cap and Precipitation Boundaries

From the above illustrations, it is clear that the region of polar cap is rather small in all of the local time sectors and also that, in the quiet time, the soft electron precipitation region is extremely wide in latitude. In this section, we examine statistically the spatial distribution of the polar cap and the auroral electron precipitation regions based on the latitudes of the poleward, transition, and equatorward boundaries during quiet geomagnetic conditions from 434 polar pass observations. We have examined the average boundary locations in the northern and southern hemispheres separately to search for possible seasonal variations. Over the northern hemisphere, there were 114 winter observations (October to March) and only 41 summer ones (April to September). For the southern hemisphere observations, there were 62 winter passes (April to September) and 217 summer passes (October to March). Since the northern hemispheric electron precipitation data were mostly obtained in the winter season and the southern ones were mostly obtained in the summer season, the average electron precipitation patterns are thus grouped only by the local season, irrespective of the hemisphere. These data were subgrouped into four magnetic local time (MT) sectors, namely, from 0300 to 0900, 0900 to 1500, 1500 to 2100, and 2100 to 0300 MLT.

Figure 4 illustrates the average locations of the poleward, transition, and equatorward boundaries of the precipitation region in the winter and summer hemispheres during geomagnetically quiet periods. Because of the limited coverage of DMSP satellite orbits, observations from 1200 to 1800 and 0000 to 0300 MLT zones were not abundant compared with other sectors. Therefore, the average location of boundaries in the noon sector (0900 to 1500 MLT), the evening sector (1500 to 2100 MLT), and the midnight sector (2100 to 0300 MLT) were determined by using the data mainly from 0900 to 1200, 1800 to 2100, and 2100 to 0000 MLT, respectively. In this average precipitation pattern during quiet times (Fig. 4), one of the interesting results is that the averaged location of the poleward boundary in both winter and summer polar regions is at very high geomagnetic latitudes in all local time sectors. It is at about 82° to 84° in the morning, noon, and evening sectors and at about 81° to 82° in the midnight sector. The standard deviation of the poleward boundary location in the midnight sector is larger than that in other magnetic local time sectors because of greater scattering. The average size of the polar cap of the very quiet magnetosphere is about 12° to 14° in diameter.

It is important to point out that the average locations of the auroral equatorward and transition boundaries between the local winter and the local summer hemisphere are nearly identical, except in the noon sector (0900 to 1500 MLT). The average location of the equatorward boundary is at about 70.0° to 70.2° , 68.6° to 68.9° , and 69.5° to 69.7° in the evening, midnight, and morning sectors, respectively. The transition boundary is at about 73.4° to 73.5° , 71.3° to 71.6° , and 75.4° to 75.5° in the evening, midnight, and morning sectors. In the noon sector, there is a slight difference between the winter and the summer hemisphere in the averaged equatorward and transition boundary locations. The locations are at 70.0° and 76.7° in the winter hemisphere and 70.8° and 77.5° in the summer hemisphere, perhaps indicating that,

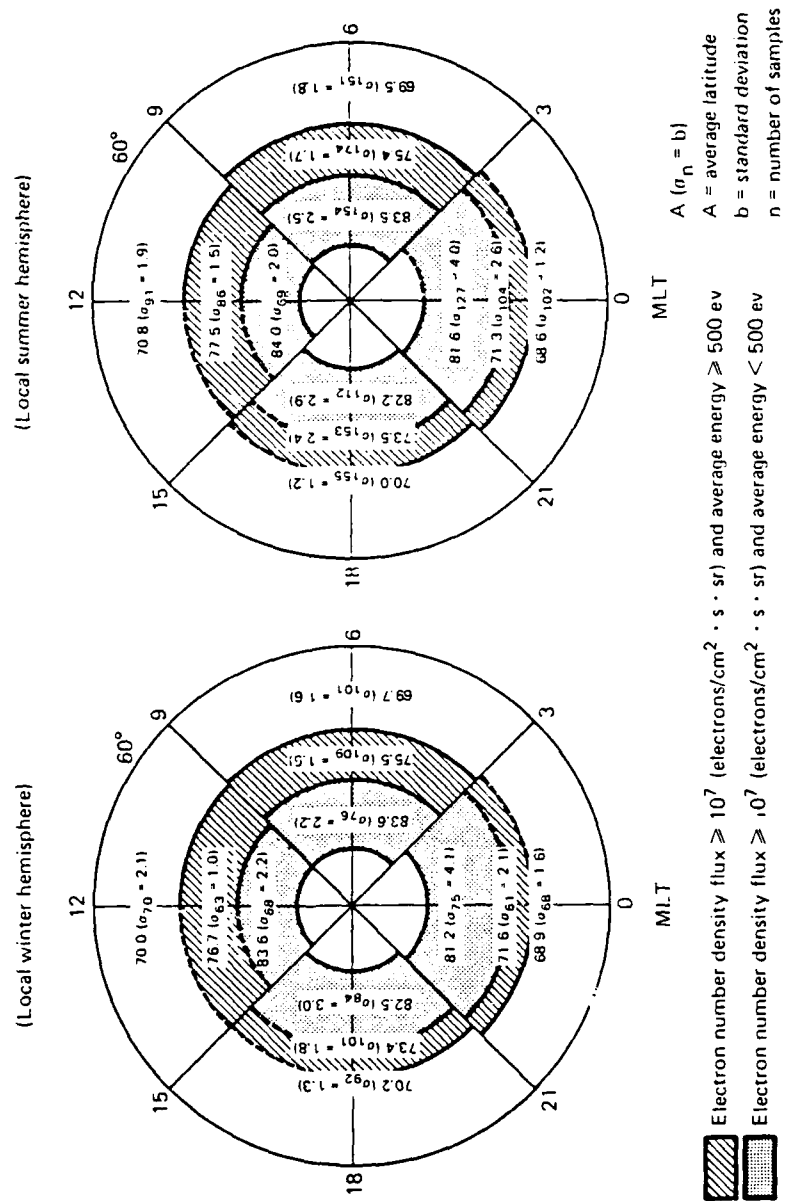


Fig. 4. Average distribution of auroral electron precipitation on the local winter and the local summer hemispheres during geomagnetic quiescence. The lightly shadowed region corresponds to the poleward low-average-energy auroral electron precipitation region, and the heavily shadowed region corresponds to the equatorward high-average-energy auroral electron precipitation. Note that the boundaries of poleward precipitation are statistically located at very high latitude, above 80° in all local time sectors during very quiet periods.

in the noon sector, the region of high-average-energy electron precipitation in the summer hemisphere is located about 1 degree higher than it is in the winter hemisphere.

Is this statistical result of a very small polar cap during geomagnetic quiescence consistent with other observations of the polar cap region? The most direct way to define the polar cap is from global imaging of the auroral display. Usually imaging the very quiet time auroral oval is rather difficult due to the very low auroral emission intensity. The auroral scanner on the ISIS-2 satellite made many global auroral distributions during the very quiet geomagnetic condition. A very small polar cap and a widened auroral oval were observed (MURPHREE *et al.*, 1982); it confirms the earlier suggestion of MENG (1981b). Thus the present DMSP electron observation is certainly consistent with that optically imaged, small polar cap distribution during the geomagnetic quiescence.

4. Quiet-Time Electron Precipitation Boundaries and IMF B_z Component

The relationship of average locations of the quiet-time poleward, transition, and equatorward boundaries of auroral precipitation with the IMF B_z component is examined statistically in this section. Figure 5 shows scatter diagrams of the three boundaries subgrouped into four MLT sectors (0900–1500, 1500–2100, 2100–0300, and 0300–0900). Within each diagram, boundary locations are plotted according to the concurrent hourly average of the IMF B_z value. Since DMSP electron data used here were selected during the quiet period, the concurrent hourly average value of IMF B_z was mostly northward ($>80^\circ$). The poleward, transition, and equatorward boundaries are represented by circles, triangles, and solid dots, respectively. The linear regression was calculated for each type of boundary by using the least-squares-fit method, and the correlation coefficients are shown on the figure. There are large scatters with respect to the linear regressions; however, some general trends of these boundaries can be stated.

It is noticed that responses of the poleward, transition, and equatorward boundaries to the IMF B_z fluctuation are similar in all local time sectors. Generally, the latitudinal position of the poleward boundary of auroral electron precipitation was proportional to the magnitude of the northward IMF B_z component. The average displacement rate of the poleward boundary in the noon, evening, midnight, and morning sector was about 0.14° , 0.37° , 0.43° , and 0.26° per 1 nT change of the IMF B_z , respectively. This indicates an increase of the polar cap radius by $\sim 0.3^\circ$ per 1 nT of southward IMF B_z . The effect of IMF B_z on the transition and equatorward boundaries during quiet times was quite different from that of the poleward boundary. The transition boundary moves only slightly equatorward with the increasing northward IMF component in all local time sectors, whereas the equatorward boundary did not show any significant variation with the northward change of IMF B_z magnitude. These results indicate that, in all local time sectors, the width of the region of low-average-energy electron precipitation (between the poleward and transition boundaries) expanded both poleward and equatorward with increasing northward IMF B_z intensity; however, the width of the region of high-

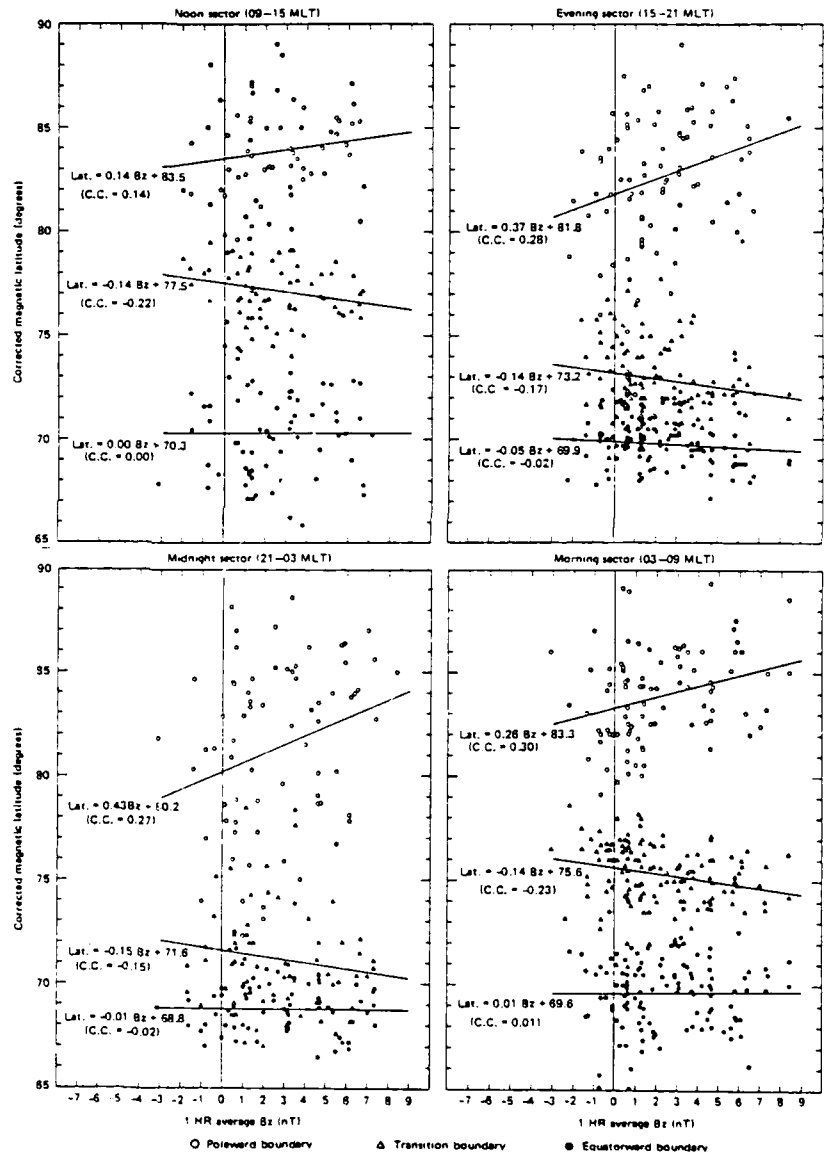


Fig. 5. The scatter plot of the poleward, transition, and equatorward boundaries of the auroral electron precipitation in the four MLT sectors (09-15, 15-21, 21-03, and 03-09). The poleward, transition, and equatorward boundaries are represented by circles, triangles, and solid dots, respectively. The linear regression was calculated for each type of boundary by using the least-squares-fit method; the correlation coefficients (c.c.) are also shown.

average-energy electron precipitation (between the transition and equatorward boundaries) slightly reduced its latitudinal width with the increasing northward IMF component. The poleward shift of the poleward precipitation boundary with increasing northward IMF component. The poleward shift of the poleward precipitation boundary with increasing northward IMF implies the reduction of the polar cap size with the increasing magnitude of positive B_z . Such a gradual poleward movement of the poleward edge of the auroral oval is very consistent with the distribution of discrete auroras in different IMF conditions reported by LASSEN and DANIELSEN (1978), since the discrete arcs occur in the poleward part of the auroral oval.

5. General Variations of Polar Cap and Auroral Oval

Previous sections concern the morphology of the polar cap and auroral oval in the very quiet geomagnetic condition. In this section, their morphology under different geomagnetic conditions and IMF B_z component is examined statistically based on 246 dawn-dusk orbits selected from June to August 1978.

The equatorward, transition, and the poleward boundaries of the precipitation region at various magnetic local times were analyzed, together with the corresponding hourly average AE index during the satellite traverse over the polar region. The locations of these boundaries are determined with an accuracy of 0.1° . These dawn-dusk DMSP passes were subgrouped according to three ranges of the hourly AE index, namely, $0 \leq AE \leq 150$ (nT), $150 < AE \leq 400$ (nT), and $AE > 400$ (nT); there are 100 passes in $0 \leq AE < 150$ (nT), 85 passes in $150 < AE \leq 400$ (nT), and 61 passes in $AE > 400$ (nT). We also subgrouped the data into four dawn-dusk magnetic local time sectors, 1700 to 1900 and 1900 to 2100 MLT in the evening sector and 0600 to 0800 and 0800 to 1000 MLT in the morning sector.

Figure 6 shows the average locations of the poleward, transition, and equatorward boundaries of the precipitation region during geomagnetically quiet periods when the hourly average AE index was less than 150 nT. The light- and heavy-hatched areas indicate the low-energy and the high-energy electron precipitation regions, respectively. The poleward boundary of the low-energy electron precipitation region is located at about 80° to 82° in both the evening and morning sectors. The transition boundary is seen at about 73° to 75° in both the evening and morning sectors, and the equatorward boundary is located at 69° to 71° in the evening sector and 67° to 69° in the morning sector. The latitudinal extent of the low-energy electron precipitation region is about 7° to 8° in both the evening and morning sectors, while the width of the high-energy electron precipitation region is about 4° in the evening sector and 6° in the morning sector. The polar cap size and locations of various boundaries are somewhat different from those in Fig. 4, indicating a larger polar cap and the equatorial shift of the auroral oval. It is contributed by including a slightly disturbed condition and using a less stringent definition of geomagnetic quietness.

Figure 7 shows the average width of the electron precipitation region during disturbed periods ($AE > 400$ nT). The poleward boundary is located at about 73° to 75° in the evening sector and 76° to 77° in the morning sector. The transition and the

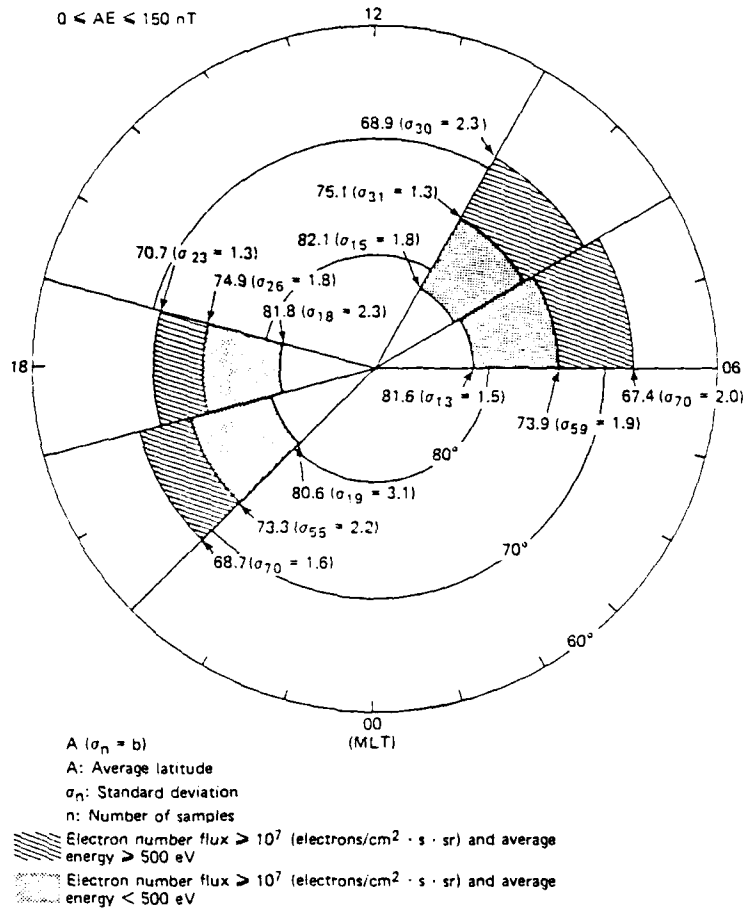


Fig. 6. Averaged auroral electron precipitation distribution on the dawn-dusk side during quiet geomagnetic conditions ($0 \leq AE \leq 150$ nT). The poleward light-shadowed region corresponds to the low-energy auroral electron precipitation region, and the equatorward heavy-shadowed region corresponds to the high-energy auroral electron precipitation region. Note that the poleward precipitation boundary is statistically above 80° geomagnetic latitude during moderately quiet times.

equatorward boundaries are located at about 70° to 72° and 64° to 66° , respectively, in both the evening and morning sectors. The polar cap size is much larger than that of the quiet condition with the diameter increased from only $\sim 12^\circ$ to 14° of very quiet to $\sim 16^\circ$ to 18° of moderately quiet and finally to $\sim 30^\circ$ wide in latitude during this moderately active time. During magnetic storms, the polar cap size is even larger to $> 50^\circ$ wide in latitude (MENG, 1984). The average width of the low-energy electron precipitation region during disturbed time is about 1° to 4° in the evening sector and

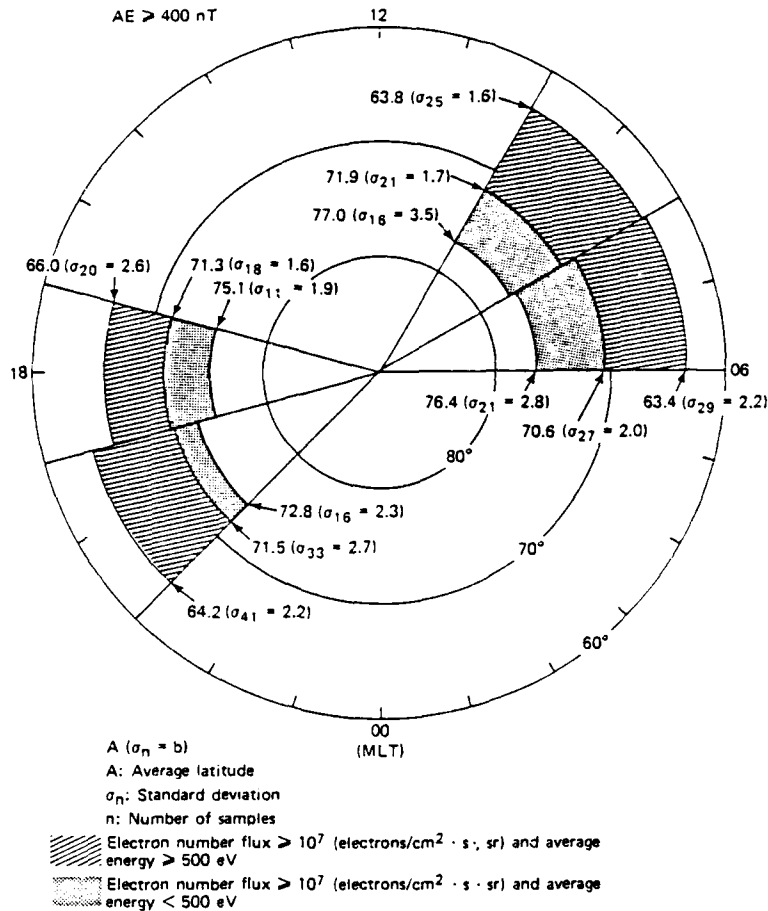


Fig. 7. The same as Fig. 6, but for the geomagnetically active time ($AE > 400$ nT). Note the equatorward shift of the averaged poleward boundary of 5° in the morning sector (0600-1000 MLT) and of 7° to 8° in the evening sector (1700-2100 MLT). The reduction of the auroral oval width is about 2° to 4° in the evening and less than 1° in the morning sectors from the average quiet conditions.

about 5° to 6° in the morning sector, while the width of the high-energy electron precipitation region is about 5° to 7° in the evening sector and about 7° to 8° in the morning sector. The location of the poleward, transition, and equatorward boundaries for moderately active periods ($150 \text{ nT} < AE \leq 400 \text{ nT}$) falls between the above two geomagnetic conditions. Generally, as the geomagnetic activity increases, the polar cap size increases, the width of the low-energy auroral electron precipitation region decreases, and the width of the high-energy auroral electron precipitation region increases.

The locations of the poleward, transition, and equatorward boundaries and their relationships to the IMF B_z component were also statistically examined. The three boundaries were subgrouped for two magnetic local time sectors (1700-2100 and 0600-1000) and then were compared with the concurrent hourly IMF B_z components and also at 1 hour preceding the satellite crossing. Figures 8(a) and 8(b) show the scatter plot of the poleward, transition, and equatorward boundaries and the corresponding hourly average values of the IMF B_z component at the hour of and 1 hour before the satellite pass, respectively. The poleward, transition, and equatorward boundaries are represented by open circles, triangles, and dots, respectively. The left and right panels show variations in the evening and morning sectors. The correlation coefficient and the linear regression by the least-squares method were calculated for the entire B_z range and for positive and negative ranges separately, as is illustrated in the diagram.

The responses of the equatorward boundary of the precipitation region to the positive and negative IMF B_z were established by HARDY *et al.* (1981). From our analysis, it is clear that a linear correlation is present between decreasing B_z values at the hour and 1 hour before, and the equatorial displacement of the poleward, transition, and equatorward boundaries, when B_z is negative.

Figure 8(a) shows that the average poleward, transition, and equatorward boundaries move toward lower latitudes by about 1.1°, 0.37°, and 0.66° per 1 nT, respectively, in the evening sector and about 0.77°, 0.54°, and 0.55° per 1 nT, respectively, in the morning sector.

Similar tendencies can be recognized in Fig. 8(b). It shows that the average poleward, transition, and equatorward boundaries move toward lower latitudes by about 0.98°, 0.42°, and 0.85° per 1 nT in the evening sector and about 0.96°, 0.52°, and 0.65° per 1 nT in the morning sector. Both figures show that the correlation can also be seen between the increasing values of the positive B_z component and the poleward displacement of the poleward boundary of the extended precipitation region.

The above analyses reveal that both the poleward and equatorward auroral precipitation boundaries are located at higher latitudes during quiet periods than during disturbed periods, indicating a drastic variation of the polar cap size. It was also found that there is a widening of the precipitation region during quiet periods that coincides with periods of positive IMF B_z . This results from the fact that the poleward boundary shifts poleward considerably more than the equatorward boundary. It is also shown that the poleward boundary moves toward lower latitudes with a decreasing IMF B_z value. Further, the shift of the equatorward boundary can be seen only when IMF B_z is negative. However, there is no distinct correlation between the positive B_z magnitude and the displacement of the equatorward and transition boundaries in both the dawn and dusk sectors.

6. Dynamic Variation of the Auroral Oval

The above observations indicate that the unusually high latitude of the precipitation poleward boundary (i.e., a small polar cap) is the consequence of a very

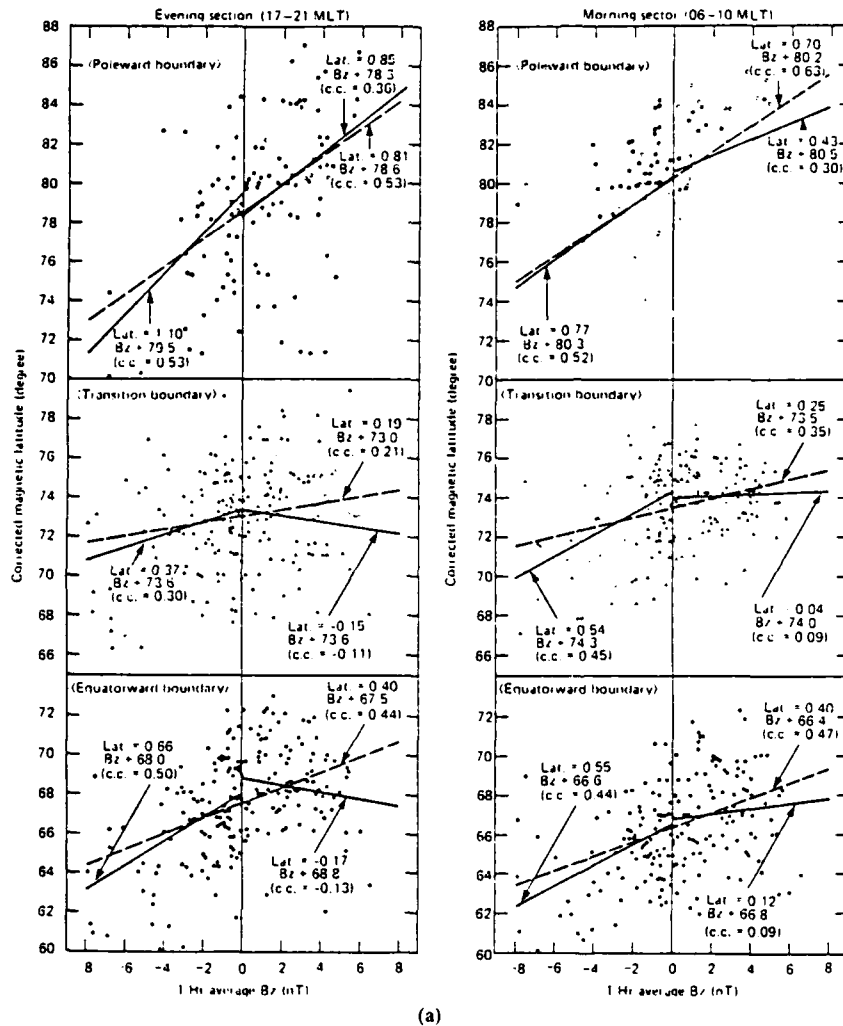
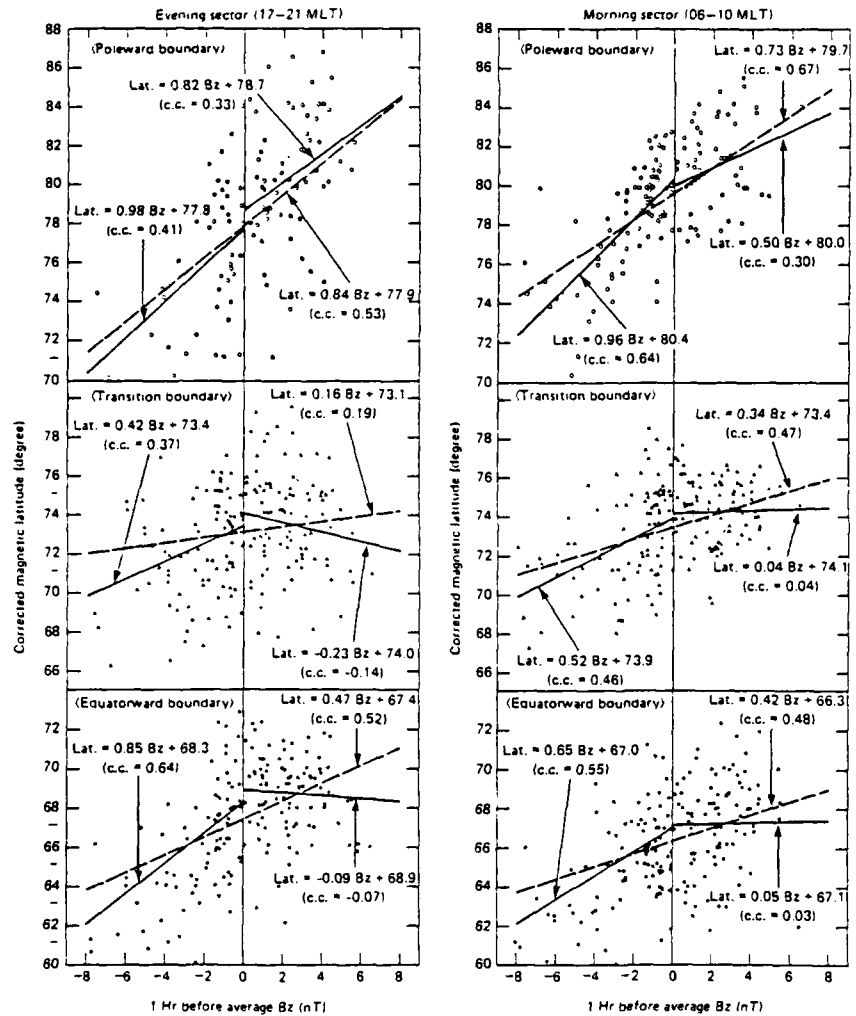


Fig. 8. (a) The scatter plot of the poleward transition and equatorward boundaries of the auroral electron precipitation in the magnetic local time 1700–2100 MLT and 0600–1000 MLT and their relationship to the corresponding hourly average values of the IMF B_z component at the hour of the polar pass. The poleward transition and equatorward boundaries of the auroral electron precipitation are represented by open circles, triangles, and dots, respectively. The solid lines give the least-squares fit to the data points with IMF $B_z > 0$ nT and $B_z < 0$ nT separately. The dotted lines give the least-squares fit for points without B_z separation. The correlation coefficients (c.c.) are also shown in this figure. (b) The scatter plot of the poleward transition and equatorward boundaries of the auroral electron precipitation in the magnetic local time 1700–2100 MLT and 0600–1000 MLT and their relationship to the corresponding hourly average values of the IMF B_z at 1 hour preceding the polar pass. The format of the presentation is the same as that of Fig. 8(a).



(b)

small number of geomagnetic flux lines interconnected with the IMF during a northward IMF condition. They also imply that the size of the polar cap is inversely controlled by the magnitude of the northward B_z component. The insensitivity of the transition and equatorward precipitation boundaries to the northward IMF B_z can be used to infer that their dynamics are dominated by internal magnetospheric processes and not by direct solar-magnetospheric interactions. In this section, we will present the evolution of the polar cap size with the IMF and substorm variations based on

observations from a pair of DMSP satellites.

Figure 9 illustrates typical electron precipitation profiles along the dawn-dusk meridian for three consecutive northern polar region crossings during the development of a magnetospheric substorm. The upper panel from 0231 to 0311 UT was obtained during a quiet period ($AE(\text{hourly})=32$ nT) before the onset of a substorm on October 8, 1978. The AE index at the time of the top panel is shown by the arrow (a) in Fig. 10. From the electron number flux and energy flux data, the region of enhanced electron precipitation extended from gm latitude $\sim 69^\circ$ to $\sim 80^\circ$ in the dusk sector and from $\sim 71^\circ$ to $\sim 84^\circ$ in the dawn sector, respectively. The high-average-energy electron precipitation region was located between 69° and 71° in the dusk sector and between 71° and 75° in the dawn sector. The low-average-energy electron precipitation region was located between 71° and 80° in the dusk sector and between 75° and 84° in the dawn sector. The latter can be distinguished from the former by its highly structured features. The polar cap was $\sim 16^\circ$ wide in latitude. The middle panel was observed between 0432 and 0450 UT during the moderately disturbed period ($AE(\text{hourly})=200$ nT); see the arrow (b) in Fig. 10. From the middle panel data, one can see that the electron precipitation region clearly shifted equatorward after the previous polar crossing. The high-average-energy electron precipitation region was located between $\sim 69^\circ$ and $\sim 67^\circ$ in both the dawn and dusk sectors. The low-average-energy electron precipitation region extended from $\sim 69^\circ$ to $\sim 71^\circ$ in the dusk sector and from $\sim 73^\circ$ to $\sim 81^\circ$ in the dawn sector with a polar cap width of $\sim 28^\circ$. The lower panel was observed from 0613 to 0630 UT during a disturbed period ($AE(\text{hourly})=250$ nT) in the recovery of a substorm; see the arrow (c) in Fig. 10. The high-average-energy electron precipitation region was detected from $\sim 65^\circ$ to $\sim 72^\circ$ in the dusk sector and from 65° to 74° in the dawn sector. The low-average-energy electron precipitation region cannot be identified in the dusk sector and were from 74° to 78° in the dawn sector. The polar cap was about 30° wide in the dawn-dusk orientation.

If the precipitation boundary can be defined by the poleward edge of the elevated level of the low-average-energy electron precipitation region, this sequence of DMSP polar crossings suggests that the poleward boundary of the low-average-energy electron precipitation region shifted drastically equatorward and thus the dawn-dusk distance between the precipitation boundaries (i.e., the polar cap) distinctly increased during this disturbed period. Note that there were a few bursts of electron precipitation in the polar cap thus defined during the quiet and moderately disturbed periods, but they disappeared during the highly disturbed periods. By using consecutive observations from two identical DMSP satellites made over both polar regions, the dynamic variation in the polar cap dimension can be inferred. In this analysis, Akasofu's solar wind input ϵ parameter ($\epsilon = VB^2 \sin^4(\theta/2) h_0^2$) is calculated using the ISEE-3 IMF data by assuming that the solar wind velocity is constant (400 km/sec). We examined in detail 15 examples, but, for presentation purposes, we selected two typical examples in the dawn-dusk sectors and one in the noon-midnight sectors.

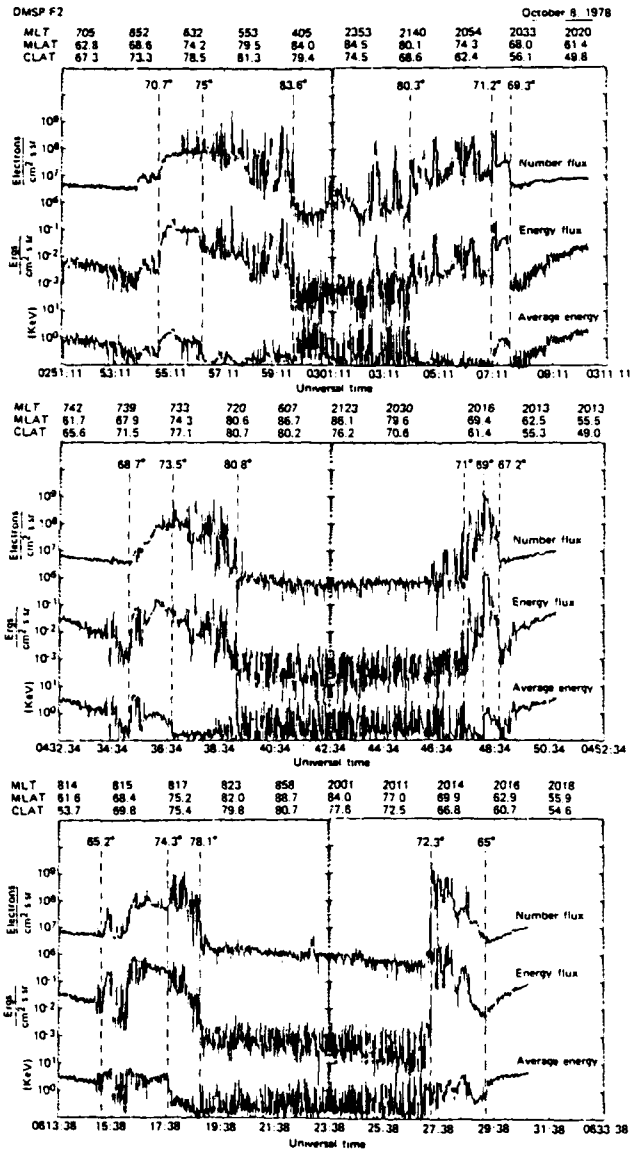


Fig. 9. Typical electron precipitation profile along the dawn-dusk meridian for three consecutive northern polar region crossings. The upper panel was obtained during a quiet period ($AE=32$ nT), the middle panel was observed during the moderate disturbed period ($AE=200$ nT) and the lower panel was observed during a disturbed period ($AE=250$ nT).

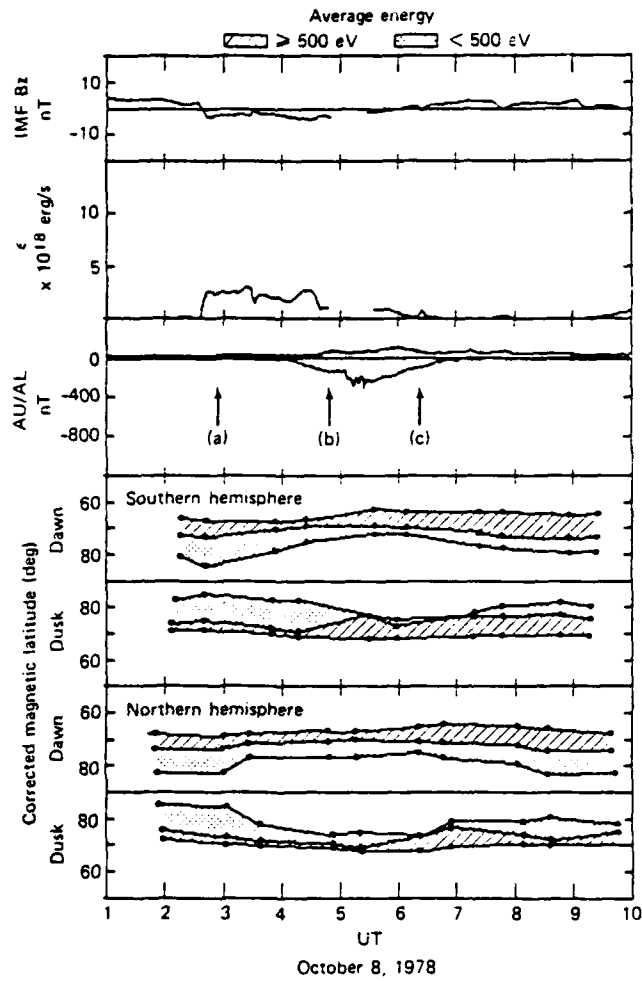


Fig. 10. Temporal and spatial variations of the polar cap size and of the electron precipitation region in the dawn-dusk sector with the IMF B_z , ϵ , and AE index. The lightly shaded region (poleward) corresponds to the low-average energy electron precipitation region ($E_{avg} < 500$ eV), and the hatched region (equatorward) corresponds to the region of high-average-energy electron precipitation ($E_{avg} > 500$ eV). Note that there is about a 1 hour time delay for the solar wind to propagate between the ISEE-3 location and the magnetosphere. Thus, both the IMF B_z and ϵ data should be shifted to the right by about 1 hour in order to examine them in conjunction with the DMSP observation and the AE index.

6.1 October 8, 1978

In Fig. 10, temporal and spatial variations of the polar cap size and of the electron precipitation region are plotted, together with the IMF B_z , ϵ , and AE index. From the AE index, one can see that an isolated substorm occurred during this period. The electron precipitation regions along the dawn-dusk meridian observed from both the southern and northern hemispheres are shown in the two bottom panels. The electron precipitation data are obtained by combining observations from the DMSP-F2 and -F3 satellites, enabling us to determine the boundaries with time resolution of ~ 30 min on the average. Note that the observed locations of these electron precipitation boundaries were normalized to those of the 1800 MLT in the dusk sector and the 0600 MLT in the dawn sector by assuming a circular distribution with the center shifted by 4.2° from the geomagnetic pole toward the 0015 MLT (MENG *et al.*, 1977).

As shown in this figure, during the period of the northward IMF and low ϵ values (namely, before 0230 UT), the poleward boundaries of the low-average-energy electron precipitation region were located at 80° in gm latitude or higher. Thus, the dimension of the polar cap in the dawn-dusk direction during the quiet period was about 15° or less. Note that there is about a 1 hour time interval for the solar wind to propagate from the ISEE-3 location to the magnetosphere. Therefore, both the IMF B_z and ϵ data should be shifted to the right by about 1 hour in order to examine them in conjunction with the DMSP observations and the AE index.

Associated with a negative excursion of the IMF B_z component and the associated increase of the ϵ parameter after 0230 UT, the poleward boundary of the electron precipitation region began to shift equatorward. By combining both the northern and southern polar data, one can infer that the shift began between 0300 and 0320 UT (at about the time when the southward-directed IMF reached the magnetosphere). The geomagnetic activity represented by the AE index began gradually at about 0400 UT and reached the maximum values at about 0515 UT. The polar cap became largest at about 0530 UT; the maximum dimension of the polar cap was 33° in the southern hemisphere and 31° in the northern hemisphere. On the other hand, the equatorward shifts of both the equatorial boundary of the high-energy precipitation region and the transition boundary between the high- and low-energy precipitation regions were much less.

After 0430 UT, the ϵ parameter began to decrease. Subsequently, the substorm activity began to decline after 0520 UT. The poleward boundary of the electron precipitation region gradually shifted poleward after 0600 UT. As a result, the distance between the precipitation boundaries was reduced. Note that this reduction lasted well after the substorm activity (represented by the AE index) ceased and the ϵ parameter became less than 10^{18} erg/sec.

6.2 August 18-19, 1978

Figure 11 shows an example that covers the recovery phase of one substorm and the development of a new substorm activity with a fairly quiet period between them. The recovery of the first substorm was associated with the northward turning of the IMF. During this interval, the poleward boundary of the auroral electron precipita-

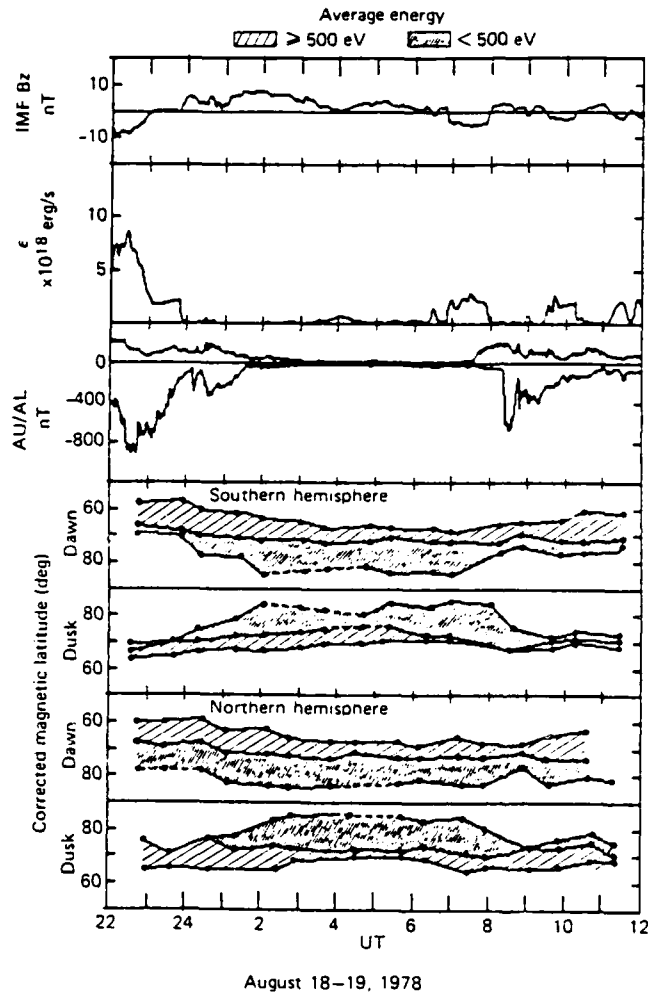


Fig. 11. The format in the figure is the same as that for Fig. 10. The poleward boundary of the electron precipitation region in both hemispheres began to shift poleward (equatorward) after the northward (southward) turning of the IMF and the corresponding decrease (increase) of the ϵ parameter at ISEE-3 at 2300 UT (0600 UT).

tion region gradually shifted poleward. After 0200 UT on August 19, the poleward boundary was located at latitudes higher than 80° in both hemispheres. Between ~ 0300 UT and ~ 0700 UT, the ϵ parameter was very low, and the poleward boundary of the auroral electron precipitation region remained persistently at magnetic latitudes above 80° . It should be noted that the equatorward boundary of auroral

electron precipitation regions also moved slightly poleward during this quiet period. With an increase of the ϵ parameter after 0650 UT at the ISEE-3 location, a new substorm activity began at about 0730 UT, first a significant increase of the AU and a sharp increase of AL at ~ 0815 UT. Concurrently, the poleward boundary of the electron precipitation region gradually moved equatorward and then sharply after ~ 0800 UT.

6.3 December 3-4, 1979

The previous two examples illustrate the dynamics of the precipitation region observed in the dawn-dusk sector. This example illustrates the auroral electron precipitation region in the noon-midnight sector (Fig. 12). We normalize the observed locations of these electron precipitation boundaries to the 00 MLT in the midnight sector and to the 1200 MLT sector in the noon sector as described previously. One can see that the IMF B_z component was positive until about the end of December 3, and both the ϵ parameter and the AE index were low. The poleward boundary of the auroral electron precipitation region was located at latitudes higher than 80° on the dayside and 71° on the nightside. First, the overall trend of the equatorward and poleward shifts and their relationship to the AE index (as well as to the IMF B_z component and the ϵ parameter) are quite similar to those for the dawn-dusk sector, although the shift is a little more pronounced in the midday sector than in the midnight sector. Thus, there is no doubt that the noon-midnight dimension of the polar cap is also significantly greater during a substorm than during a quiet period. The equatorward shift of the midday part of the auroral oval (the cusp) during a substorm was studied earlier by AKASOFU (1972) and EATHER *et al.* (1979). It is quite likely that the nightside shift is somewhat obscured by both gradual and rapid ($\sim 0630, 1212$ UT) poleward expansion of the aurora. Note that the nightside auroral oval consisted almost wholly of the high-average energy electron precipitation region, since the low-energy precipitation region disappeared. When the ϵ parameter began to decrease after 1500 UT, the polar cap boundaries began to shift poleward.

7. Interpretations of the Results

It may be worthwhile to summarize some of the findings before attempting to interpret the results in terms of changes of the open flux and of magnetic energy in the magnetotail as a consequence of the solar wind-magnetosphere interaction. It is quite clear that the distance between the precipitation boundaries along both the dawn-dusk and noon-midnight meridians increases during substorm activity. This feature can be considered as a response of the magnetosphere to the IMF southward turning and the resulting increase of the ϵ parameter. The increase is more prominent along the dawn-dusk meridian than in the noon-midnight meridian. In the noon-midnight meridian, the increase is more evident on the dayside than on the nightside. At times, the nightside dimension decreases for brief periods; this feature is due to the poleward expansion of the auroral bulge during a substorm.

The poleward boundary of the instantaneous auroral electron precipitation can

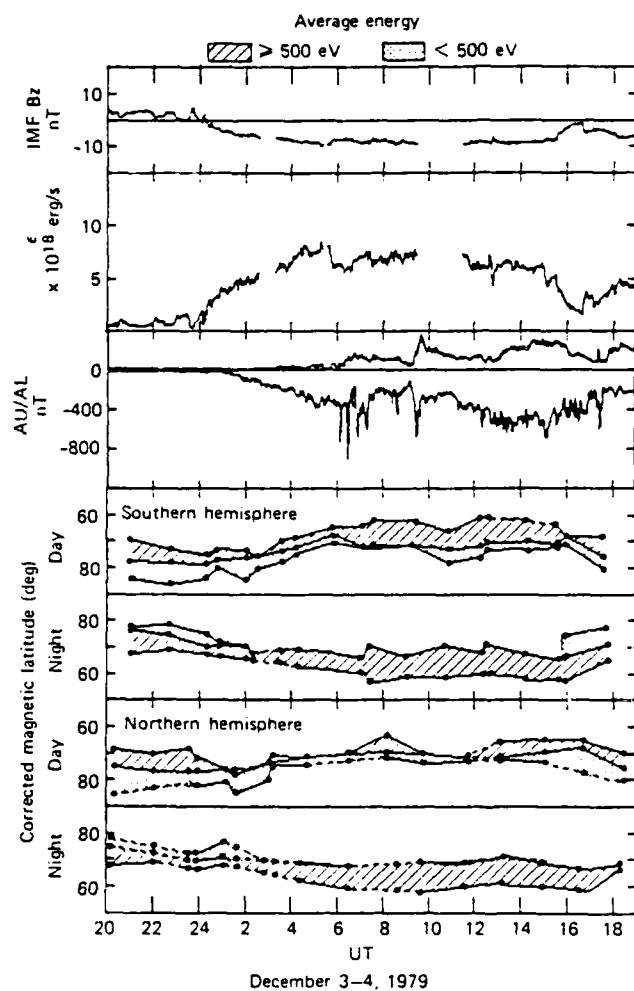


Fig. 12. Temporal and spatial variations of the polar cap size and of the electron precipitation region in the noon-midnight sector. The format in this figure is the same as that for Fig. 10. Note that the overall trend of the equatorward and poleward shifts and their relationship to the AE index (as well as to the $IMF B_z$ component and the ϵ parameter) are quite similar to those for the dawn-dusk sector.

be used to define the dimension of the polar cap. Then the polar cap begins to shift poleward slowly at about the time when the AE index begins to decline. The polar cap dimension is largest at about the period when the AE index becomes largest. However, the shift continues well after the AE index decreases to the noise level. The size of the polar cap is very small corresponding to a quiet magnetosphere. The

equatorward boundary of the precipitation region appears to respond in a similar way, but the extent of the shift is much less than that of the poleward boundary. Thus, the resulting short distance between the precipitating boundaries is characterized mainly by the poleward shift (or advance) of the poleward precipitation boundaries. Further, this poleward shift is due to widening of the low-energy precipitation region as previously suggested (MENG, 1981b). On the other hand, the low-energy precipitation region during an intense substorm becomes very narrow, particularly in the night sector. Note also that the electron precipitation pattern in the latitude range between 60° and 70° (where most *AE* stations are located) is quite insensitive to the IMF changes during the initial epoch. We schematically illustrate these main features in Fig. 13. Note that these findings are consistent with earlier results by MENG (1981b), MURPHREE *et al.* (1982), and MAKITA *et al.* (1983).

We now attempt to interpret some of these findings in terms of changes of the open geomagnetic flux and of magnetic energy in the magnetotail. The basic assumptions in this interpretation are that the poleward boundaries of the electron precipitation belt can be identified as the polar cap boundary and that the dimension of the polar cap thus is a defined measure of the amount of the open magnetic flux.

The amount of the open flux begins to increase soon after the southward turning of the IMF *B*_z reaching the front of the magnetosphere. The subsequent overall shifts of the polar cap boundary follow changes of ϵ fairly well except that the decrease continues gradually well after ϵ becomes less than $\sim 10^{18}$ erg sec.

The accompanying substorm activity expressed by the *AE* index begins often about ~ 30 min to 1 hr after the beginning of the open flux increase. This is possibly due to the fact that the *AE* stations cannot monitor geomagnetic changes that take place at latitudes higher than 70° ; thus we must be cautious about the limitation of the *AE* index in monitoring polar cap changes. The subsequent overall changes of the *AE* index and the amount of the open flux are similar. The peak periods of the *AE* and of the open flux occur at about the same time. The open flux decreases gradually well after the *AE* index is reduced to the noise level.

It is quite likely that the open flux (i.e., the size of the polar cap) is a qualitative measure of the total magnetic energy in the magnetotail. If this would indeed be the case, the above observation suggests that the total amount of magnetic energy in the magnetotail tends to vary similarly with the ϵ parameter and the *AE* index. In particular, there is no significant time shift for the period of maximum values of the polar cap dimension and the *AE* index. Therefore, substorms cannot be described as a manifestation of explosive conversion of the magnetotail magnetic energy that is accumulated prior to substorm onset. If this were the case, the polar cap dimension should decrease rapidly during the expansive phase. It may be added that AKASOFU (1972) and EATHER *et al.* (1979) found that the equatorward shift of the dayside cusp during the expansive phase is inconsistent with the hypothesis of explosive return of the magnetic flux from the magnetotail to the dayside magnetosphere. It is also interesting to note that the magnetic energy in the magnetotail can decrease gradually without significant magnetic effects in the auroral zone.

It is also interesting to speculate that the observed changes of the total open flux may be directly related to the so-called "thinning" and "thickening" of the plasma

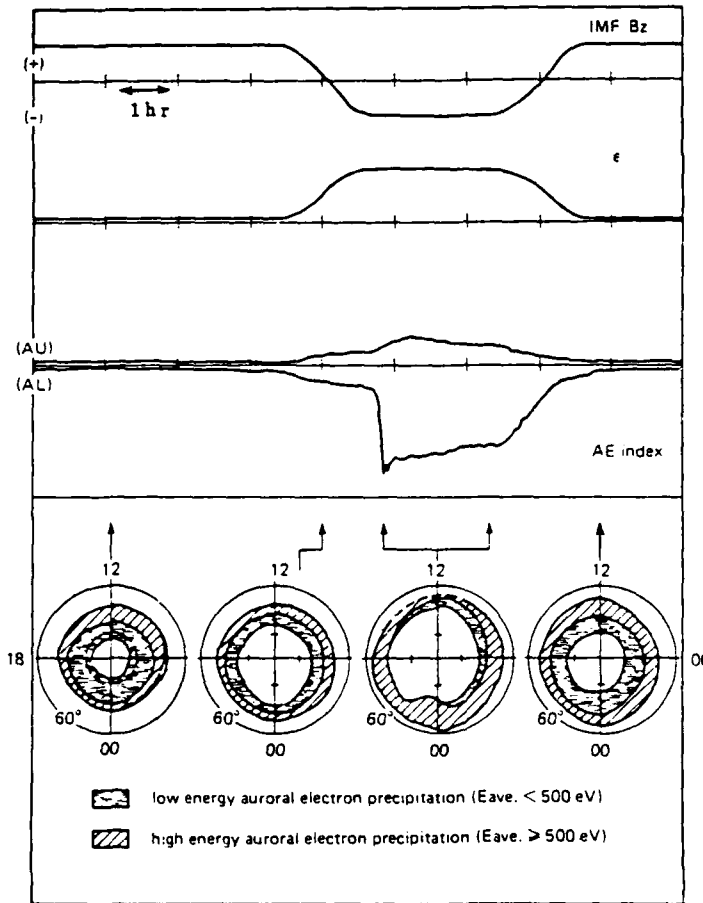


Fig. 13. Schematic presentation of the results. The contracted polar cap is seen during the northward IMF period. The size of the polar cap begins to increase soon after the southward turning of the IMF B_z at the front of the magnetosphere. The peak period of the AE and of the polar cap size is about the same. The polar cap begins to contract gradually as the ϵ parameter and AE index decrease.

sheet during a substorm. If the magnetotail cross section does not change significantly during a substorm, an increased open flux will squeeze out plasmas in the plasma sheet, resulting in thinning of the plasma sheet. As the open flux and the high-latitude lobe cross section begin to decrease during the recovery phase, the magnetosheath plasma finds its way into the plasma sheet region to fill the space created by the contracting high-latitude lobe.

This research is supported in part by the Air Force Office of Scientific Research under

Grant AFOSR 84-0049 and by the Division of Atmospheric Sciences, National Science Foundation, under Grant ATM-83-15041 to The Johns Hopkins University, Applied Physics Laboratory.

REFERENCES

- AKASOFU, S.-I., Midday auroras and magnetospheric substorms, *J. Geophys. Res.*, **77**, 244, 1972.
- AKASOFU, S.-I., A study of auroral displays photographed from the DMSP-2 satellite and from the Alaska meridian chain of stations, *Space Sci. Rev.*, **16**, 617, 1974.
- EATHER, R. H., S. B. MENDE, and E. J. WEBER, Dayside aurora and relevance to substorm current systems and dayside merging, *J. Geophys. Res.*, **84**, 3339, 1979.
- HARDY, D. A., W. J. BURKE, M. S. GUSSENHOVEN, N. HEINEMANN, and E. HOLEMAN, DMSP: F2 electron observations of equatorward auroral boundaries and their relationship to the solar wind velocity and the north-south component of the interplanetary magnetic field, *J. Geophys. Res.*, **86**, 9961, 1981.
- HOFFMAN, R. A. and J. L. BURCH, Electron precipitation patterns and substorm morphology, *J. Geophys. Res.*, **78**, 2867, 1973.
- HOLZWORTH, R. H. and C.-I. MENG, Mathematical representation of the auroral oval, *Geophys. Res. Lett.*, **2**, 377, 1975.
- LASSEN, K. and C. DANIELSEN, Quiet time pattern of auroral arcs for different directions of the interplanetary magnetic field in the Y-Z plane, *J. Geophys. Res.*, **83**, 5277, 1978.
- LIU, A. T. Y., S.-I. AKASOFU, E. W. HONES, Jr., S. J. BAME, and C. E. MCILWAIN, Observations of the plasma sheet during a contracted oval substorm in a prolonged quiet period, *J. Geophys. Res.*, **81**, 1415, 1976.
- MAKITA, K. and C.-I. MENG, Average electron precipitation patterns and visual auroral characteristics during geomagnetic quiescence, *J. Geophys. Res.*, **89**, 2861, 1984.
- MAKITA, K., C.-I. MENG, and S.-I. AKASOFU, The shift of the auroral electron precipitation boundaries in the dawn-dusk sector in association with geomagnetic activity and interplanetary magnetic field, *J. Geophys. Res.*, **88**, 7967, 1983.
- MAKITA, K., C.-I. MENG, and S.-I. AKASOFU, Temporal and spatial variations of the polar cap dimension and its relation to the energy input rate ϵ and AE index, *J. Geophys. Res.*, **90**, 2744, 1985.
- MENG, C.-I., The auroral electron precipitation during extremely quiet geomagnetic conditions, *J. Geophys. Res.*, **86**, 4607, 1981a.
- MENG, C.-I., Polar cap arcs and the plasma sheet, *Geophys. Res. Lett.*, **8**, 273, 1981b.
- MENG, C.-I., Dynamic variation of the auroral oval during intense magnetic storms, *J. Geophys. Res.*, **89**, 227, 1984.
- MENG, C.-I., R. H. HOLZWORTH, and S.-I. AKASOFU, Auroral circle-delineating the poleward boundary of the quiet auroral belt, *J. Geophys. Res.*, **82**, 164, 1977.
- MURPHREE, J. S., C. D. ANGER, and L. L. COGGER, The instantaneous relationship between polar cap and oval auroras at times of northward interplanetary magnetic field, *Can. J. Phys.*, **60**, 349, 1982.
- PIKE, C. P. (Ed.), Defense meteorological satellite program auroral-ionospheric interpretation guide, *Air Force Surv. Geophys.*, **306**, 1975.
- WINNINGHAM, J. D., F. YASUHARA, S.-I. AKASOFU, and W. J. HEIKKILA, The latitudinal morphology of 10-eV to 10-keV electron fluxes during magnetically quiet and disturbed times in the 2100-0300 MLT sector, *J. Geophys. Res.*, **80**, 3148, 1975.

Quantitative Modeling of the "Convection Surge" Mechanism of Ion Acceleration

B. H. MAUK

Applied Physics Laboratory, Johns Hopkins University, Laurel, Maryland

To explain the presence of the so-called "bounce-phase-bunched" ion distributions (eV range to ~ 20 keV) observed in the earth's geosynchronous magnetosphere, Quinn and Southwood (1982) examined the general properties of what they called the "convection surge" mechanism. This mechanism is associated with a sudden earthward displacement of curved field lines resulting from the short-lived application of an intense, east-west electric field. To explore its properties a quantitative computer model of the mechanism has been constructed that incorporates the dipolarization of the field line shapes, and recent transient electric field measurements. It is confirmed that the mechanism easily generates the bounce-phase-bunched ion distributions in question and that for some particles it can give rise to dramatic ion energization in the field parallel direction associated with the violation of the second adiabatic invariant. It is shown additionally that depending on initial conditions the mechanism can generate dramatically field aligned distributions. It is hypothesized that the convection surge mechanism is fundamentally associated with the processes responsible for transporting tail populations to the middle (geosynchronous) regions of the earth's magnetosphere, and it is proposed that a key general characteristic of geosynchronous ion pitch angle distributions, field-aligned low energies and field-perpendicular high energies, is a signature of this energization mechanism. The presence of field aligned ions cannot be presumed to be a signature of recent ionospheric extraction.

1. INTRODUCTION

Within the geosynchronous regions of the earth's magnetosphere, spatially bunched clusters of ions have been observed bouncing back-and-forth along field lines between the northern and southern hemispheres [Quinn and McIlwain, 1979]. On the nightside these so-called "bounce-phase-bunched" ion distributions are observed only at small pitch angles, involve ion energies from the eV range up to (occasionally) 20 keV, and are associated in time with the expansion phase of substorms. Because special experimental conditions must prevail in order for the bunched distributions to be observed, it is unknown whether ion bounce bunching occurs in one-to-one correlation with substorm expansions.

In order to explain the presence of bounce-phase-bunched distributions, Quinn and Southwood [1982] proposed, and discussed the general properties of, what they called the "convection surge" mechanism. The convection surge is associated with a sudden earthward displacement of curved field lines resulting from the short-lived application of an intense, east-to-west electric field. Because the surge happens quickly it can violate the second adiabatic invariant of the lower energy ions. Associated with this violation is the condition that the particles that gain the largest multiplication in their energies will be those that have very small pitch angles, and at the same time reside very close to the magnetic equator at the time of the surge. Quinn and Southwood argue that for the short period of time during the surge, the equatorial regions are a spatially confined source of relatively energetic, field-aligned ions, and that this short-lived source gives rise to the observed bounce-phase-bunched ion distributions. For one bounce-phase-bunched-ion event whose velocity dispersive properties were analyzed with particular care, it was found that the source of the ions was indeed the equatorial regions and not the ionospheric regions.

In order to confirm, illustrate, and quantify the claims made by Quinn and Southwood [1982] a numerical computer model of the convection surge process has been constructed here. Incorporated in this model are the results of recent measurements of transient electric fields, and also the dipolarization of the field line shapes. The computer model numerically integrates the equations of motion of ensembles of ions that populate a single flux tube that goes through the convection surge or "dipolarization" transformation. In addition to quantifying the points made by Quinn and Southwood, the model shows that the convection surge or dipolarization process can generate dramatically field aligned ion distributions within the near-geosynchronous regions of the earth's magnetosphere. It is argued here that this finding has important consequences with respect to the interpretation of ion distributions measured within these regions.

2. OBSERVATIONS

Figure 1 shows several examples of the "bounce-phase-bunched" ion distributions reported by Quinn and McIlwain [1979]. This figure shows greyscale, energy-time spectrograms of ion and electron data (~ 1 eV to ~ 80 keV) sampled by the ATS-6 geosynchronous satellite. The electron data is shown in the top panel of each figure and the ion data is shown on the bottom panel. Note that the energy scale of the ion display is inverted as compared to that of the electron display. The whiteness of the greyscale panels is proportional to the count rate of electrostatic, energy/charge particle analyzers (with normalized energy resolution $\Delta E/E = \text{constant}$). The count rate of such analyzers is proportional to differential energy flux (i.e., eV/cm² sr eV). Of crucial importance to the present study is the fact that the data shown were sampled by particle analyzers that were at the times shown viewing only particles traveling along the local field lines with very small pitch angles (10° to 15°).

The features of interest in Figure 1 are the repetitive dispersive streaks that appear in the ion displays. The figure shows two examples, one beginning near 0055 UT, and the other

Copyright 1986 by the American Geophysical Union.

Paper number 6A8464.
0148-0227/86/006A-8464\$05.00

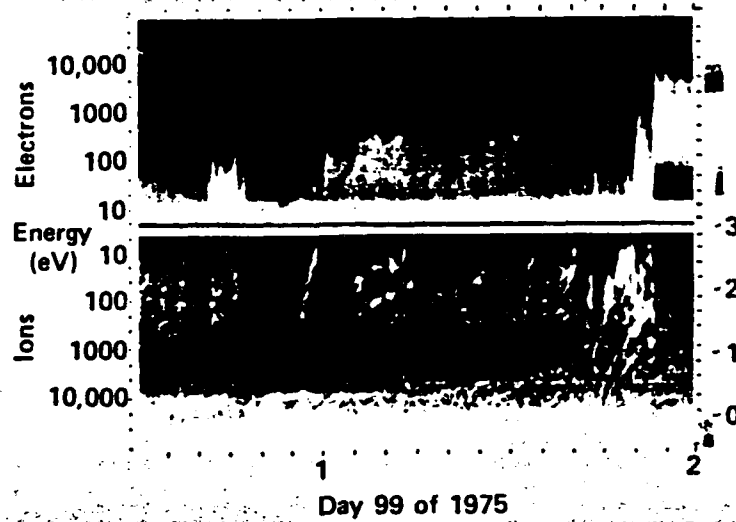


Fig. 1. From Quinn and McIlwain [1979]. Energy vs. time (top) electron and (bottom) ion spectrograms of particle data sampled by the geosynchronous ATS-6 satellite. The whiteness is proportional to energy flux ($\text{eV}/\text{cm}^2 \text{ s sr eV}$). The features of interest are the repetitive dispersive streaks within the ion display beginning near 0055 UT and again near 0143 UT. Only field-aligned pitch angle particles (10° to 20°) are shown here.

beginning near 0143 UT. Note that the streaks corresponding to the 0143 UT event extend in energy up to ~ 20 keV. As discussed by Quinn and McIlwain, the repetition period of the streaks corresponds to the bounce period (or some integer fraction thereof) of ions traveling along field lines and bouncing between hemispheres. The dispersiveness of the streaks corresponds to that fact that ions with different energies have different bounce periods. Quinn and McIlwain have reproduced the evolving dispersive characteristics of the events by hypothesizing that the source of the ions is temporally impulsive and spatially confined at specific positions along the field lines.

3. MODELING THE CONVECTION SURGE PROCESS

The top panel of Figure 2 shows the concept envisioned by Quinn and Southwood [1982] to explain the bounce-bunched distributions. The figure shows field lines before (the line labeled $k = 2$) and after ($k = 0$) the "convection surge" or "dipolarization" transformation. It is envisioned that this transformation happens quickly enough so as to violate the second adiabatic invariant of lower energy particles constrained to move within the flux tube represented on the figure.

The field lines shown on the top panel of Figure 2 were drawn using a simple analytic field line model first presented, for other purposes, by Quinn and McIlwain [1979]. It is assumed that the inclination angle I of a field line (where $\tan(I) = B_r/B_\theta$, and where B_r and B_θ are the spherical components of the magnetic field vector \mathbf{B}) varies functionally with the magnetic latitude λ as

$$\tan(I) = 2 \tan(\lambda) + k \sin(4\lambda) \quad (1)$$

The first right-hand side (RHS) term is the dipolar term, whereas the second RHS term (with parameter k) perturbs the field line away from the dipolar configuration. Assuming cylindrical symmetry about the magnetic dipole axis, Quinn and McIlwain showed that the equation for the field line is:

$$R/R_0 = \cos^2(\lambda) \exp\left[\frac{-k}{4}(1 - \cos 4\lambda)\right] \quad (2)$$

where R is the radial position of the field line at the magnetic latitude λ , and where R_0 is the equatorial (i.e. $\lambda = 0$) crossing radial position of the field line. Similarly, the variation of field strength B along the field line is given by:

$$B/B_0 = \frac{1}{\cos^3(\lambda)} [1 + (2 \tan(\lambda) + k \sin(4\lambda))^2]^{1/2} \cdot \exp\left[\frac{k}{2}(1 - \cos(4\lambda))\right] \quad (3)$$

where B_0 is the equatorial field strength (at $R = R_0$ and $\lambda = 0$). Equation (2) was used to generate the field line shapes shown on the top panel of Figure 2 (additional information, as will be seen, was needed to determine R_0). An initial value of $k = 2$ is reasonable given field inclination angle measurements that have been made in the $R = 6$ to $9 R_E$ region of the earth's magnetosphere [Fritz and Corrigan, 1977]. The final value of $k = 0$ corresponds to a purely dipolar shape. The transformation of k from 2 to 0 is intended to represent the dipolarization of the field line shapes during the initiation of the expansion phase of substorms [e.g., Nagai, 1982; Moore et al., 1981].

The field line model discussed above can only tell one the off-equatorial electric and magnetic parameters once the equatorial parameters (e.g., R_0 , B_0) are known. The time evolution of the equatorial parameters is determined by the properties of the imposed transient electric fields. Powerful transient electric fields pointing perpendicular to \vec{B} have been measured within the near-geosynchronous, near-equatorial regions by Shepard et al. [1980] and by Aggson et al. [1983]. Figure 3 shows an example of the electric field measurements taken from the Aggson et al. paper. The bottom portion shows the magnitude of the east-to-west component of the electric field measured at $R \sim 7.5 R_E$ and at a geographic latitude of $\sim 20^\circ$. There clearly occurred sharp, monopolar transients in the displayed component that reached a magnitude of ~ 30 mV/m and lasted for a combined time period of 1–2 min. The top portion of the figure shows the (approximately) radial component of the magnetic field vector. The transition that occurred in that

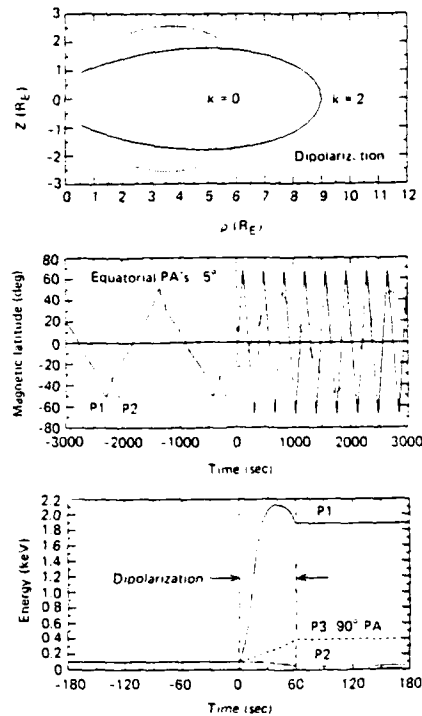


Fig. 2. (top) Field-line shapes before (labeled $k = 2$) and after ($k = 0$) the "convection surge" or "dipolarization" modeled in this study. The lines were drawn with the analytic field line model of *Quinn and McIlwain* [1979]. The condition $k = 0$ corresponds to a pure dipole. (middle) Numerically determined trajectories of two different particles constrained to the flux tube diagrammed in the top panel. The "dipolarization" transformation occurs between 0 and 60 s near the middle of this middle panel. The 2 particles (P1 and P2) both start out with energies of 100 eV and equatorial pitch angles of 5° . (bottom) On an expanded time scale, this panel shows the total energy of the two particles (P1, P2) shown in the middle panel, plus that of an equatorially mirroring particle (P3).

component corresponds to a dipolarization of the field line shapes. The correlation that appears to exist between the electric field transient and the time derivative of the magnetic field component suggests that the electric field is inductively generated by time variations in the local magnetic configuration. In the nightside regions, and relatively close to the magnetic equator, the electric field transients generally point east-to-west. However, *Aggson et al.* [1983] have emphasized the fact that well away from the magnetic equator the electric transients generally point in the west-to-east direction. This fact is consistent with the dipolarization of the field line shapes. Reexamining the top panel of Figure 2, an east-to-west electric field will indeed move the magnetic field line closer to the earth in the near equatorial regions. However, at magnetic latitudes above (for $\lambda > 0$) or below (for $\lambda < 0$) the position where the two drawn field lines cross each other, the evolution shown requires that the electric field transient point in the west-to-east direction.

For the present study the transient, equatorial electric field E_0 is represented as a step function in time, with a constant magnitude of 20 mV/m lasting for a time period T of 1 min (as viewed by the equatorial position of the evolving field line). The finer time scale fluctuations observed in Figure 3 will be ignored. This equatorial electric field vector points in the east-to-west direction, or out of the page on which the top panel of

Figure 2 is printed. Off-equatorial values of the electric field are generally not equal to 20 mV/m, but are calculated self-consistently with the field line motions (i.e., $v = cE/B$). As will be shown, the magnetic field line model described at the beginning of this section must be used to calculate the off-equatorial values. It is assumed that the free parameter k of the field line model varies linearly with time between 2 and 0 during the one minute time period T during which the electric field transient is applied.

The equatorial parameters R_0 and B_0 are determined in the following manner. The initial values of these parameters are set at $9 R_E$ and 40 nT, respectively. An additional initial equatorial parameter $\beta' [\equiv (\partial B/\partial r)/B - 1/r]$ is set equal to $-0.28/R_E$ (where r is an independent radial position parameter). Note that at $9 R_E$ the parameter β' has been set so that the spatial scale length for magnetic field strength variations is twice the dipole value, corresponding to tail-like distortions. The variation of B_0 with time, once the equatorial electric field E_0 is applied, is determined by the frozen-in condition and conservation of magnetic flux. The frozen-in condition is valid for the model because the time variations are slow compared to the cyclotron period of the particles and because there are no electric field components parallel to the magnetic field lines. Additionally, all motions parallel to the meridional planes are governed strictly by the cE/B drift.

During the dipolarization process, the conservation of flux condition for the equatorial field-line position is written

$$\frac{d(B_0 A)}{dt} = 0 \quad (4)$$

where A is the area of the equatorial cross section of the flux tube. Additionally, it is easy to show that for cylindrical symmetry about the magnetic dipole axis, the frozen-in condition gives rise to the equation:

$$\frac{1}{A} \frac{\partial A}{\partial t} = \frac{\partial V_{c0}}{\partial r} + \frac{V_{c0}}{r} \quad (5)$$

where V_{c0} is the equatorial convection speed of the plasma (i.e., of the field line position), and r is the independent equatorial radial position. Combining equations (4) and (5) with

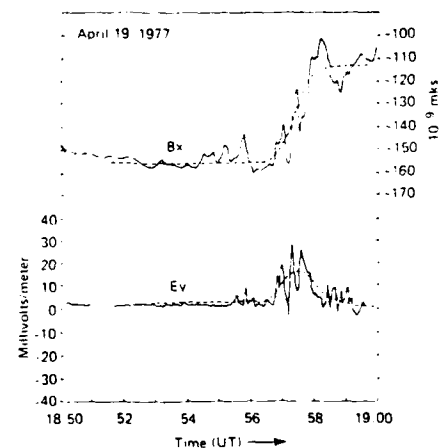


Fig. 3. From *Aggson et al.* [1983]. Measurement of dawn-to-dusk impulsive electric fields (at $\sim 7.5 R_E$) apparently generated by local variations in the magnetic configuration.

the equation for $V_{co} (= cE_o/B_o)$ one obtains the following non-homogeneous, partial differential equation for B_o :

$$\frac{\partial B_o}{\partial t} = \frac{cE_o}{B_o} \frac{\partial B_o}{\partial r} - \frac{cE_o}{r} \quad (6)$$

In deriving (6) it has been assumed that $\partial E_o/\partial r = 0$. The effects of including the term with $\partial E_o/\partial r$ can be simply approximated by modifying β' to obtain the equivalent divergence in the convection velocity. We have not carried the extra term here because obtaining an exact solution to (6) would become substantially more complex. We revisit the possible effects of a finite value of $\partial E_o/\partial r$ in the last section of this paper.

Equation (6) is solved by first rewriting it into an equation that relates the parameters (B_o/r , t , r^2). Then, by using separation of variables [$B_o/r = G(t) \cdot H(r^2)$], the equation may be solved simultaneously with $dr/dt = cE_o/B_o$ to obtain the relations:

$$\frac{B_o}{B_{oi}} = \frac{R_o}{R_{oi}} (1 + \beta'_i V_{coi} t)^2 \quad (7)$$

$$\left(\frac{R_o}{R_{oi}}\right)^2 = 1 + \frac{2V_{coi} t}{R_{oi}(1 + \beta'_i V_{coi} t)} \quad (8)$$

where β'_i is the initial value of β' [$\equiv (\partial B_o/\partial r)/B_o - 1/r$]; and B_{oi} , R_{oi} , and V_{coi} are the initial values of B_o , R_o , and V_{co} , respectively. Equation (8) was used to determine the $\sim 2.3 R_E$ net displacement of the equatorial position on the field line in the top panel of Figure 2.

So, with the equations (7) and (8) one has the solutions for the equatorial parameters $R_o(t)$ and $B_o(t)$. Combining these solutions with equations (2) and (3) results in knowledge of the radial position R of the field line of interest and the field strength B at that position for any magnetic latitude and for any time during the convection surge or dipolarization process.

There are additional parameters, as will be seen, that must be determined at all positions along the evolving field line so that the trajectories of particles constrained to follow this field line can be calculated. These parameters are V_c , $\partial B/\partial s$, R_c , and $(\partial \hat{b}/\partial t)$, which are, respectively, the perpendicular plasma (or field line) convection speed (or the equivalent off-equatorial electric field value), the gradient of the magnetic field strength B parallel to \mathbf{B} , the radius of curvature of the field line, and the time rate of change of the field line pointing direction at constant positions along the field line. The convection speed is calculated using equation (2), with equation (8), in the formula:

$$V_c = \left. \frac{\partial R}{\partial t} \right|_{\lambda} \cdot \cos(I) \quad (9)$$

where the $\cos(I)$ projects the radial motion calculation into the direction perpendicular to \mathbf{B} . One obtains:

$$V_c = \frac{R}{\zeta} \left(\frac{1}{R_o} \frac{dR_o}{dt} - \frac{1}{4} \frac{dk}{dt} [1 - \cos(4\lambda)] \right) \quad (10)$$

where

$$\zeta = (1 + (2 \tan(\lambda) + k \sin(4\lambda))^2)^{1/2}$$

where dR_o/dt is just V_{co} , and where, as should be clear from earlier discussions, dk/dt will just equal the constant value (0-2)/(60 s) during the dipolarization. The parallel field

strength gradient is straightforwardly determined using equation (3), with equation (7), and using the identity:

$$\frac{d}{ds} = \frac{1}{[R^2 + (\partial R/\partial \lambda)^2]^{1/2}} \frac{\partial}{\partial \lambda} \quad (11)$$

where the quantities in the square brackets are determined by using equation (2) with equation (8). The messy final results are not included here. The field line radii of curvature are determined by taking the reciprocal of the magnitude of the so-called curvature vector $\bar{\kappa}$, which is in turn calculated with the formula. (see for example, Lass [1950, p. 58]):

$$\kappa = \frac{d}{ds} \left(\frac{d}{ds} \mathbf{R} \right) \quad (12)$$

where

$$\mathbf{R} = \hat{i}R \sin(\lambda) + \hat{j}R \cos(\lambda)$$

and where equations (2) and (8) are used for the evaluation along with the identity (11) for the differential operator. Again, the very messy final results are not included here. Finally, $(\partial \hat{b}/\partial t)$, is determined from $(\partial(I + \lambda)/\partial t)$, where $(\partial I/\partial t)$, is related to $(\partial \lambda/\partial t)$, using equation (1), and where $(\partial \lambda/\partial t)$, is just $V_c \cdot \sin(I)/R$. The quantity $(I + \lambda)$ is used because it expresses the field line angular direction with respect to a Newtonian frame of reference.

With the calculation of R_o , B_o , R , B , V_c , $\partial B/\partial s$, R_c , and $(\partial \hat{b}/\partial t)$, one has all of the electromagnetic field quantities that one needs in order to calculate the trajectories of particles within the system.

4. PARTICLE TRAJECTORIES

The trajectories of particles confined to travel with the dipolarizing field line are calculated by numerically integrating the equations of motions. At each differential time step the perpendicular energization is calculated by conserving the first adiabatic invariant μ of each particle, i.e.,

$$\mu = \frac{\frac{1}{2} m v_{\perp}^2}{B} = \frac{\frac{1}{2} m v_{\perp i}^2}{B_i} \quad (13)$$

where B_i is the field strength at the particles starting position, and $v_{\perp i}$ is the particle's initial perpendicular velocity. The parallel motion is determined by solving the equation [see Chapman and Cowley, 1984; Northrop, 1963]:

$$\frac{m dv_{\parallel}}{dt} = -\mu \frac{\partial B}{\partial s} + m V_c \cdot \frac{d\hat{b}}{dt} \quad (14)$$

where V_c is the local perpendicular convection speed, $\partial B/\partial s$ is the gradient of the field strength parallel to \mathbf{B} (both discussed in the previous section) and \hat{b} is the unit vector in the direction of \mathbf{B} at the particles position. By decomposing $d\hat{b}/dt$ one obtains for the configuration shown in Figure 2:

$$\frac{dv_{\parallel}}{dt} = \frac{-\mu}{m} \frac{\partial B}{\partial s} - \frac{V_c v_{\parallel}}{R_c} + V_c \cdot \left(\frac{\partial \hat{b}}{\partial t} \right), \quad (15)$$

where R_c (the local field line radius of curvature) and $(\partial \hat{b}/\partial t)$, were both discussed in the previous section.

Equation (15) yields energization (or deenergization) in the direction parallel to \mathbf{B} . This parallel energization can be understood heuristically by performing a reference frame change. In the frame of reference where locally (and at a given instant) the electric field (and V_c) has zero magnitude, the particle's parallel velocity vector changes direction differentially as the

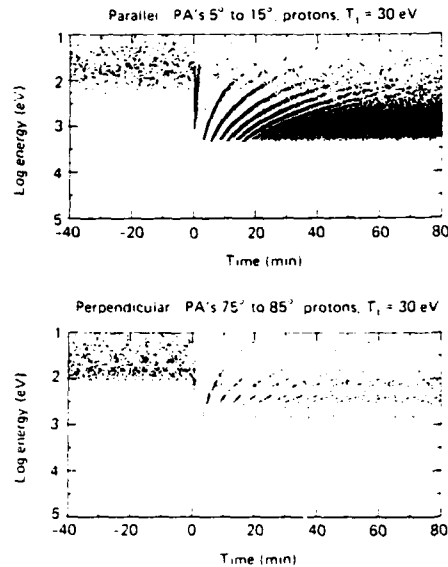


Fig. 4. Simulated energy-time ion spectrograms generated by following the trajectories for an ensemble of particles constrained to the flux tube diagrammed on the top panel of Figure 2. On average the initial ensemble is Maxwellian as a function of energy at each position along the initial field line and angularly isotropic, but with empty loss cones. Each point on the displays correspond to the time and energy of each particle every time it crosses the magnetic equator. The top panel was generated by selecting only "parallel" particles, with pitch angles between 5° and 15° . The bottom panel shows only "perpendicular" particles, with pitch angles between 75° and 85° . The density of points is approximately proportional to the particles' differential energy flux ($\text{eV cm}^{-2} \text{s sr eV}$), as is the whiteness of the data shown on Figures 1. The initial distribution used here consisted of protons with a Maxwellian temperature of 30 eV.

guiding center of particle moves differential distances along its curved trajectory (the total energy remains unchanged). One might think of this differential change of direction as being equivalent to a rubber ball taking a shallow, glancing bounce off of a stationary brick wall. Under idealized conditions the energy of the ball does not change; only its velocity vector direction changes. After the differential velocity direction change, or after the rubber ball has bounced, one then transforms back into the frame of reference where the electric field is finite, or equivalently the brick wall is moving rapidly along its normal vector direction. One finds that the transformed final energy of the particle has changed, and that the energy gain or loss appears in the field parallel direction. The form of equation (15), and the heuristic arguments given here, make it clear that the parallel energy change tends to be most rapid in the regions where the radii of curvature of the field lines are the smallest. It is for this reason that the equatorial regions are so key to the results that will be presented here. (Note, however, that the last term of (15) favors the regions away from the equator.)

Equation (15) is a second order differential equation and must be integrated twice to yield the trajectory information of interest. Because of the changing shape and length of the field line, it is difficult to conceptualize the absolute position along the field line, which would be the results of the twice integrated equation (15). It is thus convenient to use the particles magnetic latitude λ_p as the positional parameter. This parameter can be determined by replacing the second integration of equation (15) with the integration of the equation:

$$\frac{d\lambda_p}{dt} = \frac{1}{R} [v_{\parallel} \cos(I) + V_c \sin(I)] \quad (16)$$

where, the reader will recall, equation (1) is used to evaluate $\cos(I)$ and $\sin(I)$. Thus, all trajectory parameters of interest: perpendicular energy, parallel energy, magnetic latitude, particle pitch angle, etc., can be determined by numerically solving in parallel the equations (13), (15), and (16). A first-order Runge-Kutta procedure, with variable time steps, is used here to solve these equations. At each time step the field quantities given in the preceding section are updated.

The bottom two panels of Figure 2 show examples of such trajectory information for several particles with specific initial conditions. The middle panel shows the magnetic latitude versus time of two different particles, P1, and P2, with initial energies of 100 eV and initial equatorial pitch angles of 5° . The only difference between the two particles is the time phasings of their bounce motions along the field line. The convection surge or dipolarization occurs briefly between 0 and 60 s near the very center of the panel. During the rest of the time period shown the field lines are stationary and the electric fields have zero magnitudes. This middle panel shows dramatically that the response that the particles have to the dipolarization process depends critically on the phasings of the particles' bounce motions.

This effect is demonstrated even more graphically in the bottom panel of Figure 2, which shows the particles' total energy displayed on an expanded time scale. The particle labeled P1, that on the middle panel was very close to the magnetic equator during the dipolarization, has gained a factor of ~ 19 in energy. In contrast, the particle labeled P2, that was well away from the equator at the time of the dipolarization, has actually lost half of its energy (the phasings of P1 and P2 were chosen to be extremum cases for the given initial conditions). The bottom panel of Figure 2 also shows the change in energy of an equatorially mirroring particle, labeled P3. This particle has gained a factor of ~ 4 in energy. The special particle with a small equatorial pitch angle and located close to the equator during the dipolarization has gained much more energy than has the equatorially mirroring particle, which means that the second adiabatic invariant has been very substantially violated. Had the dipolarization occurred slowly, so as to preserve the second adiabatic invariants of the 5° particles, each of these particles would have gained in energy only a factor of ~ 1.7 , less than that gained by the equatorially mirroring particle.

The results shown in Figure 2 quantitatively confirm the claims made by Quinn and Southwood [1982]. What is unclear at this stage is the relative number of particles gaining substantial energy in the parallel direction. The conditions for the substantial energization may be quite restricted. These questions will be explored in the following section.

5. ION DISTRIBUTION RESPONSES TO THE DIPOLARIZATION

Figure 4 shows, in simulated spectrogram form, the response of an ensemble of particles to the dipolarization process. This figure was generated by loading the initial field line shown on Figure 2 with particles such that at each position along the field line the ion distribution is, on average, Maxwellian in energy distribution, angularly isotropic out of the loss cone, and empty within the loss cone. The distribution was generated by weighting the output of random number

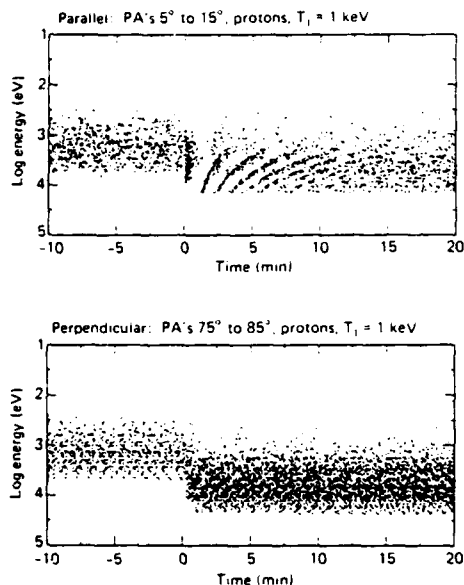


Fig. 5. Same as Figure 4 but for a proton distribution with an initial Maxwellian temperature of 1.0 keV rather than 30 eV.

generators. The trajectory of each of the resulting 10,000 particles was then followed before, during, and after the dipolarization process. Everytime a particle crossed the equatorial plane, its energy, pitch angle, and crossing time were recorded. Each point on Figure 4 corresponds to one recorded crossing. The figure shows particle energy versus time for two selected pitch angle windows. The top panel shows the "parallel" spectrogram, representing pitch angles between 5° and 15° ; while the bottom panel shows the "perpendicular" spectrogram, with pitch angles between 75° to 85° . The density of points on the display is at each position approximately proportional to the differential energy flux ($\text{eV}/\text{cm}^2 \text{ s sr eV}$) of the distribution, just as is the whiteness of the data displays shown in Figure 1. (The appearance of nonrandomness in the predipolarization, perpendicular spectrogram results from the fact that statistical fluctuations are propagated, given the procedures used, and from the shorter bounce periods for perpendicular particles as compared to parallel particles at the same energy.) For the simulation run shown in this figure, the initial distribution consisted of protons with a Maxwellian temperature of 30 eV.

The dipolarization process occurred on Figure 4 during the one minute period that began at time $t = 0$ on the horizontal axis. This proton distribution has clearly responded quite dramatically to that process. Also, the response in the parallel direction was, for the case shown, much more dramatic than was the response in the perpendicular direction, with much higher final energy fluxes recorded and a higher mean energy in the final distribution.

Of most immediate interest are the very striking and high contrast dispersive streaks that appear in the top panel. The repetition period of the streaks at any one energy corresponds to half the intrahemispherical bounce period of those particles. It is an obvious conclusion that these simulated streaks correspond to the dispersive streaks observed within the data on Figure 1. The model calculations clearly support the conclusion that the "bounce-phase-bunched" ion distributions are generated by the convection surge or dipolarization process, particularly since the electric field transient values used in the

model correspond to observed values. Dispersive streaks also appear in the perpendicular spectrogram. These streaks have lower contrast than those observed in the upper panel, and the overall flux levels are very substantially lower. These conditions may explain why the streaks have not been noticed on the nightside in the measured perpendicular spectrograms.

Figure 5 shows that the response that a particle ensemble has to the dipolarization depends critically on the temperature of the initial distribution. Here an initial proton temperature of 1 keV was used. Bounce dispersive streaks still appear in the parallel spectrogram, but with lower contrast than was observed with the lower temperature case. The dispersive streaks have disappeared in the perpendicular spectrogram, despite the fact that the net energization appears to have been

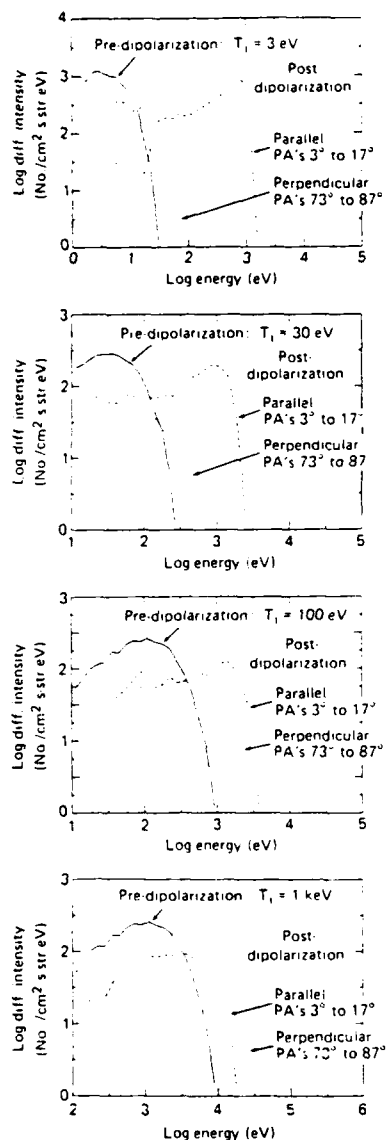


Fig. 6. Simulated predipolarization and postdipolarization ion differential intensities for four different initial proton temperatures ranging from 3 eV for the top panel and 1 keV for the bottom panel. On each panel the solid line corresponds to the initial, isotropic, predipolarization distribution while the short dashed and long-dashed lines correspond to the postdipolarization "perpendicular" and "parallel" distributions, respectively.

higher in the perpendicular as compared to the parallel spectrogram.

Figure 6 shows a more quantitative view of the net changes in the distributions that are caused in the model by the dipolarization process. Each panel shows differential intensity, on a logarithmic scale, plotted versus a logarithmic energy scale. On each panel the initial, predipolarization distribution is shown as a solid line and the final distribution is shown as a short-dashed line for "perpendicular" particles and a long-dashed line for "parallel" particles. All 4 panels correspond to proton distributions with predipolarization temperatures of 3 eV, 30 eV, 100 eV, and 1 keV for panels 6a-6d, respectively. For the lowest two proton temperatures used, dramatically field-aligned distributions have been generated by the dipolarization process. For the highest initial temperature, 1 keV, the perpendicular fluxes are highest; and it is again of interest (as shown on Figure 5) that field-aligned dispersive streaks are generated even when the perpendicular fluxes dominate. At an initial temperature of 100 eV the final distribution is still substantially field-aligned at the higher energies. The transition between field-aligned and strictly field perpendicular final proton distributions occurs for initial temperatures of several hundred (~ 300) eV.

Quantitatively the results change very substantially when heavy ions are used. Figure 7 shows the results of a simulation using an initial oxygen distribution with a temperature of 1 keV. Here, despite the high initial temperature, a dramatically field aligned final distribution is generated. At the same temperature the average velocity of an oxygen ion is slower than the average proton. Hence, the equatorial occupation times (the amount of time the ions spend in the high field line curvature regions) is longer for the heavier ions, and those ions receive greater parallel energization.

There are several more subtle conclusions that can be drawn from Figures 6 and 7. Note that for the three lowest temperature cases on Figure 6, the peak of the final field aligned distribution occurs at about 1 keV, independent of initial temperature. For the initial temperatures that give rise to field-aligned distributions, the final mean energy appears to be more a property of the electromagnetic accelerating fields and less a property of the initial particle parameters. From Figure 7 one can surmise that the final field-aligned oxygen distributions will quite generally peak between 10 and 20 keV for the electromagnetic fields used. The final mean energy in the parallel direction appears to be linearly related to the particle mass, at least at intermediate energies. This condition clearly breaks down at high energies, as the second adiabatic invariant starts becoming valid.

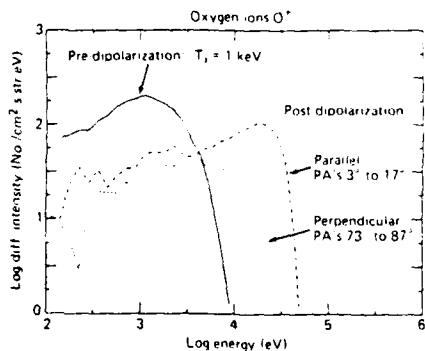


Fig. 7. Same as Figure 6, but for oxygen ions with an initial, predipolarization temperature of 1 keV.

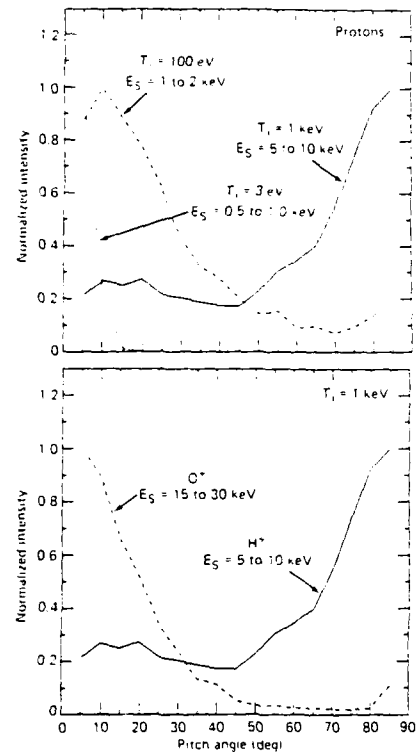


Fig. 8. Pitch angle distributions for selected energy bandpasses generated by the simulation runs of Figures 4-7. For each case T_i is the initial Maxwellian temperature and E_s is the range of energies sampled for the pitch angle plot. In each case the E_s range is centered on the peak of the postdipolarization differential energy flux spectrums. The top panel shows, for one mass species, the changes that result from changing the initial temperature. The bottom panel shows, for one initial temperature, the effect of having different mass species.

One final observation about Figure 6 is that despite the generation of "beaming" in the sense of having directionally anisotropic fluxes, the dipolarization mechanism did not generate a beam in the sense of having $\partial f / \partial v > 0$, where f is the time average velocity distribution and v is speed. (The distribution f can be calculated by dividing each point of the differential intensity with the corresponding energy.) The last term of equation (15) makes it technically possible for the condition $\partial f / \partial v > 0$ to be generated, but that condition has not been generated for any initial conditions used in this study. (The beaming condition does exist, however, during the periods before the bounce-bunching phase-mixes away.)

As a final format for displaying the results of the dipolarization model, Figure 8 shows, for selected energy bandpasses, the pitch angle distributions expected for the simulation runs discussed in this section. The top panel shows results from three of the proton simulations. On this panel the T_i correspond to the initial temperatures, and the E_s ranges correspond to the ranges of energies in the final distributions that were sampled. In each case the E_s ranges are centered on the peaks of the final differential energy flux profiles. One can see that the lowest initial temperature has given rise to a very narrowly collimated field aligned distribution. At the highest initial temperature the perpendicular fluxes dominate over the parallel fluxes, but yet there is the hint of a field-aligned feature between 10° and $\sim 45^\circ$. This feature eventually disappears as still temperatures are used.

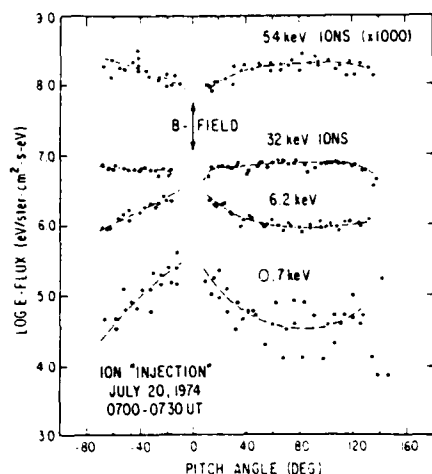


Fig. 9. From Mauk and McIlwain [1975]. Pitch angle distributions actually measured in the geosynchronous orbit by the ATS-6 geosynchronous satellite. The data were sampled near 0100 LT and within an hour of a local substorm injection. The field-aligned character of the lower energy ions is of particular interest.

The bottom panel of Figure 8 shows the pitch angle distribution comparison between 1 keV temperature protons and oxygen ions. The dipolarization mechanism not only can separate our different mass species in energy, but in pitch angle as well. For instance if the initial conditions are such that there exists a mixed plasma cloud of H^+ and O^+ ions, the dipolarization process could well cause a preponderance of oxygen ions to precipitate into the ionosphere with numbers out of proportion to the initial density ratios.

6. DISCUSSION AND CONCLUSIONS

The properties of a mechanism that can easily generate field-aligned ion distributions have been explored here. A very common feature of ion populations observed within the geosynchronous regions is the field aligned character of the lower energies. An example is shown in Figure 9, which displays data taken by the ATS-6 geosynchronous satellite. The figure shows the pitch angle distributions of four selected energy (E/q) channels. Clearly the lower energy channels, at 0.7 and 6.2 keV/ q , show field-aligned distributions, while the higher energy channels, at 32 and 54 keV/ q , show nearly isotropic and field perpendicular distributions, respectively. The field aligned character of the lower energies extends in energy up to ~ 10 keV for the time period sampled. The data shown was sampled just following (within 30–60 min) a local particle injection associated with a substorm expansion phase. Even in the absence of recent substorms, substantially field aligned ions for energies up to several keV are observed in the geosynchronous regions, as has been shown by Fennel *et al.* [1981] and Kaye *et al.* [1981].

In previous studies the field aligned character of the lower energy ions within the geosynchronous regions has been taken as a signature of recent ionospheric extraction [Mauk and McIlwain, 1975; Lennartsson and Reasoner, 1978; Young, 1979; Horwitz, 1980; Fennel *et al.*, 1981; Kaye *et al.*, 1981]. It is clear from the present study that this conclusion was premature. The observed characteristics are just what would be expected based on the convection surge or dipolarization mechanism. Certainly, upflowing ionospheric ions have been observed at low altitudes within the auroral regions [Shelley *et*

al., 1976]. The question that remains is where and in what form do those ions end up? It has, for instance, been argued [Lyons and Evans, 1984, and references therein] that the regions of the discrete aurora (where one might expect the ionospheric extraction of the sort observed by Shelley *et al.* to occur) corresponds (by means of magnetic mapping) to the outer edges of the plasma sheet population. In contrast, the geosynchronous injected plasmas are commonly associated (if in an energized form) with the inner edge of the plasma sheet population [McIlwain, 1974; Kivelson *et al.*, 1980] and with the diffuse auroral regions [Meng *et al.*, 1979]. Hence, it is likely that in order to associate the geosynchronous, keV-range field-aligned ions with recent ionospheric extraction one must concern oneself with the subsequent transport of those ions from the outer to the inner edges of the plasmasheet population. It has been argued [Cladis and Francis, 1985] that that transport is of an extremely turbulent nature, to the extent that pitch angle structure could be eliminated.

Certainly one cannot exclude the possibility that the signature of ionospheric extraction persists within the intermediate energy geosynchronous particle populations. What one can say is that the success of the modeling discussed in this paper (using observed parameters) in terms of reproducing the commonly observed "bounce-phase-bunched" ion distributions, and the corresponding ease by which the model generates field-aligned ion distributions, means that the convection surge mechanism must play an important role in forming the observed pitch angle distributions. This statement is supported additionally by the evidence [Mauk and Meng, 1983, 1986] that all transport to the geosynchronous regions occurs in association with impulsive, spatially localized processes, presumably driven by the inductive electric fields discussed in this report. It is here hypothesized that the convection surge or dipolarization mechanism is a fundamental component of the processes that transport particles to the middle magnetospheric regions.

As a final point of discussion it should be noted that the model that has been explored here is very restricted [see Cladis, 1968]. For instance, very special assumptions have been made concerning the properties of the electric field transients. The finer time scale fluctuations have been ignored, and also the condition $\partial E_0/\partial r = 0$ as viewed by the evolving equatorial position of the field line has been used. A relaxation of this latter assumption could enhance (or reduce) the perpendicular acceleration (as noted earlier, the consequences of a finite $\partial E_0/\partial r$ can be approximated by altering β_i). Clearly a great deal of parametric exploration remains to be done before the properties of the mechanism are fully understood. Additionally, the self consistency between the stresses of the fields and particles must eventually be incorporated into any complete model. Finally, in the absence of very cool background electron populations, the mechanism will try to separate positive and negative charges along the field line. The consequences of this effect have not been incorporated into the model. In terms of comparing the results of the model to the observed distribution characteristics, clearly the shape of the source distribution will be a key input (multiple energy components are clearly evident in the data) as will be the shape of the electric field transients as viewed by the field line (rather than the shape viewed by a stationary satellite). And it must be recognized that adiabatic convection will cause a strong evolution in distributions generated by nonadiabatic processes. Unfortunately it is likely to be very difficult to ob-

servationally assess the relative contributions of ionospheric extraction and dipolarization to forming the character of middle magnetospheric ion pitch angle distributions.

Acknowledgments. We thank C.-I. Meng, D. G. Mitchell, and J. M. Quinn for helpful discussions. This work was supported by the Atmospheric Sciences Division, National Science Foundation grant ATM-8315041, and by the Air Force Office of Scientific Research grant 84-0049, and by NASA contract to Johns Hopkins University Applied Physics Laboratory and Department of the Navy under task I2UOS1P of contract N00024-85-C-5301.

The Editor thanks J. B. Cladis and B. A. Whalen for their assistance in evaluating this paper.

REFERENCES

- Aggson, T. L., J. P. Heppner, and N. C. Maynard, Observations of large magnetospheric electric fields during the onset phase of a substorm, *J. Geophys. Res.*, **88**, 3981, 1983.
- Chapman, S. C., and S. W. H. Cowley, Acceleration of lithium test ions in the quiet time geomagnetic tail, *J. Geophys. Res.*, **89**, 7357, 1984.
- Cladis, J. B., Dynamical motion of geomagnetic flux tube resulting from injection of high energy particles, in *Earth's Particles and Fields*, edited by B. M. McCormac, Reinhold, New York, 1968.
- Cladis, J. B., and W. E. Francis, The polar ionosphere as a source of the storm time ring current, *J. Geophys. Res.*, **90**, 3457, 1985.
- Fennell, J. F., D. R. Croley, Jr., and S. M. Kaye, Low-energy ion pitch angle distributions in outer magnetosphere, ion zipper distributions, *J. Geophys. Res.*, **86**, 3375, 1981.
- Fritz, T. A., and J. P. Corrigan, Significant initial results from the environment measurements experiment on ATS-6, *NASA Tech. Pap.*, 1101, 34 pp., 1977.
- Horwitz, J. L., Conical distributions of low-energy ion fluxes at synchronous orbit, *J. Geophys. Res.*, **85**, 2057, 1980.
- Kaye, S. M., E. G. Shelley, R. D. Sharp, and R. G. Johnson, Ion composition of zipper events, *J. Geophys. Res.*, **86**, 3383, 1981.
- Kivelson, M. G., S. M. Kaye, and D. J. Southwood, The physics of plasma injection events, in *Dynamics of the Magnetosphere*, edited by S. I. Akasofu, pp. 385-405, D. Reidel, Hingham, Mass., 1980.
- Lass, H., *Vector and Tensor Analysis*, McGraw-Hill, New York, 1950.
- Lennartsson, W., and D. L. Reasoner, Low-energy plasma observations at geosynchronous orbit, *J. Geophys. Res.*, **83**, 2145, 1978.
- Lyons, L. R., and D. S. Evans, An association between discrete aurora and energetic particle boundaries, *J. Geophys. Res.*, **89**, 2395, 1984.
- Mauk, B. H., and C. E. McIlwain, UCSD auroral particles experiment, *IEEE Trans. Aerosp. Electron. Syst.*, **AES-11**, 1125, 1975.
- Mauk, B. H., and C.-I. Meng, Dynamical injections as the source of near geostationary quiet time particle spatial boundaries, *J. Geophys. Res.*, **88**, 10,011, 1983.
- Mauk, B. H., and C.-I. Meng, Macroscopic ion acceleration associated with the formation of the ring current in the earth's magnetosphere, in *Geophysical Monograph on Ion Acceleration, Geomogr. Ser.*, vol. 38, edited by T. Chang, pp. 351-361, AGU, Washington, D. C., 1986.
- McIlwain, C. E., Substorm injection boundaries, in *Magnetospheric Physics*, edited by B. M. McCormac, p. 143, D. Reidel, Hingham, Mass., 1974.
- Meng, C.-I., B. H. Mauk, and C. E. McIlwain, Electron precipitation of evening diffuse aurora and its conjugate electron fluxes near the magnetic equator, *J. Geophys. Res.*, **84**, 2545, 1979.
- Moore, T. E., R. L. Arnoldy, I. Feynman, and D. A. Hardy, Propagating substorm injection fronts, *J. Geophys. Res.*, **86**, 6713, 1981.
- Nagai, T., Observed magnetic substorm signatures at synchronous altitude, *J. Geophys. Res.*, **87**, 4405, 1982.
- Northrop, T. G., *The Adiabatic Motion of Charged Particles*, Interscience, New York, 1963.
- Quinn, J. M., and C. E. McIlwain, Bouncing ion clusters in the earth's magnetosphere, *J. Geophys. Res.*, **84**, 7365, 1979.
- Quinn, J. M., and D. J. Southwood, Observations of parallel ion energization in the equatorial region, *J. Geophys. Res.*, **87**, 10,536, 1982.
- Shelley, E. G., R. D. Sharp, and R. G. Johnson, Satellite observations of an ionospheric acceleration mechanism, *Geophys. Res. Lett.*, **3**, 654, 1976.
- Shepard, G. G., R. Bostrom, H. Derblom, C.-G. Falthammar, R. Gendrin, K. Kaila, A. Korth, A. Pedersen, R. Pellinen, and G. Wrenn, Plasma and field signatures of poleward propagating auroral precipitation observed at the foot of the GEOS-7 field line, *J. Geophys. Res.*, **85**, 4587, 1980.
- Young, D. T., Ion composition measurements in magnetospheric modeling, in *Quantitative Modeling of Magnetospheric Processes, Geophys. Monogr. Ser.*, vol. 21, edited by W. P. Olson, p. 340, AGU, Washington, D. C., 1979.

B. H. Mauk, Applied Physics Laboratory, Johns Hopkins University, Laurel, MD 20707.

(Received March 13, 1986;
revised July 18, 1986;
accepted August 11, 1986.)

Relations Between the Interplanetary Magnetic Field B_z , AE Index, and Cusp Latitude

J. F. CARBARY AND C.-I. MENG

The Johns Hopkins University Applied Physics Laboratory, Laurel, Maryland

The connection between the interplanetary magnetic field (IMF) B_z , AE index, and magnetospheric cusp location is examined qualitatively. Seven months during 1979-1980 were searched for periods of low auroral activity and/or periods when the IMF B_z component and the AE index varied inconsistently (i.e., southward B_z and quiescent AE). During quiet auroral conditions, the IMF B_z , AE index, and equatorward cusp boundary generally tend to act coherently, although during very quiet times the cusp may exhibit considerable variability that is apparently unassociated with either B_z or AE . We found a number of instances in which the cusp location clearly followed B_z more closely than AE , especially when a time delay of ≤ 1 hour was assumed. However, we cannot conclude that either B_z or AE exerts a dominant influence on the latitudinal position of the polar cusp. The effects of B_z and AE variations on the cusp are quite complicated and the observations simply do not indicate clear cusp response to one or the other. The largest equatorward cusp motions seem to occur as a result of prolonged southward B_z lasting 3 hours or more, and cusp latitude appears to depend strongly on time-accumulated B_z .

INTRODUCTION

The ultimate source of energy for magnetospheric processes is the solar wind, and numerous studies have revealed connections between interplanetary parameters and auroral phenomena. Early work suggested that the interplanetary magnetic field (IMF) should control auroral activity [e.g., Dungey, 1961]. Subsequent research has strongly confirmed the close association of IMF orientation with auroral substorm activity [Fairfield and Cahill, 1966]. Indeed, correlating interplanetary and auroral parameters has always proved a fashionable enterprise [e.g., Pike et al., 1974; Burton et al., 1975; Kamide et al., 1976; Rostoker, 1980; Reiff et al., 1981; Zanetti et al., 1982; Bythrow and Potemra, 1983].

Considerable research has been done in searching for conclusive evidence of IMF control by relating the latitudinal position of the magnetospheric cusp with the interplanetary magnetic field. (See reviews by Burch [1979] and Shepherd, [1979].) Russell et al. [1971] first reported evidence of cusp motion in response to changes in the IMF B_z . Later workers demonstrated a substantial connection between southward (northward) turnings of B_z and equatorward (poleward) movement of the auroral zone [Akasofu et al. 1973; Pike et al., 1974; Horwitz and Akasofu, 1977; Makita et al., 1983]. Recent studies utilizing ground-based photometers [Sandholt et al., 1983, 1985] and low-orbiting solar satellites [Meng, 1982, 1983] also indicate that the position of the polar cusp depends closely on the orientation of the IMF.

However, substorm activity may also influence cusp location. Kamide et al. [1976] demonstrated that the latitude of the cusp depends not only on the orientation of B_z but also on substorm activity as reflected in the AE index. Prevailing opinion accepts the contention that both IMF orientation and substorm activity control the location of the magnetospheric cusp [Sandholt et al., 1985]. However, an extreme view holds that substorm activity alone controls the location of the polar cusp [Eather et al., 1979; Eather, 1985]. Eather [1985] reexamined previously published data and concluded that cusp location was,

in fact, better correlated with the AE index than with the interplanetary B_z ; any significant IMF influence on cusp location was repudiated.

The implication of exclusive substorm control is important. If the standard model of dayside merging is accepted, then the IMF orientation would naturally control the position of the polar cusps as a result of the change of magnetospheric configuration. On the other hand, if magnetosphere/ionosphere currents exert the dominant influence on the cusp, then substorm activity would logically control the cusp location. We wish to emphasize the important distinction between the effects of merging (represented by measurements of B_z) and the effects of magnetospheric currents (represented by measurements of AE). The former is external—the latter is internal. We need assume no specific model of merging or flux transfer to make this distinction.

The researcher will, of course, encounter much difficulty in separating IMF effects from substorm effects, since the IMF is closely associated with substorm indicators such as the AE index. In this paper, we attempt to separate substorm and IMF effects by two methods. First, we examine periods of predominantly quiescent auroral conditions (i.e., $AE \leq 120 \gamma$). Any cusp movements occurring during such periods of low substorm activity would presumably be the result of IMF fluctuations. Second, we seek conditions of contradictory IMF and AE variations. We specifically wish to find conditions of southward IMF B_z in conjunction with quiet AE , and vice versa. Such periods of contradictory IMF/ AE conditions should give a clear indication of the principal influence on cusp location.

DATA SETS

Three data sets are utilized in this study. The first data set is the AE index provided by the World Data Center (Kyoto). The AE indices represent data taken from the 12 standard stations located in the northern hemisphere. The time resolution of the indices is one minute, although this study uses 15- or 5-minute averages. Fifteen-minute averages are used for examining long time periods (≤ 1 day) and gaining an overall perspective. Five-minute averages are used to display the same data at the higher time resolution needed for detailed study. Coverage of the AE index is continuous over the 7-month period of this study.

Copyright 1986 by the American Geophysical Union.

Paper number 5A8817.
0148-0227/86/005A-8817\$05.00

TABLE 1. Cusp Signatures Database

Date	Kp (Sum)	AE (Daily Average)
Aug. 14, 1979	15 -	108
Aug. 15	9 +	104
Aug. 16	11 -	108
Aug. 17	14	127
Oct. 3	20 +	193
Oct. 4	13 +	121
Oct. 5	11	135
Oct. 6	33	305(D)
Oct. 7	34	308(D)
Oct. 8	36	463(D)
Oct. 16	15	124
Oct. 17	9	43
Oct. 18	5 +	52
Oct. 19	10	52
Oct. 20	13 +	120
Nov. 23	8	55
Nov. 24	30	126
Nov. 25	19 +	438(D)
Nov. 26	8	163
Nov. 27	9 -	59
Nov. 28	3	83
Jan. 14, 1980	17 +	132
Jan. 15	12 -	89

D is disturbed.

The second data set is from the Goddard Space Flight Center (GSFC) magnetometer on the IMP 8 spacecraft. Magnetometer data are provided at 15.36-second time resolution. As with the AE data, the magnetometer data are averaged over 5 or 15 minutes, depending on whether a detailed or coarse examination is desired. Because of the orbital motion of IMP 8, coverage of the IMF B_z component is incomplete. Magnetometer data are used only for periods during which $X_{SM} > 0$. This restriction ensures the selection of interplanetary fields rather than magnetotail fields. To a lesser extent, some gaps in the coverage further reduced the magnetometer data set, especially in 1980.

The third data set derives from the 50-eV to 20-keV electron measurements from the Defense Meteorological Satellite Program (DMSP) F2 and F4 satellites. The DMSP electron data have an ultimate time resolution of 1 second, although, at best, cusp observations themselves were attainable only twice per satellite orbit of 101 minutes. Cusp data are generally "snapshots" about an hour apart. By combining observations from two DMSP spacecraft, we can occasionally achieve a time resolution of 30 minutes or better.

This study is based on the data obtained in a 7-month period from August 1979 through February 1980. During this period, the DMSP F2 and F4 satellites orbited in the noon-midnight sectors. We determined cusp locations for 23 full days. The cusp data were merged with AE (12) data and IMP 8 magnetometer data. We chose to correlate the DMSP, AE (12), and IMP 8 data sets on account of their availability and their continuity of coverage. Table 1 lists the 23 days and indicates the daily Kp sum and a 24-hour average of the AE index. The 24-hour AE average was computed from hour averages found in the works by *Kamei and Maeda* [1982] and *Kamei et al.* [1983].

As mentioned in the introduction, the two primary criteria for the selection of data were (1) quiet geomagnetic conditions as reflected in the AE index ($AE \leq 120 \gamma$) and/or (2) disparate conditions of the IMF and AE index in which B_z was southward (northward) and AE was inactive (active).

Quiet auroral conditions were generally plentiful during the 7-month period of this study so that criterion 1 could be readily satisfied. However, satisfaction of criterion 2 proved much more difficult and, in fact, greatly reduced the size of the usable data set.

A diligent search was made to find events in which the IMF B_z direction disagreed with the AE activity. A time lag of up to 1 hour was allowed between a change in the B_z direction and the corresponding effect in the AE profile. In no case was there a prolonged period (≥ 1 hour) of southward B_z without significant AE activity ($\geq 100 \gamma$), nor was there a prolonged northward B_z without a quiescent AE profile ($\leq 100 \gamma$ and fairly steady).

Nevertheless, we found a number of brief but significant events in which the variations of IMF B_z and the AE index seem unrelated. These cases are usually characterized by brief southward excursions of B_z that produce no effect on a quiet AE profile. This lack of response by the AE index could possibly be explained as the result of inadequate coverage by the ground stations that contribute to the measurement of the AE index [e.g., *Baumjohann*, 1985]. In any case, many of the events cited in the following sections are atypical in the sense that the AE index is not responding to changes in the IMF B_z direction.

CUSP BOUNDARY DETERMINATION

The determination of cusp boundaries follows the studies of *Meng* [1982, 1983]. Routine DMSP processing generates time profiles of auroral electron fluxes (J), energy fluxes (J_E), and average energies (E_{AV}). The cusp may be identified by intense fluxes of low-energy electrons. These characteristics may be recognized in the DMSP time profiles by enhanced electron fluxes and lowered average energies. A good cusp signature involves the elevation of J to values exceeding $\sim 10^8 \text{ el cm}^{-2} \text{ s}^{-1} \text{ sr}^{-1}$ and the lowering of E_{AV} to below $\sim 200 \text{ eV}$. Optimally, such changes occur at both the poleward and equatorward boundaries on time scales of a few seconds. In addition, the cusp signature will occur within a few hours of noon MLT in longitude.

Regrettably, cusp signatures are usually not optimal during quiet times. Discrete auroral arcs may tend to obscure cusp boundaries and the width of auroral oval/cusp increase, or the elevation of J may be too slow to permit concise definition of the cusp. Determination of the poleward cusp boundary is especially hazardous [cf., *Meng*, 1983]. A somewhat subjective assessment of the cusp location is inevitable and the researcher can only attempt to be consistent.

In an effort to mitigate this situation, we have classified DMSP cusp signatures into three categories depending on quality (or confidence) of cusp identification. A cusp signature was rated "good" if both poleward and equatorward boundaries were clearly determinable. A rating of "fair" was assigned to a cusp signature for which only one boundary was clearly discernible. Almost always, a fair signature indicates a clearly defined equatorward boundary. A "poor" rating was given to a cusp signature in which neither boundary was clearly well determined. In such cases, the experimentalist exercised consistent but subjective judgment in marking the cusp. In addition to this classification scheme, the identified cusp signatures were generally restricted to the MLT range from 0800 to 1400. Only rarely was a cusp signature observed outside this longitudinal range.

Examples of the three categories of signatures are shown in Figure 1. Figure 1a shows a classic cusp signature in which the

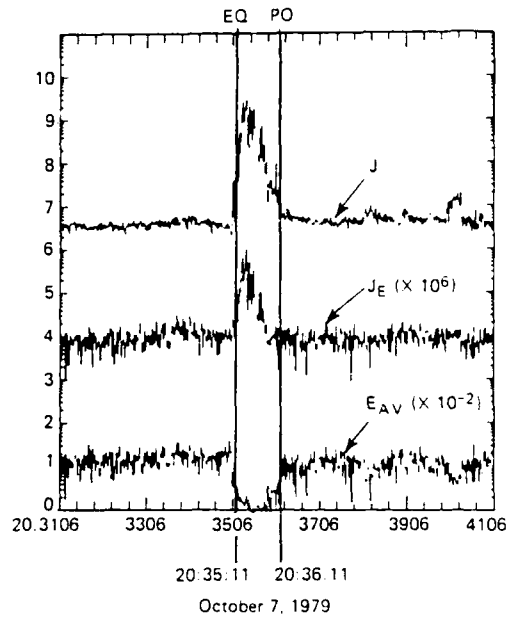


Fig. 1a. Example of a "good" cusp signature. The flux J is enhanced and the average energy E_{AV} is decreased at two well-defined boundaries. "EQ" indicates the equatorward boundary and "PO" indicates the poleward boundary.

total flux J is enhanced and the average energy is depressed. Both the poleward and equatorward boundaries are clearly delineated. Figure 1b shows a less well defined cusp signature in which the researcher has several choices for the poleward boundary. Finally, Figure 1c demonstrates a poor cusp signature in which neither boundary is clearly determined. In such cases of ambiguous boundaries, the time of greatest change in J was taken as the boundary mark.

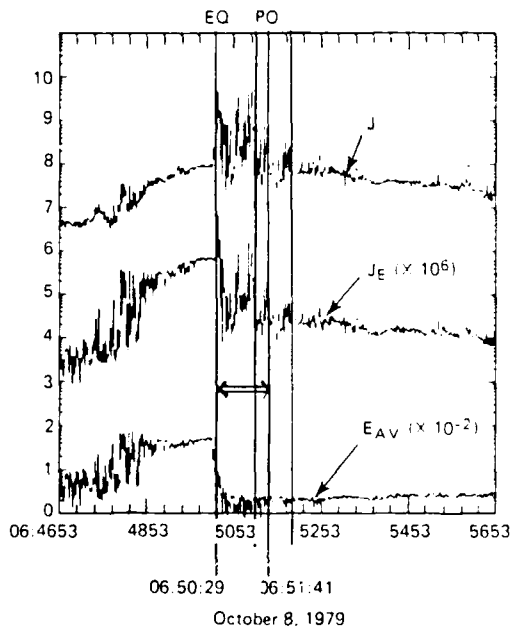


Fig. 1b. Example of a "fair" cusp signature. The equatorward boundary at 0650:20 is clearly defined, but the poleward boundary is difficult to determine. The heavy arrow denotes the boundaries actually accepted.

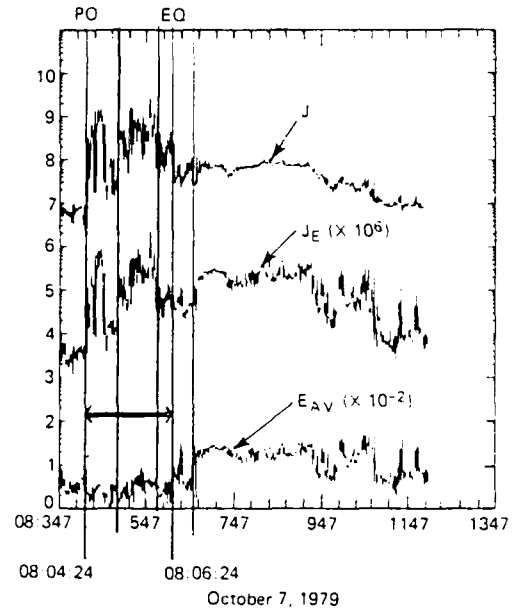


Fig. 1c. Example of a "poor" cusp signature. The researcher has a choice of possible signatures. Neither the poleward nor the equatorward boundary is well determined.

The time boundaries of the cusp are converted to boundaries in MLT and magnetic latitude by examining count rate and trajectory data at the full 1 second time resolution. The magnetic latitude is then normalized to the noon meridian by assuming a circular auroral zone centered at 4° away from the geomagnetic pole toward local midnight [Holtzworth and Meng, 1975]. This normalization is discussed succinctly by Meng [1984]. The normalization is required for compensating the local time variation of the auroral oval configuration of which the cusp may be considered a segment.

EXAMINATION OF DATA

Format

The IMF, cusp, and AE data are displayed in a three-panel format exemplified by Figure 2. The top panel shows the solar-magnetospheric B_z component of the IMF as measured by the IMP 8 magnetometer. The B_z profile here represents 15-minute averages of samples at 15.36-second resolution. The magnetometer data have not been adjusted to take into account any time delay between the point of IMF measurement and the magnetospheric interaction region or the auroral oval reaction time. The middle panel displays the latitudinal extent of the cusp as determined from DMSP electron data. Solid lines indicate observations from northern hemisphere passes while dotted lines indicate observations from southern hemisphere passes. Symmetry between northern and southern hemispheres has been demonstrated previously [Candide and Meng, 1984]. The cusp boundary latitudes shown in these figures have been normalized to the MLT noon meridian. Finally, the bottom panel displays 15-minute averages of the AE (12) index, which was originally provided at 1-minute time resolution.

Figure 2 spans 48 hours. Some figures may show higher time resolution data to examine detailed variations. Specific features worthy of discussion are marked on each figure.

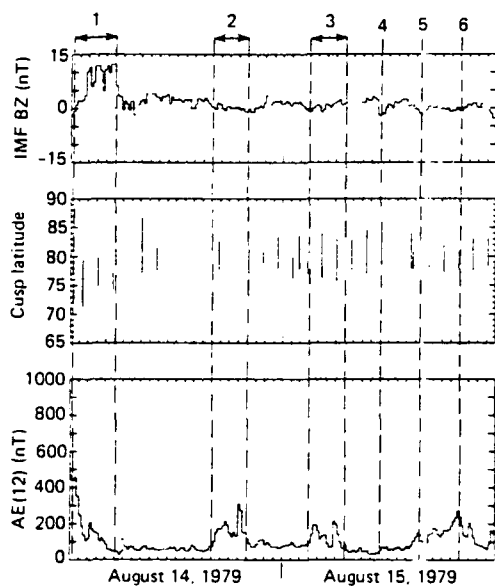


Fig. 2 August 14–15, 1979. The AE and B_z profiles are 15-minute averages. Cusp latitudes have been normalized to noon. The latitudinal extent of the cusp is indicated by the lines in the middle panel. Solid lines denote cusp measurements from the northern hemisphere while dotted lines denote measurements from the southern hemisphere.

August 14–15, 1979 (Figure 2)

This first example shows two days that are typical of the quiet periods examined in this paper. For most of the 48 hours covered in Figure 2, neither B_z nor AE exhibits large variation. The B_z component is strongly northward for a few hours on August 14 (feature 1), but otherwise remains close to zero and slightly northward. The IMF never has an extended southward component although B_z does have short duration southward "dips," as in feature 4 on August 15.

As one would expect from such lethargic interplanetary conditions, the AE index remains below 100 nT except for several minor substorms (features 1, 2, 3, and 5). The enhancements in the AE index do not appear to be strongly correlated with variations in the IMF B_z component. Indeed, the most prominent southward turning of B_z (feature 4) does not correspond to any significant enhancement in AE .

Because variations of AE and B_z are not well correlated, and because B_z is so close to zero, the August 14–15 period seemed a good time to investigate for possible relations between AE and the cusp position. Unfortunately, the resulting comparisons are ambiguous.

As can be seen in the middle panel of Figure 2, the position of the cusp varies several degrees throughout the 2-day period. The equatorward boundary achieves a minimum value of 71° early on August 14 (feature 1). This event occurs about an hour after B_z turned northward and also after AE maximized in excess of 400 nT. The poleward cusp boundary reaches a maximum of $\sim 86^\circ$ on two occasions: after feature 1 and at feature 4. At these times auroral activity is low and the cusp has its greatest latitudinal width. However, an extended cusp is also seen for feature 3 when the AE index indicates auroral activity. Except for feature 1, the cusp boundaries and width exhibit essentially no dependence on either B_z or AE . For most of the period, the equatorial and poleward cusp boundaries vary randomly between 75° and 80° .

Figure 2 typifies the problems encountered in using quiet times to relate cusp position to B_z and AE . Quiet periods display random cusp motions not clearly associated with either B_z or AE , and we must seek slightly more active periods.

August 16–17, 1979 (Figure 3)

The next example provides just such a slightly more active period (Figure 3a). On these days, moderate substorm activity occurs and the AE index exceeds 300 nT on several occasions (features 1, 4, and 7). In addition, the IMF B_z component achieves southward extrema of 3–5 nT for periods of up to an hour. Furthermore, the equatorward boundary of the cusp varies in a nonrandom fashion between 74° and 84° .

For the most part, B_z , AE , and both cusp boundaries apparently act coherently as one would expect. That is, southward turnings of B_z are followed by enhancements in AE and equatorward motions of the cusp. An outstanding example of this behavior is feature 4, which displays these essentials. Also, notice that the two-peak structure seen in both B_z and AE in feature 7 appears to be closely reflected in the movement of the cusp.

However, closer scrutiny reveals significant discrepancies between the variation of cusp location and the B_z or AE profiles. For instance, a relatively strong and significant southward B_z in feature 2 produces relatively little enhancement in AE or movement of the cusp. In feature 6, another southward B_z appears to generate a small enhancement in AE (~ 200 nT) but produces no significant movement of the equatorward cusp boundary. (Notice, however, that the poleward boundary moves equatorward.)

Profiles at higher time resolution allow closer examination. Figure 3b displays an 8-hour time interval centered roughly on feature 1 of the previous figure. In Figure 3b, the B_z and AE profiles represent 5-minute averages. Only the locations of the equatorward cusp boundary are shown. Solid triangles mark the "poor" cusp signatures, and we have drawn a suggestive line through all the signatures.

Features A, B, and C represent magnetic field extrema in which $B_z = -3$ nT. In the cases of A and B, equatorward

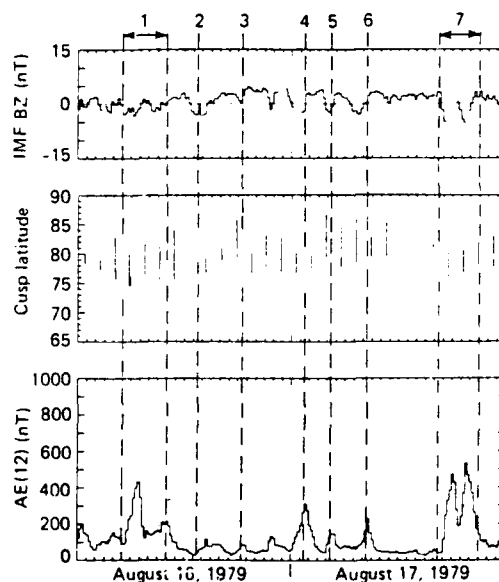


Fig. 3a. August 16–17, 1979. Same format as Figure 2.

motion of the cusp boundary occurs in close association with southward B_z . For feature C a southward B_z appears to be related to a poleward motion of the cusp. For feature A, the AE index exhibits a minimum of less than 100 nT; and the cusp boundary, also a minimum at 74° , appears to reflect variations in the interplanetary field. For feature B, the AE index achieves a maximum of nearly 500 nT, but the latitude of the cusp boundary actually moves poleward to $\sim 75^\circ$. In feature C, the IMF B_z again achieves a minimum of -3 nT while the cusp boundary moves to nearly 79° and the AE profile is essentially flat at ~ 150 nT. The profile of the cusp variation, revealed by the line in the middle panel, most closely parallels that of the IMF B_z , if one excludes the two "poor" signatures following event C.

October 16-17, 1979 (Figure 4)

As seen in Figure 4a, moderate auroral activity of ~ 300 nT occurs several times on October 16, 1979 (features 1, 2, and 3). A southward B_z precedes each of the enhancements in AE on this day. The cusp exhibits a general tendency to move equatorwards for all three features, although the correlation is most prominent in features 1 and 3.

October 17 is the quietest day in the 7-month survey interval. On this day the AE index averages somewhat less than 50 nT and only once achieved a value significantly above 100 nT. The DMSP satellites apparently covered the polar cusp regions quite completely during the first 6 hours of October 17, and this time interval includes a small but significant equatorward motion of the cusp (feature 4). Feature 4 shows a brief southward B_z followed within an hour by an equatorward movement of the cusp. The AE index shows no response. We note that, as *Eather* [1985] has implied, the latitudinal positions of auroral magnetometer stations during the 0000-0600 UT interval are appropriate for monitoring quiescent auroral conditions such as occur on this day.

Figure 4b displays feature 4 with a higher time resolution.

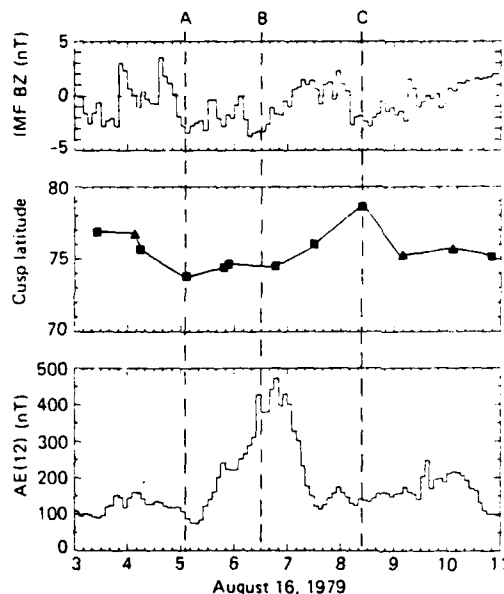


Fig. 3b. Detail of feature 1 in Figure 3a. The AE and IMF B_z profiles represent 5-minute averages. Only the equatorward cusp boundary is shown. "Poor" cusp boundaries are circled. Note the scale changes on the Y axes.

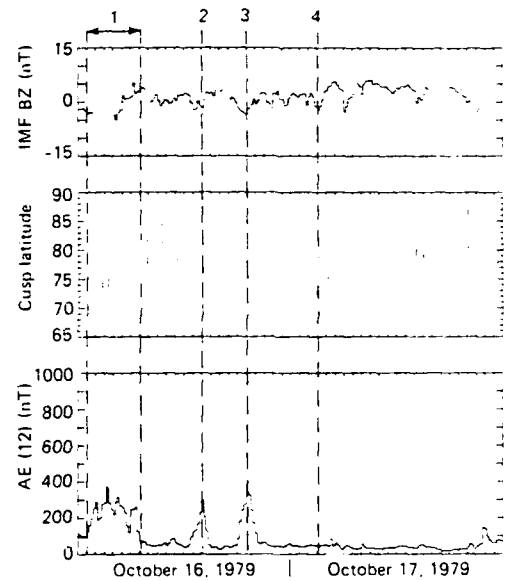


Fig. 4a. October 16-17, 1979. Same format as Figure 2.

This figure covers the first 6 hours of August 17. The IMF B_z and the AE index are 5-minute averages, and only the latitude of the equatorward cusp boundary is shown. Features A and B mark southward excursions of the IMF B_z component, although feature B is deeper (-4 nT) and lasts longer. The equatorward boundary of the cusp reaches a minimum of $\sim 74^\circ$ within an hour of feature B, at which time the AE index is essentially flat. The only significant variation of the AE index is feature C, which occurs 40 minutes after the cusp has achieved a minimum latitude.

Conceivably, the coverage afforded by the AE ground stations might have been insufficient to record the electrojets generated by this admittedly small and brief dip in the IMF B_z .

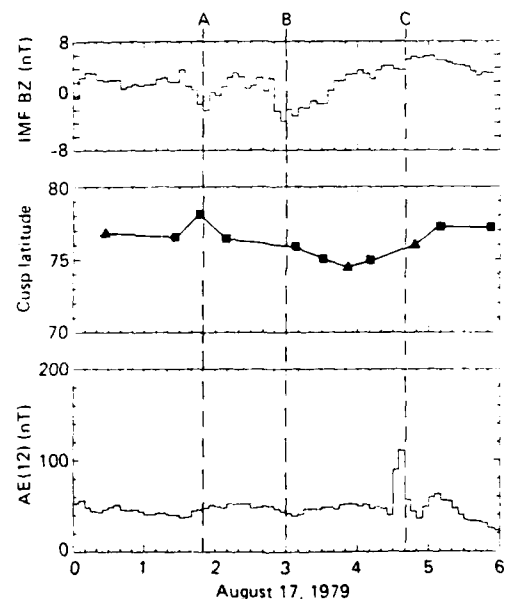


Fig. 4b. Detail of feature 4 in Figure 4a. Same format as previous high time resolution plot (Figure 3b).

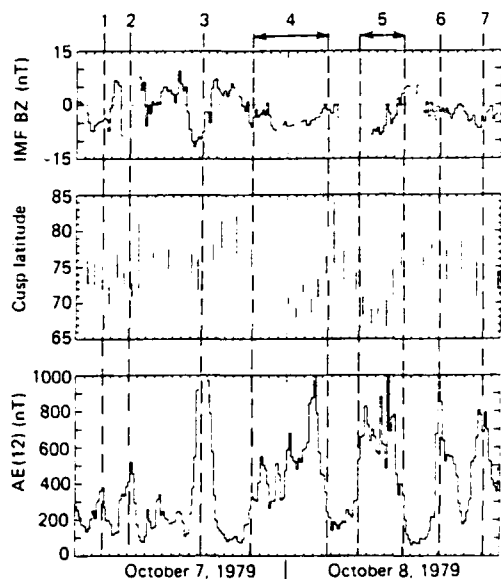


Fig. 5a. October 7-8, 1979. A disturbed period. Same format as Figure 2.

Eather [1985] has suggested that because of the latitudinal positions of recording stations, the AE index in the 2300-0900 UT time sector may be invalid during substorm activity, although there is little evidence of substantial substorm activity during this time interval. At any rate, we regard feature B as an example of an instance in which the cusp location follows B_z more closely than an auroral index.

October 7-8, 1979 (Figure 5)

Unlike the other days discussed previously, October 7 and 8 exhibit very strong substorm activity and probably represent the most active two days in the survey period. The AE index achieves values exceeding 1000 on four occasions (features 3,

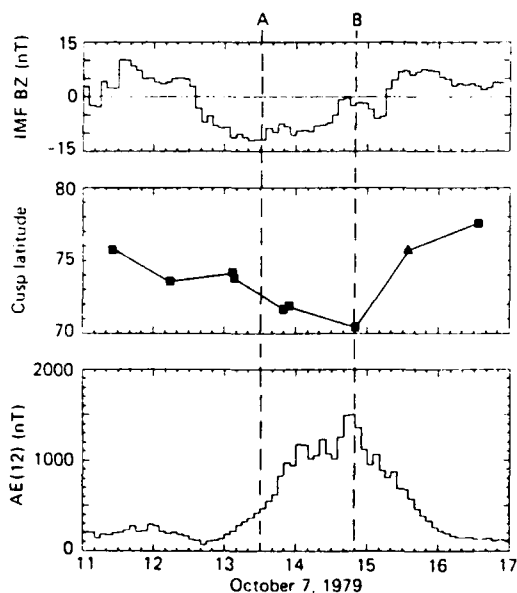


Fig. 5b. Detail of feature 3 in Figure 5a. Same format as Figure 3b.

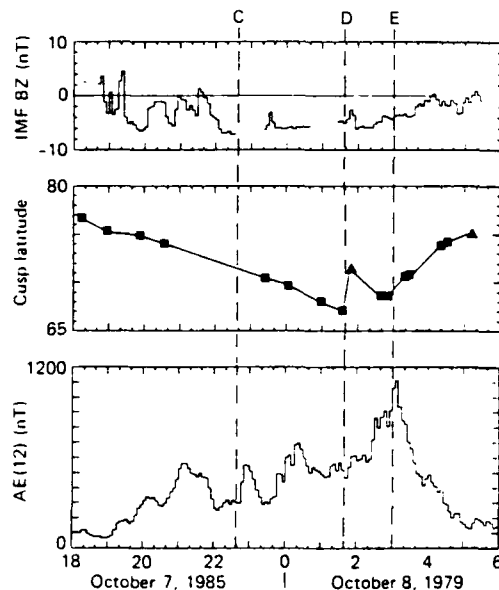


Fig. 5c. Detail of feature 4 in Figure 5a. Same format as Figure 3b.

4, 5, and 6), and the peak of one event (feature 3) is over 1500 nT. This auroral activity coincides with extended periods (≥ 2 hours) of southward B_z (≥ 5 nT). The cusp moves to latitudes as low as 67° on two occasions (features 4 and 5).

Generally, the features in all three panels show qualitative agreement. That is, AE enhancements and low cusp latitudes usually coincide with or follow closely (within an hour) southward turnings of the IMF B_z . Indeed, the substantial variations in IMF B_z , cusp location, and AE index are generally easier to interpret in disturbed conditions than in quiet conditions.

However, the correlation is only qualitative. Consider features 3 and 4, for instance. In feature 3, a deep minimum of -10 nT in the IMF B_z component gives rise to an enhancement of the AE index of over ~ 1500 nT, the most significant substorm activity of these two days. The cusp, however, does not move below $\sim 70^\circ$. The longer lasting substorm of feature 4 includes cusp movement to well below 70° . In this case, the AE index remains below ~ 600 nT and $B_z \sim -6$ nT for most of the event. Apparently, the latitude of the cusp does not vary with the magnitude of the southward B_z or with the size of the AE enhancement.

The data displayed in Figure 5 suggest that the latitude achieved by the equatorward boundary depends not only on the magnitude but also on the duration of southward IMF. For example, the cusp reaches its lowest latitudes in features 4 and 5 only after prolonged southward B_z . In feature 3, the southward B_z is larger but does not last as long, and the cusp does not reach as low a latitude. Such considerations suggest that the latitude of the equatorward cusp boundary is related to the time integral of B_z :

$$\lambda \propto \int_0^T B_z(t) dt$$

where T is the time since B_z turned southward. Several authors [e.g., Burch, 1972; Holzer and Slavin, 1978, 1979] have similarly suggested that the time integral of solar wind parameters correlates well with the time-integrated AE index. We empha-

size here that our approach specifically assumes the nonequivalence of the time integrals of B_z and AE and that the effects of AE and B_z may be determined separately.

Figures 5b and 5c show features 3 and 4 in detail at higher time resolution. As before, the IMF B_z and the AE index are represented by 5-minute averages, and only the equatorward cusp boundary is shown.

Figure 5b details feature 3. The B_z component reaches a minimum of about -12 nT (at feature A) over an hour prior to the peak of 1500 nT in the AE index (at B). The cusp apparently achieves its most equatorward position of nearly 70° in association with the strong peak in the AE index. A time delay of 80 min would be necessary to explain the cusp minimum at B as a result of the IMF minimum at A. In this instance, therefore, cusp behavior does indeed follow the AE profile more closely than B_z .

Figure 5c shows the details of feature 4. Gaps in the magnetic field data prevent complete coverage of the B_z component, although the field appears to reach an extremum of -7 nT near feature C. The cusp reaches its lowest latitude of 67° near D, at which point the AE index is actually at a relative minimum of 500 nT. The 1100 -nT peak of the AE index (at E) occurs during a period of apparent IMF B_z and cusp recovery. In this case, none of the three profiles is in good agreement with any other profile.

CONCLUSIONS AND DISCUSSION

An attempt has been made to determine whether interplanetary magnetic fields or magnetospheric currents exert dominant control over the location of the polar cusp. We have examined predominantly quiet times and times during which AE and B_z behaved contrarily. This approach tacitly assumes, of course, that the effects of internal magnetospheric currents (AE) may be ascertained independently of the effects of external magnetic fields (B_z).

We have qualitatively examined more than 23 days of DMSP data over 7 months during 1979 and 1980 and have compared cusp variations with IMF B_z to the AE index. Generally, the IMF B_z , AE index, and equatorward cusp boundary tend to act coherently; that is, southward B_z occurs in conjunction with an equatorward motion of the low-latitude cusp boundary and enhanced AE activity. This conclusion agrees substantially with results of previous workers [e.g., Kamide *et al.*, 1976]. However, during relatively quiet times, the cusp boundary may exhibit considerable variability that does not appear to be associated with variations in B_z or AE . In several instances, the cusp location followed B_z more closely than AE . During more active times, large spikes in AE may not coincide with either B_z or the cusp position. The largest equatorward movements of the cusp seem to occur as a result of prolonged southward B_z , lasting over 3 hours. The time integral of the southward B_z may exert a dominant influence on the latitude at the equatorward boundary of the cusp.

One of the major difficulties in conducting a study of this nature is the reliability of the auroral activity index (AE here) that is used to represent magnetospheric substorm activity. Since only 12 widely spaced stations collect the data, a substantial possibility exists that some auroral disturbances will slip between the ground stations and escape detection [e.g., Baumjohann, 1985]. This problem grows especially acute when one attempts to investigate quiet-time auroral correlations, as in this study.

The determination of the IMF represents another difficulty

that may be just as severe. The use of the IMF B_z assumes that the measurement from a single spacecraft can determine the global condition of the interplanetary field as it interacts with the terrestrial magnetosphere. Two time delays must be considered. The first involves the travel time of the IMF variation from the point of measurement to the region of magnetospheric interaction where merging occurs, and the second involves the response time of the auroral zone itself. The exact sizes of these delays are not known, however, since the location of the interaction region is not known, nor is the speed at which the auroral zones respond.

In a previous section we already enumerated the difficulties involved with determining the cusp location. In addition, the time resolution of cusp measurements from DMSP satellites may not be adequate to track the changes in AE and the IMF.

With these caveats in mind, we should not be surprised if the IMF B_z , AE index, and cusp latitude do not act in a completely coherent fashion; rather, we should marvel that the three exhibit any association at all. As previous investigators have found, the cusp generally appears to move to lower latitudes with southward B_z and enhanced AE , and vice versa. The situation during quiet conditions is not so simple, however. We have found cusp motions that do not seem to be correlated with AE . Small motions of the cusp may occur without any connection to either AE or the IMF B_z . Even during disturbed conditions, the cusp location may not exhibit a detailed association with AE or B_z .

These difficulties compound the problem of separating the effects of the IMF from the effects of the auroral electrojets and magnetospheric current systems. In surveying 7 months of data, we have found examples in which the IMF apparently exerts the dominant force in moving the polar cusp. At other times, we have found examples in which the cusp did not respond to either a southward B_z or an AE enhancement. Apparently, the cusp displays merely random motions during very quiet times. As suggested by some events occurring during disturbed conditions, the cusp location may properly correlate with the accumulated, or time-integrated, B_z and not with merely B_z .

Acknowledgments. This research is supported by the Air Force Office of Scientific Research under Grant AFOSR 84-0049 and by the Atmospheric Sciences Division of the National Science Foundation under Grant ATM-83-15041 to The Johns Hopkins University Applied Physics Laboratory.

The Editor thanks P. E. Sandholt and another referee for their assistance in evaluating this paper.

REFERENCES

- Akasofu, S.-I., P. D. Perrault, F. Yasuhara, and C.-I. Meng, Auroral substorms and the interplanetary magnetic field, *J. Geophys. Res.*, **78**, 7490, 1973.
- Baumjohann, W., Merits and limitations of the use of geomagnetic indices in solar-wind magnetosphere coupling studies, paper presented at Chapman Conference on Solar Wind-Magnetosphere Coupling, AGU, Pasadena, Calif., Feb. 1985.
- Burch, J. L., Preconditions for the triggering of polar magnetic substorms by storm sudden commencements, *J. Geophys. Res.*, **77**, 5629, 1972.
- Burch, J. L., Effects of the interplanetary magnetic field on the auroral oval and plasmasphere, *Space Sci. Rev.*, **23**, 449, 1979.
- Burton, R. K., R. L. McPherron, and C. T. Russell, The terrestrial magnetosphere: A half-wave rectifier of the interplanetary electric field, *Science*, **189**, 717, 1975.
- Bythrow, P. F., and T. A. Potvin, The relationship of total Birke-land currents to the merging electric fields, *Geophys. Res. Lett.*, **10**, 523, 1983.
- Candidi, M., and C.-I. Meng, Nearly simultaneous observations of the conjugate polar cusp region, *Planet. Space Sci.*, **32**, 41, 1984.

- Dungey, J. W., Interplanetary magnetic field and the auroral zones, *Phys. Rev. Lett.*, **6**, 47, 1961.
- Eather, R. H., Polar cusp dynamics, *J. Geophys. Res.*, **90**, 1569, 1985.
- Eather, R. H., S. B. Mende, and E. J. Weber, Dayside aurora and relevance to substorm current systems and dayside merging, *J. Geophys. Res.*, **84**, 3339, 1979.
- Fairfield, D. H., and L. J. Cahill, Jr., Transition region magnetic field and polar magnetic disturbances, *J. Geophys. Res.*, **71**, 155, 1966.
- Holzer, R. E., and J. A. Slavin, Magnetic flux transfer associated with expansion and contraction of the dayside magnetosphere, *J. Geophys. Res.*, **83**, 3831, 1978.
- Holzer, R. E., and J. A. Slavin, A correlative study of magnetic flux transfer in the magnetosphere, *J. Geophys. Res.*, **84**, 2573, 1979.
- Holzworth, R. H., and C.-I. Meng, Mathematical representation of the auroral oval, *Geophys. Res. Lett.*, **2**, 377, 1975.
- Horwitz, J. L., and S.-I. Akasofu, Response of dayside aurora to sharp northward and southward transitions of the interplanetary magnetic field and to magnetospheric storms, *J. Geophys. Res.*, **82**, 2723, 1977.
- Kamei, T., and H. Maeda, Auroral electrojet indices (AE) for July-December 1979, Data Anal. Cent. for Geomagn. and Spacemagn., Kyoto Univ., Japan, 1982.
- Kamei, T., H. Maeda, and T. Araki, Auroral electrojet indices (AE) for January-June 1980, Data Anal. Cent. for Geomagn. and Spacemagn., Kyoto Univ., Japan, 1983.
- Kamide, Y., J. L. Burch, J. D. Winningham, and S.-I. Akasofu, Dependence of the latitude of the cleft on the interplanetary magnetic field and substorm activity, *J. Geophys. Res.*, **81**, 698, 1976.
- Makita, K., C.-I. Meng, and S.-I. Akasofu, The shift of the auroral electron precipitation boundaries in the dawn-dusk sector in association with geomagnetic activity and interplanetary magnetic field, *J. Geophys. Res.*, **88**, 7967, 1983.
- Meng, C.-I., Latitudinal variation of the polar cusp during a geomagnetic storm, *Geophys. Res. Lett.*, **9**, 60, 1982.
- Meng, C.-I., Case studies of the storm time variation of the polar cusp, *J. Geophys. Res.*, **88**, 137, 1983.
- Meng, C.-I., Dynamic variation of the auroral oval during intense magnetic storms, *J. Geophys. Res.*, **89**, 227, 1984.
- Pike, C. P., C.-I. Meng, S.-I. Akasofu, and J. A. Whalen, Observed correlations between interplanetary field variables and the dynamics of the auroral oval and the high-latitude ionosphere, *J. Geophys. Res.*, **79**, 5129, 1974.
- Reiff, P. H., R. W. Spiro, and T. W. Hill, Dependence of polar-cap potential drop on interplanetary parameters, *J. Geophys. Res.*, **86**, 7639, 1981.
- Rostoker, G., Magnetospheric and ionospheric currents in the polar cusp and their dependence on the B_z component of the interplanetary magnetic field, *J. Geophys. Res.*, **85**, 4167, 1980.
- Russell, C. T., C. R. Chapell, M. D. Montgomery, M. Neugebauer, and F. L. Scarf, Ogo 5 observations of the polar cusp on November 1, 1968, *J. Geophys. Res.*, **76**, 6743, 1971.
- Sandholt, P. E., K. Hendrikson, C. S. Deehr, G. G. Sivjee, G. J. Ronrick, and A. Egeland, Dayside cusp auroral morphology related to nightside magnetic activity, *J. Geophys. Res.*, **85**, 4132, 1980.
- Sandholt, P. E., A. Egeland, B. Lybakk, C. S. Deehr, G. G. Sivjee, and G. J. Romick, Effects of interplanetary magnetic field and magnetospheric substorm variations on the dayside aurora, *Planet. Space Sci.*, **31**, 1345, 1983.
- Sandholt, P. E., A. Egeland, J. A. Holtet, B. Lybakk, K. Svenes, S. Asheim, and C. S. Deehr, Large- and small-scale dynamics of the polar cusp, *J. Geophys. Res.*, **90**, 4407, 1985.
- Shepherd, G. G., Dayside cleft aurora and its ionospheric effects, *Rev. Geophys.*, **17**, 2017, 1979.
- Zanetti, L. J., T. A. Potemra, J. P. Doering, J. S. Lee, J. F. Fennell, and R. A. Hoffman, Interplanetary magnetic field control of high-latitude activity on July 29, 1977, *J. Geophys. Res.*, **87**, 5963, 1982.

J. F. Carbary and C.-I. Meng, The Johns Hopkins University Applied Physics Laboratory, Johns Hopkins Road, Laurel, MD 20707.

(Received August 5, 1985;
revised September 25, 1985;
accepted October 11, 1984.)

Low Altitude Observations of Dispersionless Substorm Plasma Injections

PATRICK T. NEWELL AND CHING-I. MENG

The Johns Hopkins University Applied Physics Laboratory, Laurel, Maryland

The substorm injection boundary model proposed by McIlwain (1974) and since adopted by many researchers describes the phenomenology of plasma introduction into the middle magnetosphere during a magnetic substorm: at the time of the substorm onset, both electrons and ions of all energies share a common Earthward boundary. Such an injection should leave a clear signature in the auroral precipitation data. We used the Defense Meteorological Satellite Program (DMSP) F6 and F7 satellites to search for such signatures in the ≤ 30 -keV auroral electron and ion data. Clear examples of an equatorward leap of the previously energy dependent equatorward cutoff in auroral precipitation to a cutoff boundary common to ions of all energies measured (i.e., dispersionless up to 30 keV) and electrons up to several keV (usually less than 10 keV) were observed in the near-midnight sector at a time corresponding to substorm onset. A collection of 10 such events occurring over a 1-month interval was studied, providing unusually direct confirmation that the phenomenological model of an initially dispersionless boundary accurately describes at least some injections. The DMSP data show the injection boundary to be dispersionless over a wide longitudinal range, but often only a dispersive injection is seen at dawn.

1. INTRODUCTION

Substorm activity appears to be always accompanied by the introduction of plasma into regions of the middle magnetosphere Earthward of the presubstorm plasma sheet. The physical mechanisms involved in this process are still controversial. Studying particle signatures seen at geosynchronous orbit by ATS 5, McIlwain [1974] observed that if the trajectories of particles of various energies encountered by ATS 5 were traced back (he used his own electric field model E3H and magnetic field model M2), the particles of all energies for both electrons and ions often seemed to coincide at a common injection boundary at a time which corresponded to the substorm onset as observed by ground-based magnetometers. This phenomenological injection boundary model, originally supposed to result from in situ heating, has been adopted by many workers as giving a good fit to a variety of data, without explaining the underlying physical mechanism behind such a dispersionless injection. Konradi *et al.* [1975] showed that Explorer 45 storm time observations of electrons and ions were consistent with the injection boundary model. Mauk and Meng [1983a], using a dipole magnetic field and a uniform cross-tail potential, showed that there are seven different qualitative particle dispersion signatures observable from a geosynchronous satellite if an initially dispersionless injection is assumed, and they found examples of each in the SCATHA and ATS 6 data set. Greenspan *et al.* [1985] showed that some high-energy electron and ion signatures observed by ISEE 1 were consistent with an initially dispersionless substorm injection boundary. Mauk and Meng [1983b, 1986] have taken the position that plasma is never introduced into the middle magnetosphere (that is, geosynchronous orbit and within) via steady state convection-forming Alfvén layers, but that instead injections always occur in highly impulsive events with time varying electric fields. Some indirect evidence against the steady state Alfvén layer picture is inferred from observations of the energy dependence in the equatorward cutoffs of diffuse auroral precipitation [Newell and Meng, 1987].

The substorm injection boundary as first postulated extended only from dusk to about midnight [McIlwain, 1974]. Over the

years the postulated longitudinal extent of the boundary has grown steadily, extending to dawn [Konradi *et al.*, 1975] and finally completely encircling Earth [McIlwain, 1985]. There has been other research into the probable characteristics of the injection boundary. Mauk and Meng [1983a] proposed that the point of closest approach of the boundary to Earth (an inflection point in the double spiral curve) is rotated 1-2 hours toward dawn. Quinn and Johnson [1985], backtracking field-aligned oxygen ion observations, concluded that the injection boundary can, at least at times, be the location of direct ionospheric input into the trapped energetic particle population. Finally, Moore *et al.* [1981], studying simultaneous measurements from two approximately geosynchronous satellites, have proposed a possible explanation for the dispersionless boundary in terms of an Earthward propagating compression wave which carries an east-west-oriented current sheet and is the agent for the injection of plasma into the middle magnetosphere. All of this has been difficult to verify.

A single geosynchronous satellite directly observes the temporal structure of an injection, but only makes spatial inferences by indirect means. However, in the case of a low-altitude polar-orbiting satellite, which rapidly cuts across L shells, the spatial dispersion or lack thereof is much clearer (at the expense of time resolution). A polar-orbiting satellite gives an essentially projection screen view of a cut through the magnetosphere. Hence if ions and electrons occupy a common energy independent boundary at substorm onset, it would be recognizable by a satellite that crossed the boundary close enough to the injection time. Here we report what is apparently the first search for such events, and indeed, report that dispersionless injections can be seen fairly frequently. Two of these events are described in detail in section 2. It should be noted that Whalen [1983], using an array of ground- and air-based ionospheric sounders, concluded that during a substorm the integral flux into the diffuse aurora can display an unusually abrupt equatorward edge. Since the integral energy flux is dominated by electrons of a limited energy range, Whalen's observations are a necessary but not sufficient condition for a dispersionless boundary shared by electrons and ions of all energies.

The introduction of plasma into the middle magnetosphere is reflected in the Defense Meteorological Satellite Program (DMSP) data by the extension of the diffuse auroral precipitation to lower

Copyright 1987 by the American Geophysical Union.

Paper number 6A8904.
0148-0227/87/006A-8904\$05.00

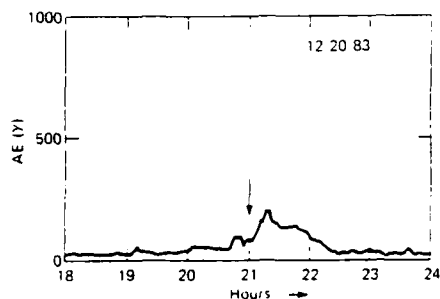


Fig. 1 The AE index near the time of the December 20, 1983, injection. The arrow marks the time the particle data observed the injection.

latitudes; a dispersionless injection implies that both electrons and ions occupy a common energy independent equatorward cut-off in diffuse auroral precipitation. Before identifying such distinct dispersion signatures, it is first necessary to know the "typical" behavior. We have previously investigated the phenomenology of the equatorward cutoffs in auroral precipitation as a function of energy, local time, and magnetic activity [Newell and Meng, 1987]. It was found that during times of moderate magnetic activity (the large majority of the time) in the midnight region, the ordering of the equatorward precipitation edges for both electrons and ions is $\lambda_{100} < \lambda_{1000} < \lambda_{3000}$, where λ refers to a cutoff latitude and the subscripts are energies in eV. The equatorward cutoff usually is the farthest poleward for ions of a few keV energy, and above this energy the cutoff again moves farther equatorward (an example can be seen in Plate 1c). This dispersive pattern holds most of the time, although during times of profound magnetic quiet the cutoffs at all energies coincide. At later local times (toward morning) the ion dispersion increases; toward dusk the dispersion is smallest. Ordinarily, electron precipitation cuts off equatorward of the ion precipitation in all local time sectors except near dusk, where the ions cut off farther equatorward than the electrons. Thus the signature of a substorm particle injection event is indeed readily identifiable: an abrupt shift of the diffuse auroral precipitation equatorward to a common dispersionless boundary coinciding with substorm onset as determined from ground-based magnetometers.

Our results depend on making inferences about the Earthward edge of the plasma sheet from measurements of the equatorward edge of the diffuse aurora. That such a mapping generally exists is the consensus of most researchers. Horwitz *et al.* [1986] have recently examined this proposition in detail. They used DE 1 and DE 2 to compare approximately simultaneous measurements of the diffuse aurora equatorward edge and the plasma sheet Earthward boundary for electrons at 100 eV, 1000 eV and 10 keV in the dusk to midnight sector. They found that the boundaries, when mapped along field lines, agreed very well at each of these energies. A related study is that of Fairfield and Viñas [1984]. They found that at the inner edge of the plasma sheet there was an enhancement of field aligned electrons, an effect they attribute to drift shell splitting. Such an effect would, of course, not hinder the ability of low-altitude satellites to infer the Earthward edge of the plasma sheet.

We herein report the results of a search for signatures such as described above. It is found that dispersionless injections are indeed frequently recognizable from the signature described above in the DMSP data set. This is by far the most direct evidence to date that the concept of the substorm injection boundary at least sometimes correctly describes the substorm introduction of

plasma into the middle magnetosphere. The present study does not attempt to establish that dispersionless injections are the only means of plasma injection, but it does show conclusively that some injections can be so described.

2. DATA PRESENTATION

We examined an approximately 1-month interval—December 1 to December 25, 1983—a period for which the ground-based magnetometer AE data are available, as well as DMSP F6 and F7 data. These satellites are both in sun synchronous polar orbits at about an 840-km altitude. DMSP F6 is in approximately the 0640–1840 local time meridian, and DMSP F7 the 1035–2235 meridian. The particle spectrometers on DMSP F6 and F7 are identical cylindrical electrostatic analyzers, measuring electrons and ions from 30 eV to 30 keV, covering the complete spectrum in 1 s. The detector apertures are always pointed toward local zenith, so that at the high latitudes of interest, only particles well within the loss cone are observed. The instrumental complement of F6 and F7 is discussed in greater detail by Hardy *et al.* [1984] and Gussenhoven *et al.* [1985].

During the 25-day period examined, we identified 10 dispersionless injection events, a few of which contained multiple injections. This number is somewhat arbitrary in that it represents the minimum number of dispersionless injections we felt it suitable to study. Section 3 discusses the probable frequency of such injections.

Section 2.1 describes an example of a well-isolated dispersionless injection occurring during extreme magnetic quiet; section 2.2 discusses a dispersionless injection which, while occurring during more normal moderate level AE activity, is nonetheless well defined; and section 2.3 reports on some more general statements and observations about the entire set of injection observations. We briefly add the caveat that what is referred to here as "an injection" is, of course, the situation within a few minutes after an injection, that is, postinjection.

2.1 An Isolated Injection: December 20, 1983

We show here an example of an isolated weak substorm, quite small but still clearly identifiable from the ground-based magnetometers used in compiling AE . The injection occurred on December 20, 1983, at about 2103 UT (75800 s). Figure 1 shows the AE magnetometer tracings for the interval of interest, with an arrow marking the time the particle data show an injection. Because none of the stations used in producing AE were near midnight, the injection time cannot be determined very accurately from the magnetic tracings, but it is still clear that there is a geomagnetic disturbance associated with the particle injection.

As seen in Figure 1, prior to the disturbance there had been a long period of quiet. Hence, as shown in Plate 1a, the auroral precipitation was at higher latitudes with fairly little dispersion: for ions in the 30-eV to 30-keV range the cutoffs near 0030 magnetic local time (MLT) as measured by DMSP F7 were between 67.3° and 67.5° magnetic latitude (MLAT); for electrons in the 100- to 3000-eV range the cutoffs were from 67.4° to 67.8° MLAT. The high-resolution (1 s) data used for these determinations have about 0.1° MLAT accuracy, which is thus the limiting accuracy to which the cutoffs can be determined. The injection, as shown in Plate 1b, left ions (in the previously cited energy range) with cutoffs between 65.7° and 65.8° MLAT, while the electrons ranged between 65.6° and 65.9° MLAT. The highest-energy electrons often, as in this example, do not share the otherwise common cutoff boundary, but rather cut off poleward of

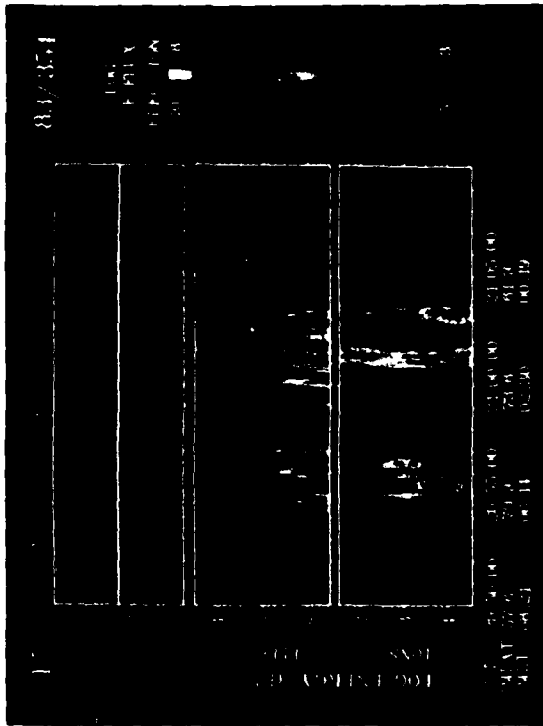


Plate 1b. A spectrogram for the DMSP F7 pass which observed the injection. Notice how the ion cutoffs at all energies and the electron cutoffs below several keV coincide in the midnight region.

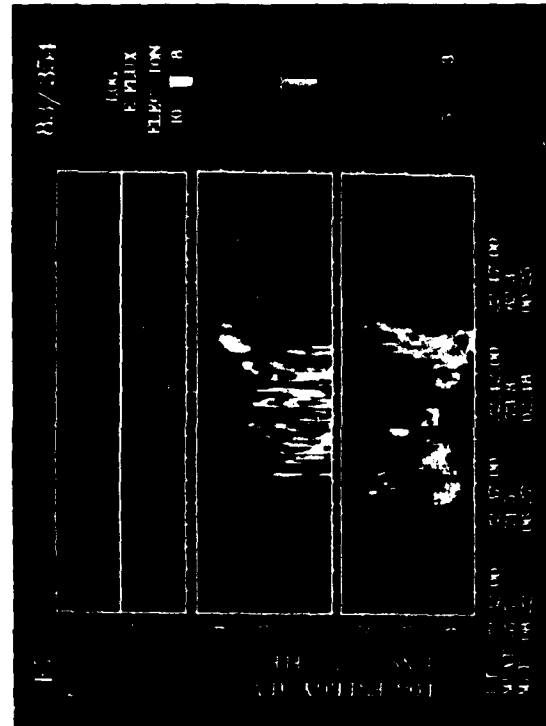


Plate 1c. The DMSP F7 northern hemisphere data on the next pass after the injection. Notice the strong dispersion that has already developed, particularly for the ions. The C-shaped curve with the intermediate energy ions cutting off farthest poleward is the most commonly observed dispersion pattern.

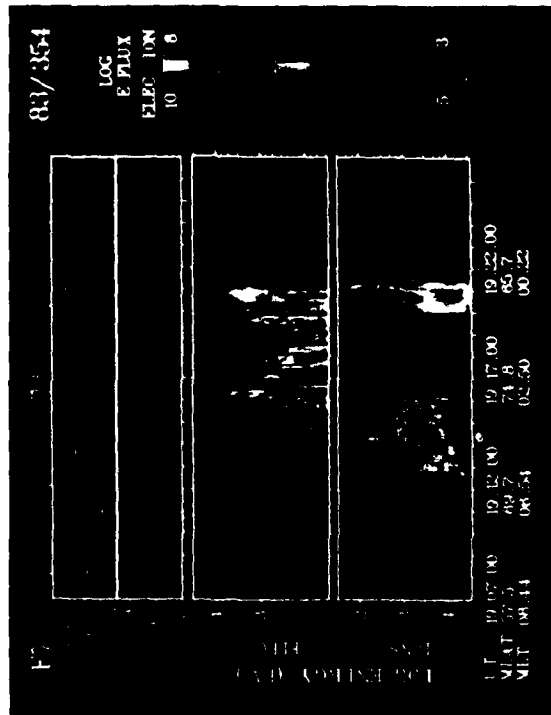


Plate 1a. A spectrogram of the DMSP F7 particle data for the very quiet time period immediately preceding the December 20 injection. Notice that the ion energy scale is inverted, with higher energies downward, so that the low energy particles of both species appear in the center of the figure. The color scale axes differential energies flux in units of eV/cm^2 sr eV^{-1} . The line plot of energy flux in the top panel is in eV/cm^2 sr eV^{-1} and the average energy in eV. The energies covered for both electrons and ions are 0.1 eV to 30 keV.

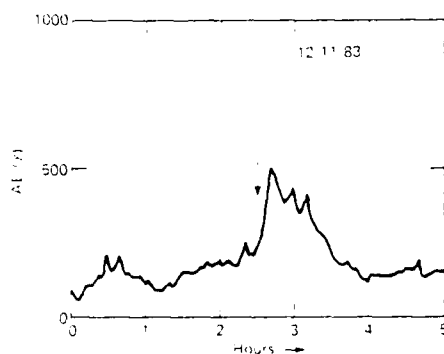


Fig. 2. AE index for the time near the injection of December 11, 1983. The arrow shows the magnetometer injection time, which is taken to be the leading edge of the sharp decrease in H for one of the stations that make up the AE index.

it. This subject is treated in detail in section 3. When viewing Plate 1 it is necessary to keep in mind that only precipitating particles are being observed. Hence the most spectacular feature in Plate 1*b* is the discrete aurora which formed farther poleward. However, for the present discussion it is the fainter signature of the diffuse aurora edge (which maps to the plasma sheet edge) that is most important. The equatorward jump to the position shown in Plate 1*b* represents an Earthward extension of the plasma sheet from what is certainly outside geosynchronous orbit to what is probably near geosynchronous orbit [e.g., Meng, 1979], and thus is an example of what a geosynchronous satellite would see as an injection event (which may or may not be dispersive, depending on the position of such a satellite). There is in this event direct substantiation of the hypothesis that this injection occurs up to a common energy and species (electrons or ions) independent boundary.

This injection is particularly interesting because the newly injected ions form a population that is clearly spatially distinct from the old ions. For the electrons there is not such a clear separation. The separation seen in the ions is not the most typical behavior, but it is not unique. It is evident that if the plasma were being introduced into the middle magnetosphere simply by the inward convection of preexisting Alfvén layers by an enhanced cross-tail electric field, one would not expect such a separation.

Once the plasma is introduced into the middle magnetosphere, it quickly develops the more characteristic dispersed form. Plate 1*c* shows that 101 min later (the satellite orbital period), the equatorward cutoffs near midnight have already lost the dispersionless boundary. The ions range from 65.3° to 68.4° MLAT, and the electrons (below 3 keV) from 64.1° to 64.6° MLAT. The "typical" dispersion pattern of up to a few degrees latitude reported previously [Newell and Meng, 1987], which holds except during times of prolonged quiet or immediately after an injection, can be observed. The dispersion shown in Plate 1*c* with intermediate-energy ions (a few keV) cutting off farthest poleward, is a good example of the dispersion most commonly seen by DMSP. There is here a two-stage process [compare with Mauk and Meng, 1986]: the dispersionless injection of the plasma into the middle magnetosphere behind a common boundary, and the subsequent dispersive evolution in this plasma.

In this example we concentrated on the behavior near midnight; and unfortunately comparatively little can be directly ascertained about the local time extent of this particular injection. The first F6 encounter with the auroral oval was not until more than a half hour after the injection. This encounter, near 0440

MLT, showed that the equatorward cutoffs for particles of all energies (except the highest-energy electrons) had shifted equatorward. However, if the injection ever was dispersionless in this sector, it had already dispersed, for there was not a common cutoff. The orbits of F6 and F7 over the southern hemisphere at this time were not such as to encounter the auroral oval. As shown in Plate 1, F7 did encounter the auroral oval near 0730 MLT near the time of the injection. In the morning to noon sector it is not as easy to determine whether an injection is occurring as it is near midnight. In the former region one must be careful to make a distinction between the auroral oval and the "mantle" aurora [Meng and Akasofu, 1983]. The mantle aurora is caused by precipitating electrons with energies greater than about 10 keV in the morning to noon sector, and it originates in injections closer to midnight which convect around Earth along roughly constant geomagnetic latitude. The auroral oval occurs at higher latitudes at later local times and is presumed to represent the extension of the plasma sheet around toward the day-side. McIlwain [1985] has argued that a signature of the injection boundary in this local time zone should coincide with the auroral oval, rather than the more equatorward mantle aurora.

In examining Plate 1*b*, therefore, one should look for the injection boundary at about 70° MLAT (given by a tick mark at top), rather than at the farthest equatorward extent of 3-keV electron precipitation. In fact, this does indeed represent an equatorward extension of the ion precipitation and electron precipitation below 3 keV (ignoring the isolated lower-latitude 3-keV precipitation). It is evident that a clear-cut, sharp boundary cannot be identified here as it can in the near-midnight sector, although it appears significant that an equatorward extension of the diffuse auroral precipitation near 0730 MLT occurs nearly simultaneously with the midnight region injection.

2.2 An Injection During Typical Activity: December 11, 1983

For a second example, we show a dispersionless injection that can be identified clearly in both the particle and magnetic field data, during low to moderate level AE activity more typical of the majority of the time. Figure 2 shows the AE index for the interval of interest. An arrow marks the particular injection to be discussed here, which, as determined from the magnetometer data, occurred at about 0238 UT, December 11, 1983 (9500 s UT). (We used the superposed 11 individual magnetometer stations that make up the AE index to make this determination. The superposed tracings are hard to reproduce here.)

The precipitation prior to the injection of immediate interest is shown in Plate 2. Although the evening dispersion pattern of the equatorward edge of the diffuse aurora in this example is not as clear and smooth a curve as, say, Plate 1*c*, the general tendency for intermediate-energy ions to cut off farthest poleward is manifest, as is the pattern of lower-energy electrons to extend equatorward of the several-keV electrons (since we have chosen to present differential energy flux rather than number flux, the higher-energy electrons are the brighter color when the number fluxes are within a few orders of magnitude). Thus the approximately normal preinjection situation is apparent. Near the midnight region, the ions cut off near 66° MLAT (the lowest- and highest-energy ions extending up to a degree farther equatorward) and the electrons about the same. The dispersion in each is about 1° .

Plate 2*b* shows the particle precipitation around the time of the injection as inferred from the magnetometer signature. Near the midnight sector a fairly dispersionless injection can be dis-

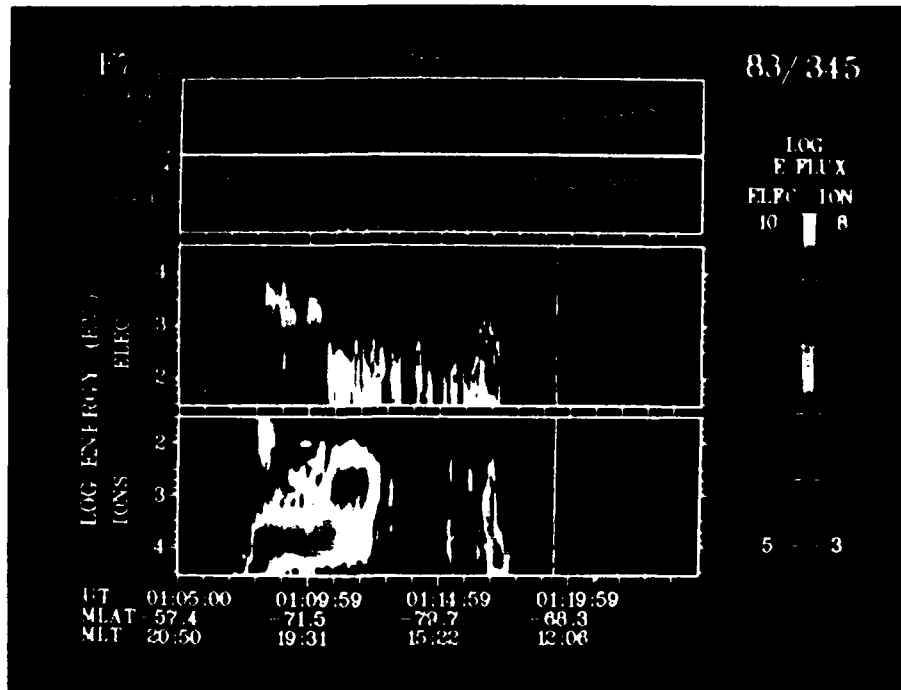


Plate 2a. A spectrogram of the DNISP F7 data for the pass preceding the December 11, 1983, injection. Although the ion "C" shape is not well defined, the equatorward edge of the diffuse precipitation is highly dispersive, and in general the intermediate energy ions cut off equatorward of the lower- and higher-energy ions.

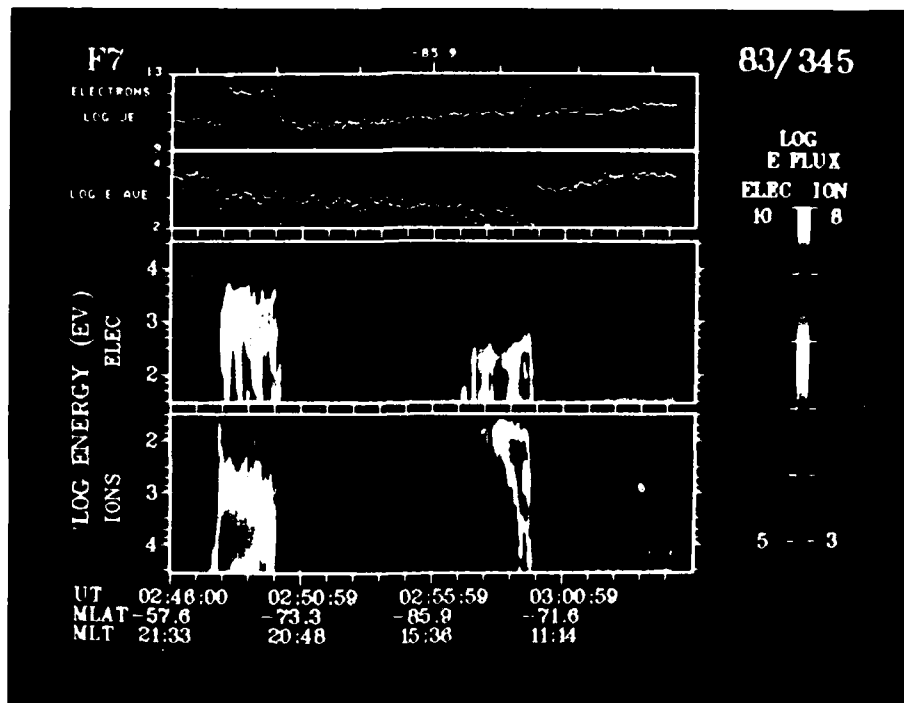


Plate 2b. The DNISP F7 particle data for an injection. Near local midnight, the ion cutoff is extended farther equatorward and the ions and electrons of all energies share a common boundary for a sharp flux decrease at 61.0° MLAT. Note that even for the highest energy ions there is a sharp flux decrease at this common injection boundary. At the highest ion energies, ions are drifting westward from closer to midnight.

TABLE 1. List of the 10 Dispersionless Injections Studied in Detail for the Present Report

Day in Dec. 1983	UT Injection Observed at Midnight	Magnetometer Injection Signature	Dawn MLT Type Injection	Prenoon MLT Type Injection	Dusk MLT Type Injection
3	1314	1302	-----	1010 dispersionless injection	-----
5	0230	0238	0510 dispersive injection	-----	1740 dispersionless injection
7	0728	0720	0700 dispersive injection	0940 no clear injection	1912 dispersionless injection
10	0916	0915	0701 dispersionless injection	1040 dispersionless injection	ambiguous
11	0248	0238	0513 dispersive injection	ambiguous	1740 dispersive injection
12	1016	not clear	0750 dispersive injection	1045 dispersionless injection	1740 no clear injection
13	0955	0955	0740 dispersive injection	1040 no injection	1750 dispersionless injection
18	1457	1446	-----	ambiguous	-----
20	2103	2113?	0440 dispersive injection	0740 ambiguous	-----
24	2126	2118	0740 no clear injection	0745 no clear injection	-----

A horizontal bar indicates no data available. Each entry gives the MLT the appropriate satellite was at when the auroral oval crossing closest in UT to the injection observation near local midnight occurred, and the type of injection seen at that MLT. All of these injections appeared dispersionless near midnight.

*No data available at time of the midnight injection listed. There was a second injection around 1533 UT which was dispersionless at dawn and dusk.

tinguished around 63.0° MLAT. These midnight sector observations were taken at about 0248 UT (10070 s), about 10 min after the magnetometer signature of substorm onset. Although at the highest energies sampled a slightly farther equatorward extension of the ion population can be discerned, the original common injection boundary can still be clearly observed. In this example it is clear that what will first disturb the dispersion of the injection is the arrival of high-energy ions from further toward midnight where the injection extends closer to Earth. As is usually the case in the events we studied, the precipitating electrons share the common injection boundary only up to a few keV, above which point their count rate is not statistically significant. Nonetheless, it is remarkable how dispersionless the boundary is, compared to the normally observed state of affairs. Indeed, considering how highly dispersive the preinjection boundaries are, the most striking feature of the injection is how well the electron and ion postinjection boundaries essentially coincide, a fact in agreement with long-standing inferences from geosynchronous data. The subsequent pass of F7 through the midnight auroral zone 101 min later (not presented here) showed dispersive features again setting in, although a faint remnant of the original injection boundary could be seen. Here we have an example of the initially dispersive equatorward boundary becoming comparatively dispersionless during the plasma injection into the middle magnetosphere.

Concerning the dayside (prenoon) injection, we have the rather curious case of an extremely sharp boundary, which, however, seems to correspond to the cusp rather than to the auroral oval. It appears as though there is no "auroral oval" in the prenoon

sector at the time of the injection. The average energy and spectra of the electrons and ions poleward of this boundary strongly suggest an identification with the cusp. In the subsequent pass, high-energy auroral oval electrons and ions are again to be observed equatorward of the cusp in this MLT sector. The same behavior occurs in several of the dispersionless injections we have studied, and its meaning is not clear to us. The signatures seen in the dawn and dusk sectors by F6 during the injection are discussed in the next section.

2.3 Observations from the Set of Dispersionless Injections

Table 1 lists the 10 injections that were dispersionless near midnight as seen by DMSP F7 and that we studied for the present work. A chief consideration of this section is how these injections looked at other magnetic local times. The injection times inferred from the magnetometer data as listed in Table 1 correspond most nearly to the leading edges of substorm activity. This was found to agree most closely with the injection time as seen in the particle data. When comparing times in Table 1, recall that the particle observation of the injection time is a lower limit, since DMSP F7 crosses the midnight region auroral oval only twice every 101 min. In all cases there was corresponding magnetic activity; usually a fairly clear magnetic signature could be discerned corresponding to the injection.

The dawn sector data are from F6. For each dispersionless injection observed near midnight by F7, the observations of the auroral edge made by F6 closest in time to the injection were recorded in Table 1. Seven of the eight injection events for which there are dawn sector data show an injection, but only in one

case, near 0710 MLT, was a dispersionless injection observed (the December 10 event, at about 33200 s UT). This injection consisted of a large flux enhancement around -67° latitude, which was not the equatorward edge of high-latitude precipitation, but should presumably represent the equatorward edge of the auroral oval according to the views of *McIlwain* [1985] and *Meng and Akasofu* [1983]. In all other cases the precipitation did shift equatorward, but a clear boundary of dispersionless flux enhancement could not be distinguished.

The prenoon sector measurements, made by F7 on the same polar pass in which the dispersionless injection was seen near midnight, show three clear examples of dispersionless injections. The December 10, 1983, injection was exceedingly sharp, with ions of all energies and electrons of up to several keV changing from a preinjection mildly dispersive cutoff around 73.8° – 74.4° MLAT to a postinjection common cutoff at 72.7° MLAT. As is typical of such injections, the equatorward edge remained dispersionless for only the single pass; the next crossing of the auroral zone in this region showed the usual dispersion (a few degrees latitude) in the equatorward cutoffs. The prenoon sector data also show, however, four cases for which no sign of an injection could be discerned. That is, for these cases the equatorward edge did not move to lower latitude, and there was no clear flux enhancement at a common boundary. Section 3 contains some discussion of the possible meaning underlying this lack of a response. There were also four unclear cases, primarily such as in Plate 2b, where a sharp dispersionless boundary formed but appeared to correspond to the cusp boundary rather than to a dispersionless auroral boundary.

In the dusk sector measurements (from DMSP F6), there were three dispersionless injections identified; one ambiguous case; one dispersive injection; one case where no injection (whether dispersive or not) could be identified in the dusk data closest to the time of the midnight sector injection; and four cases where dusk sector data were not available close enough to the time of the midnight sector observation of an injection to allow any hope of making a meaningful conclusion (more than a half hour separation from the injection at midnight). More is said about the timing of the dawn–dusk observations versus those in the pre-midnight regime in section 3. The dispersionless injections in the dusk sector were always taken to be the equatorwardmost auroral precipitation, although sometimes a clear bifurcation (i.e., spatial separation) could be observed between the preinjection precipitation and the “new” precipitation (similar to the effect shown in Plate 1b for ions).

Altogether our collection of 10 events in which a dispersionless injection was seen in the near-midnight regime shows that there can be an accompanying injection at other local times with a longitudinal extent at least from 1740 MLT to 1040 MLT. As a comparison between Plates 1b and 1c illustrates, the relaxation time scale following an injection into a state in which the equatorward cutoffs in auroral precipitation are highly dispersive is short, less than one orbital period (101 min). This is typical of nearly all the injections observed, the chief exceptions being cases where a subsequent injection occurs.

All of the “dispersionless” injections studied here had a cutoff boundary which was dispersionless for the electrons and ions at least up to 3 keV in order to be included in the set. It turned out that such events ordinarily were moreover approximately dispersionless for the ions up to 30 keV, the highest energy measured; whereas for the electrons the energy at which dispersiveness appeared usually occurred below 10 keV. As seen at pre-midnight,

in the injection events the higher-energy electrons usually cut off poleward (hence tailward in the equatorial plane) of the few-keV electrons. Sample energy spectra are given in section 3, along with a comparison with typical geosynchronous observations.

3. DISCUSSION

The primary purpose of this study was a straightforward investigation of the premise that plasma is introduced into the middle magnetosphere during substorms in a highly characteristic way; namely, behind a dispersionless boundary common to both electrons and ions. According to the mapping subscribed to by general consensus, this should be reflected in the low-altitude, high-latitude precipitation (as measured, for example, by DMSP) in an equatorward shift of the equatorward cutoffs in electron and ion diffuse auroral oval precipitation to a common energy independent boundary. A complication is that substorm injections are generally accompanied by a dipolarization; that is, the tail field lines become more dipolelike. Thus the Earthward movement of the plasma tends not to be fully reflected in a corresponding equatorward shift of the diffuse aurora (that is, there is a tendency for the field lines and plasma to move in together). The present study is confined to cases in which a clear equatorward shift of the diffuse auroral oval was identifiable.

Ordinarily, the precipitation cutoffs vary up to several degrees as a function of energy [*Horwitz et al.*, 1986; *Newell and Meng*, 1987], corresponding to up to a few Earth radii in the equatorial plane. The DMSP data set shows that such low-latitude signatures do indeed occur: that coinciding with ground-based magnetometer signatures of substorm onset, the auroral oval near midnight (and at least sometimes at much earlier and later local times as well) can leap equatorward from a dispersive state to a comparatively dispersionless boundary.

We have here presented 10 events selected from a 25-day period. However, substorms occur, generally, several times a day. It is probable that each of these involves some energization or Earthward transport of plasma. However, only a subset of these meet our criterion of a greater than 1° shift in the equatorward edge of the auroral oval (so that we only study events which clearly involve Earthward transport). Moreover, for DMSP F7 to see a dispersionless injection, it must cross the midnight auroral oval within about 10 min of the injection, which a priori has about a 10–20% chance of occurring. Finally, we were reluctant to include many events that occurred during very active times, when it was difficult to see the effects of a single injection. It was necessary to examine the entire 25-day interval quite carefully to pick out 10 suitable injections. However, given the aforementioned constraints, this seems entirely consistent with the supposition that a dispersionless injection is associated with every substorm.

Another important question is the longitudinal extent of such injections. In at least some cases, the injection which appeared dispersionless at midnight appeared so also at local times as varied as 1040 MLT or 1740 MLT. It must be emphasized that what is referred to here are nearly simultaneous measurements (within less than 20 min). It is thus clear that it is not simply a case of particles injected near midnight subsequently convecting around, for this would result in much longer time delays. Similarly, a simple substorm enhancement of the cross-tail electric field cannot be an adequate representation of an injection event (a model investigated, for example, by *Ejiri et al.* [1980]), for in this case there would again be longer time delays before such significant flux enhancements and movement to lower latitudes were noticed, especially away from midnight. Therefore a process which

is qualitatively different from steady state convection is involved in the substorm introduction of plasma into the middle magnetosphere.

There remains the question of whether the existing structure (that is, the dispersive character) of the plasma sheet inner edge is preserved when plasma is introduced into, or farther into, the middle magnetosphere, as is suggested by the apparent signatures of steady state Alfvén layers in geosynchronous injection events [e.g., *Hultqvist et al.*, 1982; *Kivelson et al.*, 1980], or whether the highly impulsive substorm injection creates a new plasma sheet dispersive character, as the injection boundary model adherents must argue [*Quinn and Johnson*, 1985]. In actuality, the presubstorm character of the plasma sheet edge (insofar as it can be inferred from the high-latitude precipitation profile) is not consistent with the Alfvén layer picture to begin with [*Newell and Meng*, 1987]: an observation which still does not render moot the aforementioned question. *McIlwain* [1974, p.143] was of the opinion that "The ATS-5 data show considerable evidence for the presence of simple inward motion and compressive heating. Other aspects of the data indicate that inward convection is far from the whole story." *Mauk and Meng* [1983b, 1986], however, cast some doubts as to whether such inward motion ever introduces plasma into the middle magnetosphere. Many of the events listed in Table 1 are of injections which do not preserve the preexisting structure. For example, Plates 2a and 2b show how profoundly an injection can alter the Earthward edge of the plasma sheet.

As noted in Table 1, very often an injection which is seen as dispersionless near midnight by F7 will appear at dawn or dusk to be dispersive. These would appear to contradict the model of a dispersionless injection boundary which encircles the Earth [*McIlwain*, 1985]. It is necessary, however, to be careful about the precise timing of the observations at different local times, since a dispersionless injection boundary ordinarily disperses into an energy dependent boundary in less than one orbital period. In Table 1, a capsule summary entry in the dawn and dusk sectors is made if a relevant auroral oval encounter occurred within 20 min of the observation of the injection near midnight. It turns out that the measurements made by DMSP F6 in the dawn sector were in fact much closer in universal time (typically < 7 min) to the injection time than were those in the dusk sector. Thus, for example, in the single injection which appeared "dispersive" at dusk as reported in Table 1 (the December 11 event), there was a 15-min delay between the midnight observation and the dusk observation. In the "no clear injection" event of December 12, the two passes nearest in time were 18 min before the midnight observation and 36 min after the midnight observation. The former was used in the table as the closest entry; if the latter had been used, a "dispersive injection" would have been recorded. In fact, there is no evidence at all based on the current collection of events that a dispersionless injection at midnight is not always accompanied by an initially dispersionless injection at dusk.

However, because of the close time agreement between the dawnside observations and those at midnight, the evidence is much stronger that some injections which are dispersionless near midnight are dispersive near dawn. At prenoon the measurements are always separated from those at premidnight by about 10 min (earlier or later, depending on whether the satellite is in the northern or southern hemisphere, respectively). The events marked "no injection" in the prenoon sector remain in that category even

if the next encounter after the premidnight sector observation of the injection event is always used. There is, of course, the problem that ions of only a few keV and all electrons convect toward dawn, thus tending to obscure the equatorward edge of the possible injection boundary. Nonetheless, in each case marked "dispersive injection" in Table 1, an unsuccessful attempt was made to locate a common injection boundary at latitudes above the equatorward edge of precipitation. Hence the data indicate that an event that is seen as a dispersionless injection at premidnight will consistently be seen as an injection at dawn, sometimes dispersionless and sometimes not; and at still later local times (prenoon), the injection will sometimes not be (promptly) observable at all, will sometimes be observed as dispersionless, and will sometimes be dispersive.

The most straightforward interpretation of the data is that the substorm injection boundary extends from at least 1740 MLT to midnight and sometimes but not always extends into the morning sector. It is not incompatible with the injection boundary model to argue that during a substorm there is an enhanced cross-tail electric field; indeed, this appears to be a consensus view. Thus the events in which the "injection" appears dispersive at dawn may in fact be simply a movement of the plasma sheet as a whole (or perhaps the more Earthward portion of the plasma sheet) toward Earth. From this viewpoint, the cases in which no prompt injection was seen in the prenoon sector represent cases in which neither the plasma sheet nor the substorm injection boundary extended this far into the dayside. Such a conclusion must, of course, be quite tentative on the basis of the present data alone.

Figures 3a and 3b show a sample ion and electron spectrum, respectively, from a dispersionless substorm injection event observed by DMSP F7. These spectra are taken from the December 13, 1983, event listed in Table 1; they represent a 4-s average (during which the satellite covered about 0.5° latitude) over the equatorwardmost region of the injection at premidnight. Figure 3c, from *Kaye et al.* [1981], is for comparison; it represents the storm time plasma sheet at geosynchronous orbit as observed by SCATHA. The geosynchronous plasma, which is refreshed (enhanced) during each substorm, consists of a relatively soft field-aligned component, with a characteristic temperature of a few keV, and a more energetic isotropic component with a temperature, in this particular case, of around 10 keV. The lower-energy field-aligned ions have a highly enhanced oxygen component and are believed to be primarily of ionospheric origin. The transition between flux dominance of the two populations occurs in this example between 2 and 4 keV. *Quinn and Johnson* [1985] have discussed the role of the inner edge of the injection boundary as a source region for energizing oxygen during substorms.

Recall that the DMSP observations are only of the precipitating and hence field-aligned component. Referring to Figure 3a, the lower-energy portion of the ion injection measured by DMSP is approximately a 2-keV quasi-Maxwellian population and is therefore likely, according to the reports of *Fennell et al.* [1981] and *Kaye et al.* [1981], to be of ionospheric origin with an enhanced oxygen component. The bump seen at larger energies is said to be primarily an isotropic hydrogen plasma; DMSP is therefore only seeing that portion which is pitch angle scattered into the loss cone. *Kaye et al.* believe that this portion of the ion population is produced by inward convection from the plasma sheet. We will not here argue for a particular mechanism for the plasma injection; however, we wish to point out an often

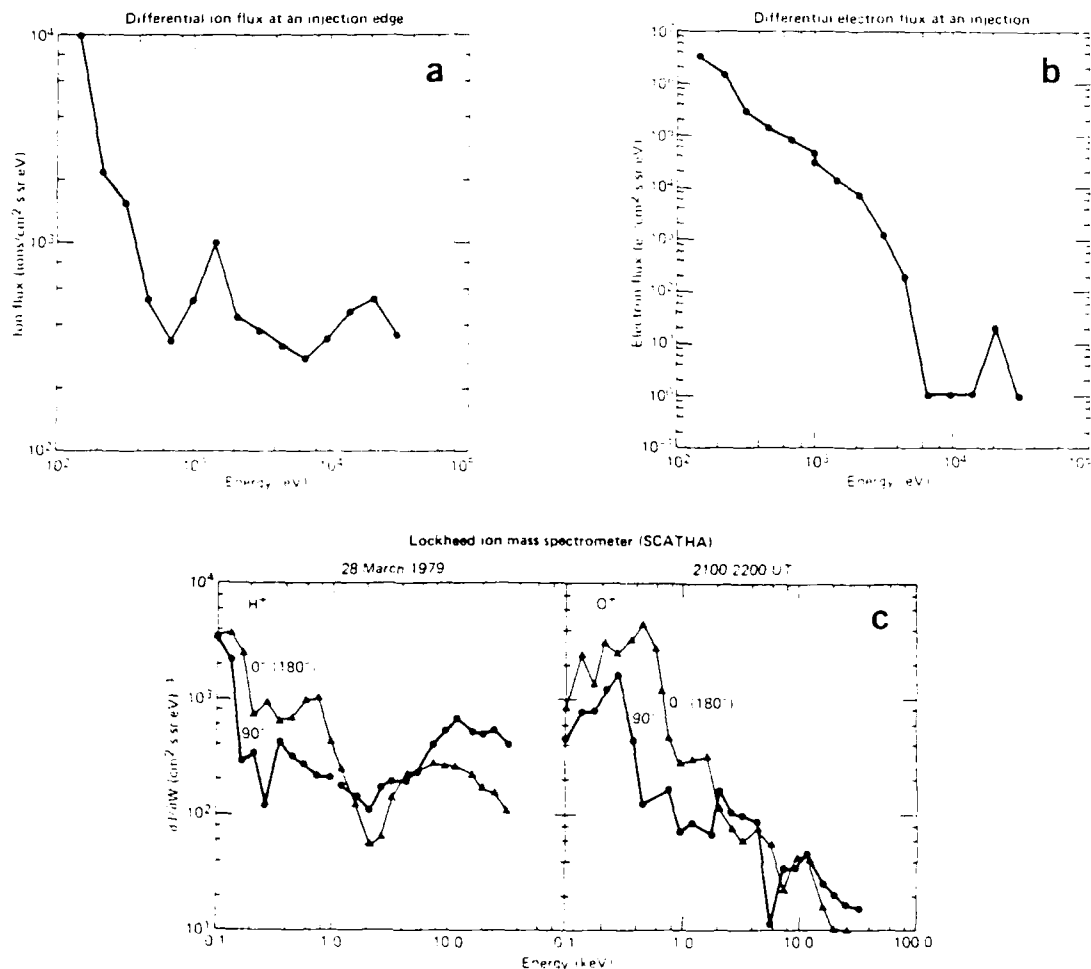


Fig. 3. (a) The ion flux averaged over 4 s (about 0.5° MLAT) at the equatorward edge of the newly injected flux for the event of December 13, 1983 (refer to Table 1). (b) Same as Figure 3a, except for the electron flux. (c) Some geosynchronous measurements of substorm injected ions, adapted from Kuvé *et al.* [1981]. Notice the bump at about 10 keV for the hydrogen, but not for the oxygen.

seen feature of the injection phenomenology, namely, the close coincidence in equatorward extent (Earthward penetration) of both ion populations.

The electron spectra observed at low altitudes by DMSP in these injection events are much cooler than in the dispersionless plasma injections reported by, say, ATS 6 and SCATHA. For example, the spectrum shown in Figure 3b corresponds to a temperature of about 600 eV. Other examples are somewhat higher, but Figure 3b is representative of most events. The DMSP electron observations show that the electron cutoff is common with the ion cutoff at all energies up to a few keV (at least 3 keV, usually not much more than 10 keV). Above a certain energy the electrons still show signs of an injection—that is, a movement of the cutoff to lower latitudes—but the injection is dispersive (thus the high-energy electrons are not represented in the spectrum of Figure 3b, since they were not present on the equatorwardmost edge). It seems very likely that this discrepancy is again related to the fact that the DMSP detectors count only electrons that are well within the loss cone. There is no reason to believe that pitch angle scattering occurs at the strong diffusion rate [Fairfield and Vörös, 1984]. Because of the very fast loss rate through

precipitation of field-aligned high-energy electrons, it may be that the introduction of plasma this close to Earth results quickly in a cooling among the electron population that is near the loss cone. Moore *et al.* [1981] discussed the degradation of the electron spectrum following an injection due to interaction with the ionosphere. The time scale for this process is about 1 hour, where our observations of the postinjection structure are always within about 10 min of the ground-based magnetometer signature.

It might be supposed that an independent check on whether the dispersionless injection boundaries reported on here are indeed examples of the boundary referred to in the substorm injection boundary models [McIlwain, 1974; Mauk and McIlwain, 1983a; etc.] would depend on whether the latitudinal position as a function of Kp of our boundary observations corresponds to the substorm injection boundary model position as specified by, say, McIlwain [1986]. In fact, such a comparison is circular. Formulas such as McIlwain's are based on data, similar to that of the DMSP satellites, on the statistical average position of the equatorward edge of the auroral oval. Our observations are precisely of the energy dependence of the equatorward edge of the oval. The present investigation simply shows that during a st

storm, immediately following an equatorward jump of the diffuse auroral oval edge, the precipitation cutoff is indeed often energy independent for ions of all energies measured and for electrons up to several keV.

4. SUMMARY AND CONCLUSIONS

We conclude that the substorm injection boundary model accurately describes at least some of the events in which plasma is introduced into (or deeper into) the middle magnetosphere. In the past, evidence for the phenomenological model of an initially dispersionless substorm injection boundary has been inferred by fairly indirect means, such as backtracking particle motions under assumed electric and magnetic fields to the initial boundary [e.g., McIlwain, 1974]. The present data on auroral precipitation cutoffs as a function of energy show that during substorms, abrupt equatorward jumps of the cutoffs are indeed often to an initially dispersionless boundary. Previous geosynchronous-based observations have been able only indirectly to infer the existence of a dispersionless injection boundary, and the DMSP observations are thus probably the most direct evidence to date for the hypothesized spatial characteristics of the substorm injection boundary model. By comparing the spectra with previous geosynchronous observations, we infer that the lower-energy ions (typically 1 to a few keV) probably belong to a field-aligned population of recent ionospheric origin, whereas the higher-energy ions are part of an isotropic hydrogen plasma. Both populations share a common boundary in these ion injection events. This dispersionless boundary can extend at least as far toward the duskside as 1740 MLT and at least as far past dawn as 1045 MLT. However, it is often the case that an injection which appears dispersionless in the premidnight regime will appear dispersive near dawn, even when the measurements are closely coincident in time. A more comprehensive statistical study of a larger data set should help clarify the morphology of dispersionless injections.

Acknowledgments. We thank the referees for thoughtful comments. This work was supported by the Atmospheric Sciences Division, National Science Foundation, grant ATM-8315041, and by the Air Force Office of Scientific Research, grant 84-0049.

The Editor thanks J. F. Fennell and another referee for their assistance in evaluating this paper.

REFERENCES

- Ejiri, M., R. A. Hoffman, and P. Smith, Energetic particle penetrations into the inner magnetosphere, *J. Geophys. Res.*, **85**, 653-663, 1980.
- Fairfield, D. H., and A. F. Viñas, The inner edge of the plasma sheet and the diffuse aurora, *J. Geophys. Res.*, **89**, 841-854, 1984.
- Fennell, J. F., D. R. Cowley, and S. M. Kaye, Low-energy ion pitch angle distributions in the outer magnetosphere: Ion zipper distributions, *J. Geophys. Res.*, **86**, 3375-3382, 1981.
- Greenspan, M. E., D. J. Williams, B. H. Mauk, and C.-I. Meng, Ion and electron energy dispersion features detected by ISEE 1, *J. Geophys. Res.*, **90**, 4079-4089, 1985.
- Gussenhoven, M. S., D. A. Hardy, F. Rich, W. J. Burke, and H.-C. Yeh, High-level spacecraft charging in the low-altitude polar auroral environment, *J. Geophys. Res.*, **90**, 11009-11023, 1985.
- Hardy, D. A., L. K. Schmitt, M. S. Gussenhoven, F. J. Marshall, H. C. Yeh, T. L. Shumaker, A. Hube, and J. Pantazis, Precipitating electron and ion detectors (SSJ-4) for the block 5D flights 6-10 DMSP satellites: Calibration and data presentation, *Rep. AFGL-TR-84-0317*, Air Force Geophys. Lab., Hanscom Air Force Base, Mass., 1984.
- Horwitz, J. L., S. Menteer, J. Turnley, J. L. Burch, J. D. Winningham, C. R. Chappell, J. D. Craven, L. A. Frank, and D. W. Slater, Plasma boundaries in the inner magnetosphere, *J. Geophys. Res.*, **91**, 8861-8882, 1986.
- Hultqvist, B., H. Borg, L. A. Holmgren, H. Keme, A. Bahnsen, M. Jespersen, and G. Kremser, Quiet-time convection electric field properties derived from keV electron measurements at the inner edge of the plasma sheet by means of GEOS-2, *Planet. Space Sci.*, **30**, 261-283, 1982.
- Kaye, S. M., E. G. Shelley, R. D. Sharp, and R. G. Johnson, Ion composition of zipper events, *J. Geophys. Res.*, **86**, 3383-3388, 1981.
- Kivelson, M. G., S. M. Kaye, and D. J. Southwood, The physics of plasma injection events, in *Dynamics of the Magnetosphere*, edited by S.-I. Akasofu, pp. 385-394, D. Reidel, Hingham, Mass., 1980.
- Konradi, A., C. L. Semar, and T. A. Fritz, Substorm-injected protons and electrons and the injection boundary model, *J. Geophys. Res.*, **80**, 543-552, 1975.
- Mauk, B. H., and C.-I. Meng, Characterization of geostationary particle signatures based on the "injection boundary" model, *J. Geophys. Res.*, **88**, 3055-3071, 1983a.
- Mauk, B. H., and C.-I. Meng, Dynamical injections as the source of near geosynchronous quiet time particle spatial boundaries, *J. Geophys. Res.*, **88**, 10011-10024, 1983b.
- Mauk, B. H., and C.-I. Meng, Macroscopic ion acceleration associated with the formation of the ring current in the earth's magnetosphere, in *Ion Acceleration in the Magnetosphere and Ionosphere*, *Geophys. Monogr. Ser.*, vol. 38, edited by T. Chang, pp. 351-361, AGU, Washington, D. C., 1986.
- McIlwain, C. E., Substorm injection boundaries, in *Magnetospheric Physics*, edited by B. M. McCormac, pp. 143-154, D. Reidel, Hingham, Mass., 1974.
- McIlwain, C. E., Equatorial magnetospheric particles and auroral precipitations, in *Results of the ARC-AD 3 Project and of the Recent Programmes in Magnetospheric and Ionospheric Physics*, pp. 275-280, Cepadues-Editions, Toulouse, France, 1985.
- McIlwain, C. E., A Kp dependent equatorial electric field model, in *Proc. COSPAR Meeting*, Toulouse, France, July, 1986, Committee on Space Research, Pergamon Press, 1986.
- Meng, C.-I., Conjugate low energy electron observations made by ATS-6 and DMSP-32 satellites, in *Quantitative Modeling of Magnetospheric Processes*, *Geophys. Monogr. Ser.*, vol. 12, edited by W. P. Olson, pp. 96-109, AGU, Washington, D. C., 1979.
- Meng, C.-I., and S.-I. Akasofu, Electron precipitation equatorward of the auroral oval and the mantle aurora in the midday sector, *Planet. Space Sci.*, **31**, 889-899, 1983.
- Moore, T. E., R. L. Arnoldy, J. Feynman, and D. A. Hardy, Propagating substorm injection fronts, *J. Geophys. Res.*, **86**, 6713-6726, 1981.
- Newell, P. T., and C.-I. Meng, Energy dependence of the equatorward cutoffs in auroral electron and ion precipitation, *J. Geophys. Res.*, **92**, 7519-7530, 1987.
- Quinn, J. M., and R. G. Johnson, Observation of ionospheric source cone enhancements at the substorm injection boundary, *J. Geophys. Res.*, **90**, 4211-4220, 1985.
- Whalen, J. A., A quantitative description of the spatial distribution and dynamics of the energy flux in the continuous aurora, *J. Geophys. Res.*, **88**, 7155-7169, 1983.

C.-I. Meng and P. T. Newell, Applied Physics Laboratory, Johns Hopkins Road, Laurel, MD 20707.

(Received December 30, 1986;
revised April 28, 1987;
accepted May 5, 1987.)

Simultaneous Polar Cap and Magnetotail Observations of Intense Polar Rain

M. E. GREENSPAN¹ AND C.-I. MENG

The Johns Hopkins University Applied Physics Laboratory, Laurel, Maryland

D. H. FAIRFIELD

Goddard Space Flight Center, Greenbelt, Maryland

Six prolonged episodes of intense polar rain with average or above average temperatures occurred during the four-month period from mid-February to mid-June 1978. Electrons with energies up to 1 keV are observed throughout these events, and 9-keV electrons occasionally are detected. To investigate whether this intense polar rain is accelerated within the magnetosphere, we compare DMSP F2 electron measurements made at low altitudes over the polar cap with near-simultaneous ISEE 1 electron measurements made in the northern tail lobe at distances between 10 and 22.6 R_E . In some cases, the electron spectra measured at low altitude are nearly identical to those measured in the tail lobe. In other cases, intensities are similar, but the phase space densities measured by DMSP exceed those measured by ISEE at energies above 500 eV. The episodes with extremely similar spectra show that intense polar rain can pass through the tail lobes without undergoing acceleration between 22.6 R_E and 800 km altitude. Three-dimensional ISEE measurements of electron distribution functions suggest that the field-aligned pitch angle anisotropy of the tail lobe electron population may account for most if not all of the differences when the spectra do not match.

INTRODUCTION

The term "polar rain" was introduced by Heikkila [1972] to describe the uniform, low-intensity precipitation of low-energy (< 1 keV) electrons over the earth's polar caps. This phenomenon was studied in more detail by Winningham and Heikkila [1974] and others. Detectable polar rain electrons typically have energies ranging from a few to a few hundred eV and temperatures below 100 eV. A typical integral flux (over the energy range 50 eV to 20 keV) is between 10^6 and 2.5×10^7 (cm² s sr)⁻¹ and a typical energy flux between 10^{-4} and 10^{-2} erg/(cm² sr s) [Winningham and Heikkila, 1974; Gussenhoven et al., 1984; Riehl and Hardy, 1986].

Examples of more intense and energetic polar cap precipitation have been observed by Winningham and Heikkila [1974], Foster and Burrows [1976], and Meng and Kroehl [1977]. Foster and Burrows reported unusually intense, energetic electron precipitation seen over the polar cap by instruments on ISIS 2 during quiet times after large storms. This precipitation was spatially uniform over large areas of the polar cap, and on one pass over the entire polar cap. The differential flux spectra measured during such precipitation had high-energy tails in the keV range. During magnetic storms, Meng and Kroehl observed electron fluxes as much as two orders of magnitude more intense than normal polar rain across the entire polar cap. This enhanced precipitation had spectra harder than those of normal polar rain. In addition to polar rain, Winningham and Heikkila [1974] defined two other classes of polar cap precipitation involving more energetic particles, "polar showers" and "polar squalls."

It has been proposed that solar wind electrons are the ultimate source of polar rain. This hypothesis is strongly support-

¹Now at Regis College Research Center, Weston, Massachusetts.

Copyright 1986 by the American Geophysical Union.

Paper number 5A8158.
0148-0227/86/005A-8158\$05.00

ed by studies that demonstrate that precipitation is more intense over one polar cap than the other. These studies have included both extended periods of typical polar rain [Fennell et al., 1975; Yeager and Frank, 1976; Mizera and Fennell, 1978; Gussenhoven et al., 1984] and selected intervals of unusually intense and energetic polar rain [Meng and Kroehl, 1977]. The preferred polar cap shows the same dependence on interplanetary magnetic field (IMF) sector structure as that observed when solar flare particles precipitate over the polar caps. This supports the idea, developed to explain polar cap observations of solar flare particles, that one polar cap is connected to field lines leading directly to the sun while the other polar cap is connected to IMF lines leading far out into the solar system. Fennell et al. [1975] suggest that the electrons moving outward from the sun that produce the more intense precipitation over the preferred polar cap are associated with the interplanetary heat flux.

Fairfield and Scudder [1985] discovered a field-aligned anisotropy in magnetotail observations of polar rain electrons. These authors argue that this observation confirms the solar wind source of the polar rain and, more specifically, that it identifies the field-aligned, hot component of the solar wind known as the "strahl" [Rosenbauer et al., 1976, 1977; Feldman et al., 1978; Pilipp et al., 1981; Ogilvie and Scudder, 1981] as the source of polar rain electrons above 100 to 200 eV. The strahl is believed to be made up of solar coronal electrons that make few collisions and undergo little scattering between the corona and 1 AU [Fairfield and Scudder, 1985]. As these electrons travel outward from the sun into regions of much weaker magnetic field, conservation of the first adiabatic invariant causes them to become extremely field-aligned. Because it is so narrowly confined to the field direction, the strahl is very difficult to measure; it was unknown at the time of early polar rain observations. If the first adiabatic invariant of solar wind electrons is conserved as they move into the much larger magnetic field of earth's magnetosphere, it is only such extremely field-aligned electrons that can reach the polar caps.

Fairfield and Scudder suggest that a well-developed strahl and

intense polar rain should occur when the density of the solar wind is low and velocity is high so that fewer electrons will be coulomb scattered away from field alignment as they move earthward from the inner solar corona. They point out that early observations showing similarity between the distribution functions of precipitating electrons over the polar cap and those of solar wind electrons with arbitrary pitch angles [Fennell *et al.*, 1975] were made when the solar wind was dense, and the strahl was apt to be less well-developed and anisotropies to be minimal.

Comparisons of polar rain and tail lobe electron spectra with magnetosheath and solar wind spectra have supported the hypothesis that typical polar rain reaches the polar caps from the solar wind without undergoing significant acceleration [Fennell *et al.*, 1975]. For more intense and energetic precipitation [Winningham and Heikkila, 1974; Foster and Burrows, 1976, 1977; Fairfield and Scudder, 1985], the situation is not so clear.

Foster and Burrows [1976, 1977] found no similarity between electron spectra measured during their observations of intense, energetic precipitation and near-simultaneous solar wind electron spectra and concluded that the precipitating electrons were energized within the magnetosphere. Fairfield and Scudder [1985], however, suggest that the source of the precipitation could have been energetic field-aligned interplanetary electrons that were too collimated to be detected. They hypothesize that the solar wind strahl may have been unusually well developed at the time of the observations by Foster and Burrows, allowing an anomalously large number of energetic solar electrons to reach the earth. An exceptionally low solar wind density at that time supports this view.

The two categories of energetic precipitation reported by Winningham and Heikkila [1974] are different in character from the energetic events described by Foster and Burrows [1976, 1977] and Meng and Kroehl [1977]. It is now clear that polar showers are associated with polar cap auroral arcs [Hardy, 1984]. Polar squalls extend over larger areas than showers, up to 3° or 4° of magnetic latitude. During squalls, total electron fluxes are greater than 10^7 (cm² sr s)⁻¹, and energy fluxes can be more than 0.1 erg/(cm² sr s). It is tempting to identify polar squalls with the intense, energetic precipitation reported by Foster and Burrows and Meng and Kroehl. However, squalls have limited spatial extent. Winningham and Heikkila have noted similar phase space densities of squall electrons and adjacent regions of polar rain, and, during squalls, differential electron fluxes sometimes show a marked secondary peak in the keV range. These observations suggest an acceleration process. Secondary peaks are characteristic of the spectra of auroral zone electrons that are accelerated by parallel electric fields. (See Meng [1978] for a review.) Parallel electric fields that might accelerate such electrons are also suggested by occasional observations of downcoming as well as upgoing ionospheric photoelectrons [Winningham and Heikkila, 1974; Winningham and Gurgiolo, 1982] and by accelerated barium ions [Heppner *et al.*, 1981].

The differences in the phase space densities of polar rain and of solar wind electrons and the presence of spatial gradients in the polar rain intensity and mean energy are not consistent with the unimpeded access of solar wind electrons to the polar cap. In the energy range from 50 to 250 eV, the phase space density of polar rain is typically an order of magnitude less than that of field-aligned solar wind electrons [Gussenhoven *et al.*, 1984; Feldman *et al.*, 1975]. Meng *et al.* [1977] reported gradients in the polar rain intensity along the dawn-dusk trajectory

of Defense Meteorological Satellite Program (DMSP) 32, and their control by the IMF B_y . Gussenhoven *et al.* [1984] made a statistical study of polar rain intensity and mean energy over the entire polar cap. They found that these quantities vary with location. The gradient of the average intensity runs from slightly premidnight (lowest intensity) to slightly prenoon (highest intensity), and the gradient of the average energy runs in the opposite direction, with lowest energy slightly prenoon and highest energy premidnight. Fairfield and Scudder [1985] propose the existence of a modest, spatially varying electric field in the vicinity of the magnetopause boundary layer. By impeding the direct entry of solar wind electrons, such a field could account for both the differences in the phase space densities of solar wind and polar rain electrons and the gradients. Gussenhoven *et al.* [1984] suggest that the gradients may result from acceleration by an electric field within the magnetosphere.

Our goals in this work are to determine whether acceleration processes are necessary to explain the energies and temperatures of the electrons seen during periods of intense polar rain, and to understand whether and how the occurrence of intense polar rain is controlled by the IMF and solar wind. The availability of near-simultaneous DMSP data from the northern polar cap and ISEE data from the northern tail lobe for many hours during a period of four months provides a unique opportunity to investigate the first of these questions. To search for evidence of an acceleration region, we compare DMSP observations of the precipitating electrons over the polar cap with simultaneous ISEE 1 electron measurements in the conjugate tail lobe at distances between 10 and 22.6 R_E . To explore the second question, we examine the solar wind and IMF conditions during which the intense polar rain events occur.

OBSERVATIONS

Electron data from the satellites DMSP F2 and ISEE 1 are used in this paper. The DMSP F2 spacecraft was launched in July 1977 into a low-altitude (840 km), circular, polar orbit. Immediately after launch, the orbit plane was centered near the 0700–1900 LT meridian. The orbit gradually precessed toward later local times, so that by June 1978 it was located near the 0800–2000 LT meridian. The precipitating electron detector had two cylindrical-section electrostatic analyzers that measured fluxes in 16 energy channels between 50 eV and 20 keV once each second. The low-energy analyzer, measuring particles with energies between 50 and 1045 eV, had an angular acceptance of 4° by 5°. The high-energy analyzer, measuring electrons with energies between 1060 eV and 20 keV, had an angular acceptance of 2° by 10°. The analyzers looked along the local zenith, within ~10° of the magnetic field direction over the polar cap. At DMSP's low altitude, electrons with such small pitch angles belong to the precipitating rather than the trapped or backscattered population [Hardy *et al.*, 1982].

ISEE 1 was launched on October 22, 1977, into an eccentric orbit with an apogee of 22.6 R_E and a perigee of 700 km. The orbit had an inclination of 30° and a period of 57 hours. In 1978, tail lobe data were available only in the northern hemisphere. In this paper, we examine measurements made by the low-energy electron spectrometer. This instrument had 16 logarithmically spaced energy channels, covering one of three energy ranges, 7.5 to 512 eV, 11 to 2062 eV, and 109 to 7285 eV. The ISEE 1 data presented in this paper were taken when the instrument was operating in the 11- to 2062-eV or the 109- to 7285-eV range. The experiment consisted of two sets of three

orthogonal cylindrical-section electrostatic analyzers with 8.5° by 11° viewing angles. Each of these six detectors made six 0.5-s energy sweeps during a 3-s satellite spin period to give good measurements of the three-dimensional electron distribution function. For a more complete description of the instrument, see *Ogilvie et al.* [1978].

SELECTION OF PERIODS OF INTENSE POLAR RAIN FOR ANALYSIS

For our study, we have selected periods of polar rain with above average intensity and with average or above average electron temperature. The most intense and highest temperature cases in our study have intensities and temperatures in some energy ranges that equal or exceed those of the intense, energetic polar rain reported by *Meng and Kroehl* [1977] and the intense polar cap precipitation reported by *Foster and Burrows* [1976]. It thus seems reasonable to initiate a search for evidence of acceleration with this subset of polar rain passes. A further reason for using this subset of the data is that the high intensities during these time periods result in optimum counting statistics at both DMSP and ISEE.

The following criteria were used to select periods of polar rain for analysis: that the total flux in the energy range 50 eV to 20 keV exceed 10^7 electrons/($\text{cm}^2 \text{ s sr}$), that the ratio of counts in the 50-eV to those in the 660-eV channel be less than 4, and that the ratio of counts in the 110-eV to those in the 1060-eV channel be less than 20. These criteria were chosen to permit the easy recognition of intense polar rain with average or above average temperature from plots of count rates and integral fluxes. The criteria are equivalent to requiring that the ratio of phase space density at 50 eV to that at 660 eV be less than 8.8×10^2 and the ratio of phase space density at 110 eV to that at 1060 eV be less than 5.5×10^3 . Since the temperature of a Maxwellian is inversely proportional to the slope of a plot of $\ln(f)$ versus E , this definition is equivalent to requiring effective "temperatures" in the two intervals that are greater than 90 eV (1.04×10^6 K) and 110 eV (1.28×10^6 K), respectively. Our criteria were met for at least one minute during a polar cap pass by the eyeball average of the count rates (using 25-min line plots) and the total electron flux (using 10-min line plots). Passes for which the line plots showed large or rapid fluctuations in count rates or total flux were eliminated from the study. One minute of data corresponds to satellite motion through approximately 3.5° or 450 km along the orbit. In most of the observed cases, the intense polar rain extended over most or all of the polar cap, covering distances much greater than this lower bound.

We have searched the four-month period during which both DMSP polar cap data and ISEE 1 tail lobe data are available in order to identify episodes of polar rain that meet our criteria. This period lasted from February 10, 1978 to June 10, 1978 (two years prior to solar maximum). We identified six prolonged occurrences of such intense polar rain, lasting from 26 hours to 4.5 days, during this interval. These events begin on March 9, April 3, April 11, April 14, April 18, and May 30. There were a few briefer periods that met the criteria for inclusion in this study. During the study period, there were 12 days when DMSP electron data were not available or were contaminated by solar protons. Although solar protons were present on April 18, careful examination of the DMSP data and comparison with IMP 8 energetic particle measurements show that solar proton fluxes

were not large enough to affect significantly the spectra shown in Figures 1, 3, or 4e.

Roughly 10% of polar rain meets our criteria for intensity and temperature. *Gussenhoven et al.* [1984] found that 19% of passes with polar rain have fluxes greater than 10^7 /($\text{cm}^2 \text{ s sr}$). We found 240 DMSP polar rain passes that met this intensity criterion during the four-month period studied. Of these passes, 129 (or 54%) met our temperature criteria as well.

The three distribution functions of Figure 1 are calculated from averages of sixteen 1-s energy scans. The distributions of 1010:42 UT, March 9, 1978, and 1030:45 UT, April 18, 1978 meet the criteria for inclusion in this study, while that of 1125:35, May 26, 1978 does not. This example of low-temperature, low-intensity polar rain is included for comparison. The distribution of March 9 is one of the less intense, lower-temperature examples to meet our criteria, while that of April 18 is among the most intense and energetic observed. Using a linear least-squares fit, we have determined the slopes of the best-fit straight lines through the five lowest energy points of the three curves of Figure 1. The abscissas of the points lie between 51 and 264 eV. On March 9, the reciprocal of the slope indicates a "temperature" of 95 eV and on April 18, 155 eV, while on May 26, the effective temperature in this range is 48 eV. In all three cases, the correlation coefficients exceed 0.97. At higher energies, the spectrum for May 26 becomes similar to that of March 9. In contrast, on April 18, the phase space density falls off slowly with increasing energy at energies less than 1600 eV, and then begins to decrease fairly rapidly.

Count rates across the polar cap for the three passes during which the distribution functions of Figure 1 were measured are shown in Figure 2. The left column shows the low-intensity, low-temperature polar rain of May 26, 1978, the center column, the moderately intense and more energetic polar rain of March 9, 1978, and the right column the very intense and high-temperature polar rain of April 18, 1978. The increase in the count rates from left to right is clear. On April 18, 1978, count rates exceed those typical of polar rain at energies up to 8990 eV. The central and right columns demonstrate the occurrence of intense polar rain over the entire polar cap, with an absence of abrupt spatial and temporal variations.

Figures 1 and 2 illustrate that polar rain varies in both spectral shape and intensity. Figure 3 contrasts the three examples of Figure 1 with the average polar rain spectra from *Gussenhoven et al.* [1984] and with the extremely intense and energetic polar cap precipitation observed by *Foster and Burrows* [1976]. In Figure 3, the spectra labeled "Gussenhoven et al. 1 and 2" are averages at opposite boundaries of the polar cap: spectrum 1 of data taken at local noon and 79° magnetic latitude and spectrum 2 of data taken at local midnight and 75° magnetic latitude. The averages include only the data from the hemisphere in which polar rain is most probable and most intense—the northern hemisphere when $B_z < 0$, and the southern hemisphere when $B_z > 0$. As *Gussenhoven et al.* [1984] pointed out, these spectra show that the polar rain intensity decreases and temperature increases from the dayside to the nightside edge of the polar cap. An average spectrum from within the polar cap would be intermediate in intensity and temperature. The data of the three examples from Figure 1 were taken on the nightside of the polar cap.

On May 26, 1978, the intensity of the polar rain was very low. The spectral shape is similar to that of spectrum 1 of *Gussenhoven et al.* [1984], although that spectrum represents an

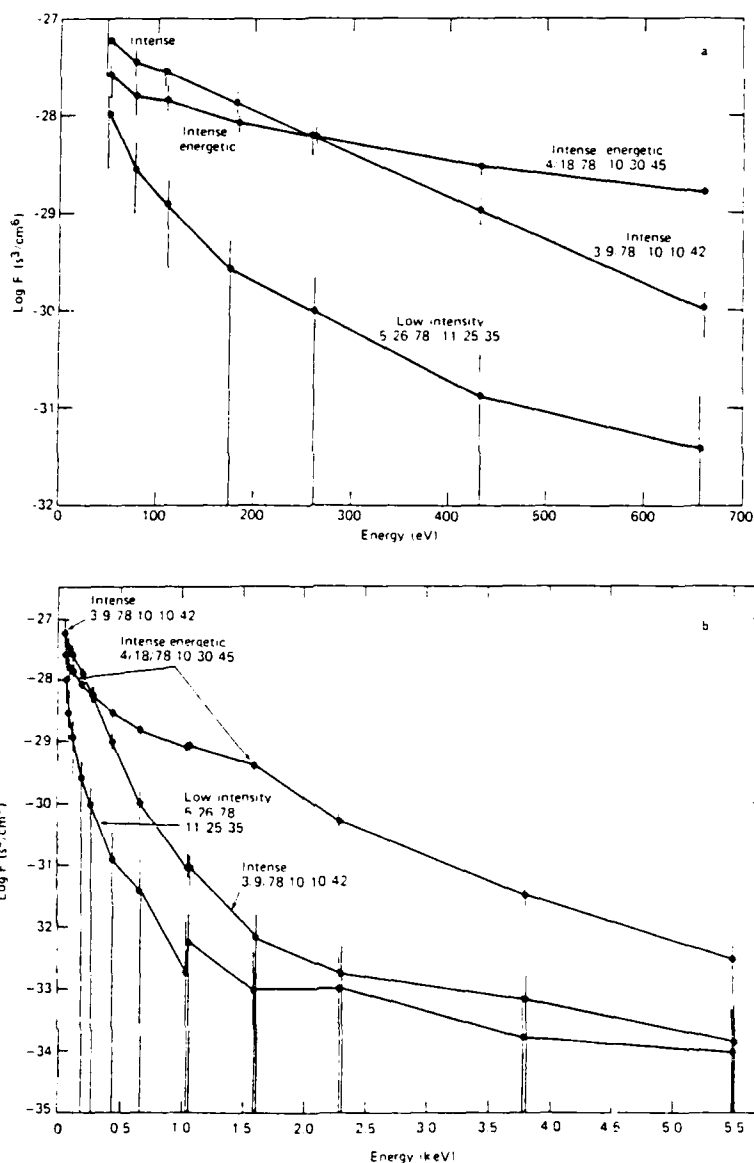


Fig. 1. Distribution functions illustrating the non-Maxwellian distributions and variable intensities of the polar rain measured by DMSP F2. Each distribution is computed from the average of sixteen 1-s energy scans. Figure 1a shows phase space densities in the energy range 0-700 eV, and Figure 1b phase space densities in the range 0-5500 eV. The error bars indicate one standard deviation in count rates.

average of data taken on the noon edge of the polar cap, while the May 26 data were taken on the nightside of the magnetic pole. In contrast, the two spectra that meet the criteria for inclusion in this study, those of March 9, 1978 and April 18, 1978, exceed the average polar rain intensity. On March 9, the spectrum resembled spectrum 2 of Gussenhoven et al., from the midnight edge of the polar cap, while the April 18 spectrum is clearly harder over the energy range from 200 to 1600 eV.

The March 10, 1972 spectrum of Foster and Burrows [1976] differs from our March 9, 1978 and April 18, 1978 cases. It is extremely intense, and the differential flux spectrum shows an increase in temperature or decrease in spectral index at 700 eV. Foster and Burrows [1977] point out that this may indicate the presence of two particle populations with different origins.

It is to explain this type of spectrum that Foster and Burrows [1977] postulate the existence of a fluctuating electric field. Because of the difference in the character of this spectrum and the intense polar rain analyzed in this study, we cannot be certain that the two have the same origin or that conclusions based on our data apply to the event of Foster and Burrows.

COMPARISON OF LOW ALTITUDE POLAR CAP AND DISTANT TAIL LOBE MEASUREMENTS

A crucial question about the unusually intense fluxes of polar rain electrons observed by DMSP is whether they have unimpeded access from the solar wind or are accelerated in the distant magnetotail. The unusually high temperatures during some of these events make the question more pressing. In this

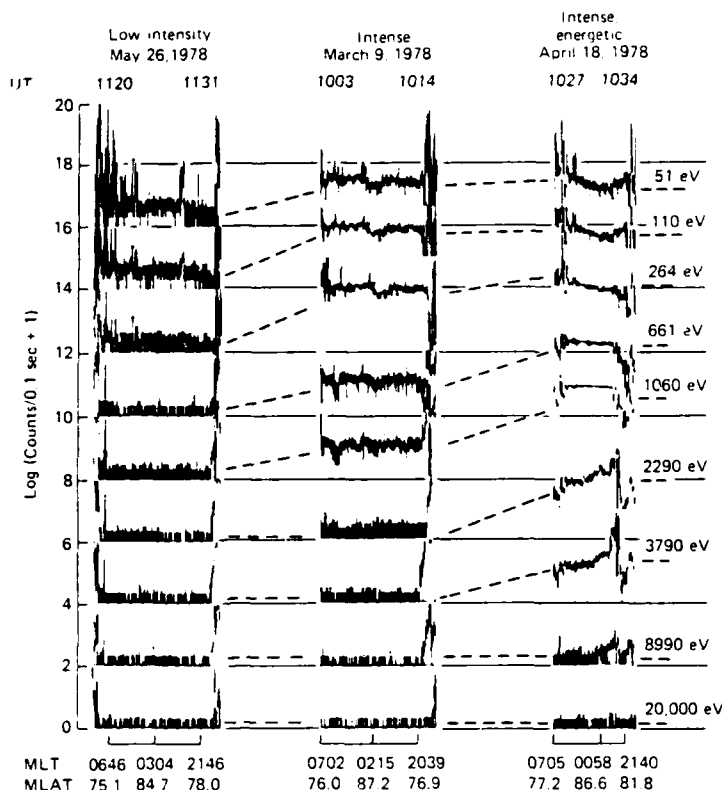


Fig. 2. Count rates across the polar cap during the three passes during which the distribution functions of Figure 1 were measured. The left column shows low-intensity, low-temperature polar rain occurring between 1120 UT and 1131 UT, May 26, 1978, the middle column intense polar rain occurring between 1005 UT and 1012 UT on March 9, 1978, and the right column intense, quite energetic polar rain occurring between 1028 and 1032 on April 18, 1978. Magnetic local time (MLT) and latitude (MLAT) are shown across the bottom of the count rate plots, and universal time (UT) across the top. The logarithms (base 10) of $(1 + \text{counts per } 0.1\text{-s accumulation period})$ are shown for nine energies between 51 eV and 20 keV. The energies are given on the right. The baseline for 20 keV is at the bottom of the figure, and each successively lower-energy channel is displaced upward by two decades. The dashed lines connect count rates at the same energies.

section, we compare DMSP electron spectra with those measured at ISEE. Our goal is to determine whether the source of the electrons detected by DMSP is the population measured by ISEE, and, if so, whether the electrons are accelerated between ISEE's location at 10 to 20 R_E in the tail lobe and the position of DMSP 840 km above the earth in the polar cap.

Simultaneous northern polar cap data from DMSP and northern tail lobe data from ISEE are available during four of the six prolonged intense precipitation events that occurred during the period studied. Figure 4 shows spectra measured at the two satellites during these four events and, for comparison, spectra measured at the two satellites during the low-temperature, low-intensity period of polar rain on May 26, 1978. The DMSP spectra are averages of sixteen 1-s energy sweeps. At ISEE 1, it is important to use measurements made as close to the magnetic field direction as possible because electrons precipitating at DMSP have pitch angles less than 2° at ISEE. For this reason, we select and average those ISEE 1 measurements made nearest to the magnetic field direction during individual 3-s spin periods. The averages include 8 to 12 sequential measurements and cover time periods ranging from 100 to 200 s. The numbers adjacent to the ISEE spectra give the averages of the pitch angles at which the ISEE measurements were made.

The times at which each set of spectra was measured, the magnetic coordinates of DMSP, the radial coordinate of ISEE

1 in earth radii, and the location of the foot of the ISEE 1 field line according to the *Mead and Fairfield* [1975] magnetic field model are shown on each plot in Figure 4. The captions show that we have been able to obtain near-simultaneous and approximately conjugate data from the two spacecraft. Because electron count rates are fairly uniform across large regions of the polar cap during these events, exact magnetic conjugacy of the two spacecraft is not necessary for a meaningful comparison.

Figure 4a shows spectra taken during the May 26, 1978 period of low-intensity and low-temperature polar rain that was illustrated in Figure 2. The two spacecraft were at different local times when the data of Figure 4a were obtained. However, Figure 2 shows that polar rain fluxes were fairly uniform across the polar cap, with no dawn-dusk gradients apparent during this time. The polar cap distribution function measured by DMSP and the tail lobe distribution function measured by ISEE on May 26 during this period are similar in shape. For both spacecraft, counting rates are very low at energies above 300 eV, and the data are not plotted. Below 200 eV, the spectra from both DMSP and ISEE have apparent temperatures on the order of 40 eV. These temperatures are smaller than those measured during the periods of intense polar rain included in this study.

Figure 4 reveals two patterns of similarities and differences between the electron distribution functions observed by DMSP

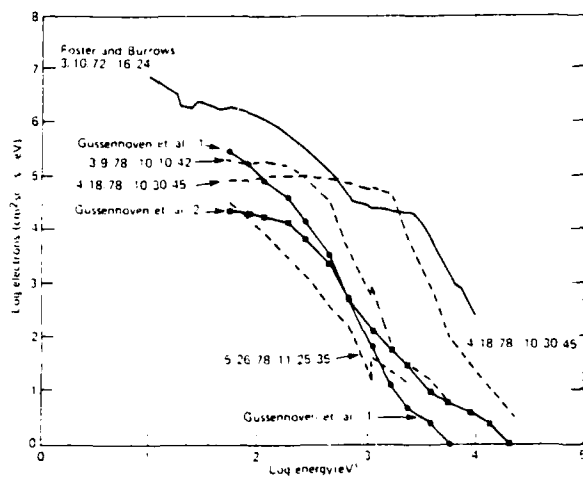


Fig. 3. Comparison of the spectra of Figure 1 and the observations of other authors. The dashed spectra are differential fluxes calculated from the DMSP data displayed as phase space densities in Figure 1. The curve labeled "Foster and Burrows" is an ISIS 2 polar cap spectrum measured at 1629 UT on March 10, 1972, during a period of very intense, uniform polar cap electron fluxes [Foster and Burrows, 1976, Figure 3]. The curves labeled "Gussenhoven et al. 1 and Gussenhoven et al. 2" are average polar rain spectra from Gussenhoven et al. [1984, Figure 6]. Both spectra are averages over data taken when $B_z > 0$ ($B_z < 0$) in the northern (southern) polar cap. Gussenhoven et al. 1 is an average spectrum at 79° corrected geomagnetic latitude (CGL) at local noon, and Gussenhoven et al. 2 at 75° CGL at local midnight.

and ISEE during the selected periods of intense polar rain. The spectra of March 10, 1978 (Figure 4b), and May 30, 1978 (Figure 4c) are virtually identical in phase space density at energies below 800 eV where counting statistics are best. (The error bars show one standard deviation.) In Figures 4b (March 10) and 4c (May 30), the average pitch angle at which the ISEE measurements were made first decreases and then remains nearly constant with increasing energy at energies where meaningful comparisons can be made. The striking similarities between the DMSP and ISEE spectra during these two time periods suggest that the electrons that DMSP observes at low altitude over the polar region have traveled through the tail lobes without undergoing significant acceleration between the two satellites.

On April 11, 1978 (Figure 4d) and April 18, 1978 (Figure 4e), the electrons observed by DMSP appear to have a higher temperature than those observed by ISEE. (ISEE and DMSP spectra from hour 3 on April 18 are compared in Figure 4e because ISEE 1 tail lobe data were not available during hour 10 when the April 18 DMSP measurements shown in Figures 1 through 3 were made.) At high energies, the ISEE phase space densities are smaller than those seen at DMSP. For these two spectra, the average pitch angles at which the ISEE measurements were made increase with energy and exceed 20° at 1 keV. A probable cause for the differences between the electron distribution functions measured at DMSP and at ISEE on April 11, 1978 (Figure 4d) and April 18, 1978 (Figure 4e) is pitch angle anisotropy in the tail lobe electron population. ISEE measurements of tail lobe electron distribution functions show marked pitch angle anisotropies [Fairfield and Scudder, 1985]. At a fixed energy, the distributions show peaks in the measurements made close to 0° and 180° . The field alignment becomes more pronounced with increasing energy. Figure 5 shows an example. These data were taken during the same time period as the April 18 spectra

shown in Figure 4e. Field alignment becomes noticeable at energies greater than or equal to 180 eV. This energy is close to that at which the ISEE distribution function begins to fall below that measured at DMSP. The degree of field alignment at ISEE increases with increasing energy until counts fall close to background at all pitch angles at 1.03 keV.

The magnetic field increases by three orders of magnitude from ISEE's location to DMSP's. Conservation of the first adiabatic invariant means that only particles with pitch angles less than 2° at ISEE will reach DMSP. The ISEE electron spectrometer does not always sample these particles, which, in any case, are confined to a solid angle less than the 8.5° by 11° aperture of the detector. The critical question then is how well the sampled electrons represent the extremely field-aligned population that will reach DMSP. The increase in phase space density at pitch angles approaching 0° and 180° illustrated in Figure 5 and typical of ISEE tail lobe data suggests that phase space densities within 2° of the field line may be still higher and increase with increasing energy at energies above 180 eV. The cases of Figures 4b and 4c in which ISEE and DMSP distribution functions are extremely similar are those in which the pitch angles of the ISEE measurements decrease with increasing energy up to 800 eV and are only 12° at 1 keV. The two cases of Figures

May 26, 1978

Time
 ---- DMSP 11:25:51 - 26:07
 — ISEE 11:13:10 - 15:36

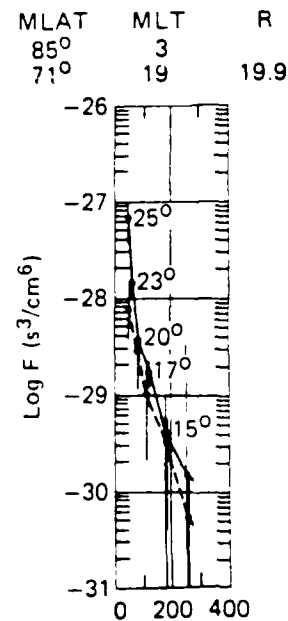


Fig. 4a. Near-simultaneous DMSP F2 polar cap and ISEE 1 tail lobe distribution functions during a period of low-intensity and low-temperature polar rain on May 26, 1978. The DMSP distributions are calculated from averages of sixteen 1-s energy scans. The ISEE distributions are averages of data from 8 to 12 satellite spins. The error bars for the DMSP spectrum indicate one standard deviation in the count rates, and those for the ISEE spectrum, one standard deviation in the phase space density. The numbers adjacent to the ISEE distribution functions are averages of the pitch angles at which the ISEE measurements were made.

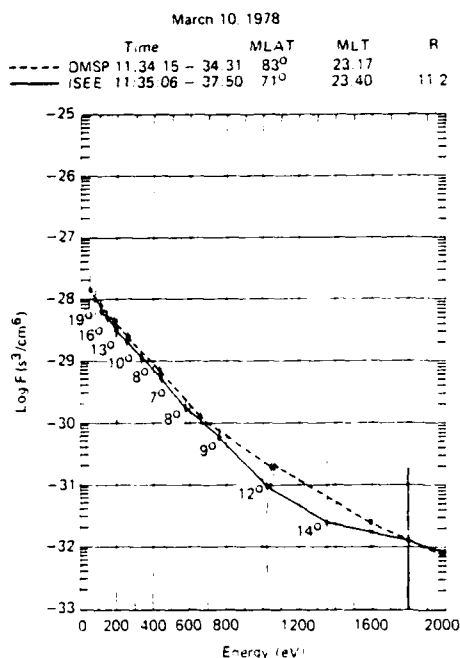


Fig. 4b. DMSP F2 and ISEE 1 distribution functions during a period of intense polar rain on March 10, 1978. The ranges of energy and phase space density shown are larger, but the format is otherwise the same as that of Figure 4a.

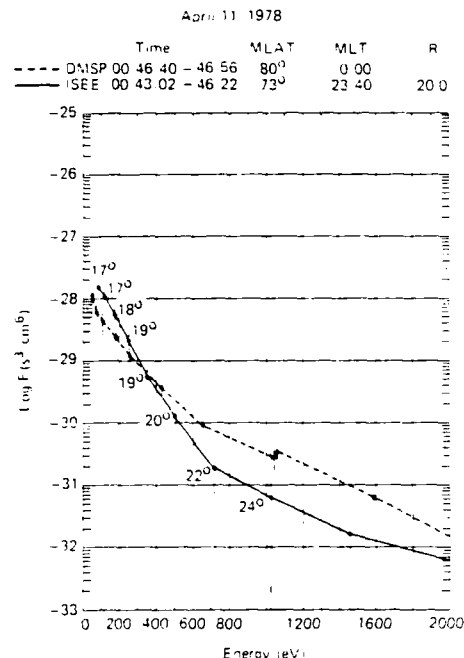


Fig. 4d. DMSP F2 and ISEE 1 distribution functions during intense polar rain on April 11, 1978. Same format as Figure 4b.

4d and 4e, where ISEE and DMSP distribution functions diverge at high energies, are those in which the ISEE pitch angles increase with increasing energy, up to 20° at 1 keV. These data do not permit us to rule out the presence of an acceleration region, but do suggest that the pitch angle anisotropy of the tail lobe electron population plays the major role in producing the differences between the ISEE and the DMSP spectra.

COMPARISON WITH IMF SOLAR WIND,
AND MAGNETOSPHERIC ACTIVITY

The existence of a clear relationship between the occurrence of unusually intense or energetic polar rain and the solar wind velocity and density, the magnitude and direction of the IMF, or the level of magnetospheric activity could provide valuable information about the origin of polar rain. *Fairfield and Scud-*

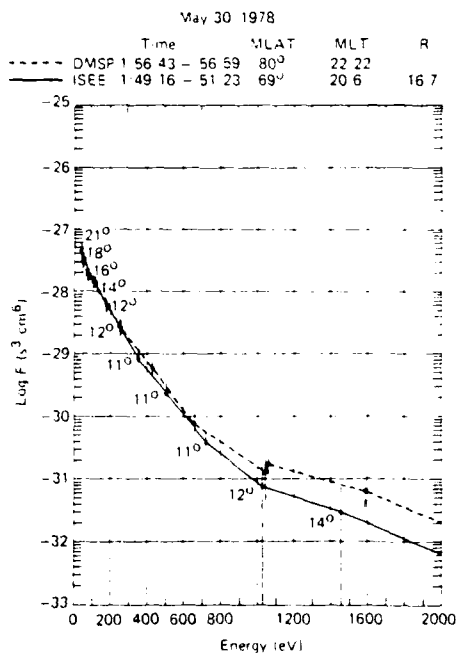


Fig. 4c. DMSP F2 and ISEE 1 distribution functions during intense polar rain on May 30, 1978. Same format as Figure 4b.

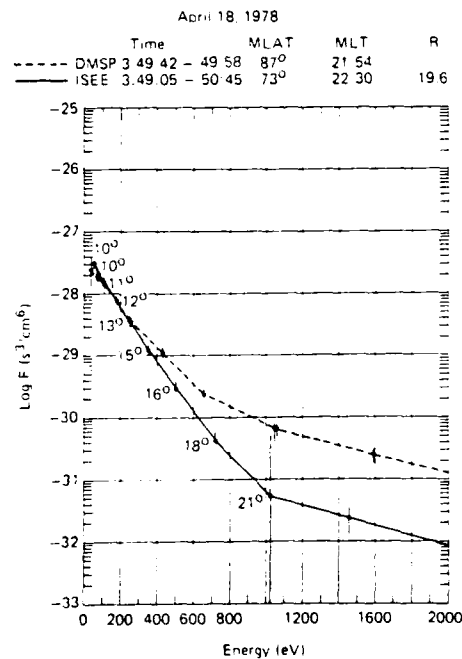


Fig. 4e. DMSP F2 and ISEE 1 distribution functions during intense polar rain on April 18, 1978. Same format as Figure 4b.

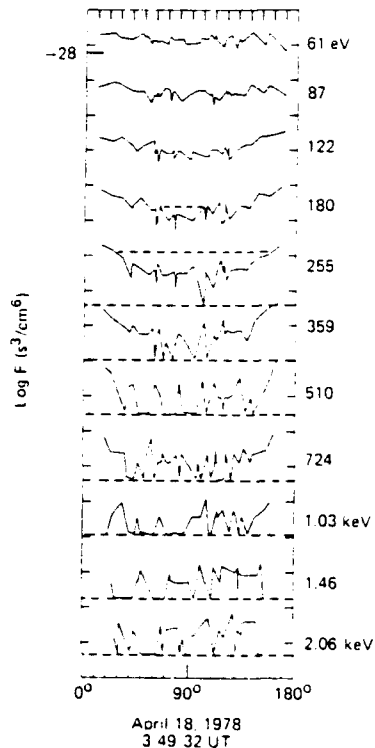


Fig. 5. Phase space density as a function of pitch angle for various electron energies measured by the Goddard vector electron spectrometer on ISEE 1. Each trace is offset by 1.25 decades to prevent overcrowding. The dashed lines indicate the instrumental one count level.

der [1985] suggest that intense and energetic polar rain should appear preferentially during periods of high solar wind velocity and low density, when an intense strahl is most likely to exist. Control of the hemisphere in which intense polar rain occurs by the IMF sector structure would confirm that this precipitation behaves in the manner typical of polar rain, a manner that suggests a solar wind source [Fennell, 1973; Fennell et al., 1975; Yeager and Frank, 1976; Meng and Kroehl, 1977; Meng et al., 1977]. The sign of the IMF B_z has a strong influence over polar cap conditions, and a strong dependence of the probability of occurrence of intense polar rain on the sign of B_z would constrain models of its origin. A tendency for the intense polar

rain of our study to occur during disturbed magnetospheric conditions might suggest a magnetospheric source or acceleration mechanism. To search for such relationships, the four-month period during which both DMSP polar cap data and ISEE 1 tail lobe data were available was surveyed.

Clear relationships between the probability of occurrence of intense polar rain and the solar wind velocity and density, the amount of geomagnetic activity as indicated by the daily sum of K_p or the sign of the IMF B_z were not found. Figure 6 illustrates the lack of such clear relationships. Periods of intense polar rain that met the study criteria are indicated by shading. Five of the six prolonged intervals of intense polar rain found during our study took place during the time span shown by the figure. They began on March 9, April 3, April 11, April 14, and April 18. The figure shows that such intervals may begin at or shortly after large increases in the solar wind velocity, as on April 11, several days after such an increase but while the solar wind velocity is still high, as on April 14, or during times when the velocity is less than 450 km/s, as on April 19. The very intense and energetic event of April 18 through 20 takes place during a time when the solar wind density swings rapidly from fairly high to extremely low and back. It is at such times of extremely low solar wind density that Fairfield and Scudder [1985] predict the most intense strahl. The event of March 9 through 13 also occurs during a period when the density is less than $10/\text{cm}^3$. However, four of the events occur during peaks in the solar wind density. The four April events occur at or near peaks in the daily sum of K_p , but the event of March 9 through 13 and that of May 30 through June 1 occur when the sum of K_p is fairly low, indicating less active conditions within the magnetosphere.

Intense polar rain occurs during a wide range of IMF B_z values. There are 37 polar cap passes during our study during which intense polar rain was observed and IMF data are available. The hourly average IMF B_z was < 0 during 17 of these passes, and ≥ 0 during 20 passes, ranging in values from -9.1 nT to 6.4 nT. B_z may change signs several times during a prolonged period of intense polar rain. Neither is there a clear relationship between the onset of these events and IMF sector crossings. These results show that the occurrence of intense polar rain is not strongly correlated with the solar wind velocity or density, the degree of magnetospheric activity, or the direction of the IMF B_z . The lack of a clear relationship with solar wind bulk parameters does not prove that intense polar rain occurs independently of solar wind electron conditions, but may sim-

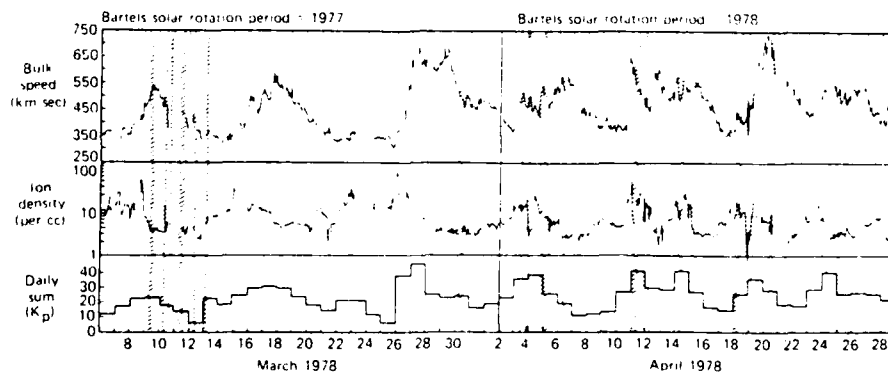


Fig. 6. Shaded bars mark occurrence of intense polar rain that met the study criteria during Bartels rotations 1977 and 1978. Also shown are solar wind velocity, solar wind density, and daily sum of K_p .

ply indicate that the bulk parameters, which are determined by the protons, do not reflect changes in the solar wind electron distribution function.

Intense polar rain that meets the criteria for inclusion in this study usually occurs over the northern polar cap during IMF away sectors and over the southern polar cap during toward sectors. This is the behavior shown by more typical polar rain and by energetic solar particles [Fennell, 1973; Morfill and Scholer, 1973; Paulikas, 1974; Fennell et al., 1975; Yeager and Frank, 1976; Meng and Kroehl, 1977; Meng et al., 1977]. Such behavior is expected if these fluxes originate in the anisotropic solar wind electron population and travel adiabatically to the polar caps. Hourly averages of spacecraft measurements of the IMF were available for 35 of the polar cap passes included in this study [King, 1983]. In these cases, the IMF sector was determined by assuming that GSE longitudes in the range 45° to 225° indicated away sectors and all other longitudes indicated toward sectors. For 67 more passes, we used the IMF sector inferred from ground magnetograms and reported by Lincoln [1978]. Combining the two sets of data, we found that intense polar rain with temperature at or above average occurred in the predicted hemisphere during 81 passes, and in the other hemisphere during 21 passes.

Perfect agreement is not expected for several reasons. Most cases of intense polar rain in the unexpected hemisphere occurred on days when such precipitation was observed in both hemispheres or during a transition between solar wind sectors or both. The IMF sector is inferred from ground magnetograms, which depend on the sign of B_z , by assuming that the IMF is in one of the normal garden hose quadrants [Svalgaard, 1974]. This is untrue approximately 17% of the time [Wilcox, 1968]. Neither an hourly average nor a sign inferred from ground magnetograms for a half-day period is the same as an instantaneous determination of the IMF sector. It is also possible that, because of small-scale twisting of the IMF, the sector determined from near-earth measurements occasionally may be incorrect.

DISCUSSION

Prolonged episodes of intense polar rain with electron temperatures at or above the polar rain average are fairly common in DMSP data. As is typical of polar rain, the electron distribution functions during such episodes are non-Maxwellian, with high-energy tails. The spectral shape of the intense polar rain included in this study remains quite constant during a single DMSP pass across the polar cap. However, variations in the spectra occur from pass to pass during an event, and from event to event. As Figure 1 shows, such variations can occur in different parts of the energy range 50 eV to a few keV. Count rates are large enough that these differences cannot be attributed simply to shifts in the intensity of the precipitation.

The electron distribution functions measured at DMSP and at ISEE during the periods of intense polar rain included in our study sometimes are almost identical over the energy range in which counting statistics allow a meaningful comparison. In these cases, the simplest explanation is that the polar rain electrons pass through the tail lobes without undergoing significant acceleration between the altitude of ISEE and the altitude of DMSP. In other cases, the DMSP and ISEE electron distributions differ, with DMSP electron fluxes exceeding those seen at ISEE at high energies. Our work suggests that the field-aligned pitch angle anisotropy of the tail lobe electron population is the major factor responsible for this difference.

Neither the differences between the DMSP and ISEE distribution functions at high energies nor their similarities at low energies are consistent with the existence of a static potential structure between the two satellites. If electrons were accelerated by a potential Φ between ISEE and DMSP, the DMSP electron distribution function above the energy $e\Phi$ would have the same shape as the ISEE electron distribution function when both were plotted versus energy. Above energy $e\Phi$ the two could be matched by translating the ISEE distribution function along the energy axis by $e\Phi$. No resemblance would be expected between the DMSP electron spectrum at energies less than $e\Phi$ and the ISEE spectrum, because all electrons observed by ISEE would acquire energies greater than $e\Phi$ before arriving at DMSP, and upgoing electrons present at low altitudes with energies below $e\Phi$ would be reflected by the potential barrier before reaching ISEE. This prediction of maximum similarity at high energy and minimum similarity at low energy is the opposite of what is actually seen.

The data used in this study cannot rule out the existence of a region tailward of ISEE or between ISEE and DMSP where electrons are accelerated by a fluctuating electric field. Measurements of the most field-aligned component of the electron population at ISEE's altitude could prove or disprove the presence of electron acceleration between ISEE and DMSP. Two- or three-dimensional measurements of the electron distribution function at low altitude over the polar caps could reveal boundaries in phase space between populations of different origin. Such boundaries can provide evidence for or against the existence of an acceleration region and information about its location, if it exists. The data used in this study cannot provide such information.

However, our data show that another factor plays an important role in creating the differences between the distribution functions measured by ISEE and by DMSP. This factor is the field-aligned pitch angle anisotropy of the tail lobe electron population. This anisotropy is observed by ISEE at energies above 200 eV and increases with increasing energy. Magnetic mirroring reflects all but the most field-aligned tail lobe electrons before they can reach DMSP, while ISEE measures lobe electrons with somewhat larger pitch angles. This difference in the population sampled may explain why the DMSP distributions sometimes exceed those measured by ISEE, and why the difference grows with increasing energy.

The intense polar rain fluxes included in our study usually occur over the northern polar cap when IMF $B_z < 0$, and over the southern polar cap when IMF $B_z > 0$, as would be expected if they originated in the anisotropic solar wind electron population and traveled adiabatically to the polar caps. The temperature of the subset of intense polar rain studied is on the order of 100 eV at energies below a few hundred eV. This is similar to the observed temperature of strahl electrons [Feldman et al., 1978]. The temperature of our cases at energies above 500 eV is similar to that predicted for high-energy strahl by Scudder and Olbert [1979]. These facts support the conclusion that the electrons of intense polar rain, as well as those of normal polar rain, originate in the interplanetary medium, and that the spectral differences between normal and intense polar rain are the result of temporal variations in the source solar wind electron population.

Acknowledgments. The authors express appreciation to K. W. Ogilvie, the principal investigator on the ISEE 1 vector electron spectrometer experiment for contributing his data to this study and to the Space

Physics Analysis Network (SPAN) for the use of networking facilities. This research was supported in part by the Air Force Office of Scientific Research under grant AFOSR 84-0049 and by the Division of Atmospheric Sciences, National Science Foundation, under grant ATM 83-15041, both to The Johns Hopkins University Applied Physics Laboratory, and by the JHU/APL independent research and development program under Navy contract N00024-85-C-5301.

The Editor thanks two referees for their assistance in evaluating this paper.

REFERENCES

- Fairfield, D. H., and J. D. Scudder, Polar rain: Solar coronal electrons in the earth's magnetosphere, *J. Geophys. Res.*, **90**, 4055-4068, 1985.
- Feldman, W. C., J. R. Asbridge, S. J. Bame, M. D. Montgomery, and S. P. Gary, Solar wind electrons, *J. Geophys. Res.*, **80**, 4181-4196, 1975.
- Feldman, W. C., J. R. Asbridge, S. J. Bame, J. T. Gosling, and D. S. Lemons, Characteristic electron variations across simple high-speed solar wind streams, *J. Geophys. Res.*, **83**, 5285-5295, 1978.
- Fennell, J. F., Access of solar protons to the earth's polar caps, *J. Geophys. Res.*, **78**, 1036-1046, 1973.
- Fennell, J. F., P. F. Mizera, and D. R. Croley, Low energy polar cap electrons during quiet times, *Conf. Pap. Cosmic Ray Int. Conf. 14th*, 4, 1267-1272, 1976.
- Foster, J. C., and J. R. Burrows, Electron fluxes over the polar cap, 1, Intense keV fluxes during poststorm quieting, *J. Geophys. Res.*, **81**, 6016-6028, 1976.
- Foster, J. C., and J. R. Burrows, Electron fluxes over the polar cap, 2, Electron trapping and energization on open field lines, *J. Geophys. Res.*, **82**, 5165-5170, 1977.
- Gussenhoven, M. S., D. A. Hardy, N. Heinemann, and R. K. Burkhardt, Morphology of the polar rain, *J. Geophys. Res.*, **89**, 9785-9800, 1984.
- Hardy, D. A., Intense fluxes of low-energy electrons at geomagnetic latitudes above 85°, *J. Geophys. Res.*, **89**, 3883-3892, 1984.
- Hardy, D. A., W. J. Burke, and M. S. Gussenhoven, DMSP optical and electron measurements in the vicinity of polar cap arcs, *J. Geophys. Res.*, **87**, 2413-2430, 1982.
- Heikkila, W. J., Penetration of particles into the polar cap and auroral regions, in *Critical Problems of Magnetospheric Physics, Proceedings of the Symposium Jointly Sponsored by COSPAR, IAGA, and URSI*, edited by E. R. Dyer, pp. 67-82, IUCSTP Secretariat, Washington, D. C., 1972.
- Heppner, J.-P., M. L. Miler, M. B. Pongratz, G. M. Smith, L. L. Smith, S. B. Mende, and N. R. Nath, The Cameo barium releases: E1 fields over the polar cap, *J. Geophys. Res.*, **86**, 3519-3542, 1981.
- King, J. H., Interplanetary medium data book, supplement 2, 1978-1982, *Rep. NSSDC/WDC-A-R&S 83-01*, NASA Goddard Space Flight Center, Greenbelt, Md., 1983.
- Lincoln, J. V., Geomagnetic and solar data, *J. Geophys. Res.*, **83**, 2727, 3367, 3906, 4417, and 4882, 1978.
- Mead, G. D., and D. H. Fairfield, A quantitative magnetospheric model derived from spacecraft magnetometer data, *J. Geophys. Res.*, **80**, 523-534, 1975.
- Meng, C.-I., Electron precipitation in polar auroras, *Space Sci. Rev.*, **22**, 223-300, 1978.
- Meng, C.-I., and H. W. Kroehl, Intense uniform precipitation of low-energy electrons over the polar cap, *J. Geophys. Res.*, **82**, 2305-2313, 1977.
- Meng, C.-I., S.-I. Akasofu, and K. A. Anderson, Dawn-dusk gradient of the precipitation of low-energy electrons over the polar cap and its relation to the interplanetary magnetic field, *J. Geophys. Res.*, **82**, 5271-5275, 1977.
- Mizera, P. F., and J. F. Fennell, Satellite observations of polar, magnetotail lobe, and interplanetary electrons at low energies, *Rev. Geophys.*, **16**, 147-153, 1978.
- Morfill, G., and M. Scholer, Study of the magnetosphere using energetic solar particles, *Space Sci. Rev.*, **15**, 267-353, 1973.
- Ogilvie, K. W., and J. D. Scudder, Observations of the "strahl" by the solar wind electron spectrometer on Mariner 10, in *Solar Wind Four*, edited by H. Rosenbauer, pp. 226-240, Max-Planck-Institut für extraterr. Phys., Garching, Federal Republic of Germany, 1981.
- Ogilvie, K. W., J. D. Scudder, and H. Doong, The electron spectrometer experiment on ISEE-1, *IEEE Trans. Geosci. Electron. GE-16*, 261-265, 1978.
- Paulikas, G. A., Tracing of high-latitude magnetic field lines by solar particles, *Rev. Geophys.*, **12**, 117-128, 1974.
- Pilipp, W. G., R. Schwenn, E. Marsch, K.-H. Muhlhauser, and H. Rosenbauer, Electron characteristics in the solar wind as deduced from Helios observations, *Rep. MPAE-W-100-81-31*, edited by H. Rosenbauer, pp. 241-249, Max-Planck-Inst. für Aeron., Katlenburg-Lindau, and Max-Planck-Inst. für extraterr. Phys., Garching, Federal Republic of Germany, 1981.
- Riehl, K. B., and D. A. Hardy, Average characteristics of the polar rain and their relationship to the solar wind and interplanetary magnetic field, *J. Geophys. Res.*, **91**, 1557-1571, 1986.
- Rosenbauer, H., H. Miggenrieder, M. Montgomery, and R. Schwenn, Preliminary results of the Helios plasma measurements, in *Physics of Solar Planetary Environments*, Vol. 1 edited by D. J. Williams, pp. 319-331, AGU, Washington, D.C., 1976.
- Rosenbauer, H., R. Schwenn, E. Marsch, B. Meyer, H. Miggenrieder, M. D. Montgomery, K. H. Muhlhauser, W. Pilipp, W. Voger, and S. M. Zink, A survey on initial results of the Helios plasma experiment, *J. Geophys. Res.*, **42**, 561-580, 1977.
- Scudder, J. D., and S. Olbert, A theory of local and global processes which affect solar wind electrons, 1, The original of typical 1 AU velocity distribution functions—Steady state theory, *J. Geophys. Res.*, **84**, 2755-2772, 1979.
- Svalgaard, L., The relationship between the azimuthal component of the interplanetary magnetic field and the geomagnetic field in the polar caps, in *Correlated Interplanetary and Magnetospheric Observations*, edited by D. E. Page, pp. 61-84, D. Reidel, Hingham, Mass., 1974.
- Wilcox, J. M., The interplanetary magnetic field. Solar origin and terrestrial effects, *Space Sci. Rev.*, **8**, 258-328, 1968.
- Winningham, J. D., and C. Gurgiolo, DE-2 photoelectron measurements consistent with a large scale parallel electric field over the polar cap, *Geophys. Res. Lett.*, **9**, 977-979, 1982.
- Winningham, J. D., and W. J. Heikkila, Polar cap auroral electron fluxes observed with ISIS 1, *J. Geophys. Res.*, **79**, 949-957, 1974.
- Yeager, D. M., and L. A. Frank, Low energy electron intensities at large distances over the earth's polar cap, *J. Geophys. Res.*, **81**, 3966-3976, 1976.
- D. H. Fairfield, Goddard Space Flight Center, Code 695, Greenbelt, MD 20771.
- M. E. Greenspan, Regis College Research Center, 235 Wellesley Street, Weston, MA 02193.
- C.-I. Meng, The Johns Hopkins University Applied Physics Laboratory, Johns Hopkins Road, Laurel, MD 20707.

(Received July 22, 1985;
revised April 30, 1986;
accepted May 15, 1986.)

Long-Period Polar Rain Variations, Solar Wind and Hemispherically Symmetric Polar Rain

K. MAKITA¹ AND C.-I. MENG

The Johns Hopkins University, Applied Physics Laboratory, Laurel, Maryland

On the basis of electron data obtained by the Defense Meteorological Satellite Program (DMSP) F2 satellite the long-period variations of the polar rain flux are examined for four consecutive solar rotations. It is clearly demonstrated that the asymmetric enhancement of the polar rain flux is strongly controlled by the sector structure of the interplanetary magnetic field (IMF). However, the orbit-to-orbit and day-to-day variations of the polar rain flux are detected even during a very stable sector period, and the polar rain flux does not have any clear relationship to the magnitude of the IMF B_z or B_y . Thus the polarity of B_z controls only the accessibility of a polar region. It is also noticed that the intensity of polar rain fluxes does not show any relationship to the density of the solar wind, suggesting that the origin of the polar rain electrons is different from the commonly observed part of the solar wind electron distribution function. In addition to the asymmetric polar rain distribution, increasing polar rain fluxes of similar high intensity are sometimes detected over both polar caps. An examination of more than 1 year's data from the DMSP F2 and F4 satellites shows that simultaneous intense uniform precipitations ($>10^7$ electrons/cm² s sr) over both polar caps are not coincidental; it also shows that the spectra are similar. The occurrence of hemispherically symmetric events is not common. They generally are observed after an IMF sector transition period, during unstable periods in the sector structure, and while the solar wind density is high.

INTRODUCTION

The presence of low-energy electrons over the polar cap was first revealed by the ISIS 1 satellite [Heikkila, 1972]. Those electrons, mostly below 1 keV, precipitate rather uniformly over the entire polar cap and have been called the "polar rain" by *Winningsham and Heikkila* [1974]. *Fennel et al.* [1975] suggest that such precipitation consists of interplanetary electrons gaining direct access to the polar cap through the magnetotail. Since the field lines of the tail lobe link with the polar cap region, it is expected that electron fluxes measured over the polar cap are connected to the tail lobe fluxes. *Yeager and Frank* [1976] reported the observation of low-energy electrons similar to the polar rain electrons in the northern geomagnetic tail lobe at 3-7 R_E by IMP 5 and also found that their intensities are high during the interplanetary magnetic field (IMF) away sector and low during the toward sector. Asymmetric distributions are also found at low altitudes over the polar cap [Meng and Kroehl, 1977; Mizera and Fennel, 1978]. The hemispherical asymmetry of the polar rain flux and its dependence on the sector structure of the IMF suggest a solar wind origin for the electrons. Recently, *Fairfield and Scudder* [1985] found field-aligned fluxes of electrons of a few hundred electron volts in the geomagnetic tail lobe and suggested that the polar rain electrons originated from the solar wind "strahl" (field-aligned) component. Also, *Greenspan et al.* [1986] reported the nearly identical spectra between intense polar rain and electrons in the magnetotail. However, magnetospheric acceleration is proposed as a possible explanation of intense energetic (≥ 1 keV) polar rain fluxes [Foster and Burrows, 1976, 1977]. The plasma mantle is also proposed as an alternative source region of the polar rain electrons [Gusenhoven et al., 1984].

The general trend of the asymmetric distribution of the intense polar rain flux with the structure of the IMF sector has been established mostly on case studies or statistically [Riehl and Hardy,

1986]. Further studies of its temporal evolutions and possible anomalies are needed to better understand the processes of particle entry and transport. For example, the reason for variations of the northern and southern polar rain fluxes, while the earth is immersed within a sector of given polarity, is not well understood; neither are the long-duration temporal variations and any repeatable patterns in consecutive solar rotation periods. Also, we do not know whether there is a one-to-one relationship between the variation of the polar rain flux and the variations of the IMF B_z and B_y magnitudes. Although the solar wind is thought to be the origin of the polar rain, it is not known whether the polar rain intensity is associated with the solar wind density.

Since the long-duration temporal variations of polar rain fluxes in both hemispheres and their relationships to solar wind and IMF parameters over a long period of time have not been examined, the polar rain variation during four consecutive solar rotations is studied here. From this examination of long-period polar rain data it is found that significant polar rain fluxes can sometimes occur over both polar regions for extended durations. This type of polar rain event is certainly different from the well-established asymmetric hemispherical polar rain distribution. The occurrence of this apparently hemispherically symmetric polar rain event is examined in the second part of this article.

DATA SELECTION

The electron data obtained by the Defense Meteorological Satellite Program (DMSP) F2 satellite during the period January 24, 1979, to May 11, 1979 (that is, solar rotations 1989-1992) are used to study the polar rain long-period variations. The spacecraft was launched into a dawn-dusk circular polar orbit at 840-km altitude in July 1977. A perfect sun-synchronous orbit was not achieved, and its orbital plane slowly precessed toward the later local time. By early 1979 the DMSP F2 orbit was near the 9:00 A.M.-9:00 P.M. meridian at the equator. However, its exact orbit track over the polar region in the geomagnetic latitude (MLAT) and local time (MLT) coordinates varied with universal time (UT) because of the offset between the geomagnetic and geodetic poles. Electron detectors on board DMSP satellites are always aligned with the geocentric zenith and detect precipitating low-energy electrons

¹ Permanently at Takushoku University, Bunkyo, Tokyo 112, Japan.

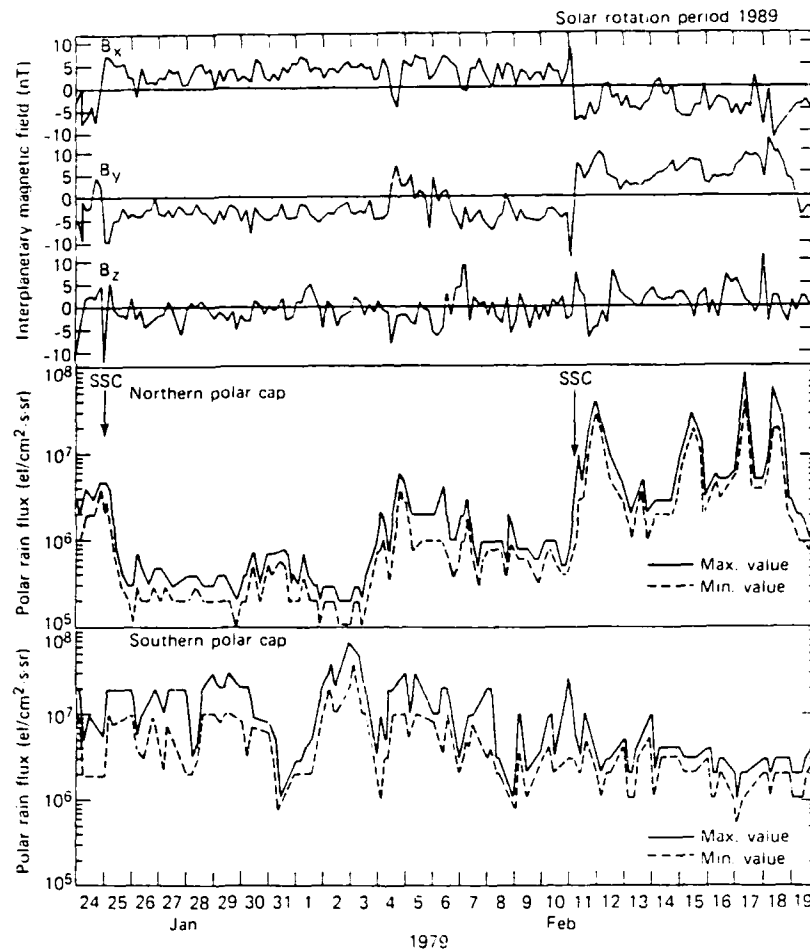


Fig 1a. IMF B_x , B_y , B_z and polar rain flux in both hemispheres during the period January 24 to February 19, 1979, for solar rotation period 1989. Since the polar rain has spatial gradients, the maximum and minimum values are shown as solid and dotted lines, respectively. Note that the polar rain flux in the southern hemisphere is almost continuously larger than that in the northern one during the period January 25 to February 10 in the toward sector and that the asymmetry is reversed after February 10 in the away sector.

(50 eV to 20 keV) over the polar cap and auroral ovals. A more detailed description of the DMSP F2 electron detectors has been given by *Hardy et al.* [1979].

The selection of these four solar rotations is based on the most extended coverage of continuous interplanetary data with distinct sector structures given by *King* [1983]. Furthermore, this period is around the equinox when the seasonal geometric asymmetry between the two polar regions is near minimum. In determining the polar rain intensity a few caveats have to be considered, particularly, the orbit trajectory variation from orbit-to-orbit and the polar rain spatial gradient. In order to reduce complications only the satellite passes that traverse higher than 80° MLAT and its particle data revealing a clearly identifiable polar cap region were used; about 50% of the orbits satisfy this criterion. Since there is no quantitative model to normalize the known dawn-dusk [*Meng et al.*, 1977] and noon-midnight [*Gussenhoven et al.*, 1984] gradients, both the maximum and the minimum of the polar rain intensity during each high-latitude pass were determined and used in analysis. Thus the temporal variation of the polar rain can be detected on the basis of relative changes of either maximum or minimum intensity profiles, and the impact of the polar rain gradient is qualitatively minimized but not quantitatively corrected. Also, to

avoid contamination and misidentification of the polar rain intensity, electron data from each polar crossing are examined carefully to be certain that only the polar rain flux is used to determine intensity. The short-duration precipitation spikes associated with polar cap auroral arcs are excluded. The occasional polar cap absorption events associated with the entry of very energetic particles related to solar flares are also eliminated from the data base; they are characterized by the nearly constant enhanced count rate in all energy channels above 1 keV. When there is any doubt in defining the polar cap flux, the observation of that polar pass is not used in this study. Data from 1845 polar region crossings are included in the analysis.

POLAR RAIN VARIATIONS AND SECTOR STRUCTURE

The long-period intensity variations in the polar rain are the main interest of this study; the short-period polar rain fluctuations of a few hours' scale are beyond its scope. Also, the variation, if any, due to the diurnal changes of the DMSP trajectory over the polar cap is not considered. Figures 1a-1d illustrate the polar rain flux and three components of the IMF (B_x , B_y , B_z) for four consecutive solar rotations.

Figure 1a illustrates the IMF and polar rain flux variations from

AD-A195 972

INVESTIGATIONS OF MAGNETOSPHERE-IONOSPHERE COUPLING
RELEVANT TO OPERATION (U) JOHNS HOPKINS UNIV LAUREL MD
APPLIED PHYSICS LAB C I MDX 11 AL. FEB 88

2/2

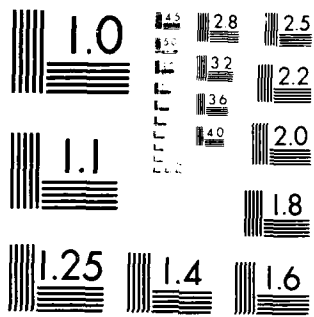
UNCLASSIFIED

AFOSR-TR-88-0622 AFOSR-84-0049

F/G 4/1

NL

END
DATE
FILMED
9 88



MICROCOPY RESOLUTION TEST CHART
NATIONAL BUREAU OF STANDARDS-1963-A

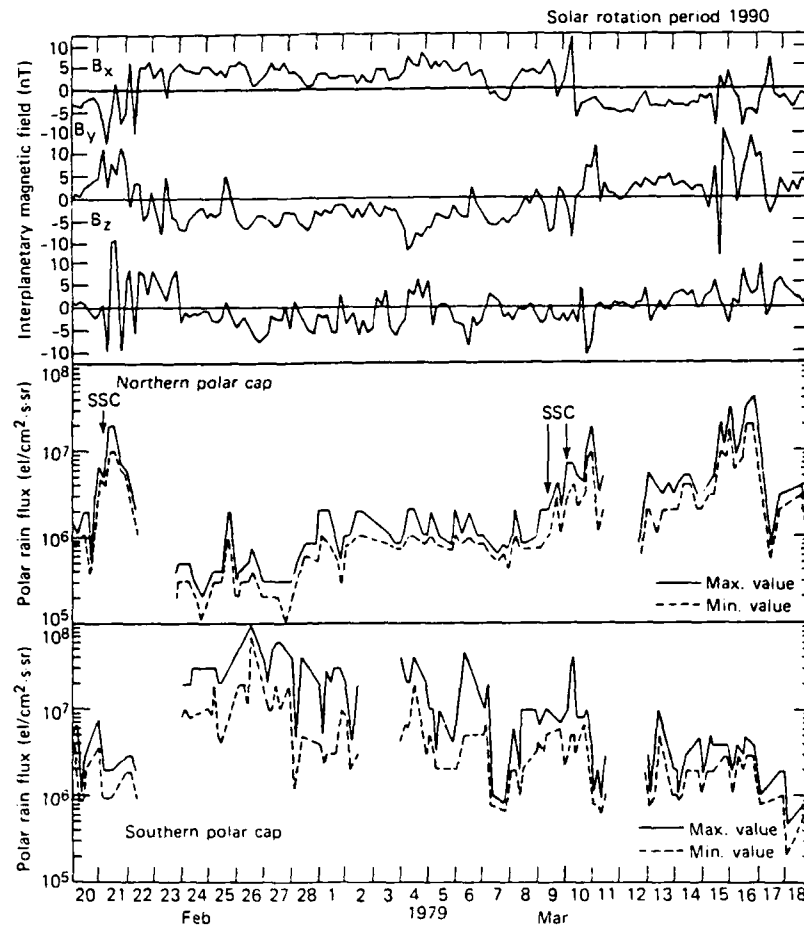


Fig. 1b. Same as Figure 1a but for the period February 20 to March 18, 1979, for solar rotation period 1990. The polar rain flux in the southern hemisphere is almost continuously higher than that in the northern one from February 22 to March 10 in the toward sector and is reversed after March 10 in the away sector

January 24 to February 19, 1979, for solar rotation period 1989. The top panel shows the three components of the IMF, and the bottom panel reveals the variation of the polar rain flux integrated from 50 eV to 20 keV in the northern and southern polar caps. The polar rain maximum and minimum intensities determined from those polar cap crossings, as described in the previous section, are connected except that the data gaps are more than 15 hours long. Consistent daily data gaps exist from about 1500–0100 UT and about 1300–2400 UT in the northern and southern hemispheres, respectively. They are attributed to the diurnal variation of satellite trajectories that do not reach 80° . The temporal profiles of maximum and minimum polar rain flux vary coherently; the difference is generally within a factor of 2. A sudden storm commencement (SSC) is observed at 0139 UT on January 25, 1979, in the ground magnetogram data [Coffey, 1979]. Correspondingly, in the IMF data the sector structure changes suddenly from the away direction ($B_x < 0$) to the toward direction ($B_x > 0$) during this period. A fairly stable toward sector structure continues to February 10, except for a fluctuation in B_x and B_y from February 4–6. The IMF changes its sector direction from toward to away after another SSC at 0147 UT on February 11.

Variations of the polar rain flux with sector polarity can be seen in both hemispheres. During the toward sector from January 25 to February 10, the intensity of the polar rain flux in the southern hemisphere is $\sim 10^7$ electrons/cm² s sr, which is almost 1 or-

der of magnitude higher than that in the northern hemisphere. When the polar rain flux increases in the southern polar cap, the polar rain flux in the northern polar cap decreases simultaneously. However, in the period February 4–6, after an SSC, the northern polar rain increases to $\sim 3 \times 10^6$ electrons/cm² s sr, while the southern polar cap flux is still 2×10^7 electrons/cm² s sr. Following a distinct sector change from the toward to away direction on February 11, the polar rain flux in the northern hemisphere becomes more intense than that in the south. It is also obvious that intensities of polar rain flux in both hemispheres are very irregular with fluctuations of up to a factor of 10 even within a stable IMF sector. A gradual polar rain intensity decrease (or increase) may exist in the southern hemisphere (or northern hemisphere) during this solar rotation period.

Figure 1b shows the second solar rotation period (1990), from February 20 to March 18. After the SSC at 0301 UT on February 21, the fairly stable toward sector continues to March 9, when two SSCs at 0809 and 2318 UT occur. The polar rain flux in the southern hemisphere is higher than that in the northern hemisphere cap from February 23 to March 9. A simultaneous enhancement of polar rain fluxes is observed in both northern and southern hemispheres in association with the SSC on March 9 and with a sector change. The magnitude of polar rain flux is similar for the two hemispheres to about March 14. This may indicate an unusual symmetrical distribution of polar rain and will be discussed

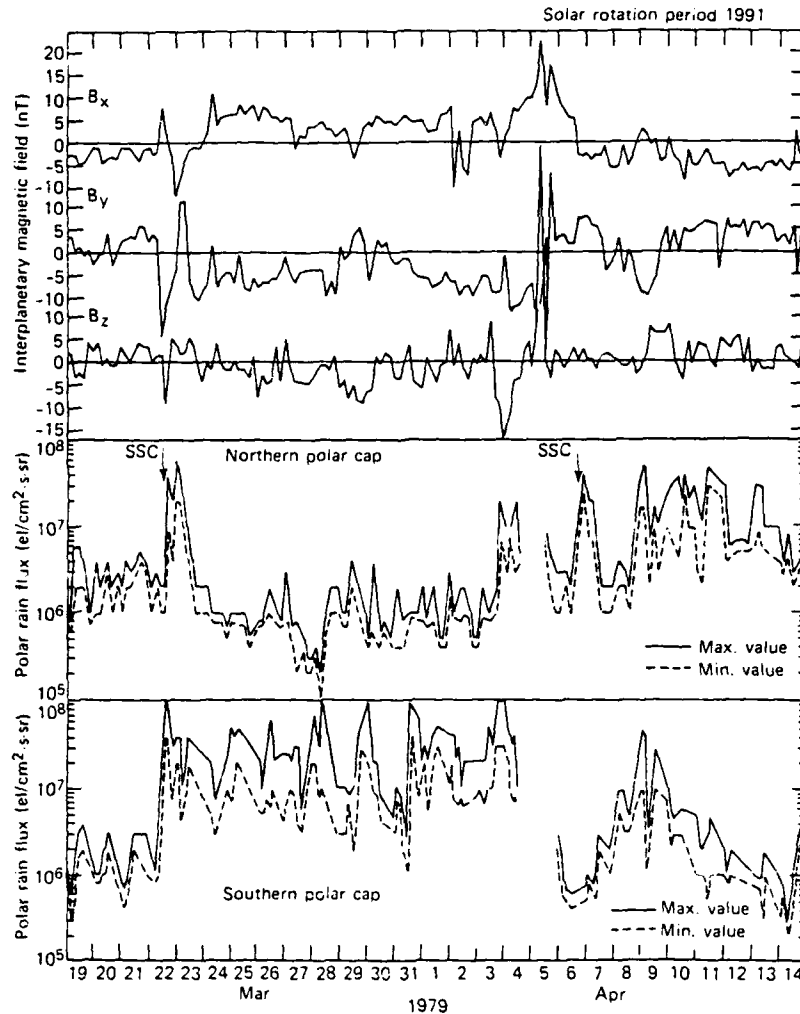


Fig. 1c. Same as Figure 1a but for the period March 19 to April 14, 1979, for solar rotation period 1992.

later. During the away sector from March 15 to March 22, the polar rain flux in the northern hemisphere is generally higher than that in the southern hemisphere, as expected.

Figure 1c shows the third consecutive rotation period (1991), from March 19 to April 14. The sector structure changes from away to toward after an SSC at 0826 UT on March 22. A sudden intense enhancement of polar rain flux occurs in both hemispheres at about 1900 UT on March 22, and the similar intensity over both hemispheres lasts for about one day (that is, another symmetric polar rain case). During the stable toward sector after March 23, the polar rain flux in the southern hemisphere is distinctly higher, by more than 1 order of magnitude, than that in the northern hemisphere. A general anticorrelation is seen between the southern and northern hemispheres. On March 28 the polar rain flux in the southern hemisphere increases to about 10^8 electrons/cm² s sr, whereas in the northern hemisphere it decreases to about 10^5 electrons/cm² s sr with a difference of about 3 orders of magnitude. After an SSC at 1000 UT on April 3, the enhancement of polar rain flux is seen in both hemispheres. This symmetric enhancement lasts for about 12 hours and is similar to an event on March 22. During the away sector (after April 6), the polar rain flux in the northern hemisphere is generally higher than that in the southern, except on April 8 and 9 when an enhancement is observed over the southern hemisphere.

Figure 1d shows the fourth solar rotation period (1992), from April 15 to May 11. The IMF sector changes from the away to the toward direction on April 21, and the southern polar rain flux increases markedly after this turning, while no significant change is seen over the northern polar cap. Associated with an SSC at 2358 UT on April 24, the polar rain flux intensifies in both hemispheres. During the away sector, the intensity of polar rain flux in the northern hemisphere is higher than that in the southern hemisphere, as expected.

From the analysis of these four consecutive solar rotations it is concluded that the polar rain flux variation is indeed controlled by the IMF sector structure. The asymmetric distribution pattern in the flux is repeated in successive solar rotations. However, the polar rain flux in each hemisphere is not at all constant during a stable period of away (or toward) sector structure. Sometimes, a simultaneous enhancement of intense polar rain flux with similar intensity is observed over both polar caps. This will be examined later.

POLAR RAIN FLUX AND IMF B_x , B_y MAGNITUDES

The polarity of the IMF controls the occurrence of the polar rain in a polar cap. Thus, it would be interesting to know whether the magnitude of IMF B_x and B_y components has any effect on the intensity of the observed polar rain flux. For each orbit

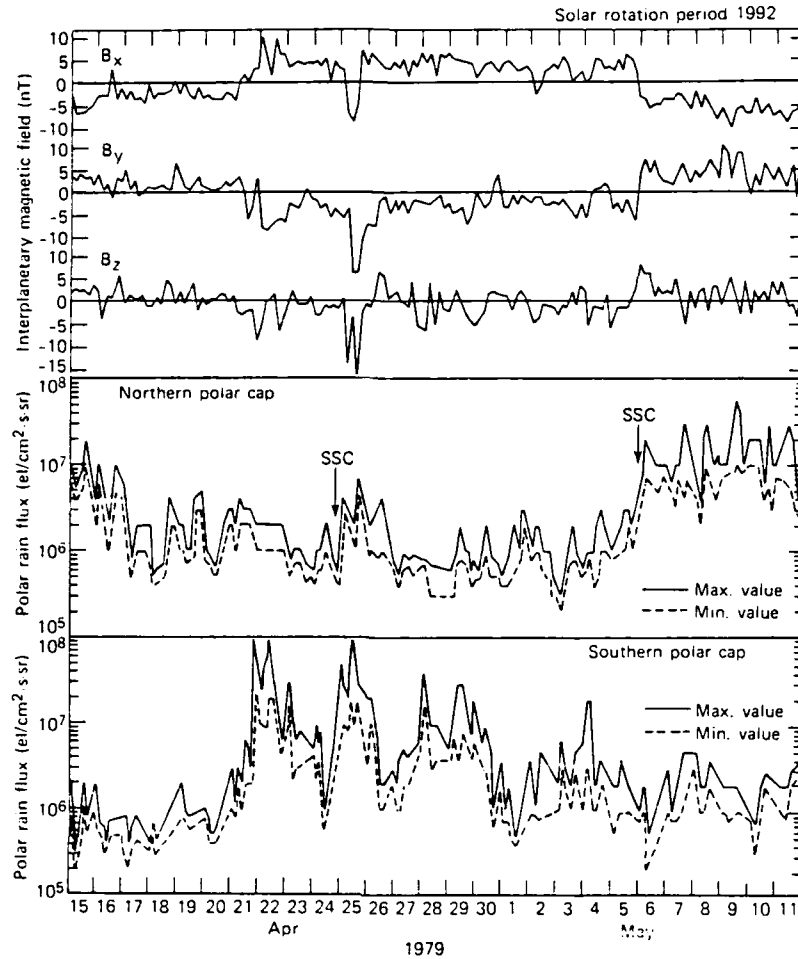


Fig. 1d. Same as Figure 1a but for the period April 15 to May 11, 1979, for solar rotation period 1992.

the maximum polar rain flux in any one of the two hemispheres is compared with simultaneous IMF B_x and B_y values. Since the intensity level of the weak and moderate polar rain flux is usually at about 1 to 5×10^6 electrons/cm² s sr [Makita and Meng, 1984; Gussenhoven et al., 1984; Riehl and Hardy, 1986], the more intense polar rain ($>6 \times 10^6$ electrons/cm² s sr) events are used in this analysis in order to reveal a more distinct relationship, if there is one. A total of 264 polar passes is selected within the period January 24 to May 11, 1979. If the polar rain intensity is very similar in two hemispheres (that is, if there are symmetric types of polar rain events), that orbit is eliminated in analysis because of the difficulty in determining the dominant polar cap with the larger flux and also the independency to the IMF polarity. Only 17 out of 264 passes ($\sim 6\%$) are deleted, and this procedure should not affect the result. A scatter plot of the polar rain flux in the dominant hemisphere with IMF B_x and B_y values is illustrated in Figures 2a and 2b. The open and solid circles correspond to the more intense polar rain that occurred in the northern and southern hemispheres, respectively. It is clear that the higher polar rain flux is detected predominantly ($\sim 96\%$) in the northern hemisphere for the negative B_x (or positive B_y) condition corresponding to the away sector structure of a typical garden-hose configuration. For the positive B_x (or negative B_y) condition the higher intensity is observed mainly ($\sim 97\%$) in the southern hemisphere. These results are consistent with the previously reported asymmetric distribution of the polar rain. However, there are few exceptions

($\sim 3\text{--}4\%$) even after cases of anomalous symmetric distribution are deleted in the analysis.

For completeness in the analysis we also calculated the correlation coefficients for the magnitudes of positive (negative) B_x and the southern (northern) polar rain flux. They are very low, about 0.2 and -0.2 , respectively. The correlation coefficient for the positive B_y and the northern polar rain flux is slightly higher at about 0.4 and that for the negative B_x and the southern polar rain flux is about -0.3 . These results suggest that the intensity of polar rain flux is not closely related to the magnitude of IMF B_x or B_y , irrespective of the direction, at least for more intense ($>6 \times 10^6$ electrons/cm² s sr) polar rain events.

In addition, we examined the relationship between the occurrence of SSCs and the enhancements of polar rain flux. Within the four solar rotations from January 24 to May 11, 1979, there are 18 SSC events. We found that 13 of them ($\sim 72\%$) are distinctly related to the enhancement of polar rain flux in either the southern or the northern hemispheres within 12 hours. Therefore the polar rain flux is more likely to occur after an interplanetary shock front passes by the magnetosphere.

POLAR RAIN FLUX AND SOLAR WIND DENSITY

Since the polar rain is expected to be of solar or interplanetary origin, it is of interest to determine if the polar rain is due to the direct entry into the magnetotail and the consequent precipitation of solar wind electrons. We compared the variations of polar rain

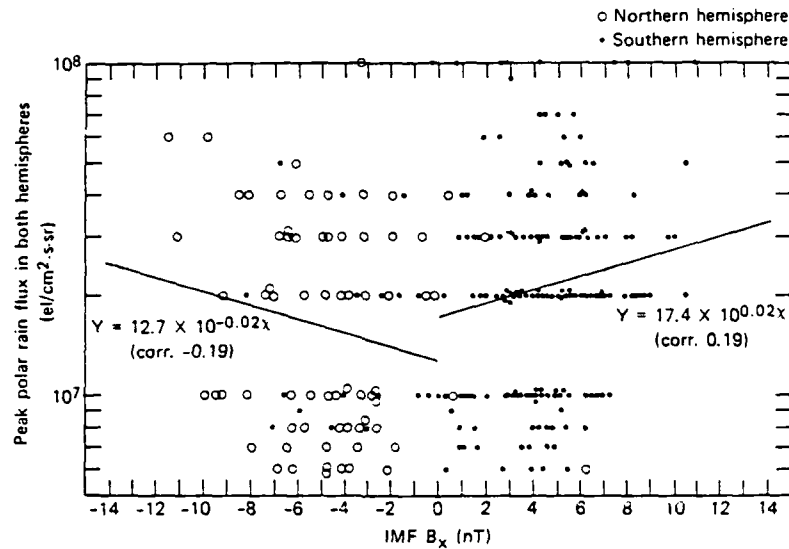


Fig. 2a. The scatter plot between the polar rain flux and the IMF B_x value. The open circles and solid circles correspond to the polar rain flux in the northern and southern hemispheres, respectively. The correlation coefficients for the positive B_x and the southern polar rain flux and also for the negative B_x and the northern polar rain flux are about 0.2 and -0.2 , respectively.

flux with those of the solar wind density, assuming that the electron density of the solar wind is identical to the proton density. The latter is used in this analysis because of its availability in the work by King [1983]. The data base is for the same four consecutive solar rotations from January 24 to May 11, 1979. Figure 3a illustrates temporal variations of the density of the solar wind and the peak polar rain flux obtained over both hemispheres during the first solar rotation from January 24 to February 19. The top panel shows the hourly averaged values of the solar wind density; there are several distinct periods of sharp increases as on January 25 and February 3, 11, 12, and 18. The diagram reveals that periods of enhanced solar wind density do not coincide with periods of very large polar rain flux, indicating a lack of clear correlation. In fact, most of the intense polar rain events took place during

periods of low solar wind density ($< 10 \text{ cm}^{-3}$), suggesting an anticorrelation between the solar wind density and the polar rain flux.

In order to determine the general trend all four solar rotations must be examined. The second period, from February 20 to March 18, is shown in Figure 3b. Sharp increases of solar wind density occur on February 21 and March 4, 9, 15, and 17. Some of the increases in polar rain intensity may be related to variations in solar wind density as on February 21 and March 4 and 10. However, the anticorrelation can also be recognized on March 15 and 17. Furthermore, the intense polar rain flux on February 26 occurs during a period of fairly low solar wind density ($< 5 \text{ cm}^{-3}$).

The third solar rotation, from March 19 to April 14, is shown in Figure 3c. In the top panel the distinct enhancement of the solar wind density takes place on March 22 and 28 and April 1, 3,

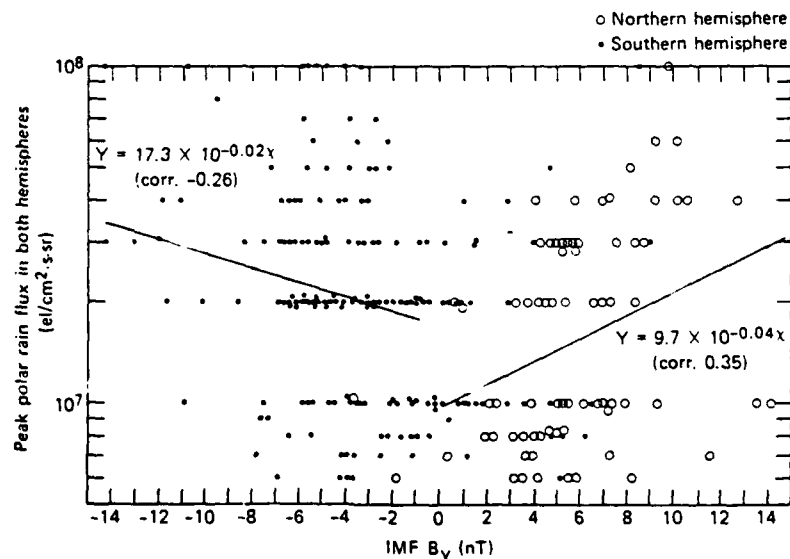


Fig. 2b. A scatter plot of the polar rain flux and IMF B_y values. The correlation coefficients for the positive B_y and the northern polar rain flux and also for the negative B_y and the southern polar rain flux are 0.35 and -0.26 , respectively.

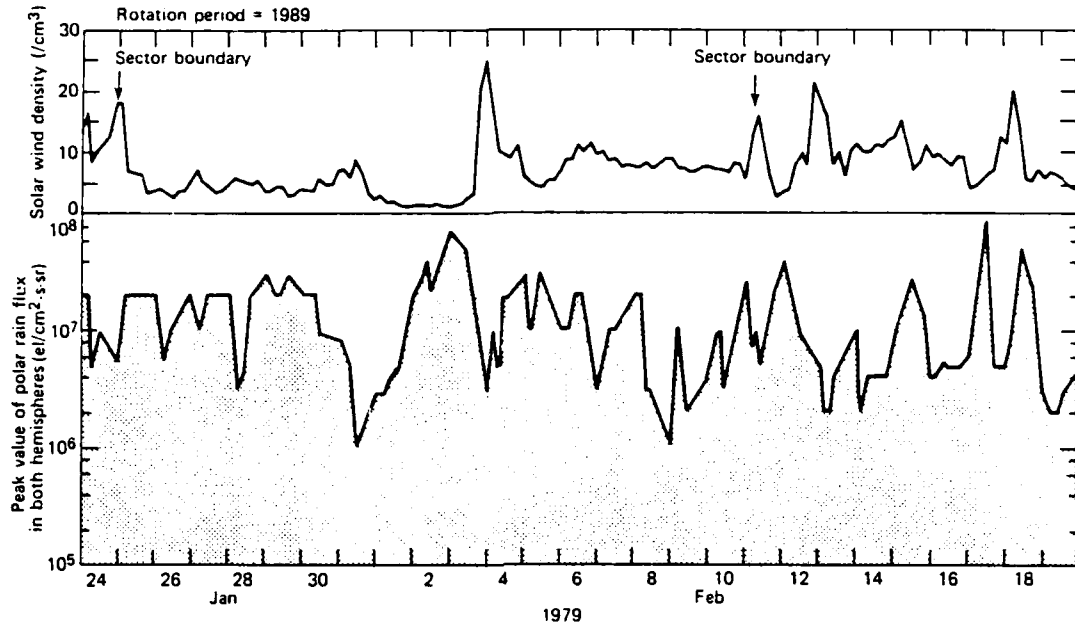


Fig. 3a. The solar wind density and peak polar rain flux detected over two polar caps during the period January 24 to February 19, 1979. Notice that the large polar rain flux is mostly seen during the period of low solar wind density ($< 10 \text{ cm}^{-3}$).

5, and 10. Enhancements of the polar rain flux coincide with increases of the solar wind density on March 22 and April 1, 3, and 10. The anticorrelation is seen also, for example, from March 27 to March 29. Figure 3d shows the last of the four solar rotations. Distinct enhancements of the solar wind density can be seen on April 21 and 25 and May 5 and 8. An enhancement of the polar

rain flux on April 25 can be related to the increase of the solar wind density, but in other periods, as on May 5 and 8, an anticorrelation exists. On April 21 there may even be an obvious time delay between the two.

These four solar rotations certainly do not show any clear consistent relationship between the two parameters except in several

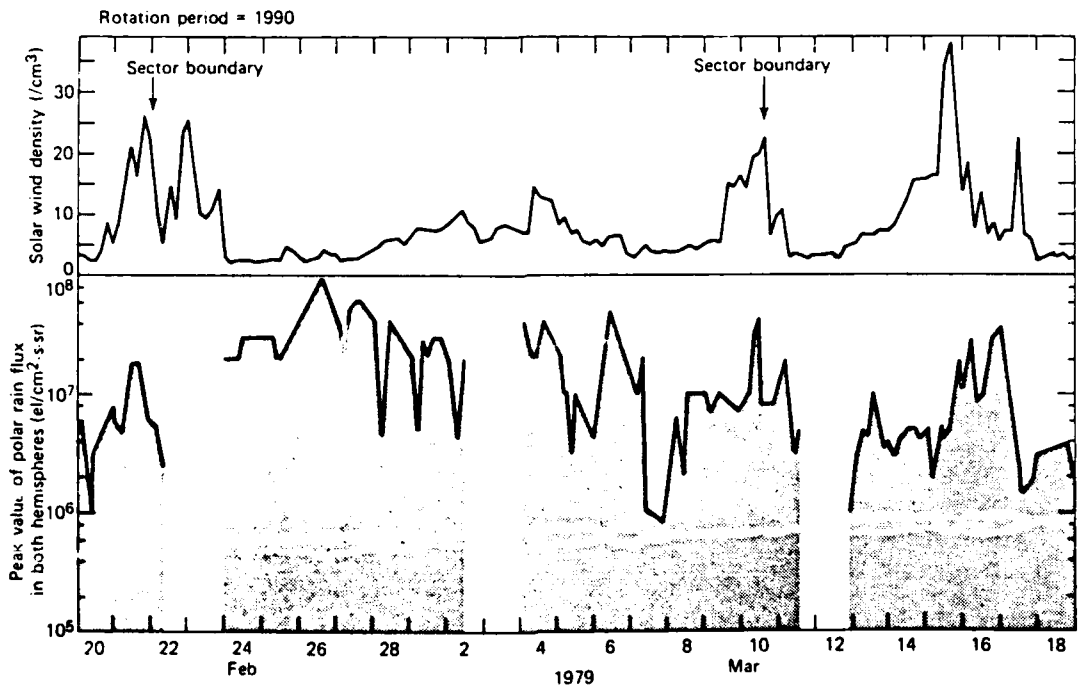


Fig. 3b. The solar wind density and peak polar rain flux obtained in two hemispheres during the period February 20 to March 18, 1979. Although the large polar rain flux corresponds partly to the period of high solar wind density on February 21, March 4, and March 10, most of the large polar rain fluxes are seen during the period of low solar wind density.

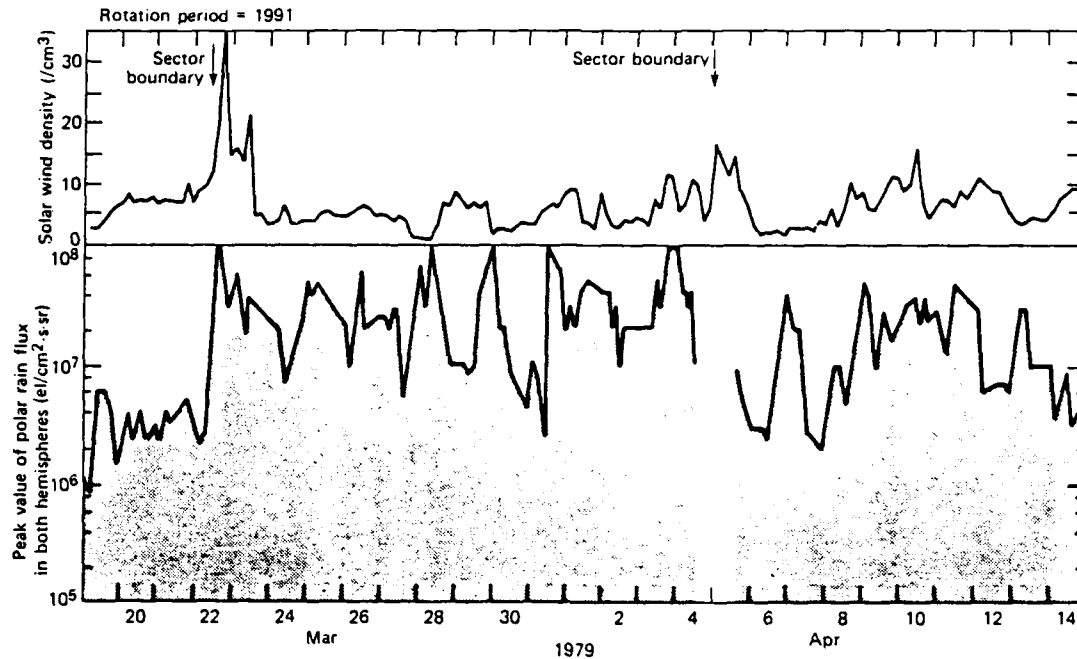


Fig. 3c. The solar wind density and peak polar rain flux obtained in two hemispheres during the period March 19 to April 14, 1979. Although the enhancement of polar rain flux corresponds to the increase of solar wind density on March 22 and April 1, 3, and 10, most of the other large polar rain fluxes are seen during the period of low solar wind density.

isolated instances. In order to investigate their relationship statistically we made a scatter plot of the solar wind density and the peak polar rain flux of each orbit. No clear relationship is found. The calculated linear regression between the polar rain flux and the solar wind density has an extremely low correlation coefficient of

-0.04 , as reported by *Riehl and Hardy* [1986]. Therefore we can conclude that the intensity of polar rain flux is independent of the solar wind density, on the basis of these four solar rotations, even though a few cases show a clear positive correlation related to SSC activity. In these unusual events the polar rain fluxes are

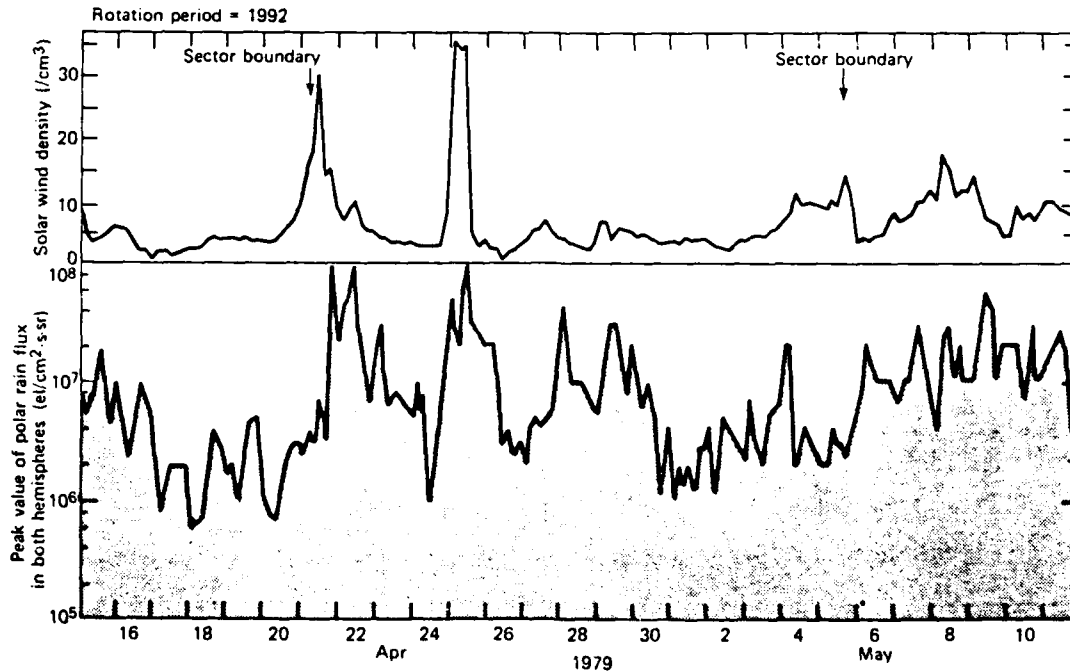


Fig. 3d. The solar wind density and peak polar rain flux obtained in two hemispheres during the period April 15 to May 11, 1979.

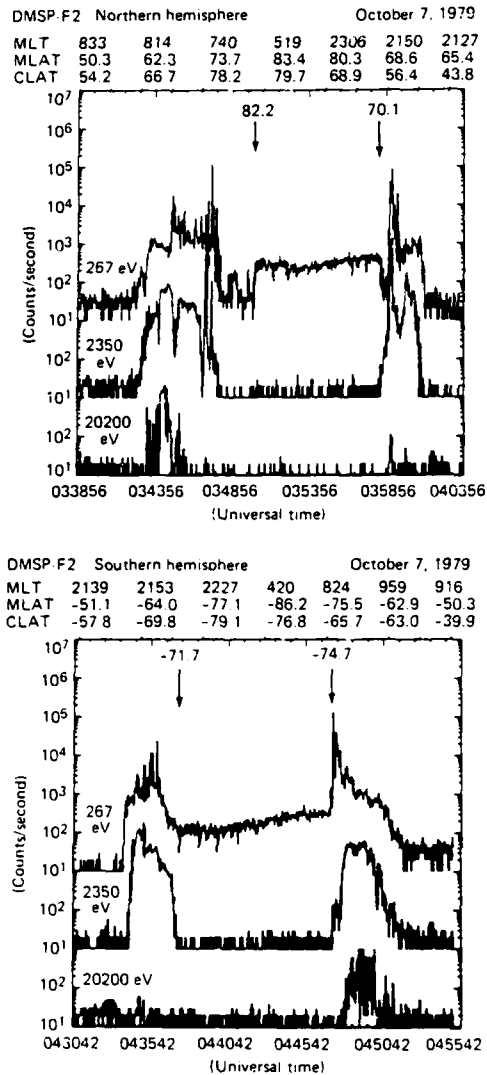


Fig. 4. An example of a hemispherically symmetric polar rain distribution. The top and bottom panels show the counting rate of three selected energy channels at 267, 2350, and 20,200 eV obtained over the northern and southern polar regions, respectively. For the lowest energy channel at 267 eV the intense uniform polar rain precipitation is seen between 82.2° and 70.1° in the northern polar cap and between 71.7° and 74.7° in the southern polar cap. Near the center of the polar cap over the northern and the southern polar passes the counting rate of the 267-eV channel is the same (about 2×10^2 counts/s).

generally distributed symmetrically in both hemispheres. The symmetric polar rain event is different from the well-established asymmetric polar rain enhancement observed only in one hemisphere.

HEMISPHERICALLY SYMMETRIC ENHANCEMENT OF POLAR RAIN

From our routine examination of the polar region precipitation and long-term polar rain variation shown in Figure 1 we notice that a significant enhancement of polar rain precipitation with similar intensity was detected over both polar caps for several consecutive orbits. This is not an isolated occurrence. In contrast to the typical polar rain enhancement that generally is far more in-

tense in one hemisphere than in the other (that is, an asymmetric enhancement), this type of polar rain phenomenon may be labeled the hemispherically symmetric enhancement of polar rain.

Figure 4 illustrates the observation of symmetric enhancement of polar rain. The top and bottom panels show the electron precipitation counting rate profiles obtained over the northern and southern polar regions, respectively. Each panel consists of data from three selected energy channels at 267, 2350, and 20,200 eV. In the northern hemisphere the satellite traversed the polar region from the morning to the evening side between 0342 and 0402 UT on October 7, 1979. The nearly uniform distributions of polar rain precipitations are seen between 82.2° MLAT on the morning side (~0600 MLT) and 70.1° MLAT on the late evening side (~2200 MLT). The precipitation is mainly in the lowest energy channel (267 eV). Near the center of the polar cap (~84.8° MLAT), over the northern polar region, the counting rate of the 267-eV channel is about 2×10^2 counts/s. The gaps between the polar rain region and the auroral oval are below 70.1° MLAT on the evening side and below 82.2° MLAT on the morning side over the northern hemisphere. Such gaps have been reported earlier [Meng and Kroehl, 1977] and are beyond the topic of this study.

The satellite traversed the southern polar cap from the evening to the morning side about 50 min later, from 0433 to 0453 UT on October 7, 1979. The homogeneous polar rain precipitation region is seen between -71.7° MLAT on the late evening side (~2200 MLT) and -74.7° MLAT on the morning side (~0800 MLT) in the 267-eV energy channel data. The polar rain flux has a distinct gradient in this southern pass; the intensity is higher on the dayside than on the nightside, as reported by Gussenhoven *et al.* [1984]. In order to obtain a meaningful comparison of polar rain intensity between the northern and southern polar caps the observation closest to the center of the polar cap in each polar pass is used. The counting rate of the 267-eV channel is about 2×10^2 counts/s at -86.5° MLAT along the 0300 MLT meridian. Therefore the enhanced polar rain intensity is nearly identical over the center of the polar cap in both hemispheres, in contrast to the well-known asymmetric polar rain distribution. The integrated flux is $\sim 10^7$ electrons/cm² s sr over both caps.

Polar rain precipitation exists most of the time, but its intensity is usually rather low. For the 267-eV energy channel it is frequently only 20–30 counts/s and can be considered as background polar rain. The intensity of the symmetric polar rain events seen here is much larger than that of the normal background polar rain precipitation. Thus this apparent symmetry of the polar rain distribution deserves further study.

To verify this phenomenon, it is necessary to be sure that the apparent symmetry is not due to nonsimultaneous detection at opposite polar caps accompanied by temporal variations of the polar rain associated with coincidental sudden changes in the IMF B_z direction. An examination of consecutive DNISP F2 polar passes before and after those shown and of DMSF F4 satellite data obtained during this period verifies that the consistent enhancement of polar rain flux exists continuously over both the northern and southern polar caps for almost 11 hours. Thus during this event, the polar rain distribution is truly symmetric over both polar caps, and it is indeed different from the familiar asymmetric polar rain.

During the change of IMF direction, a coincidentally equal flux intensity in both hemispheres is expected in association with the decay of polar rain in one cap and its growth in the other, if the temporal variation of polar rain is a gradual one. In order to avoid such a misleading situation, only newly occurring polar rain en-

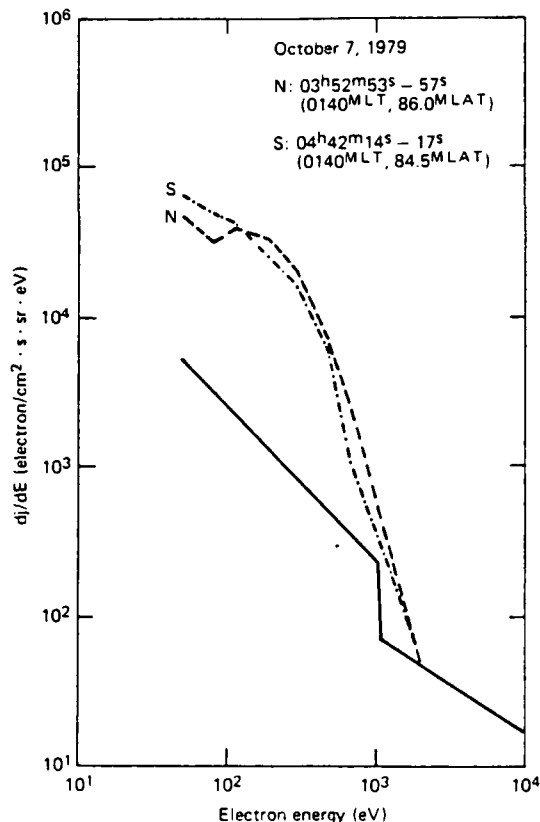


Fig. 5. The differential energy spectra of a symmetric polar rain obtained in the similar MLT sector near the center of the northern and southern polar caps. The two spectra are very similar.

enhancements simultaneously in both caps, such as the one of March 22 in Figure 1c, are selected for the study. This identification criterion for symmetric polar rain observation confines our analysis to the more intense and less ambiguous cases.

SPECTRA OF SYMMETRIC POLAR RAIN

To understand the symmetric enhancement of polar rain, it is interesting to compare the electron differential energy spectra obtained over both hemispheres. In general, differential fluxes and spectra of polar rain vary with magnetic latitude and also with magnetic local time [Meng *et al.*, 1977; Gussenhoven *et al.*, 1984]. Thus the location of the polar rain spectra measurement must be selected carefully to minimize this spatial variation and to make a meaningful comparison between the two polar caps.

For the event in Figure 4 we use spectra obtained in similar magnetic local time sectors (~ 0140 MLT) near the center of each polar cap ($\pm 85^\circ$ MLAT). In Figure 5 the dashed and dot-dashed lines show the differential energy spectra obtained in the northern and southern polar caps, respectively, averaged over 4 s. The spectral shape and intensity are very similar over both caps. The intensity of the differential flux at 100 eV is about 4×10^4 electrons/cm² s sr eV. The fluxes above 1 keV drop down to the 1 count level. The spectral similarity in this observation suggests that the enhanced polar rain electrons observed in both polar caps may come from the same source.

The hemispherically symmetric enhancements of the polar rain shown in Figure 4 are observed continuously for about 11 hours and can be defined as one event. Then the polar rain distribution

gradually becomes asymmetric. A typical asymmetric polar rain distribution is clearly observed about 20 hours after the first indication of the symmetric polar rain event.

OCCURRENCE OF SYMMETRIC POLAR RAIN

The occurrence frequency of symmetric polar rain is not as high as that of asymmetric polar rain. In order to understand this condition, observations of the symmetric type (exemplified by Figure 4) and the typical asymmetric type are compared with solar wind conditions and IMF orientations. Figure 6 illustrates the hourly values of the IMF B_x , B_y , and B_z and the solar wind density and velocity [King, 1983] together with periods of the symmetric and asymmetric polar rain observations over four consecutive days. The arrows indicate two passes of the symmetric event shown in Figure 4. Until about 28 hours before an SSC occurred at 1120 UT on October 6 the IMF showed a very stable toward sector structure. After the passing of the interplanetary shock (that is, the SSC), the IMF was no longer very stable for about 36 hours. The solar wind density gradually increased from $\sim 8\text{--}60$ cm⁻³ near the SSC; 36 hours later it dropped to a very low density, 5 cm⁻³, and the IMF showed a stable away sector orientation. The solar wind velocity suddenly jumped from ~ 350 to ~ 440 km/s near the onset of the SSC and then gradually increased to

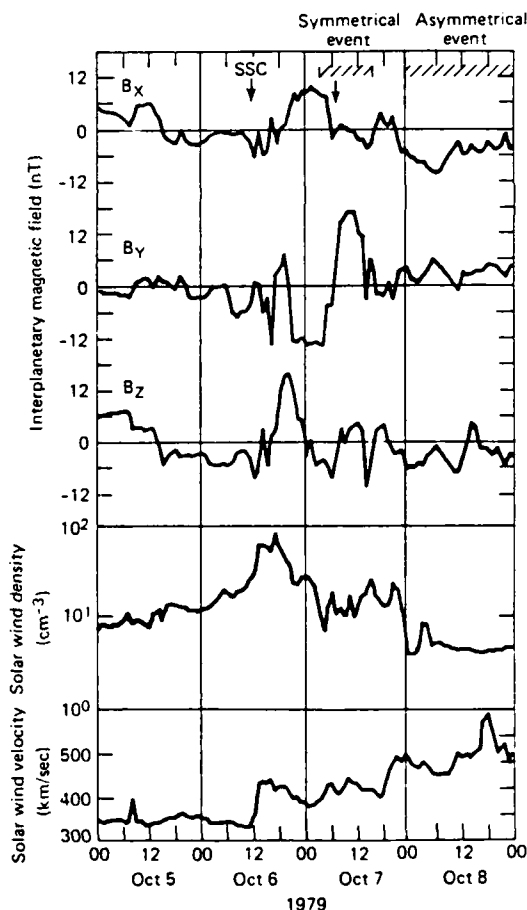


Fig. 6. The hourly average values of the IMF B_x , B_y , and B_z and the solar wind densities and velocities obtained by IMP 8. A magnetic storm sudden commencement occurred at 1120 UT. Periods of symmetric and asymmetric phenomena are indicated. The arrows indicate passes of the typical symmetric event described in Figure 4.

TABLE 1. Hemispherically Symmetric Enhancements of Polar Rain Events

Symmetrical Event (flux $> 10^7$ in both hemispheres)	Selected Polar Pass	Kp Index
Aug. 27, 1978, 1100-1500	4	4, 5-
Oct. 30, 1978, 1300 to Oct 31, 0800	16	4-, 5-, 4+, 4-, 4-, 4-, 3-
March 22, 1979, 2200 to March 23, 1000	14	3, 4-, 3+, 3, 2-
April 3, 1979, 2200 to April 4, 1300	18	8, 7-, 6+, 5+, 5+, 5-
April 9, 1979, 0000-0500	6	4, 3+
Sept. 18, 1979, 0100-1600	14	6-, 5-, 7, 6+, 6-, 6
Oct. 7, 1979, 0300-1400	8	4+, 4, 3+, 5
Nov. 12, 1979, 1300 to Nov. 13, 0100	14	2+, 2+, 2, 2-, 4
Nov. 23, 1979, 1300 to Nov. 24, 0100	10	1, 1, 2-, 2, 3

The total number of polar passes with symmetric polar rain distribution is 104, corresponding to 52 pairs of observations for both hemispheres.

above 500 km/s. The hemispherically symmetric enhancement of the polar rain was detected 16 hours after the SSC and continued for about 11 hours, between 0300 and 1400 UT on October 7, which corresponds to part of the transition period from a stable IMF toward sector to an away sector. The typical asymmetric polar rain enhancement was detected 36 hours after the SSC on October 8 during a stable IMF away sector.

In order to understand the conditions for the hemispherically symmetric enhancement of polar rain, more examples have to be examined. A fundamental question is how often does the symmetric type of polar rain occur. Using DMSP F2 and F4 electron data from August 1978 to December 1979, we searched for distinct symmetric polar rain observations with a total number flux larger than $\sim 10^7$ electrons/cm² s sr near the center of the polar caps in both hemispheres. We used somewhat intense polar rain events in order to avoid ambiguity in defining the symmetric polar rain, as was discussed previously. The count rate at ~ 200 eV is generally about 1 order of magnitude above the background. Also, the symmetric distribution has to occur for at least two orbits.

Only nine periods (Table 1) show clear hemispherically symmetric enhancement of the polar rain. The average duration of a symmetric event is about 11 hours, and the maximum and minimum durations are 19 hours and 4 hours, respectively. The total number of polar passes with intense, symmetric polar rain distribution is 104, corresponding to 52 pairs of observations from both hemispheres. Six out of nine ($\sim 70\%$) symmetric events occur within 24 hours after an SSC. Thus the occurrence of symmetric events may be related to the interplanetary shock and/or the turbulent IMF configuration. Our limited observations also reveal that the intense symmetric events occur most often when $-4 < B_z < 0$ nT (that is, B_z is southward) and when the Kp index is generally larger than 3, as shown in Table 1.

Next, we examined the relationship between the symmetric polar rain enhancement and the IMF sector structure. The concurrent values of the IMF B_x and B_y components are plotted in Figure 7. Among the data in Table 1, there are six orbits without IMF information. Of the 48 orbits of symmetric polar rain observations, 70% are associated with a typical away or toward sector structure along a general IMF garden-hose configuration. Even though almost 30% of the symmetric polar rain events are detected during an unusual IMF orientation, it is not obvious that the symmetric events are associated with some strange IMF con-

dition. However, the absolute values of B_x and B_y are rather large (> 10 nT) in most cases. Indeed, the average IMF magnitude of all these events is ~ 12 nT which is much larger than the average IMF magnitude of ~ 7 nT during 1978-1979 [King, 1981].

Another feature of the occurrence of symmetric polar rain events is the association with high solar wind density. Figure 8 shows the occurrence number of symmetric polar rain crossings versus the solar wind density. Simultaneous solar wind density data are found during 51 paired DMSP observations. During periods of symmetric events, the solar wind density is high (an average of ~ 11.4 cm⁻³), whereas the average solar wind density during 1978-1979 is only 6.6 cm⁻³, as reported by King [1983]. Recently, Fairfield and Scudder [1985] reported that the typical asymmetric enhancement of polar rain occurs during periods of low solar wind density. Therefore the occurrence conditions for the hemispherically symmetric enhancement of polar rain may be quite different from those for asymmetric ones.

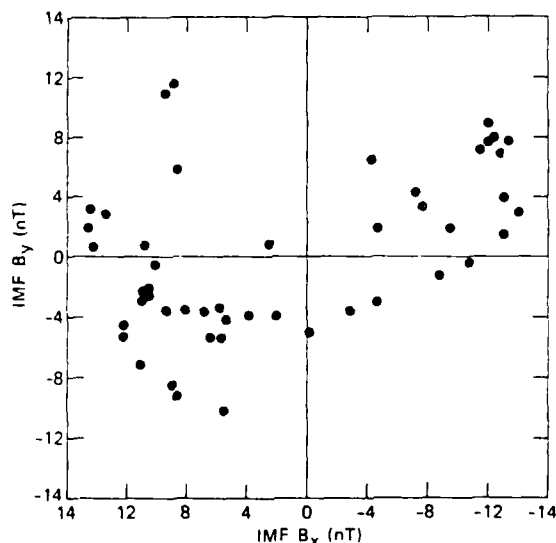


Fig. 7. A scatter plot of the IMF B_x and B_y components for all the intense symmetric events listed in Table 1. The IMF configuration of 70% of 48 symmetric events has the typical away or toward sector structure along the garden-hose direction.

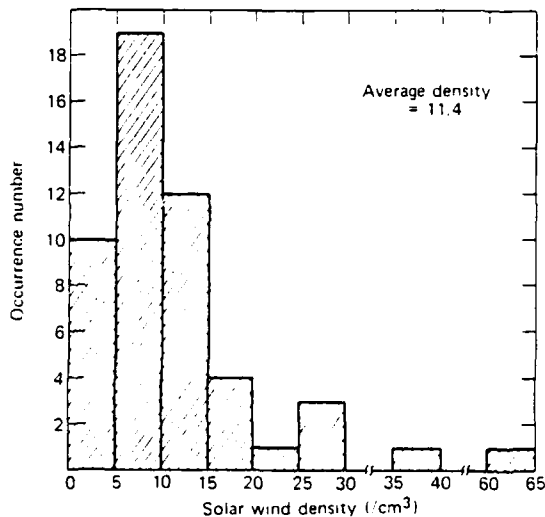


Fig. 8. The occurrence numbers of symmetric events and their relationship to the solar wind density. The average solar wind density for all these events is 11.4 cm^{-3} .

SUMMARY AND DISCUSSION

The long-period variations of polar rain precipitations are examined by using observations over four consecutive solar rotations from January 24 to May 11, 1979. The study confirms the asymmetric polar rain flux distribution reported previously from shorter duration observations or case studies [Fennel *et al.*, 1975; Meng and Kroehl, 1977; Mizera and Fennel, 1978]. Temporal variations of polar rain flux between the northern and the southern hemispheres generally are anticorrelated, and the polar rain flux varies rapidly in the order of hours.

On the basis of the statistical analysis of the polar rain flux and the concurrent IMF values we did not find any distinct correlation between the magnitude of IMF B_x and/or B_y values and the intensity of polar rain events, although a weak positive correlation (with a coefficient of 0.3) did exist between the absolute value of the IMF B_y and the polar rain intensity. This is different from the results of Riehl and Hardy [1986] that appeared during the reviewing process of our paper; they reported a higher correlation between the magnitudes of $|B_x|$ and $|B_y|$ and the polar rain intensity. This discrepancy may be due to the effect of different data sets and requires further study. The intense polar rain flux is mainly ($\sim 96\%$) observed in the northern hemisphere for negative B_x (or positive B_x) values; for positive B_x (or negative B_x) values the larger polar rain flux was observed ($\sim 97\%$) in the southern hemisphere. Thus the IMF B_x direction controls the entry of the polar rain electrons, as was previously reported, while other parameters such as the IMF magnitude do not play an important role.

An obvious parameter that may relate to the polar rain intensity is the electron density of the solar wind. However, our comparison of variations of the polar rain flux with those of the solar wind density did not reveal any significant positive intensity correlation. In fact, we found that typical asymmetric polar rain enhancements are usually observed during periods of low solar wind density ($< 10 \text{ cm}^{-3}$). Recently, Fairfield and Scudder [1985] reported that field-aligned fluxes of electrons of a few hundred electron volts are detected in the magnetotail lobe during periods of high solar wind velocity and low density; they suggested that the intense solar wind strahl [Rosenbauer *et al.*, 1976; Feldman

et al., 1978; Ogilvie and Scudder, 1981] is likely to be the source of polar rain. Our observation of the asymmetric enhancement of the polar rain flux during periods of low solar wind density is consistent with their suggestion. Furthermore, the occurrence of the strahl tends to be correlated with the sector in such a way that the strahl is usually more pronounced at the beginning of a sector structure and gradually weakens toward the end of each sector [Pilipp *et al.*, 1981]. Variations in the polar rain flux examined here sometimes show similar features.

A previously unnoticed polar rain phenomenon was recognized during this study: the simultaneous enhancement of polar rain with similar intensity over both the northern and southern polar caps. This polar rain electron precipitation is enhanced usually at energies below 1 keV, similar to typical asymmetric polar rain spectra, but it is different from the well-established polar rain feature of asymmetric enhancement occurring mainly in one hemisphere. Reported symmetric polar rain events are characterized by similar precipitation intensities over both the northern and southern polar caps. The duration of examined symmetric events is generally about 10 hours, indicating that the observed simultaneous enhancement over both polar caps cannot be coincidental. The examined differential polar rain electron spectra obtained at similar magnetic latitudes and local times over the opposite hemispheres are very similar. This spectral similarity may imply that the source for the symmetric polar rain electrons seen at low altitudes in the two polar caps is the same. Certainly, we cannot yet eliminate the possibility of a magnetospheric source for the symmetric polar rain, but the uniform distribution over both polar caps, the extended duration, the spectral similarity between the two polar caps, and the opened geomagnetic field line configuration in polar caps do not point toward any easily explainable magnetospheric origin. We noticed that most of the symmetric events are related to the IMF turbulence and the high solar wind density, whereas the asymmetric events usually occur during stable periods of away or toward IMF sector structure and low solar wind density. Fairfield and Scudder [1985] identified the higher-energy portion of the polar rain with the anisotropic strahl and also noticed that the lower-energy solar wind is more isotropic. However, it is unlikely that the observed precipitation over both polar caps is the consequence of this isotropic lower-energy electron, since the spectra of symmetric polar rain are similar to typical ones without an indication of softer precipitation. Even though the frequency of occurrence of these intense polar rain events is rather low (about one 10-hour-long event per month, or fewer), their unusual symmetric distribution is a distinct polar precipitation phenomenon associated with solar terrestrial interaction and deserves further investigation.

Acknowledgments. We would like to thank Marian Greenspan for many useful discussions and suggestions during the course of this research. This work was supported by the Air Force Office of Scientific Research grant AFOSR-84-0049 and the Atmospheric Sciences Division, National Science Foundation grant ATM-8315041 to The Johns Hopkins University Applied Physics Laboratory. K. Makita also acknowledges a partial support from the National Institute of Polar Research in Japan. Many useful comments from reviewers to improve the presentation of this paper are acknowledged.

The Editor thanks two referees for their assistance in evaluating this paper.

REFERENCES

- Coffey, H. E., *Solar-Geophysical Data Prompt Reports*, 415-419, Nat. Geophys. and Sol.-Terr. Data Cent., Nat. Oceanic and Atmos. Admin., Boulder, Colo., 1979.
- Fairfield, D. H., and J. D. Scudder, Polar rain: Solar coronal electrons in the earth's magnetosphere, *J. Geophys. Res.*, **90**, 4055, 1985.

- Feldman, W. C., J. R. Asbridge, S. J. Bame, J. T. Gosling, and D. S. Lemons, Characteristic electric variations across simple high-speed solar wind streams, *J. Geophys. Res.*, **83**, 5285, 1978.
- Fennel, J. F., P. F. Mizera, and D. R. Croley, Jr., Low energy polar cap electrons during quiet times, *Conf. Pap. Int. Cosmic Ray Conf. 14th*, 1267, 1975.
- Foster, J. C., and J. R. Burrows, Electron fluxes over the polar cap, 1, Intense keV fluxes during poststorm quieting, *J. Geophys. Res.*, **81**, 6016, 1976.
- Foster, J. C., and J. R. Burrows, Electron fluxes over the polar cap, 2, Electron trapping and energization on open field lines, *J. Geophys. Res.*, **82**, 5965, 1977.
- Greenspan, M. E., C.-I. Meng, and D. H. Fairfield, Simultaneous polar cap and magnetotail observations of intense polar rain, *J. Geophys. Res.*, **91**, 11,123, 1986.
- Gussenhoven, M. S., D. A. Hardy, N. Heinemann, and R. K. Burkhardt, Morphology of the polar rain, *J. Geophys. Res.*, **89**, 9785, 1984.
- Hardy, D. A., M. S. Gussenhoven, and A. Huber, The precipitating electron detectors (SSJ/3) for the block 5D flights 2-5 DMSP satellites: Calibration and data presentation, *Rep. AFGL-TR.-79-0210*, Air Force Geophys. Lab., Hanscom Air Force Base, Bedford, Mass., 1979.
- Heikkila, W. J., Penetration of particles into the polar cap and auroral regions, in *Critical Problems of Magnetospheric Physics*, edited by E. R. Dyer, pp. 67-82, Inter. Union Commission on Solar Terrestrial Physics, Washington, D. C., 1972.
- King, J. H., On the enhancement of the IMF magnitude during 1978-1979, *J. Geophys. Res.*, **86**, 4823, 1981.
- King, J. H., *Interplanetary Medium Data Book, S. ppl. 2 GSFC/NSSDC 83-01*, Goddard Space Flight Center, Greenbelt, Md., 1983.
- Makita, K., and C.-I. Meng, Average electron precipitation patterns and visual aurora characteristics during geomagnetic quiescence, *J. Geophys. Res.*, **89**, 2361, 1984.
- Meng, C.-I., and H. W. Kroehl, Intense uniform precipitation of low-energy electrons over the polar cap, *J. Geophys. Res.*, **82**, 2305, 1977.
- Meng, C.-I., S.-I. Akasofu, and K. A. Anderson, Dawn-dusk gradient of the precipitation of low-energy electrons over the polar cap and its relation to the interplanetary magnetic field, *J. Geophys. Res.*, **82**, 5271, 1977.
- Mizera, P. F., and J. F. Fennel, Satellite observations of polar magnetotail lobe and interplanetary electrons at low energies, *Rev. Geophys.*, **16**, 147, 1978.
- Ogilvie, K. W., and J. P. Scudder, Observations of the "strahl" by the solar wind electron spectrometer on Mariner 10, in *Solar Wind Four*, edited by H. Rosenbauer, pp. 226-240, Springer-Verlag, New York, 1981.
- Pilipp, W. G., R. Schwenn, E. Mach, K.-H. Muhlhauser, and H. Rosenbauer, Electron characteristics in the solar wind as deduced from Helios observations, in *Solar Wind Four*, edited by H. Rosenbauer, pp. 241-249, Springer-Verlag, New York, 1981.
- Riehl, K. B., and D. A. Hardy, Average characteristics of the polar rain and their relationship to the solar wind and the interplanetary magnetic field, *J. Geophys. Res.*, **91**, 1557, 1986.
- Rosenbauer, H., H. Miggenrieder, M. Montgomery, and R. Schwenn, Preliminary results of the Helios plasma measurements, in *Physics of Solar Planetary Environments*, edited by D. J. Williams, p. 319, AGU, Washington, D. C., 1976.
- Winningham, J. D., and W. J. Heikkila, Polar cap auroral electron fluxes observed with ISIS 1, *J. Geophys. Res.*, **79**, 949, 1974.
- Yeager, D. M., and L. A. Frank, Low-energy electron intensities at large distances over the earth's polar cap, *J. Geophys. Res.*, **81**, 3966, 1976.

K. Makita and C.-I. Meng, Applied Physics Laboratory, The Johns Hopkins University, Laurel, MD 20707.

(Received October 30, 1985;
revised March 10, 1987;
accepted March 27, 1987.)

Energy Dependence of the Equatorward Cutoffs in Auroral Electron and Ion Precipitation

PATRICK T. NEWELL AND C.-I. MENG

The Johns Hopkins University, Applied Physics Laboratory, Laurel, Maryland

The spectral dependence in the equatorward cutoff of diffuse auroral electron and ion precipitation is investigated using the Defense Meteorological Satellite Program F6 and F7 low-altitude polar-orbiting satellites. These equatorward boundaries are determined at 100, 1000, and 3000 eV during very quiet conditions and during normal conditions (low-level magnetic activity) in the dawn, dusk, premidnight, and prenoon sectors. We find that under normal conditions the low-energy ions cut-off equatorward of the higher energy ions at all local times, with the largest effect at dawn and the smallest at dusk. Electrons exhibit greater variability; however, at premidnight, low-energy electrons cut-off equatorward of higher energy electrons, while at dawn the electron cutoff-ordering becomes $\lambda_{100} \gg \lambda_{3000} > \lambda_{1000}$, where the subscripts are energies in electron volts. During times of prolonged and profoundly quiet conditions, the dispersion, particularly for ions, disappears; that is, the cutoffs at all three energies coincide. It is argued that these observations provide evidence against the predictions of the often considered model of steady-state Alfvén layers arising from a constant source in the magnetotail convected earthward by a Stern-Volland cross-tail electric field toward a magnetic dipole. For example, the predicted ion dispersion is never observed. Investigating the response to magnetic disturbances following times of profound quiet, we find prompt, near simultaneous reaction over a wide local time range, including dawn and dusk. Following a return to quiet magnetic conditions, the precipitation relaxes to pre-disturbance patterns in the premidnight region within 1 to 2 hours but takes several hours longer at dawn. The electron precipitation cutoffs are equatorward of the ion precipitation cutoffs in all magnetic local time sectors except dusk, where the ion precipitation extends further equatorward.

1. INTRODUCTION

The latitudinal dependence of various auroral features as a function of local time and magnetic activity has been investigated over the years (among others, *Starkov and Feldstein* [1969], *Holzworth and Meng* [1975], *Meng et al.* [1977], and *Zverev et al.* [1979]. *Gussenhoven et al.* [1981, 1983] have used the Defense Meteorological Satellite Program (DMSP) F2 and F4 satellites to systematically determine the latitude of the equatorward boundary of the diffuse auroral electron precipitation based on total energy flux as a function of magnetic local time and *Kp*. *Horwitz et al.* [1986] have recently used DE 1 and 2 observations to correlate the equatorward auroral electron boundary with the equatorial plasma sheet boundary in the evening to midnight sector. *Sauvaud et al.* [1981] reported on soft ion precipitations with an energy-dependent cutoff at the equatorward edge of the morning diffuse aurora, concluding that they could be accounted for by magnetospheric single-particle convection following substorm plasma injections. However, *Sauvaud et al.* [1985], investigating these same soft morningside ion precipitations at the equatorward edge of the ion diffuse auroral region, gave as a mechanism, upwelling ionospheric ions from the opposite hemisphere that subsequently undergo a velocity filter effect. To our knowledge there have been no previous investigations aimed at determining the behavior of both electron and ion auroral equatorward cutoffs at various magnetic local times and levels of magnetic activity as a function of energy. Such a data set, which is to be the subject of the present inquiry, has the inherent interest of auroral phenomena, as well as probable consequences for magnetospheric convection, particularly the formation of the inner edge of the plasma sheet.

The location, local time dependence, and spectral dispersion of the inner edge of the plasma sheet can provide valuable criteria

for distinguishing between models of plasma convection into (or local energization in) the middle magnetosphere. Because it is easy to work with, many workers make the assumption of a steady source in the distant magnetotail that is convected earthward by a cross-tail electric field, continuously replenishing the inner plasma sheet. There are two alternate, frequently referred to explanations for the formation of an inner boundary to this earthward convecting plasma. One is simply that the increasing influence of the earth's corotational field and curvature and gradient drifts deflects particles around the earth, thus limiting their earthward penetration (the boundaries thus formed are often called Alfvén layers). There have been numerous calculations along these lines, assuming a dipole magnetic field and a Stern-Volland cross-tail electric field (for example, *Chen* [1970], *Ejiri* [1978], *Ejiri et al.* [1980], *Kivelson et al.* [1980], and *Hultqvist et al.* [1982] among others). Because higher energy electrons drift eastward faster than lower energy electrons, they have less time to convect inward. Hence this model predicts that the inner edge of the plasma sheet for low-energy electrons lies further earthward than for higher energy electrons. Ions of zero energy would follow zero-energy electrons; ions of intermediate energy perpendicular to the magnetic field would have curvature and gradient drifts that partially cancel out the eastward convection, thus leading to the greatest earthward penetration. The theory of convection in the inner and middle magnetosphere, including magnetospheric-ionospheric coupling, has been reviewed at length in a tutorial fashion by *Wolf* [1983].

Strong diffusion has also been invoked to explain the creation of an inner boundary [*Kennel*, 1969; *Ashour-Abdalla and Thorne*, 1978; *Harel et al.*, 1981a, b]. As the plasma convects inward from the distant magnetotail, the bounce time decreases as $L^4/E^{0.5}$, where L is the McIlwain parameter and E is the particle energy. Under the strong diffusion assumption the lifetime against precipitation is $T = 2T_b/\alpha_0^2$, where T_b is the quarter bounce time and α_0 is the equatorial loss cone angle. As the particles move earthward, their lifetimes hence rapidly decrease, and a boundary is formed in which the lower energy particles penetrate to lower L

Copyright 1987 by the American Geophysical Union.

Paper number 6A8677.
0148-0227/87/006A-8677\$05.00

values because of their longer bounce time. One consequence of this model is that protons, because of their greater mass and hence longer bounce period, should convect significantly further earthward. However, *Ashour-Abdalla and Thorne* [1978] believe that the electron and ion regions of precipitation generally coincide and have suggested an explanation. They argue that the region of electron precipitation coincides with the region of field-aligned currents, which in turn excite ion mode turbulence, heating cold ionospheric electrons, thus allowing ion cyclotron waves, leading to broadband electrostatic noise and consequent ion pitch angle scattering. This model would appear to predict no energy dependence in the equatorward edge of ion precipitation, since the limit of ion precipitation is determined by the limit of field-aligned currents.

A basic underlying assumption of both these models, namely, steady state convection from the magnetotail, has been called into question on theoretical grounds. *Erickson and Wolf* [1980] have argued that adiabatic convection from essentially planar field lines toward the more dipole field lines of the earth leads to pressure constraints that are very difficult to satisfy. *Schindler and Birn* [1982] have, through the use of MHD modeling, shown that possible MHD steady state convection solutions are, because of the pressure balance problem, very unrealistic. *Lui and Hasegawa* [1986] have shown that if the source of magnetospheric plasma is from the flanks of the magnetosphere a time independent solution is not possible. *Williams* [1981] has used ISEE 1 observations to study ion beams in the plasma sheet boundary layer; he was able to account for the behavior of such ion beams based solely on single-particle convection from a tailward intrinsically sporadic source. Of course, there is no doubt that dynamic processes such as substorms play an important role in magnetospheric physics; the question is whether a steady state condition, for example, a steady state plasma sheet boundary, ever exists.

There have been numerous observations in the magnetosphere concerning the spectral effect in the plasma sheet inner edge. Most of these reports have considered only the electron and not the ion signatures and are usually confined to one particular local time zone. *Vasyliunas* [1968] reported that in the dusk sector (~ 17 – 22 hours LT) the boundary of the plasma sheet for low-energy electrons consistently lies earthward of the boundary for higher energy electrons (he reports an exponential dropoff in the electron energy at the plasma sheet boundary with a scaling distance of $0.4 R_E$ in quiet times and $0.6 R_E$ during magnetically active times). *Schild and Frank* [1970] reported similar observations near local midnight. *Kivelson et al.* [1980], using spectrograms from ATS 5 (in the equatorial geosynchronous magnetosphere), found some electron signatures in the dusk sector that they were able to model with reasonable accuracy based on a particular set of Alfvén layers. Some electron encounter signatures were interpreted in terms of the standard steady state convection, and for some they used a uniform cross-tail potential that abruptly jumps during substorms and then decays with a time constant of about 2 hours. *Hultqvist et al.* [1982], based on geosynchronous (GEOS 2) observations primarily in the premidnight local time sector, concluded that during quiet times certain electron encounter signatures could be modeled reasonably well as Alfvén layers produced by a Stern-Volland cross-tail electric field with shielding factor $\gamma = 4$.

Baumjohann et al. [1985] report on direct observations of the electric field from geostationary orbit. They find that during quiet times ($Kp = 0$ – 1), the electric field is very different from a Stern-Volland configuration, while for $Kp = 3$ – 4 the local time region

~ 12 – 21 hours closely follows a Stern-Volland field and that even in this disturbed condition, the middle magnetosphere differs radically from a Stern-Volland field near dawn.

Fairfield and Vinas [1984] used the ISEE 1 low-energy electron spectrometer to investigate whether the electric and magnetic field convection patterns or strong diffusion was more important in determining the boundaries of the inner edge of the plasma sheet. Frequent observations of large anisotropies in pitch angles and the observation that the plasma sheet sometimes extended as close as $L = 5$ at dawn led them to conclude that strong diffusion could not play a dominant role in determining the earthward penetration of electrons from the distant magnetotail. They observed that lower energy electrons usually penetrated closer to earth than higher energy electrons, that this spectral dispersion was more pronounced near dawn and dusk than near midnight, and that in agreement with single-particle convection theory, field-aligned electrons penetrate closer to earth than electrons near 90° . On the basis of DE 1 and DE 2 measurements of the electron inner edge of the plasma sheet and corresponding low-latitude electron precipitation boundary in the dusk to midnight sector, *Horwitz et al.* [1986] also argued for the importance of steady state convection in defining these boundaries.

Mauk and Meng [1983] have emphasized the importance of considering both electron and ion signatures simultaneously when investigating magnetospheric convection phenomena. Using geosynchronous data, they show that the dusk sector 0 to 5 keV plasma encounters such as investigated by *Kivelson et al.* [1980] and *Hultqvist et al.* [1982] have an ion dispersion signature opposite to the prediction of quasi steady state convection theory. They also found that the radial location of the feature did not vary with substorm activity as predicted by Alfvén layer models. Moreover, they found that the plasma dropout signatures, not considered by the previous authors, had both electron and ion signatures opposite to that predicted by Alfvén layer models. However, they found that a dynamical injection boundary model could account for both the ion and electron signatures in both cases. *Mauk and Meng* [1986] further investigated the question of plasma introduction into the near-earth (roughly geosynchronous) region. They concluded that Alfvén layer type steady state convection is never observed to convect plasma from the distant magnetotail into geosynchronous orbit. Instead, they found that plasma introduction into the near-earth region was always associated with time dependent highly inductive electric fields, followed subsequently by adiabatic convection by curl-free global convection fields (that is, single-particle motions).

In the present work we examine the energy dependence of the equatorward cutoff of diffuse auroral precipitation for both electrons and ions in the dawn, dusk, prenoon, and premidnight sectors. The most unique feature of the present study is the ion observations, which have received far less attention than the electron precipitations. We also make correlations with magnetic activity on a case study basis, allowing us to address the issue of time evolution and not just statistical averages. The data are taken from the DMSP F6 and F7 low-altitude (840 km) polar-orbiting satellites with a 101-min period. Descriptions of these satellites and the particle experiment can be found in *Gussenhoven et al.* [1985] and *Hardy et al.* [1984]. It suffices here to state that the particle spectrometers are cylindrical electrostatic analyzers that cover the range 30 eV to 30 keV for both electrons and ions in a 20-point spectrum once per second. These detectors are always directed toward local zenith, so that at the latitudes of interest here only precipitating particles are detected. Under the assumption that

precipitation boundaries map to convection boundaries, that is, assuming that if particles convect into a region, there will be some corresponding precipitation, the DMSP data are compared to the above models. We find that the energy dispersion of equatorward cutoffs is fundamentally incompatible with the predictions of steady state Alfvén layers, particularly in that the sense of dispersion that such models predict for ions is virtually never observed. The assumption that the boundaries are formed by precipitation losses at the strong diffusion rate does much better in predicting the dispersion senses; however, such models still cannot explain the observation that during very quiet times, the dispersion tends to zero, especially for the ions. Moreover, if the boundaries are formed by this loss mechanism, the ion boundaries should lie well inside the electron boundaries, which disagrees with our observations, except at dusk. Section 2 presents observations documenting these and other features, and section 3 contains a discussion of their significance.

2. DATA PRESENTATION

2.1. The Usual Precipitation Patterns

Because changes in the dispersion pattern can happen on time scales shorter than 3 hours, we preferred investigating periods in which the *AE* indices, as well as the *Kp* index, were available. DMSP F7 data are available starting in December 1983, which also is the latest month with available *AE* data; hence our study concentrates on this month. The F6 data set, available since 1982, is also crucial to our study. We have scanned through plots of electron and ion count rates throughout this month and noticed certain trends including a strong dependence of dispersion patterns on magnetic activity. In order to make a more systematic study we chose three intervals, two of which include the longest periods of nearly complete magnetic quiescence in the month. The third period is a day of fairly uniform, continuous, and modest level activity as indicated by *AE* tracings; the 3-hour *Kp* indices vary only between 2 and 3 until the final 3-hour period (when *Kp* drops to 1). The average *Kp* for the day is 2.0. This event is included to represent normal behavior and indeed appears to be typical of the dispersion patterns observed a large majority of the time. For each of these intervals the equatorward cutoff of auroral electron and ion precipitation was determined at 100, 1000, and 3000 eV from the high-resolution tables for each satellite pass. Data from both hemispheres were taken with similar results; the data presented here will be primarily from the northern hemisphere because the satellite's trajectory covers the high-latitude regions more continuously there. The particular energies used were chosen in part because the counting statistics were normally good enough to make a determination of the equatorward edge with reasonable confidence. Normally, the equatorward portion of the precipitation at any particular energy shows a sharp decline from near-peak fluxes to near-background fluxes over a narrow latitudinal range. Here we chose to define the equatorward edge as the point where this steep drop levels off at or near background rates (the equivalent converse definition moving from lower to higher latitudes is the point where a sharp rise from or near background levels to intense fluxes begins).

Because of the potential for controversy in any particular definition of the equatorward cutoff in precipitation, we further clarify our own definition with the aid of Figure 1, which shows an example of the determination of the cutoffs for morningside ions at the three energies used. It should be pointed out that for the low-energy channels, in particular, for the ≤ 1 keV ions, there is often an extended region of flat low-level count rates continu-

ing beyond the auroral zone, indeed, sometimes reaching to the limit processed, 50 Magnetic Latitude (MLAT). We take the edge of the auroral zone to be the edge of the ramp, that is, the first point at which count rates significantly above the flat background-like levels are recorded. The equatorward cutoff is, in fact, a physical effect and is not simply determined by detector threshold. Thus, for example, 1-keV electrons and ions are each measured by two different detectors with greatly different sensitivities, yet the equatorward edge as determined from either detector generally agrees reasonably well (within the much larger statistical error of the less sensitive channel). In Figure 1 the dispersion of several degrees between the equatorward extent of 100 and 3000 eV ion precipitation at dawn can be seen very clearly. Sometimes the cutoffs at the edge of the auroral zone are very sharp. We have found by scanning about a week of data that the same sense of dispersion occurs regardless of whether one considers only very sharp cutoffs or includes the less precise cutoffs such as in Figure 1, as is done in this paper. Because the latter are more common, we believe it would distort the data set to restrict it to the cases with sharp cutoffs.

Clearly, one could use alternate definitions of the equatorward edge; for example, one might use the point where the dropoff begins rather than the point (moving from lower to higher latitudes) where the rise from approximately background levels begins (as adopted here). The definition employed here seems appropriate for investigating the predictions of the models discussed in the introduction concerning the furthest earthward penetration of particles with a source in the magnetotail. Inevitably, there are occasional ambiguous cases because of very low count rates, a drop-off too gradual to define a clear cutoff edge, or other erratic behavior, where it is not practical to determine an equatorward edge; these have been excluded from our data set. Finally, we must for completeness note that we have investigated whether the contamination of the low-energy ion channels by high-energy electrons [Hardy *et al.*, 1984] is significant. Fortunately, sample calculations based on information presented in the work of Hardy *et al.* show that such contamination is consistently insignificant in the determination of the equatorward edge; this is because the electrons that have the worst contaminating effect are those above about 10 keV, and these electrons are not present at high intensities at the low-energy ion equatorward boundaries.

Figure 2 shows the typical latitudinal dispersion in equatorward edges observed in the majority of auroral oval crossings by DMSP F6 and F7 at four different local time sectors. The data are averaged over 1 day (December 2, 1983), and hence each point plotted represents the average of from 11 to 14 passes from a day of reasonably steady low-level activity. The results are representative of what is observed a large majority of the time. In all local time sectors the 100-eV ions extend to lower latitudes than do the 1000-eV ions, which in turn are equatorward of the 3000-eV ions. This dispersion is greatest in the dawn sector, where there is typically several degrees latitude between the 100- and 3000-eV ion edges and where there can be far more. Given the limited amount of data processed quantitatively, the present work is more of a case study with representative examples than a statistical study, but Table 1 gives a feeling for the significance of the separations shown in Figure 2. The uncertainties listed are the population standard deviations in the separations divided by the square root of the number of data points (11-14). Most of the separations are highly statistically significant even based on a relatively small sample size; the exception is the electron separations at dusk, which are merely suggestive.

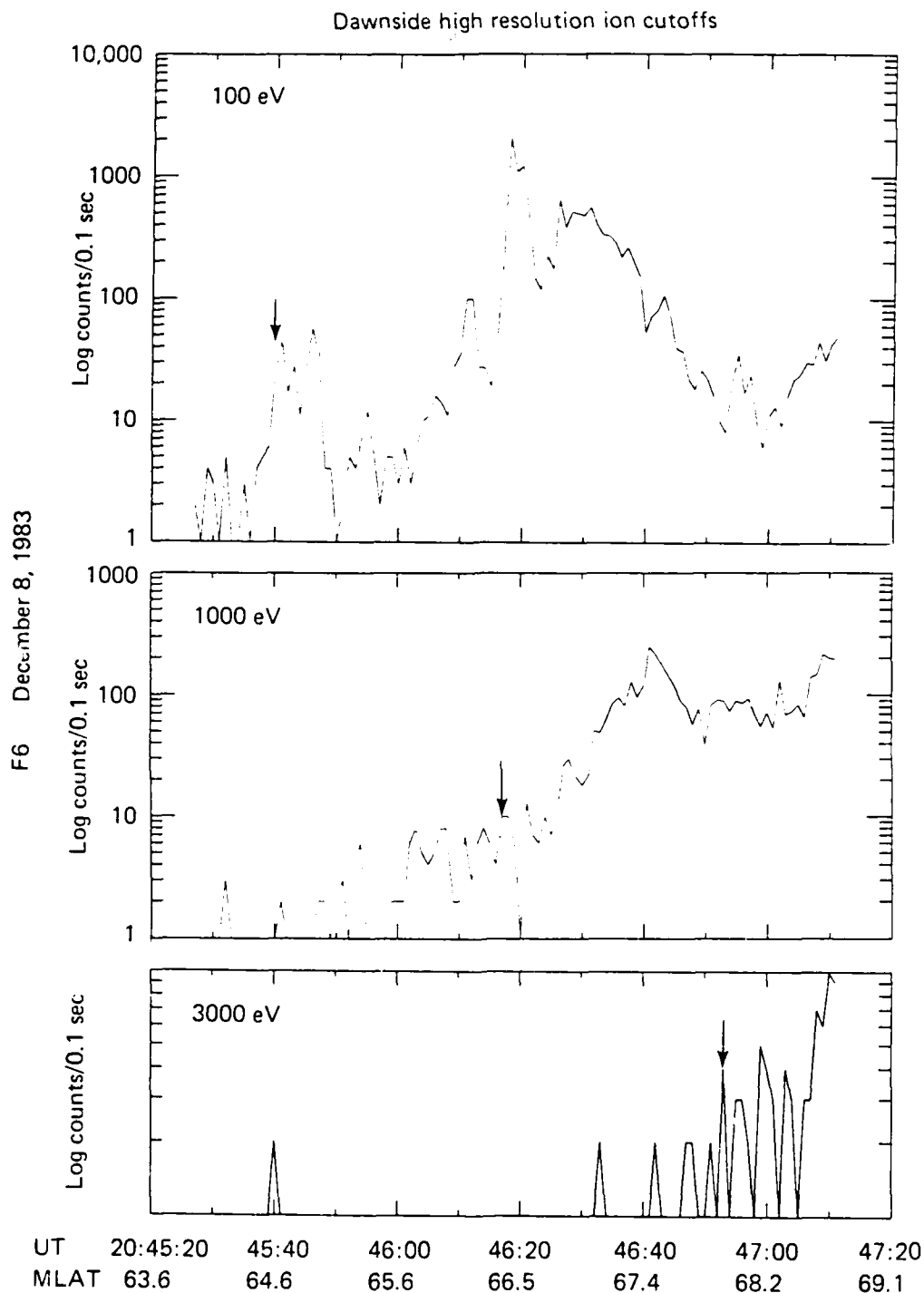


Fig. 1. A high time resolution plot of the ion precipitation edges at dawn for a typical auroral oval pass. The arrows indicate the equatorward cutoffs in auroral ion precipitation as defined in the present paper. The typical ion latitudinal dispersion at dawn in cutoffs as a function of energy is clear.

With appreciable variability, the typical ion dispersion at premidnight (2220–2335 MLT) between 100 and 3000 eV is -1.7° and is definitely smaller than the usual dispersion at dawn. At dusk the dispersion is more erratic, and some reverse signatures (higher energy further equatorward) or mixed (for example, $\lambda_{100} < \lambda_{3000}$

$< \lambda_{1000}$ are seen). However, on the average the 100 eV is about 1° below the 3000-eV ion cutoff. For the ion data the prenoon sector resembles the dawn sector, with the 100-eV cutoff usually about 2–3° below the 3000-eV cutoff.

Figure 2b shows the electron dispersion patterns averaged over

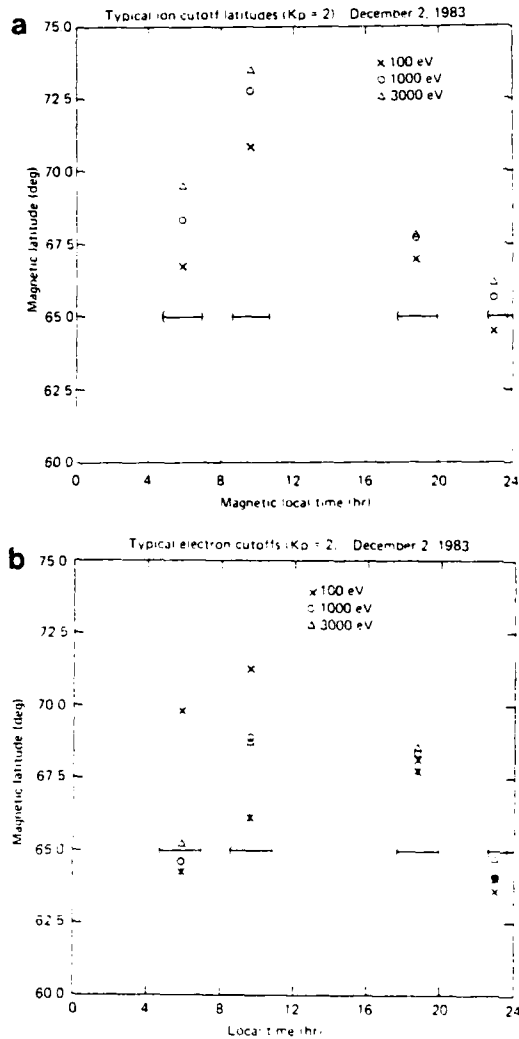


Fig. 2. Equatorward cutoff of auroral particle precipitation averaged over a typical day (northern hemisphere). Crosses, 100 eV; circles, 1000 eV; triangles, 3000 eV. Each point represents between 11 and 14 passes. (a) Ions. The bracketed intervals show the range in magnetic local time each point includes. (b) Electrons, with asterisks representing the diffuse auroral precipitation edge as reported by Gussenhoven *et al.* [1983]. To convert from counts/cm²-s-sr-eV, multiply the 100-, 1000-, and 3000-eV channels by 27.6, 2.76, and 37.8, respectively.

the same day of moderate activity. The electron dispersions are on the whole more variable than the ion dispersions. Most consistent is the premidnight sector, in which the electrons, like the ions, show the 100-eV cutoff equatorward of the 1000-eV cutoff, which itself extends below the 3000-eV cutoff. The dispersion is weaker than that of the ions, with the cutoff latitudes at 100 and 3000 eV usually differing by about only 1°, but the effect is reasonably consistent. At dawn the most common ordering is the 100-eV electron cutoff at several degrees higher latitude than the 3000-eV cutoff, which is usually slightly above the 1000-eV cutoff. It is not uncommon to see the 3000- and 1000-eV electron edges invert, but except during times of profound quiet or considerable activity (as discussed below), the 100-eV cutoff at dawn rarely extends to as low latitudes as the other cutoffs. A preliminary visual scan through a week of data not presented here indi-

cated that 300-eV electron cutoff tends to lie between the 100- and 1000-eV cutoffs. Thus under most circumstances, very low-energy electrons do not precipitate in the dawn sector to nearly as low latitudes as do medium-energy electrons. The prenoon sector is highly variable, with all six possible orderings of the three cutoffs occasionally observed. Generally, there is a rough trend for the 100-eV electron cutoff to occur at higher latitudes than do the cutoffs at higher energies. At dusk the ordering of the cutoffs is again highly variable, although there is some evidence that lower energy electrons are more likely to cut off at lower latitudes. However the dusk sector dispersions tend to be smaller than in other sectors. The very large dispersions that sometimes appear in other magnetic local time regions rarely appear at dusk.

Finally, Figure 2b includes a comparison with the data from Gussenhoven *et al.* [1983], who investigated the equatorward edge of the electron auroral precipitation based on the total electron energy flux as observed by polar-orbiting satellites. Their boundary values generally agree fairly well with our determination of the 1-keV electron flux boundary, the only exception being in the late morning (prenoon) sector. The discrepancy in the prenoon sector probably reflects the "mantle aurora" caused by tens of keV electrons that occurs at lower latitudes than the rest of the auroral precipitation [Meng and Akasofu, 1983]. The auroral "edge" as determined by Gussenhoven *et al.* [1983] is a measure of total energy flux and would be sensitive to these electron precipitations, but they are well above the highest channel (3 keV) that we studied here. The standard deviation reported by Gussenhoven *et al.* [1983] based on their rather large statistical study varies with MLT but is typically about 2°. (Our own auroral edge averages have similarly large standard deviations, reflecting the effects of varying levels of magnetic activity during the day averaged over, the varying magnetic local times covered throughout the day in each local time sector, and other factors.) Our latitudes in Figure 2 are based on between 11 and 14 points each and should be considered only as representative. Note, however, that as the data presented later here make quite clear, there is a strong hysteresis effect (that is not taken into account in the Gussenhoven *et al.* data) that in fact is the reason we chose a day with a fairly uniform level of activity to average over. The observation that the same sense of dispersion is consistently observed makes the relative differences (the dispersions) much more significant than the absolute latitude values. Thus, for example, for the 14 passes used in the average for ions in the dawn sector (Figure 2b), all 14 had the 100-eV ion cutoff at the lowest latitude, 12 had $\lambda_{1000} < \lambda_{3000}$, one had these latter two cutoffs equal, and one had the 3000-eV cutoff 0.1° below that of the 1000-eV cutoff. It is clear that the senses of latitudinal dispersions we report cannot be due to chance alone.

TABLE 1. Latitudinal Separations in the Equatorward Cutoffs of Diffuse Auroral Precipitation (in degrees) with Uncertainties in the Average Separations

	Ions		Electrons	
	$\lambda_{1000} - \lambda_{100}$	$\lambda_{3000} - \lambda_{100}$	$\lambda_{1000} - \lambda_{100}$	$\lambda_{3000} - \lambda_{100}$
Dawn	1.7 ± 0.3	2.9 ± 0.5	-4.9 ± 0.5	-4.3 ± 0.5
Prenoon	2.0 ± 0.3	2.7 ± 0.5	-2.4 ± 1.1	-2.5 ± 1.2
Dusk	0.8 ± 0.2	0.9 ± 0.3	0.1 ± 0.3	0.3 ± 0.3
Premidnight	1.2 ± 0.3	1.7 ± 0.3	0.5 ± 0.15	1.2 ± 0.2

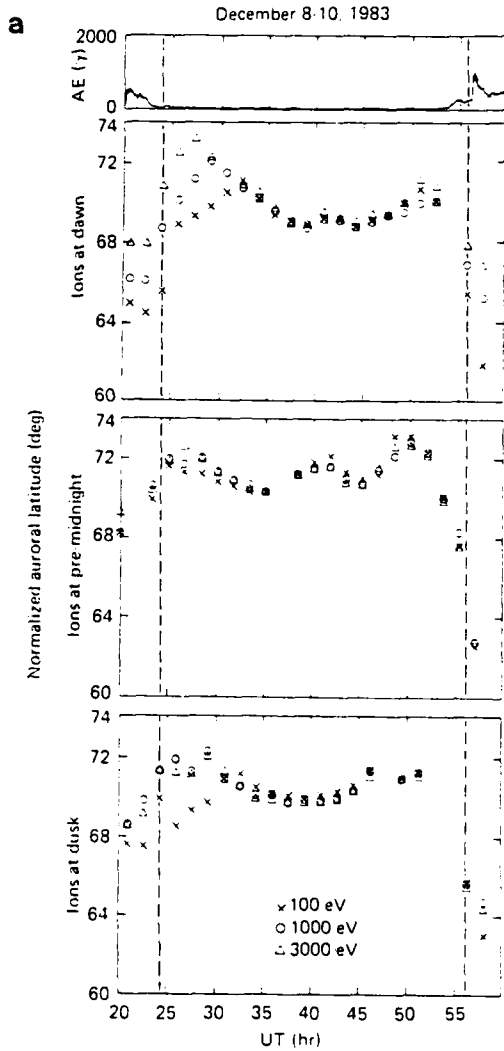


Fig. 3. Normalized auroral latitude of equatorward cutoffs during a long period of profoundly quiet AE . Each point represents a single satellite pass. Crosses, 100 eV; circles, 1000 eV; triangles, 3000 eV. The dashed lines are simply to aid the eye in lining up features in the AE tracings versus equatorward cutoffs. (a) Ions at dawn, ions at pre-midnight, ions at dusk. (b) Ions at prenoon, electrons at dawn. All the data in this figure are from the northern hemisphere.

2.2. The Effect of Substorm Activity and its Complete Absence

The previous paragraphs summarize our observations of typical electron and ion energy dispersions in precipitation cutoffs, as developed from scanning DNISP data and from the data illustrated in Figure 2. We have also investigated changes in the dispersion patterns during times of greater or lesser magnetic activity. During times of profound quiet ($AE < 25 \gamma$), the dispersion is reduced for both electrons and ions in all magnetic local time zones. The effect is particularly spectacular for ions at dawn and midnight, where during times of prolonged magnetic quiet, all three cutoffs coincide. Figure 3 shows a period of about 40 hours in which auroral electrojet activity was very low, including a brief period of activity at the start of the interval (showing a recovery) and at the end of the interval (showing the onset of renewed ac-

tivity). In Figure 3 and in the following figures, each satellite pass of the auroral zone results in a determination of the equatorward cutoff in two local time zones. At each point in time for which there is a cutoff demarcation at one energy, there are ordinarily two more for the other two energies at the same ordinate (same pass through the auroral zone); the only exceptions occur in those rare cases where there is an inability to determine an edge at a particular energy with reasonable confidence. In these figures we have plotted a "normalized" auroral latitude, determined by assuming that the auroral oval is a circle off-set 4.2° toward midnight [e.g., Meng *et al.*, 1977]. In circle this analyzer a first-order correction for the variation in magnetic local time as the earth rotates underneath the satellite is made (typically 2 or 3 hours; refer to the intervals marked in Figure 2). This processing modestly flattens the curves plotted in Figures 3 and 4 while not actually altering the dispersion.

One can observe in Figure 3 that over the course of a few hours following the quieting of AE activity that the equatorward cutoffs move to higher latitudes, and the cutoffs become dispersionless. This effect is particularly clear in the dawn sector, especially for ions. Following the resumption of magnetic activity (as indicated by the second dashed line in Figure 3), the equatorward edge of auroral precipitation moves to lower latitudes promptly (no later than 101 min, the time it takes to complete one orbit) in the dusk, midnight, and dawn magnetic local time sectors. Notice the subsequent dramatic increase in dispersion in the dawn sector ions. This (dawnside) effect appears with great consistency following an increase in AE activity. Similar dispersions often appear at midnight and at dusk but not to as great an extent. The time resolution in this example is not clear enough to show another interesting effect, discussed later, which is that the drop to lower latitudes occurs first and is subsequently followed by the increased dispersion. The dashed lines in Figures 3 and 4 are always drawn to

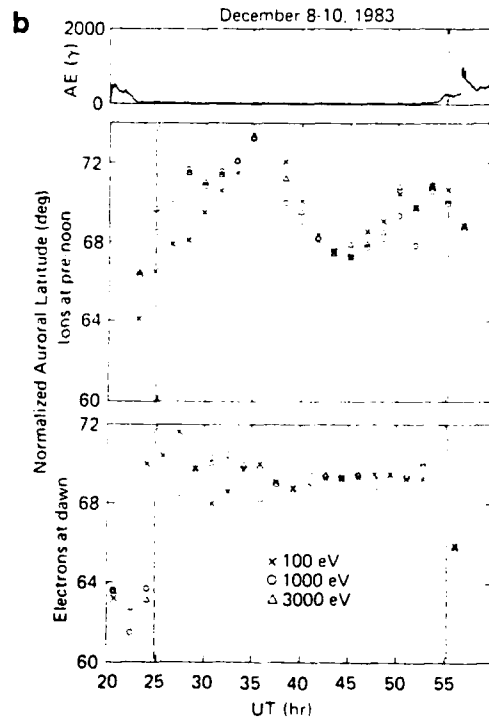


Fig. 3 (continued)

coincide with a satellite crossing of the auroral oval rather than to match a particular feature of *AE*.

The approximate simultaneity of the response over such a large longitudinal extent makes it clear that the introduction of plasma in the more earthward regions (lower latitudes) is not an initially isolated phenomena followed by subsequent convection but occurs even initially over a very wide local time range. In addition, Figure 3 suggests that the response of equatorward edges to changes in the magnetic disturbance level occurs quite promptly, within a satellite orbit period of 101 min, in the dawn, premidnight, and dusk sectors but occurs more slowly in the prenoon region (note that promptness of response is distinct from the simultaneity of the response in the different local time sectors). This impression is confirmed by the final example to be presented here.

Figure 4 shows another period of low magnetic activity that contains two fairly well isolated modest disturbances. In the initial part of this figure one can see the dispersions decreasing after magnetic activity quiets, a process that takes noticeably longer at dawn than at premidnight. In the dawn sector (the first panel) it is clear that following a magnetic disturbance the ions exhibit a greatly enhanced dispersion and that this occurs on a time scale of less than one satellite orbit. However, the time scale for subsequent recovery to a near dispersionless state appears to be several hours at dawn (refer also to the initial portion of Figure 3). The second and third panels of Figure 4 show that in the midnight sector also the equatorward edge of auroral precipitation moves to lower latitudes rapidly following an increase in *AE* activity. Notice particularly that immediately following the first disturbance (refer to the dashed line at 21.5 hours), all three boundaries coincide during the then-current satellite pass through the northern hemisphere (the satellite was not reaching high enough latitudes in the southern hemisphere to make a determination of the cutoffs possible at the time of the first disturbance). By the next pass a large dispersion has appeared (the 1000-eV and still more so the 3000-eV cutoffs have moved back up to higher latitudes). Hence the response to activity was for all three cutoffs to initially drop simultaneously, followed subsequently by time evolution into a dispersive state. The relaxation time is again short at premidnight, for the subsequent pass finds a nearly dispersionless cutoff at a high latitude. The second disturbance (also indicated by a dashed line, near 27 hours) was well under way before the first satellite pass was available to determine the dispersion, by which time the dispersion was already well developed. The recovery appeared to occur within about one orbit. Thus it appears that although the response to the onset of increasing magnetic activity is equally prompt in the midnight and dawn sectors, the "relaxation time" is shorter at midnight (~1 or 2 hours, instead of several hours). Of course, this would be the case if plasma were injected into these lower latitudes simultaneously at dawn and midnight, and subsequently, the comparatively low-energy component of the plasma at midnight convected into the dawn sector. An interesting question is whether all injections of plasma into low latitudes (and hence presumably the near-earth region) would appear initially with a dispersionless character followed by subsequent evolution, as in the first disturbance, if one were always able to make observations sufficiently promptly. This initially dispersionless signature is not the usual case in our observations, but it may simply be a matter of not having the satellite in the right place at the right time.

As mentioned above, the electrons show greater variability (or equivalently, less consistency) than do the ions. The second panel of Figure 4e shows the electron auroral cutoffs in the dawn sec-

tor. The drop to lower latitudes of the cutoffs at the times of increased magnetic activity is fairly clear, and there is also some evidence of increased dispersion, although again it must be admitted that there is considerable variability not obviously correlated to magnetic activity.

To conclude this section, we briefly call attention to the fact that the tendency for the ion dispersion at dawn to increase with increasing magnetic activity continues up to very active times (say, $Kp=6$) at which point substantial fluxes of sub-keV precipitation may extend far equatorward of the keV auroral precipitation. This process may result in low-energy ions being injected (initially along with low-energy electrons) down to very low *L* shells (at least to $L=2.4$) [Newell and Meng, 1986].

3. DISCUSSION

Let us first consider the assumption that the equatorward edge of the diffuse auroral precipitation as observed at low altitudes (840 km) maps in the equatorial plane to the earthward edge of the plasma sheet. In this view the equatorward edge of the diffuse aurora thus reflects magnetospheric convection patterns, and it is then possible to compare the present observations to the structures predicted by the various models discussed in the introduction. This certainly reflects a widespread belief, and there is published evidence for it in multisatellite comparisons of the equatorial plasma sheet with electron precipitations [Meng *et al.*, 1979; Horwitz *et al.*, 1986]. The discussion that follows is based on this premise.

We pause for a cautionary note about the usage of the term "diffuse aurora." As the auroral oval extends from the nightside into the dayside, it tends to follow a nearly circularly shaped region that is offset toward midnight from the geomagnetic pole. On the other hand, particles injected on the nightside may drift azimuthally around the earth more closely following a constant geomagnetic parallel. This is believed to be the reason, for example, why the "mantle aurora" in the midday sector is clearly equatorward of the auroral oval: It results from ≥ 10 -keV electrons drifting from the nightside [Meng and Akasofu, 1983]. Thus it may be argued that the furthest equatorward "auroral" precipitation, which is what the data here presented determine, represents drifting clouds injected on the nightside, rather than the auroral oval proper (compare the comment of McIlwain [1985] on the work of Gussenhoven *et al.* [1983]). This is, of course, exactly the appropriate measurement for making comparisons with models of single particle convection, as we wish to do. Thus even in the postmorning sector, it is reasonable to use our cutoffs, which represent the limit of the more equatorward precipitation, to investigate such models. Note that the cutoffs computed by Gussenhoven *et al.* [1983], which are based on a minimum energy flux threshold, should for this reason represent the "mantle aurora" on the dayside.

Many authors have calculated trajectories for particles convected from the magnetotail toward the earth under the influence of a dawn-dusk cross-tail electric field and a dipolar magnetic field (for example, Chen [1970], Kivelson *et al.* [1980], Hultqvist *et al.* [1982], and others). Ejiri *et al.* [1980] have made and presented calculations in a form particularly convenient for present purposes, as shown in Figure 5. Ejiri *et al.* [1980] made these calculations under the assumption of a dispersionless source in the distant magnetotail, convected by a Stern-Volland cross-tail field with shaping factor $\gamma = 2$ toward a dipolar magnetic field. (Insofar as the convection field can be represented by a Stern-Volland field, this is probably a typical value. For very quiet times, Kaye and Kivel-

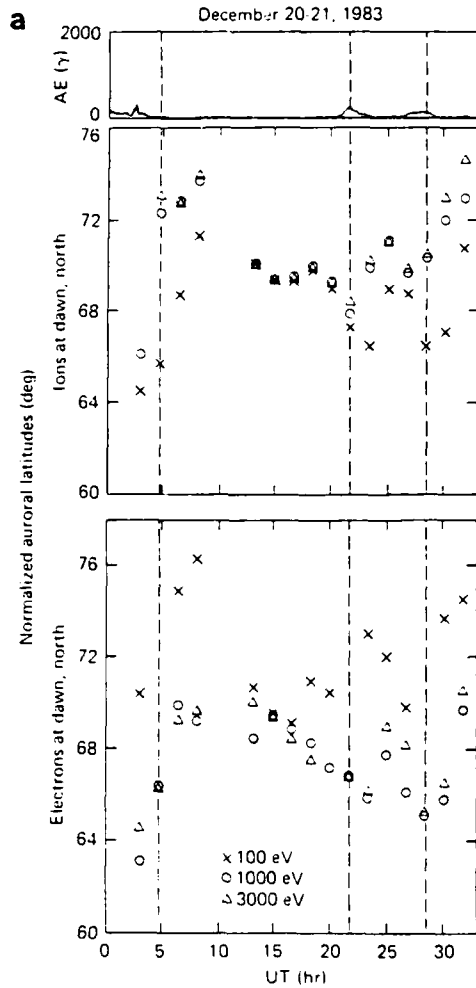


Fig. 4. Normalized auroral latitude of equatorward cutoffs during an interval of magnetic quiet containing two isolated small disturbances. Each point represents a single satellite pass. Crosses, 100 eV; circles, 1000 eV; triangles, 3000 eV. The dashed lines are to facilitate the description of certain features, as discussed in the text. (a) Ions and electrons at dawn in the northern hemisphere. (b) Ions in the premidnight sector in the northern and southern hemispheres, respectively.

son [1981] have suggested $\gamma = 3-6$ is more appropriate, whereas Baumjohann *et al.* [1985] find that under these conditions the convective flow is "quite different from the Stern-Volland model." The dashed lines in Figure 5 represent electrons and the solid lines, ions. It is assumed that the electric field is abruptly enhanced, and each successive numbering of the lines denotes the passing of an additional hour, with the initial "1" equal to $\frac{1}{2}$ hour after the electric field enhancement. The curves are the boundaries of the earthward penetration of the respective species. Thus the "infinity" curves represent the steady state Alfvén layers so often discussed. To make the radial distances at least comparable to our observations, we have scaled down the rather large electric field used by Ejiri *et al.* [1980] to investigate ring current formation during magnetic storms by a factor of 2, so that the stagnation point at dusk now occurs at a radial distance of $10 R_E$ (a value more consistent with the dusk sector observations of Vasyliunas [1968] of the plasma sheet edge at $11 R_E + 2 R_E$).

Examining first the predicted steady state boundaries (the "in-

finity" curves), we notice that in all local time sectors the intermediate (a few keV) ions are predicted to penetrate much further earthward than the lower energy ions. As discussed in section 2, the dispersion observed is nearly always of the opposite sense, with lower energy ions precipitating further equatorward of the intermediate energy ions. The exception is during times of sustained profound quiet, when a dispersionless condition appears in all sectors. The ion dispersion predicted from steady state Alfvén layers is never observed. The magnitude of the predicted dispersion varies with local time but should be more than an R_E at premidnight and even larger at dusk. In a dipole geometry this would correspond to more than a degree in latitude and would easily be detectable. Thus the ion dispersions observed are inconsistent with the steady state Alfvén layer model. For electrons the sense of the predicted premidnight dispersion agrees with observations, and is plausibly of the right size (there is considerable latitude, for example, in adjusting the size of the cross-tail field). However, the dawn sector electron dispersion, with the low-energy (~ 100 eV) electrons not reaching to as low latitudes as the higher energy electrons, is not predicted. Moreover, the predicted electron dispersion is maximal at dusk, whereas the observed electron dispersion is minimal at dusk. Finally, ions at energies below tens of kiloelectronvolts are predicted to cut-off further equatorward than electrons of all energies, in complete disagreement with observations.

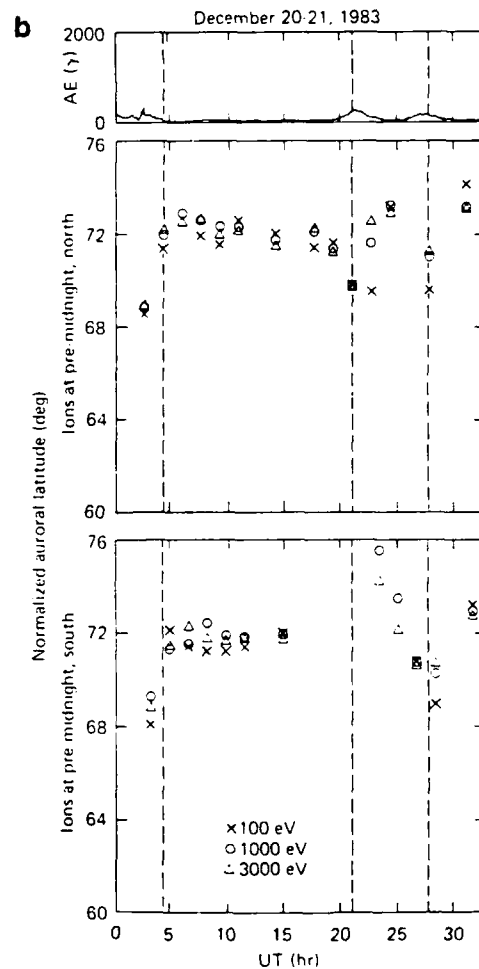


Fig. 4. (continued)

At all sectors covered except dusk we observe the electron precipitation tending to cut-off equatorward of the ion precipitation. This tendency can be observed also on individual passes, with consistency. From the above discussion it is clear that the steady state Alfvén layer model is not useful in modeling the equatorward boundaries of auroral precipitation.

It is logical to consider whether the more dynamic model represented by the numbered curves in Figure 5 does any better in agreeing with the DMSP observations. This seems plausible, since the fairly rapid loss rate through precipitation should cause the particles more recently injected to dominate. Also, for the single-particle trajectories the most earthward penetrating particles in the stable situation are those that are convected from the distant dusk flank (refer, for example, to *Chen* [1970]), which is probably not the most realistic source of, say, dawn side plasma. Thus we investigate a tentative hypothesis that ordinary times (that is, times at which the substorm activity is modest) should be represented by small-numbered curves (short times after an injection) and that quiet times should be represented by larger numbers (say, the "9" curves, 8.5 hours after the latest injection) but not by the infinity curves.

The dynamic approach does seem to at least reduce the number of apparent contradictions to the data. Recall that at dawn the static approach gives the sense of dispersion that is opposite to the precipitation cutoff data for both electrons and ions. Examining the ion curves, we find that a short time (1.5 hours or less) after an electric field enhancement the low-energy ions reach further earthward than the higher energy ions, in accordance with observation (rough quantitative agreement can also be obtained by playing with the parameters). Moreover, at increasingly later times after the injection the ions gradually become dispersionless, suggestive of our quiet time observations. For the electrons the recent injections show a behavior of intermediate energy electrons reaching further earthward than either high- or low-energy electrons. This is indeed what is observed, although the observed "intermediate" energies that penetrate close to earth are ~ 1 keV, whereas the prediction is ~ 10 keV, and the predicted dispersion does not appear to be large enough. The dynamic curves still do not agree with the observed ion dispersion in cutoffs at dusk and premidnight, but they still are of the right sense for electrons in these local time sectors. The curves in the box labeled "09 MLT" in Figure 5 approximately correspond to the prenoon (0835–1045 MLT) observations. Finally, the dynamic curves predict electrons reaching further earthward than ions at dawn but the reverse at dusk, which is in accordance with our observations and hence is an improvement over the steady state model; however, even the dynamic curves do not predict that the electrons precipitate equatorward of ions at premidnight, as we observe. Thus the dynamic approach of *Ejiri et al.* [1980] is closer to our observations than a steady state model but still cannot be used to predict the spectral dispersions in equatorward edge for both species at all local times.

As discussed in the introduction, it has sometimes been argued that particle loss through strong diffusion may play a more important role in determining the equatorward precipitation boundaries than single particle convection patterns. *Fairfield and Vinas* [1984], in their examination of this question based on ISEE 1 electron observations in the magnetosphere, concluded against the importance of strong diffusion. Their arguments were based on (1) the frequent observation of electron pitch angle anisotropies, (2) the frequent occurrence of the plasma sheet closer to the earth than would be predicted by loss at the strong diffusion rate, espe-

cially at dawn, and (3) the observation that field-aligned particles penetrate closer to the earth than those at 90° pitch angle, as expected from considerations of single particle motion. We are not aware of predictions of spectral dispersion in the cutoffs based on strong diffusion with the detail available for single-particle motion. Nonetheless, we will briefly examine how our data bear on this model. Strong diffusion does predict that lower energy particles would reach further earthward than higher energy particles (because the lower bounce rate leads to a longer loss time). This agrees with the data presented here, except for the higher latitude cutoff of low (~ 100 eV) energy electrons at dawn. However, this model also would predict that ions reach significantly further earthward than electrons because of their longer bounce time. Except at dusk, we observe the reverse effect, with electrons reaching earthward of the ions. It is also not clear how strong diffusion can account for the tendency of the dispersion (especially for ions) to approach zero during very quiet times. One possible speculation is that the strong diffusion model is only applicable to very quiet times. In this case, the boundaries are indeed found much farther from the earth (negating one point of *Fairfield and Vinas*), and the suggestion of *Ashour-Abdalla and Thorne* [1978] that ion precipitation is confined to the region of Birkeland currents might account for the coincidence of the ion cutoffs at different energies. This is only speculative, of course, and our observations can hardly be said to be confirming of the importance of strong diffusion, even under quiet conditions.

Sauvaud et al. [1981] have previously noted the softening of the ion precipitation at the equatorward edge of the diffuse ion auroral oval (note that because the electron diffuse aurora on the morningside extends below the ion diffuse aurora, as documented in Figure 2, these soft ion precipitations are still within the electron diffuse aurora). They believed that this region was limited to the local time span from about 0000 to 0500 or 0600 MLT. Actually, as our data indicate, the soft ion precipitation region can be seen at all local times, although the dispersive effect and persistence is greatest at dawn (and smallest, but still discernible, at dusk). *Sauvaud et al.* [1981] concluded that the morningside equatorward ion softening could be accounted for by *McIlwain's* injection boundary model [for example, *McIlwain*, 1974] followed by single-particle motion according to the E3 and M2 electric and magnetic field models of *McIlwain* [1974] although they did "not definitely exclude the possibility that the low-energy ions ... are at least partly of ionospheric origin." *Sauvaud et al.* [1985] re-investigated this question following AUREOL 3 results showing that the morningside soft ion precipitation contains enhanced oxygen precipitation. They argued that upward flowing ion events (UFIs) from the discrete auroral region can undergo a velocity filter effect in which the ions during a few bounce times are transported earthward (and eastward, toward the morning sector), during which the less energetic ions, because of their slower bounce time, are convected further earthward (toward lower latitudes) before they ultimately precipitate. *Sauvaud et al.* [1985] noted that the hydrogen equatorward precipitation displays the identical softening with decreasing latitude. Moreover, the precipitating hydrogen flux appears to be everywhere greater than or at least equal to the upflowing ion flux, which leads them to suggest that "particles of solar wind origin" undergoing magnetospheric convection may account for these.

Although *Sauvaud et al.*'s suggestion is intriguing, it is far from clear that UFIs found in discrete auroral regions can account for all of the softening of the ion spectra found in DMSP data. As shown in section 2 of this paper, the equatorward ion softening

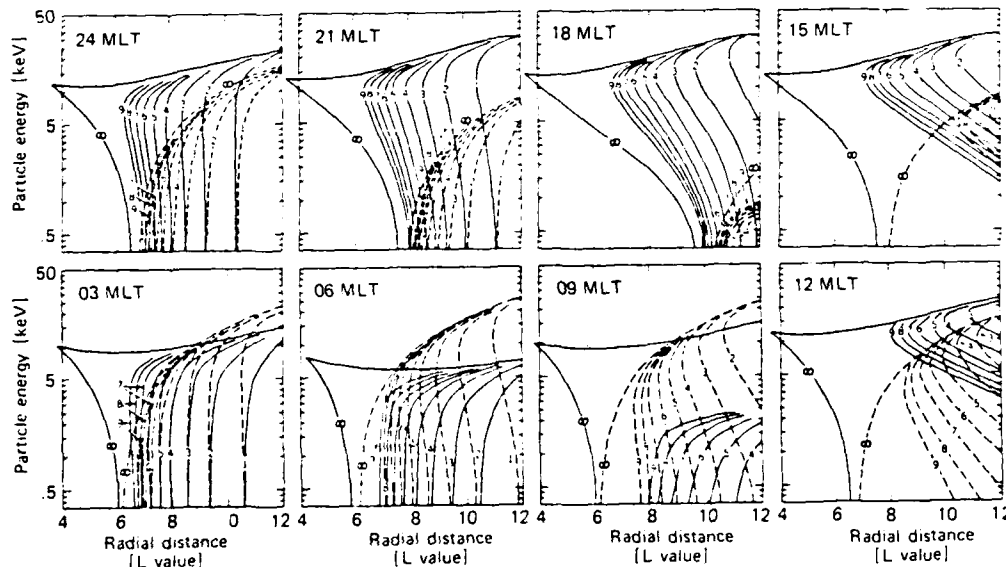


Fig. 5. Adapted from *Ejiri et al.* [1980]. Simulations based on a Stern-Volland electric field of the furthest earthward penetrations of newly injected particles. The labeled numbers 1-9 and "infinity" indicate the time at 1-hour intervals, with number 1 corresponding to +30 min after the enhancement. The solid curves represent ions and the dashed curves, electrons.

is observed at dusk, prenoon, and premidnight as well as at dawn and, except during very quiet periods, is nearly always present (the effect is, however, most profound and persistent near dawn). This question cannot be said to have been definitely resolved. An apparently distinct but closely related effect has been reported by the same group [*Bosqued et al.*, 1986] and earlier by *Winningham et al.* [1984]. This is that when an inverted V event is observed in one hemisphere, a narrow band of soft ion precipitation is observed in the conjugate hemisphere at a slightly lower latitude.

4. SUMMARY AND CONCLUSIONS

We have investigated the equatorward cutoffs in auroral electron and ion precipitation in the dawn, dusk, prenoon, and premidnight local time sectors at 100, 1000, and 3000 eV. We find that under normal (low-level magnetic activity) conditions the lower energy ions cut-off equatorward of the intermediate energy ions at all local times and that this effect is largest at dawn and prenoon with the dispersion least, but still evident, at dusk. The electron equatorward cutoffs are more erratic than the ions; however, at premidnight the lower energy electron precipitation fairly consistently extends equatorward of the intermediate energy electrons, while at dawn the ordering is $\lambda_{100} \gg \lambda_{3000} > \lambda_{1000}$. The dusk and prenoon electron cutoff patterns were not consistent enough for the present inquiry to decide anything. The DMSP data indicate that the electron precipitation extends to lower latitudes than the ion precipitation at all local times except dusk, where the ion precipitation reaches further equatorward.

During prolonged periods without AE activity (roughly $AE < 25 \gamma$), the latitudinal dispersion of the equatorward edges disappears, especially for ions. A renewal of substorm activity coincides with renewed dispersion over a wide longitudinal range extending at least from dawn to dusk. There is some evidence that this increased dispersion is a two-step process, with the particle precipitation at all energies initially extending to lower latitudes, followed subsequently by the higher energy precipitation cutoffs more quickly returning to higher latitudes.

We have discussed how our data may pertain to certain models relating to the formation of the auroral precipitation, particularly under the assumption that the equatorward edge of diffuse auroral precipitation maps in the equatorial plane to the plasma sheet inner edge [*Meng et al.*, 1979; *Horwitz et al.*, 1986]. Many authors have considered a constant source of particles in the magnetotail, convected by a cross-tail Stern-Volland electric field toward a dipole magnetic field and the steady state Alfvén layers resulting therefrom. The data presented here of equatorward cutoffs in the electron and ion 100-, 1000-, and 3000-eV diffuse auroral precipitation do not fit with the predictions of such a model, especially as regards the ions but also in certain features of the electrons. The sense of the latitudinal dispersion as a function of energy in cutoffs for the ions predicted by steady state Alfvén layers is in all sectors opposite to what we observe the great majority of the time. Even if the 100-eV ion precipitation is taken to be of ionospheric origin, it is still difficult to explain on the basis of this model why the 3000-, 1000-, and 100-eV precipitation boundaries all coincide during very quiet times (instead of having the 3000-eV ions reach closest to earth). Moreover, the model of steady state Alfvén layers also predicts that intermediate energy ions would reach earthward of electrons, also in disagreement with our observations. The DMSP observations are in this respect also in disagreement with the intriguing model of *Lyons* [1984] for diffuse auroral precipitations originating from current sheet particle interactions. This model also implies that ion precipitation extends "significantly" equatorward of electron precipitation.

Ejiri et al. [1980] have argued for the importance of dynamic effects. They have published calculations of boundaries of single-particle trajectories under the same assumptions as above (source in the magnetotail, Stern-Volland electric field, and dipole magnetic field), except that an injection is simulated by allowing a sudden enhancement of the electric field. This model agrees much better with DMSP observations but still has significant differences, such as the opposite sense of ion dispersion at premidnight. Thus it appears that alterations to this model, such as a more realistic

magnetic or electric field, or a different initial particle source distribution, are still needed.

Some authors have emphasized the importance of loss processes, often supposed to occur at the strong diffusion rate. Fairfield and Vinas [1984] have raised some compelling arguments against the importance of strong diffusion in determining the plasma sheet inner edge, including direct observations of electron anisotropies and noting that the inner edge often lies closer to the earth than would be expected if precipitation losses proceeded at the strong diffusion rate. We add the objections that during extremely quiet times the boundaries at different energies tend to coincide (especially for ions), an effect apparently not predicted by strong diffusion, and that strong diffusion would appear to imply that ions reach earthward of electrons, which is not in accordance with our observations (except at dusk).

Sauvaud *et al.* [1985] have suggested that the soft ion equatorward precipitation on the morning side of the auroral oval is of ultimately ionospheric origin, having a source in the higher latitude regions of discrete aurora, followed by earthward convection (and hence energization) in the magnetosphere before precipitating. The present observations indicate that if this is indeed the source of these ions, their sink has a much wider longitudinal distribution than previously suggested.

We hope that the observations reported here can help the efforts of future researchers in modeling auroral precipitation or the injection of plasma into the middle magnetosphere.

Acknowledgments. This work was supported by the Atmospheric Sciences Division, National Science Foundation grant ATM-8315041 and by the Air Force Office of Scientific Research grant 84-0049. We thank M. Ejiri for permission to use what is our Figure 5, and B. H. Mauk for helpful discussions.

The Editor thanks J. M. Bosqued and another referee for their assistance in evaluating this paper.

REFERENCES

- Ashour-Abdalla, M., and R. M. Thorne, Toward a unified view of diffuse auroral precipitation, *J. Geophys. Res.*, **83**, 4755-4766, 1978.
- Baumjohann, W., G. Haerendel, and F. Malzner, Magnetospheric convection observed between 0600 and 2100 LT: Variations with *Kp*, *J. Geophys. Res.*, **90**, 393-398, 1985.
- Bosqued, J. M., J. A. Sauvaud, and D. Delcourt, Precipitation of superthermal ionospheric ions accelerated in the conjugate hemisphere, *J. Geophys. Res.*, **91**, 7006-7018, 1986.
- Chen, A. J., Penetration of low-energy protons deep into the magnetosphere, *J. Geophys. Res.*, **75**, 2458-2467, 1970.
- Ejiri, M., Trajectory traces of charged particles in the magnetosphere, *J. Geophys. Res.*, **83**, 4798-4810, 1978.
- Ejiri, M., R. A. Hoffman, and P. Smith, Energetic particle penetrations into the inner magnetosphere, *J. Geophys. Res.*, **85**, 653-663, 1980.
- Erickson, G. M., and R. A. Wolf, Is steady state convection possible in the earth's magnetotail?, *Geophys. Res. Lett.*, **7**, 897-900, 1980.
- Fairfield, D. H., and A. F. Vinas, The inner edge of the plasma sheet and the diffuse aurora, *J. Geophys. Res.*, **89**, 841-854, 1984.
- Gussenhoven, M. S., D. A. Hardy, and W. J. Burke, DMSP F2 electron observations of the equatorward auroral boundaries and their relationship to magnetospheric electric fields, *J. Geophys. Res.*, **86**, 768-778, 1981.
- Gussenhoven, M. S., D. A. Hardy, and N. Heinemann, Systematics of the equatorward diffuse auroral boundary, *J. Geophys. Res.*, **88**, 5692-5708, 1983.
- Gussenhoven, M. S., D. A. Hardy, F. Rich, W. J. Burke, and H.-C. Yeh, High-level spacecraft charging in the low-altitude polar auroral environment, *J. Geophys. Res.*, **90**, 11009-11023, 1985.
- Hardy, D. A., L. K. Schmitt, M. S. Gussenhoven, F. J. Marshall, H. C. Yeh, T. L. Shumaker, A. Hube, and J. Pantazis, Precipitating electron and ion detectors (SSJ/4) for the block 5D/flights 6-10 DMSP satellites: Calibration and data presentation, *Rep. AFGL-TR-84-0317*, Air Force Geophys. Lab., Hanscom Air Force Base, Bedford, Mass., 1984.
- Harel, M., R. A. Wolf, P. H. Reiff, R. W. Spiro, W. J. Burke, F. J. Rich, and M. Smiddy, Quantitative simulation of a magnetospheric substorm. 1. Model logic and overview, *J. Geophys. Res.*, **86**, 2217-2241, 1981a.
- Harel, M., R. A. Wolf, R. W. Spiro, P. H. Reiff, C.-K. Chen, W. J. Burke, F. J. Rich, and M. Smiddy, Quantitative simulation of a magnetospheric substorm. 2. Comparison with observations, *J. Geophys. Res.*, **86**, 2242-2260, 1981b.
- Holzworth, R. H., and C.-I. Meng, Mathematical representation of the auroral oval, *Geophys. Res. Lett.*, **2**, 377-380, 1975.
- Horwitz, J. L., S. Menteer, J. Turnley, J. L. Burch, J. D. Winningham, C. R. Chappell, J. D. Craven, L. A. Frank, and D. W. Slater, Plasma boundaries in the inner magnetosphere, *J. Geophys. Res.*, **91**, 8861-8882, 1986.
- Hultqvist, B., H. Borg, L. A. Holmgren, H. Reme, A. Bahnsen, M. Jespersen, and G. Kremser, Quiet-time convection electric field properties derived from keV electron measurements at the inner edge of the plasma sheet by means of GEOS-2, *Planet. Space Sci.*, **30**, 261-283, 1982.
- Kaye, S. M., and M. G. Kivelson, The influence of geomagnetic activity of the radial variation of the magnetospheric electric field between $L = 4$ and 10, *J. Geophys. Res.*, **86**, 863-867, 1981.
- Kennel, C. F., Consequences of a magnetospheric plasma, *Rev. Geophys.*, **7**, 379-419, 1969.
- Kivelson, M. G., S. M. Kaye, and D. J. Southwood, The physics of plasma injection events, in *Dynamics of the Magnetosphere*, edited by S.-I. Akasofu, pp. 385-394, D. Reidel, Hingham, Mass., 1980.
- Lui, A. T. Y., and A. Hasegawa, Implications of a steady-state magnetospheric convection, *Planet. Space Sci.*, **34**, 315-318, 1986.
- Lyons, L. R., Electron energization in the geomagnetic tail current sheet, *J. Geophys. Res.*, **89**, 5479-5487, 1984.
- Mauk, B. H., and C.-I. Meng, Dynamical injections as the source of near geostationary quiet time particle spatial boundaries, *J. Geophys. Res.*, **88**, 10011-10024, 1983.
- Mauk, B. H., and C.-I. Meng, Macroscopic ion acceleration associated with the formation of the ring current in the earth's magnetosphere, in *Ion Acceleration in the Magnetosphere and Ionosphere*, *Geophys. Monogr. Ser.*, Vol. 38, edited by T. Chang, pp. 351-361, AGU, Washington, D.C., 1986.
- McIlwain, C. E., Substorm injection boundaries, in *Magnetospheric Physics*, 143-154, B. M. McCormac, ed., D. Reidel Publishing, Dordrecht-Holland, 1974.
- McIlwain, C. E., Equatorial magnetospheric particles and auroral precipitations, *Results of the ARCAD 3 Project and of the Recent Programmes in Magnetospheric and Ionospheric Physics*, 275-280, Cepadues-Editions, Toulouse, France, 1985.
- Meng, C.-I., and S.-I. Akasofu, Electron precipitation equatorward of the auroral oval and the mantle aurora in the midday sector, *Planet. Space Sci.*, **31**, 889-899, 1983.
- Meng, C.-I., R. H. Holzworth, and S.-I. Akasofu, Auroral circle—Delineating the poleward boundary of the quiet auroral belt, *J. Geophys. Res.*, **82**, 164-172, 1977.
- Meng, C.-I., B. Mauk, and C. E. McIlwain, Electron precipitation of evening diffuse aurora and its conjugate fluxes near the magnetospheric equator, *J. Geophys. Res.*, **84**, 2545-2558, 1979.
- Newell, P. T., C.-I. Meng, Substorm introduction of ≤ 1 keV plasma into the inner plasmasphere, *J. Geophys. Res.*, **91**, 11,133-11,145, 1986.
- Sauvaud, J. A., J. Crasnier, K. Moula, R. A. Kovrazhkin, and N. V. Jorjio, Morning sector ion precipitation following substorm injections, *J. Geophys. Res.*, **86**, 3430-3438, 1981.
- Sauvaud, J. A., J. M. Bosqued, R. A. Kovrazhkin, D. Delcourt, J. J. Berthelier, F. Lefevre, J. L. Rauch, Yu. I. Galperin, M. M. Mogilevsky, and E. E. Titova, Positive ion distributions in the morning auroral zone: Local acceleration and drift effects, *Adv. Space Res.*, **5**, 73-77, 1985.
- Schild, M. A., and L. A. Frank, Electron observations between the inner edge of the plasma sheet and the plasmasphere, *J. Geophys. Res.*, **75**, 5401-5413, 1970.
- Schindler, K., and J. Birn, Self-consistent theory of time-dependent convection in the earth's magnetotail, *J. Geophys. Res.*, **87**, 2263-2275, 1982.
- Starkov, G. V., and Y. I. Feldstein, Variations of auroral oval zone boundaries (in Russian), *Geomagn. Aeron.*, **9**, 759-760, 1969.
- Vasyliunas, V. M., A survey of low-energy electrons in the evening sector of the magnetosphere with OGO 1 and OGO 3, *J. Geophys. Res.*, **73**, 2839, 1968.
- Williams, D. J., Energetic ion beams at the edge of the plasma sheet: ISEE 1 observations plus a simple explanatory model, *J. Geophys. Res.*, **86**, 5507-5518, 1981.
- Winningham, J. D., J. L. Burch, and R. A. Frahm, Bands of ions and

- angular V's: A conjugate manifestation of ionospheric ion acceleration, *J. Geophys. Res.*, **89**, 1749-1754, 1984.
- Wolf, R. A., The quasi-static (slow-flow) region of the magnetosphere, in *Solar-Terrestrial Physics*, edited by R. L. Carovillano and J. M. Forbes, pp. 303-368. D. Reidel, Hingham, Mass., 1983.
- Zverev, V. L., G. V. Starkov, and Y. I. Feldstein, Influences of the interplanetary magnetic field on the auroral dynamics, *Planet. Space Sci.*, **27**, 665-667, 1979.

C.-I. Meng and P. T. Newell, The Johns Hopkins University, Applied Physics Laboratory, Johns Hopkins Road, Laurel, MD 20707.

(Received August 4, 1986;
revised February 6, 1987;
accepted February 10, 1987.)

Substorm Introduction of ≤ 1 -keV Magnetospheric Ions Into the Inner Plasmasphere

PATRICK T. NEWELL AND C.-I. MENG

The Johns Hopkins University Applied Physics Laboratory, Laurel, Maryland

Observations from the ion detectors on Defense Meteorological Satellite Program satellites F6 and F7 have revealed an interesting phenomenon, namely the existence of isolated and latitudinally narrow regions of ion precipitation up to ~ 1 keV well within the plasmasphere. Using the almost continuous coverage afforded by the 101-min polar orbits of these satellites, we are able to document in detail the process whereby such isolated precipitation patterns are established. Prolonged intense substorm activity is observed to introduce plasma of sub-keV energy from the earthward edge of the plasma sheet to deep within the plasmasphere (at least $L = 2.4$). The plasma introduction occurs over a confined magnetic local time (MLT) range extending from somewhere postmidnight to about 0830 MLT. Because of their much more rapid pitch-angle scattering into the loss cone, the energetic electrons are lost within one or two hours, whereas the ions can persist for at least a day. After being injected into low L values, the ions begin to corotate, thereby forming latitudinally narrow and well-isolated structures of ion precipitation far below the instantaneous auroral oval. The total number of ions injected over a several-hour span can be very roughly estimated to be $\sim 10^{25}$. Because of certain similarities of the injection process to observations by Lennartsson and Sharp (1982) and to the magnetic storm time observations of Shelley et al. (1972) and Strangeway and Johnson (1984), it is likely that the low-latitude precipitating ions are O^+ .

1. INTRODUCTION AND BACKGROUND

The phenomenology of electron precipitation at high latitudes has been intensively studied since 1960 [McIlwain, 1960] (see Meng [1978] for a review). Ion precipitation has received far less attention; for example, a recent useful auroral review by Feldstein and Galperin [1985] neglects the ion population altogether. The energy flux of electrons precipitating into the auroral oval is typically about 20 or 30 times greater than the energy flux of precipitating ions, which has led to the relative scarcity of observations of, and attention paid to, high-latitude ion precipitation. Most of the research on ion precipitation has focused on energies > 1 keV [for example, Hultqvist, 1979]. There is, however, the work of Frank and Ackerson [1971], studying typical auroral precipitation patterns. Shelley et al. [1972] and Sharp et al. [1974] observed heavy ion precipitation at mid-latitudes during magnetic storm activity. With the comparatively recent inclusion of ion detectors covering from 30 eV to 30 keV on Defense Meteorological Satellite Program (DMSP) satellites [Hardy et al., 1985], a much more systematic study of the precipitating ion population using approximately continuous data should be possible.

For several decades there have been ground-based observations of the proton aurora. The only auroral emissions that can be unambiguously and uniquely associated with proton precipitation are the weak hydrogen Balmer lines, a circumstance that has held progress in studying proton aurora to a slower pace than that of the electron aurora. The proton aurora tends to be quite diffuse (apparently partly because of charge exchange considerations) and reaches from magnetic local midnight back toward earlier local times [Vallance-Jones et al., 1982]. This implies that the proton aurora (or at least the portion that is observable from the ground, i.e., the Balmer lines) is caused by ions of many keV or greater, since DMSP measurements show that lower-energy ions do not precipitate primarily toward dusk. (As is well known, curvature and gradient drifts cause ions of larger magnetic mo-

ment to convect westward while those of lower energy convect eastward.) As far as this paper is concerned, the important point is that ground-based observations do not appear to be sensitive to the low-energy ion precipitation (≤ 1 keV), which will be the thrust of our work.

It is worth briefly discussing the magnetospheric morphology relevant to the present work. At the equatorward edge of the belt of several-keV electron and ion diffuse auroral precipitation, the spectra of both often soften, so that there is often a region of lower-energy precipitation (for electrons, this can be inferred, for example, from the data of Meng et al. [1979] and Hardy et al. [1985]). For ions, this is particularly the case in the morning local time sector. Sauvaud et al. [1981] have shown that the equatorwardmost ion auroral precipitation in this region softens with decreasing latitude, leading to a region of a few hundred eV ion precipitation. Sauvaud et al. [1985], using AUREOL-3 data, have shown that this softer equatorward morningside ion precipitation contains an enhanced oxygen component. It has been reported that in the magnetospheric equatorial plane, the inner edge of the plasma sheet is farther earthward for lower-energy electrons than for higher-energy electrons [Vasyliunas, 1968; Fairfield and Vinas, 1984]. For electrons, this effect would be predicted on the basis of steady-state Alfvén layers; that is, on the single-particle trajectories of electrons convected from a steady source in the magnetotail by a cross-tail dawn-dusk electric field toward the earth (usually taken to have a dipole field in such models). For ions, however, the Alfvén layers would lead to the opposite dispersion, with intermediate ions reaching closer to earth (and thus causing lower-latitude precipitation) than lower-energy ions [e.g., Chen, 1970]. This is in contradiction to observation (Newell and Meng, manuscript in preparation, 1986), calling the Alfvén layer picture into question. An alternative explanation for the spectral effect in the plasma sheet edge is that as plasma convects earthward, the lowest-energy particles take longer to be lost through precipitation, since their longer bounce time gives them fewer chances to precipitate. The question as to which effect was more important was addressed by Fairfield and Vinas [1984], who concluded on the basis of electron observations only that single-particle

Copyright 1986 by the American Geophysical Union.

Paper number 6A8435.
0148-0227/86/006A-8435\$05.00

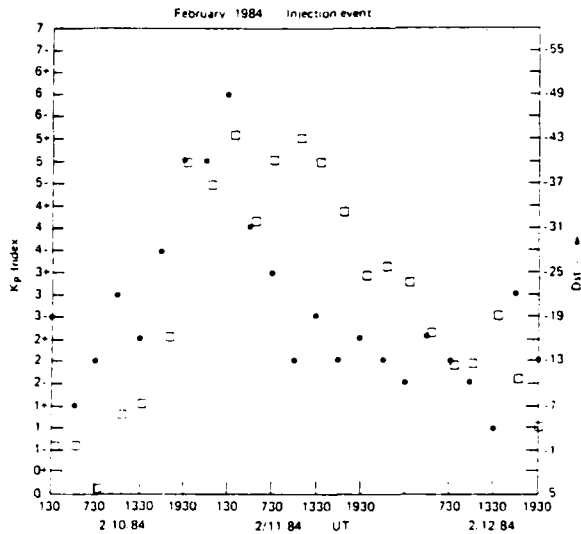


Fig. 1. Circles: 3-hr K_p indices for the quiet period prior to the injection, during the injection (beginning about 1830 UT February 10, 1984), and the quiet period following the injection. Squares: D_{st} equatorial indices (provisional) for the same time period. Every third D_{st} hourly point is plotted.

motions dominated the plasma sheet structure. The conditions under which the lower-energy precipitation region exists have not been well investigated.

The other magnetospheric structure of interest to the present work is the plasmasphere. The inner plasmasphere is cold (≤ 1 eV) and dense ($100-1000$ e^-/cm^3) extending during very quiet times out to as far as $L = 6$, and it is well developed only at lower L shells following a magnetospheric substorm [Carpenter, 1967]. The outer plasmasphere is warmer, with temperatures up to tens of eV [Chappell, 1982], and some (generally neglected) superthermal observations of ions as high as 1 keV have been reported [Young, 1983]. Chappell *et al.* [1980] have reviewed the state of plasmaspheric research.

The data used in this work are from the cylindrical electrostatic analyzers included in the SSJ/4 package on board the DMSP F6 and F7 satellites. These detectors measure both electrons and ions from 30 eV to 30 keV in 20 logarithmic steps. The low-energy ion detector (30-1000 eV) is noteworthy for its unusually large geometric factor. Both electron and ion detectors always point toward the local zenith, so that, at the latitudes of present interest, the detectors are looking well within the loss cone. Both satellites are in sun-synchronous circular polar orbits at 850-km altitude and have periods of about 101 min. DMSP F7 is in approximately the 1035 to 2335 LT meridian; DMSP F6 is in about the 0640 to 1840 LT meridian. More detailed expositions of these satellites and their instrumentation have been given by Hardy *et al.* [1984] and Gussenhoven *et al.* [1985]. All observations at the latitudes of interest herein by the DMSP detectors are well within the loss cone, so that the measurements are on precipitating rather than trapped populations.

We here report a new phenomenon revealed by the DMSP measurements. Ion precipitation up to about 1 keV, and well isolated from the auroral oval, is observed down to at least 50° magnetic latitude (MLAT). Such precipitation zones typically extend over about 2° in latitude with an enhancement of almost two orders of magnitude over background levels. The goals of this paper are (1) to document the existence of the aforemen-

tioned ion precipitation phenomena and (2) to establish the mechanism whereby these low-latitude regions of warm precipitation are created. The short (~ 100 min) orbital period of the DMSP F6 and F7 satellites allows an almost movielike coverage of the creation process, eliminating any ambiguity as to the origin of these ions. This is the injection of warm (~ 100 -eV) plasma from the earthward edge of the plasma sheet to deep within the plasmasphere (at least $L = 2.4$) in the postmidnight to dawn sector during prolonged intense magnetospheric substorm activity. Because of their higher collision rates, the electrons are quickly lost; however, the ions can persist in a narrow latitudinal range for at least 24 hr after the injection. This is a global phenomenon; that is, it is observed over both hemispheres simultaneously; and because ions of this energy convect in the direction of corotation, they are eventually seen at all the magnetic local times covered. A note on terminology: "corotation" is not used here to mean strict corotation; rather it is a looser usage denoting any convection by an electric field in the direction of corotation (i.e., corotation may here be "partial").

In this paper, we use the terms "injection" or "plasma introduction" interchangeably, to refer to the introduction of (warm) plasma into a spatial regime (specified by magnetic local time and latitude) where it was formerly absent. As will be later discussed, there is evidence to believe that in the low-latitude dawn sector this involves earthward convection from adjoining spatial regimes, although this is not intended to argue against the possibly ultimately ionospheric origin of the precipitating particles [e.g., Sauvaud *et al.*, 1985]. Thus, by using the word "injection" we are not making an identification with the phenomenon of injection boundaries seen with satellites in the equatorial magnetosphere [McIlwain, 1974; Mauk and Meng, 1983]. Moreover, our injection events are not to be confused with the "proton nose" events of Smith and Hoffman [1974], which consist of substorm injection of ~ 15 - to 20-keV magnetospheric ions at dusk down to about $L = 4.5$, that they interpret as contributing to the ring current. Specifically, our injection events consist of low-altitude high-latitude measurements of sub-keV plasma precipitation that is observed moving from just equatorward of the auroral oval in the postmidnight to dawn sector down to latitudes associated with the inner plasmasphere. At the risk of being superfluous, we add that we equally do not imply that there is no connection with injections of other types; for example, the injection of plasma into the equatorial geosynchronous magnetosphere may well be the first step in the introduction of plasma to low latitudes at dawn.

The remainder of this paper is organized as follows. Section 2 presents in detail the observations made during two injection events; section 3 rules out all potentially plausible instrumental effects and a possible data selection effect; section 4 discusses the physical interpretation of the events; and the final section contains a brief summary.

2. DATA PRESENTATION: TWO EVENTS

2.1. The Event of February 10-11, 1984

To demonstrate this new low-latitude ion precipitation phenomenon, and the injection process whereby it occurs, we chose times of relatively moderate activity ($K_p \leq 3$) followed by intense substorm activity ($K_p \geq 5$) for a few hours and relative quiet again for at least one or two days, to allow the effects of the injection to die away. Section 3 includes a discussion that should reassure the reader alarmed by this data selection procedure. Figure 1 shows the 3-hr K_p index prior to, through, and

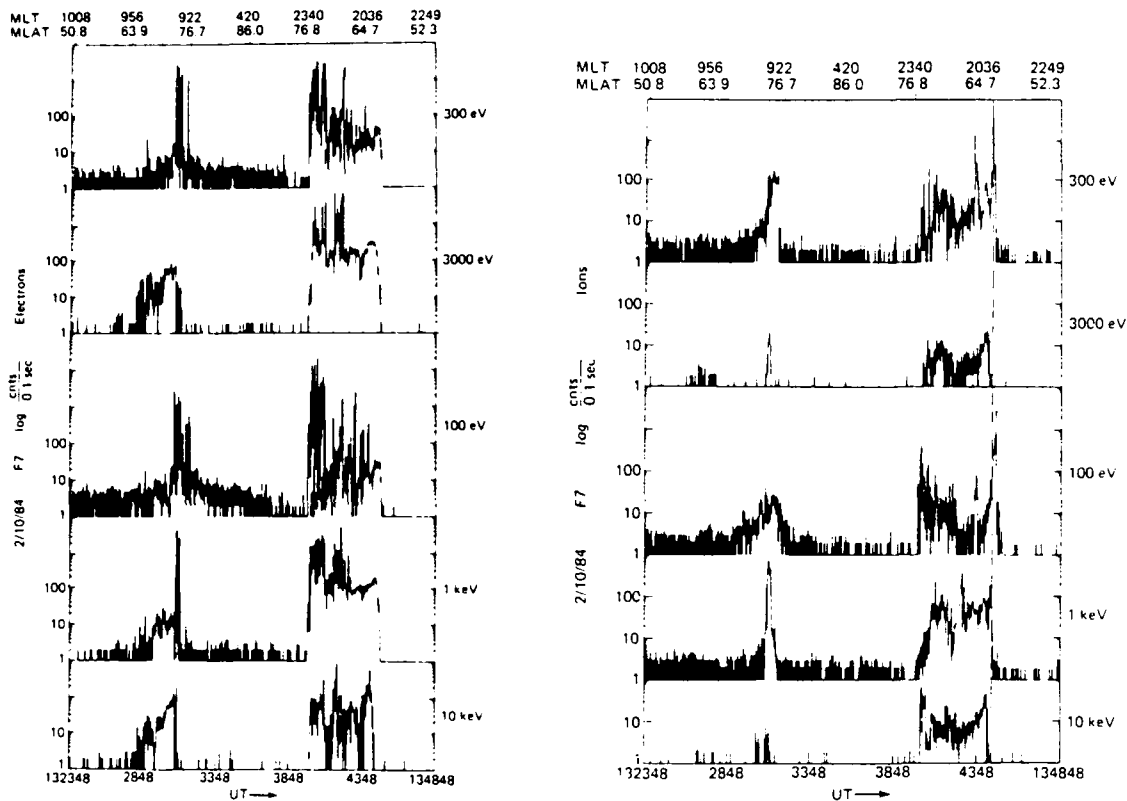


Fig. 2. The quiet high-latitude particle precipitation patterns prior to the event. Left: electrons; right: ions. The dashed line through the ion plots is to emphasize the region of soft ion precipitation. To convert from counts/0.1 s to particles/cm² s sr eV, multiply by these constants: for 300-, 3000-, 100-, 1000-, and 10000-eV electrons, respectively, 1060, 63.8, 4250, 134, and 30.9; and for 300-, 3000-, 100-, 1000-, and 10000-eV ions, respectively, 10.0, 63.8, 32.1, 3.18, and 30.9.

after the first event to be described, which commenced about 1830 UT on February 10, 1984. The more accurate (though still quite imperfect) activity index, AE , is not yet available for 1984. For completeness, Figure 1 also shows the Dst during the time period of interest, with the hourly index plotted once every 3 hr, to be consistent with the presentation of Kp .

Figure 2 (from F7) shows the typical auroral precipitation pattern for $\geq 50^\circ$ MLAT along a nearly noon-midnight orbital path during the comparatively quiet period preceding the event. This figure, like all the DMSP data to be presented herein, shows one polar pass, from 50° MLAT on either side of the pole. The magnetic field model used is the corrected geomagnetic coordinate system by *Gustafsson* [1970]. The auroral oval as seen in Figure 2 is fairly high, with the peak electron energy fluxes around 74° MLAT in both the prenoon and premidnight sectors (however, the keV electron precipitation near the midnight region extends with lower fluxes to about 63° MLAT, also a common feature). The region of soft ion precipitation discussed in the introduction can be seen in the ion data of Figure 2. On the premidnight side of the auroral oval pass, it is characterized by the 100- to 1000-eV precipitation extending to lower latitudes than do the ≥ 1 -keV particles (look near 1344 UT). The most important point here is to note the absence of significant fluxes of 100- to 300-eV ions below the auroral precipitation oval, the usual state of affairs. (The one-count level enhancement on the dayside at the lower latitudes is a direct solar UV effect. This is easily distinguishable from true precipitation, as discussed in section 3.)

The auroral region gradually expands to lower latitudes as Kp

increases, a well-established phenomenon. The injection event itself appears to commence about 1830 UT on February 10 ($Kp = 5$), as shown in Figure 3 (F7). Again we call attention to the softer electron and ion fluxes that extend equatorward of the harder precipitation. Indeed, the equatorward morningside 100- to 300-eV ion precipitation around 1833 UT (57 - 60° MLAT) already looks spatially distinct from the main region of auroral precipitation. Fifty minutes later, in the next pass of the southern polar region, it is clearly evident that plasma up to 1 keV is extending at dawn but not at dusk to latitudes far below the auroral zone. This can be seen in Figure 4 (F6), before 1940 UT, where the dawnside soft precipitation extends to about 56° MLAT. The low-latitude soft precipitation includes both electrons and ions and is highly structured. (The narrow band of apparent enhanced electron counts near 56° MLAT on the duskside is due to penetrating MeV outer belt particles; refer to section 3.) Figure 5 (F7) shows that by 2013 UT ($Kp = 5$) sub-keV plasma (electrons as well as ions) has reached the lowest magnetic latitudes ($L = 2.42$) for which we have processed data available. Notice that Figure 5 is a prenoon-premidnight northern hemisphere pass, showing that the injection is a global effect (i.e., involving both hemispheres). From Figures 4 and 5, we can state that the injection occurs in both hemispheres at approximately the same time but only toward the morning sector and not in the dusk or premidnight magnetic local time (MLT) sectors.

The 3-hr Kp indices (Figure 1) continue high until 0300 UT February 11. The low-latitude extent of the plasma precipitation waxes and wanes moderately during this period, reaching a fi-

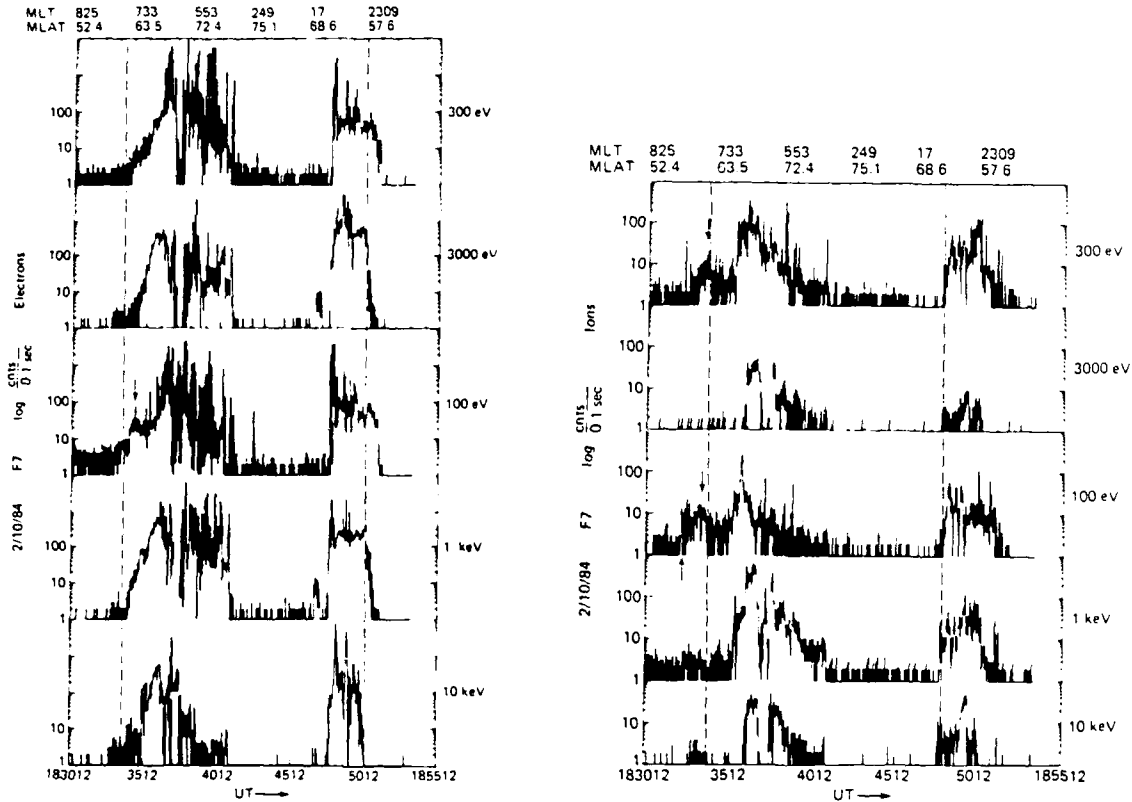


Fig. 3. Beginning of the injection event: the equatorward expansion of auroral precipitation. Left: electrons; right: ions. To convert to physical units, refer to the caption for Figure 2. The downward pointing arrows are only to call attention to the features of interest. The upward pointing arrow for the ions shows the low-latitude extent of the soft precipitation: 56.1° . The dashed lines are at 60° MLAT for reference.

nal maximum at about 0225 UT ($Kp = 6$). As the Kp index starts to fall, the auroral oval begins its recovery to higher latitudes. The electrons injected into the lowest latitudes are lost more quickly than are the ions. Figure 6 (F6), which extends to 0405 UT, illustrates these last two effects clearly. Indeed, it seems probable that the equatorward edge of the 100- to 1000-eV electron precipitation on the dawnside in Figure 6 (left) is the plasmopause (about 59° MLAT). Inside this boundary, the energetic electrons should be quickly pitch-angle scattered into the loss cone by the dense ambient thermal plasma. This topic is discussed further in section 4.

It should be noted that, even for 1-keV ions, corotation dominates over gradient and curvature drifts, and for 100-eV ions the latter are insignificant. Thus the ions at lowest latitudes should be seen to convect in the direction of corotation. One therefore expects that the low-latitude ions will disappear from the dawnside and appear on the duskside. Indeed, this is the case. As one proceeds to quieter times, the 100-eV ions disappear from the dawnside, and the first isolated low-latitude ions at dusk appear (0634 UT) as seen in Figure 7 (left). We here switched to presenting a northern hemisphere view only to get better time resolution for the first appearance on the duskside of isolated low-latitude ions; Figure 7 (right) shows the identical behavior occurring in the southern hemisphere 30 min later. Limits on the magnetic local time extent of the injection can be estimated by noting that the first ions reached low latitudes around 2013 UT February 10 on the dawnside (Figure 5) and by corotating reached 1821 MLT by 0634 February 11 (Figure 7, about 10 hr later).

Thus the injections could not have extended far beyond 0820 MLT as indicated in Figure 5. This is confirmed by the southern polar passes during the injection, which covers the noon magnetic local time. (Unfortunately, at this time the F7 ion detector, when near 50° MLAT, is looking close enough at the sun to be contaminated by solar UV and is reaching up to a uniform rate of 2 counts/0.1 s in the low-energy ion detector. Nonetheless, no evidence of injection near 1200 MLT is seen.) Figure 5 and numerous other passes (which lack of space prohibits our showing) indicate that the injection did not extend to the premidnight regime. There is no DMSP coverage available for the postmidnight magnetic local times. Thus we can conclude that the injection occurred in the sector from somewhere after midnight up to about 0820 MLT.

Following the cessation of intense substorm activity, the auroral oval starts to return to higher latitudes. However, isolated pockets of ion precipitation remain at low latitudes. Figure 8, which covers 0930 to 1000 UT February 11 (about 14 hr after the injection), is an example of several regions of low-latitude ion precipitation that have no corresponding electron precipitation. It is clear from the sequence presented that electrons along with ions were originally injected into those regions but that the electrons, because of their more rapid pitch-angle scattering, were lost more quickly. On the other hand, the low-latitude ion precipitation continues in both hemispheres with diminishing fluxes, rotating through the different magnetic local times until about 0600 UT February 12. Figure 9 shows the last observation of an enhancement in the soft ion count rate at these low latitudes,

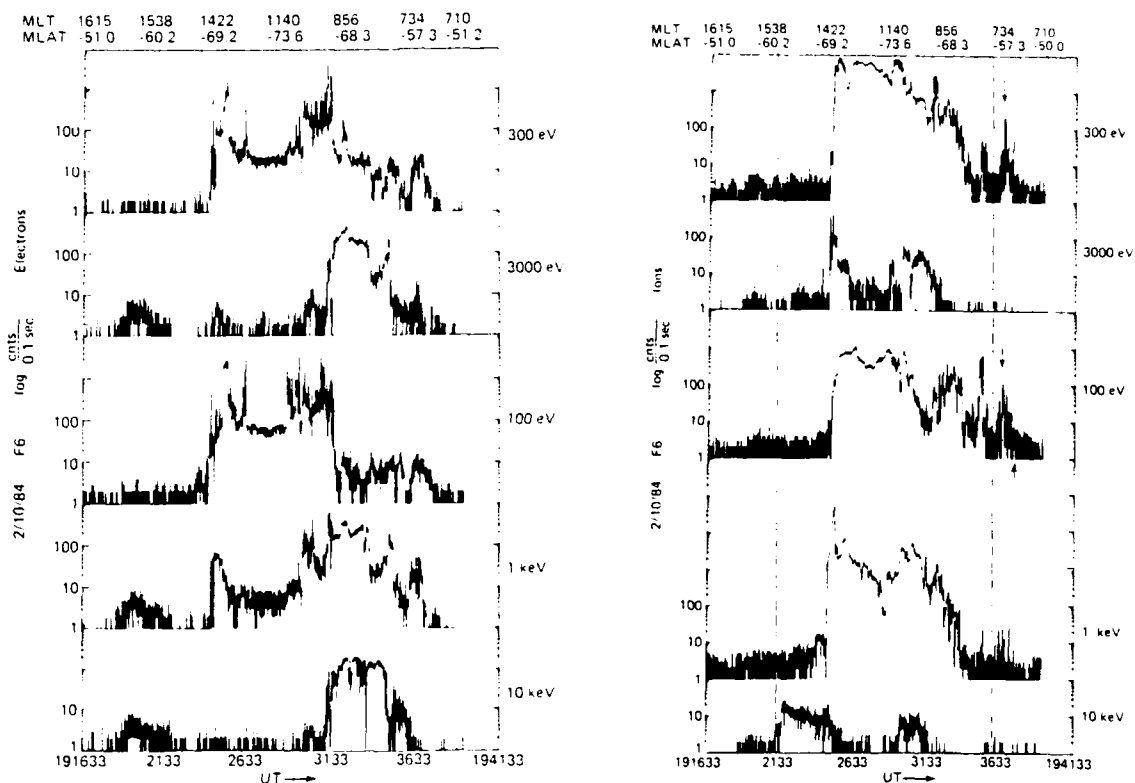


Fig. 4. Sub-keV plasma being convected to low latitudes at dawn but not at dusk in the southern hemisphere. Left: electrons; right: ions. The electron enhancement on the duskside at 56° MLAT is due to penetrating MeV radiation. The upward pointing arrow shows the low-latitude extent of soft ion precipitation: $\sim 53.1^\circ$. The downward pointing arrows are to draw the reader's attention to the features of interest; the dashed lines are at 60° MLAT for reference.

about 30 hr after the end of the injection. The flux enhancement referred to occurs only in the 100-eV channel at about 56° MLAT on the dawnside. (As an aside, there does seem to be evidence for a fairly uniform low-level 1-keV ion flux at about the 1-count level at low latitudes. This effect is seen fairly routinely, apparently independently of substorm activity, and does not have any obvious connection with the much larger particle and energy fluxes in the hundred-eV range addressed by the present paper.)

Figure 10 shows three sample spectra: one taken during the initial stage of the injection (2016 UT February 10, about 58° MLAT in Figure 5), one during the maximum point of the injection (0223 UT February 11, 56.4° MLAT), and one from the well-isolated ions left behind after the substorm (0634 UT February 11, about 51° MLAT in Figure 7 (left)). These spectra are presented only as examples. There is considerable variability, depending on precisely when and where one chooses to compute the spectrum. Nonetheless, the general features of Figure 10, such as the high-energy tail out to about 1 keV that is lost more rapidly than the lower-energy component, are representative. As Figure 10 shows, the ions injected into low latitudes are significantly softer than typical auroral oval spectra, which have much of their ion energy flux above 3 keV. A typical ion flux for the low-latitude precipitation phenomenon with which the present paper is concerned is, integrated over energy, $\sim 10^4$ ions/cm² s sr.

2.2. The Event of June 15-17, 1984

The event presented above is far from unique; rather it is a common feature during and after prolonged intense substorm

activity. In this section we present, in a highly abbreviated format, a second example of the injection of magnetospheric ions into the plasmasphere. This started late on June 15, 1984, with the low-latitude ion precipitation remaining until the morning of June 17, 1984. Figure 11 shows the 3-hr Kp indices and every third hourly Dst value prior to and during the time of the second example event. Once again, several days of relative quiet ($Kp \leq 3+$) is followed by an extended period of high Kp values, during which time the injection occurs. However, there is no sharp onset of the injection event; instead, activity builds gradually to very high levels. For brevity and for the resulting simplicity of presentation, we will adopt a new format in which only a very limited amount of data are shown; namely the 100- and 3000-eV ion channels from DMSP F6 passes over the southern hemisphere.

Figure 12 shows the entire event in this abbreviated format. The solid lines with single breaks at the center indicate the regions of 100-eV ion precipitation, with the solid line high for count rates $\geq 5/0.1$ s over a 4-s average (thus for fluxes $\geq 1.6 \times 10^2$ ions/cm² s sr eV) and low otherwise. Only those magnetic latitudes above 50° actually covered on a particular satellite pass are drawn in. The three magnetic local times given per row in the figure refer to the two crossings of 50° MLAT and the point of highest magnetic latitude reached. Although the magnetic local time at the latter point can vary rapidly and considerably, we are here most concerned with the lower-latitude behavior, and we point out that below 70° MLAT, the variation in magnetic local time on a given pass is typically only ~ 15 min. The hatch-

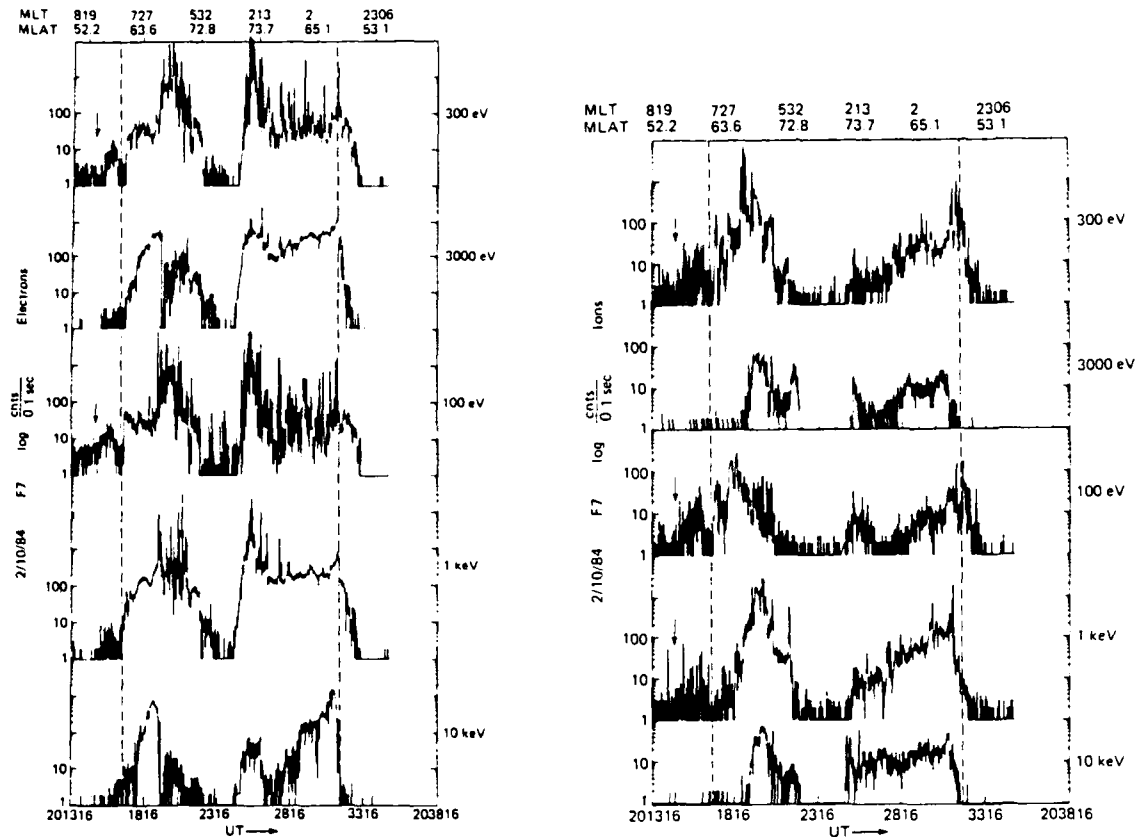


Fig. 5. Northern hemisphere pass showing soft precipitation reaching to $L = 2.5$. This occurs in the morning but not the premidnight sector. Left: electrons; right: ions. The dashed lines are at 60° MLAT. There is no clear low-latitude cutoff to the soft ion precipitation.

ing in Figure 12 indicates the region of 3-keV ion precipitation, which we take here to be the region of auroral oval ion precipitation. The universal time associated with each pass is the time the satellite reached the highest latitude rounded off to the nearest 5 min.

The top panel of Figure 12 (1200 UT June 15, 1984) shows that, even in the moderately active $Kp = 3+$ state, there are no intense fluxes of hundred-eV ions at low latitudes prior to the injection. Notice that on the dawnside there is a region of 100-eV precipitation that extends to lower latitudes than the 3-keV ions; this region is taken here to be the low-altitude projection of a soft ion population at the earthward edge of the plasma sheet. The absence of ion precipitation at latitudes below, say, 60° had been the condition for at least a day prior to the injection documented here. Events that produce persistent fluxes of ions at low latitudes involve prolonged intense activity, as measured by the Kp indices or by the low-latitude extent of the auroral precipitation, as discussed further in section 4. The event under present consideration had such activity, starting near the end of June 15 or the beginning of June 16, 1984. The second panel of Figure 12 shows that by 0150 UT June 16, sub-keV ion precipitation reached to about 55° MLAT in the dawn region but not at dusk. Meanwhile, F7 data (not shown here) indicate that in the noon-midnight meridian there is no injection to this low latitude. Thus once again the injection is limited to the postmidnight-dawn sector. The third panel of Figure 12 shows the soft ion precipitation reaching the lowest latitudes covered at about 0330 UT. In this event, unlike the one discussed in sec-

tion 2.1, there is an apparent hemispherical asymmetry, with the activity strongest in the southern hemisphere during the initial injection phase. The subsequent persistent low-latitude ion precipitation, after substorm activity returns to more moderate levels, is in both events at least approximately hemispherically symmetric.

DMSP F7 data (not presented in Figure 12) reveal that even at the peak of activity, the injection does not extend to either the premidnight or the prenoon magnetic local time sectors. As mentioned previously, the low-latitude soft ion precipitation results from prolonged activity, and the fourth panel of Figure 12 shows the injection process still continuing strong through 1011 UT June 16, 1984; thus, the initial injection lasted up to 9 hr. By this late time, F7 also shows the low-latitude soft ions near noon, although this is apparently because of convection from the injection closer to dawn.

The fifth panel of Figure 12 shows the first appearance of low-latitude ion precipitation at dusk; it occurs at 1325 UT June 16, when activity is already quieting. Notice that this is an isolated appearance at the lower latitudes, without the associated expansion of auroral precipitation in this sector having reached that low latitude. This is a clear signature that the ions reached the dusk position by corotation from the dawn injection. The timing is also consistent with corotation, for it is about 10 hr after the 100-eV ions first reached low latitudes on the dawnside (panel three). The physical reason for the sharp poleward cutoff in the low-latitude ion precipitation at dusk is likely the boundary of corotation, which is usually taken to be also the plasmapause.

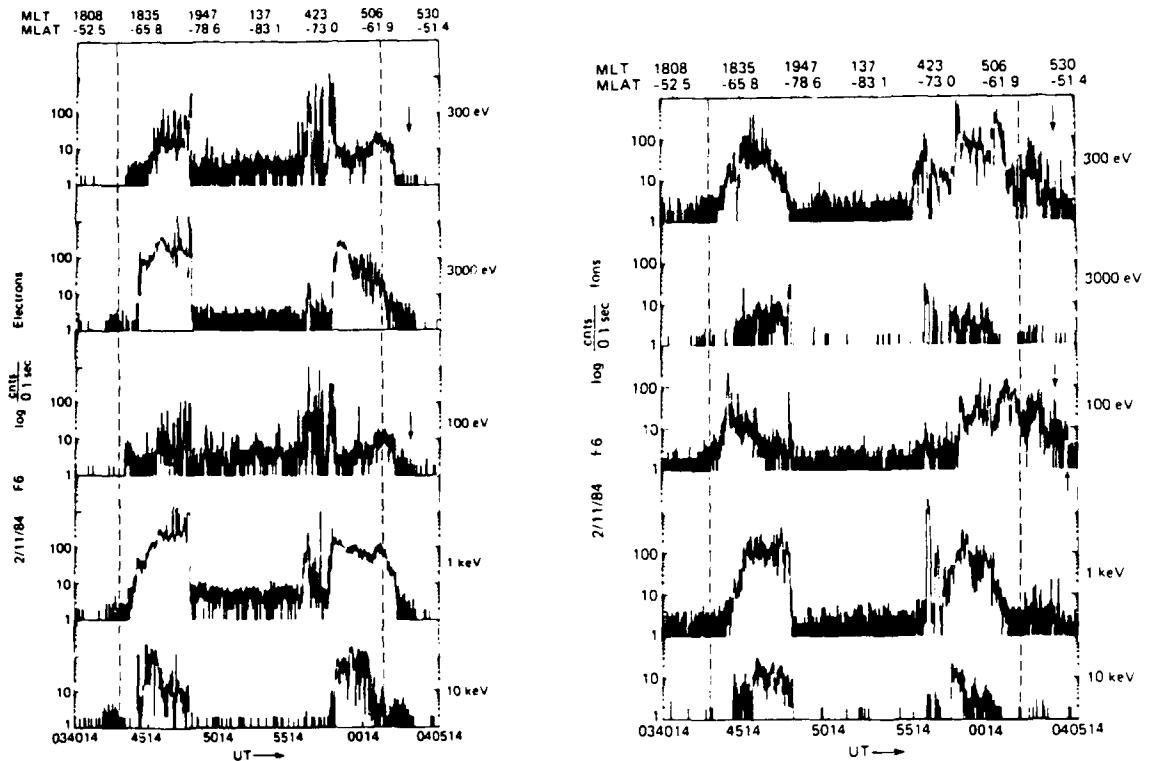


Fig. 6. The injected low-latitude electrons (left) are lost much more quickly than the ions (right). Dashed lines are at 60° MLAT. The low-latitude cutoff of the soft ion precipitation (upward arrow) is -52.1° .

Thus, a plasmopause of about 56.5° MLAT, or $L = 3.3$, is implied. A low value such as this for the plasmopause is to be expected following prolonged high-level substorm activity [e.g., Carpenter, 1966].

As activity continues to be reduced, the low-latitude soft ion precipitation zones become well isolated. The sixth panel of Figure 12 (1700 UT, 7 hr after the injection ended) is a typical example of this phenomenon. This figure also suggests that the soft ion precipitation may penetrate to even lower L values than the minimum ($L = 2.4$) for which we have data. (No 3-keV ions were seen in this satellite pass, probably due in part to the low maximum latitude that was reached.) The isolated precipitations continue for some time, a little weaker in the northern hemisphere than in the southern. The seventh panel of Figure 12 (second from the bottom) shows that even in the comparatively low $Kp = 2+$ activity, the isolated low-latitude ion precipitation continues. Thus, we are watching the survivors from the injection rather than freshly energized ions. As universal time advances, these ions can be seen to move through the different magnetic local time zones. The final observation of low-latitude ion precipitations connected with this event occurs at 0720 UT June 17, 1984, about 1 day after the injection. Thereafter, no further low-latitude ion precipitations are seen by either satellite until the next injection event. Spectra are very similar to those shown in Figure 10 for the previous event, although slightly harder.

3. POSSIBLE DATA-SELECTION AND INSTRUMENTAL EFFECTS

The data presented above give a compelling physical picture, and there is thus no particular reason to suspect instrumental effects. Nonetheless, since the phenomenon reported here is new,

we believe that a brief discussion of the possibility is in order. The best way to demonstrate that a certain instrumental effect is not responsible is to investigate examples of when the effect is operational and to determine the signature of the effect.

Solar UV may, by multiple reflections through the electrostatic analyzer, directly strike the channeltron mouth and result in a count being recorded (for the low-energy electron detector, photoelectrons from the analyzing plates would also have to be considered). The signatures of UV contamination are that it occurs when the detector is most nearly looking at the sun and is strongest in the detectors with the largest apertures, namely the high-energy electron detector and, especially, the low-energy ion detector. For both these detectors, the count rate due to solar UV is independent of the voltage on the analyzing plates. Both F6 and F7 are three-axis stabilized with the detector always pointed radially away from the earth. Thus the solar zenith angle is identical to the angle between the particle detectors and the sun. Because of its sun-synchronous nearly dawn-dusk orbit, F6 never looks close enough to the sun for a UV effect to be observed. However, F7 can look to within about 21° of the sun while still above 50° MLAT; at these times a UV effect can be seen that fits extremely well with the above description. At angles up to about 45° with the sun, a mild effect can still be seen in the low-energy ion detector. Therefore, with careful analysis, this type of contamination can be reliably discriminated against.

High-energy penetrating MeV electrons from the low-altitude horn of the outer radiation belts can also give rise to count rates independent of energy by directly stimulating the channeltrons (discussed in connection with DMSP data by Varga *et al.*, [1985]). In Figure 4, at about 57° MLAT on the duskside of the orbit, the effect of penetrating radiation can be seen. The signature is a hump-shaped pattern in which the count rate is independent

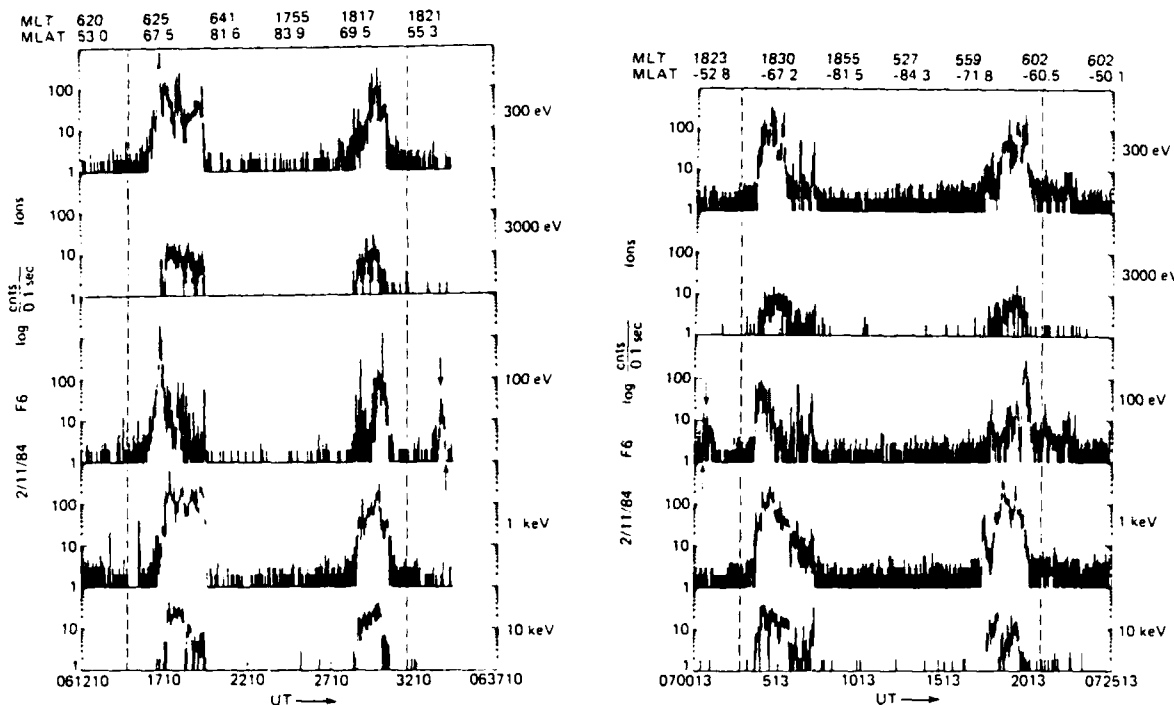


Fig. 7. The first low-latitude ions appear at dusk, by corotation from the dawn injection. Left: northern hemisphere pass; right: southern hemisphere pass. Dashed lines show 60° MLAT. The upward pointing arrow denotes the extent of the low-latitude precipitation. Left: 51.6° ; right: -52.0° .

of the resolving energy for a given detector. As seen in Figure 4, the effect is strongest in the high-energy electron detector (the 1-, 3-, and 10-keV channels are the three shown of the 10 total high-energy channels). Again, this effect can be reliably discriminated against.

Finally, spacecraft charging must also be considered. Although even the low-altitude polar-orbiting DMSP satellites can charge to high potentials for a few seconds in the auroral zone [Gusenhoven *et al.*, 1985], at the lower L values of interest to the present work a spacecraft would ordinarily be clamped to about -2 V because of the dense thermal plasma. However, on DMSP satellites, because of the operation of solar panels, the spacecraft can at times be held at -28 V (D. A. Hardy and F. Rich, personal communication, 1985). This is still far enough below the energies (100 eV to 1 keV) we consider here that it cannot be decisively affecting the data. Moreover, the energy spectra of the phenomenon discussed herein (Figure 10) bear no resemblance to spacecraft charging events [DeForest, 1972]. To minimize the importance of the often occurring -28 -V charging effect, we have not presented data below 100 eV.

In searching for events, we have concentrated on long periods (two or more days) of relatively moderate activity ($Kp < 3$), followed successively by several hours of intense substorm activity ($Kp > 5$), and then by a long enough period of moderate activity for the low-latitude precipitation to cease. Since our thesis as to the origins of the low-latitude soft ion precipitation implies their absence during times of sustained quiet, we have performed a visual scan throughout the months of February and June 1984 and confirmed that this is indeed the case. The detail with which the injections can be documented as shown in section 2 also makes clear the physical connection between substorm activity and the injection. Thus, the connection cannot be an artifact of our search procedure for events.

4. DISCUSSION

The two examples presented in section 2 are representative of a phenomenon that is typical of prolonged intense substorm activity. The injection is always seen to occur in the dawn sector, typically extending to about 0830 MLT. The earliest magnetic local time boundary of the injection cannot easily be determined from the DMSP satellites because of their limited magnetic local time coverage (specifically, there is little coverage of the post-midnight sector); however, we can conclude that it is no earlier than magnetic midnight. We should add the caveat that we have only considered the fairly frequently occurring events for which the peak Kp is in the range of 5 to 7. Thus our events, while representing intense substorm activity, do not even rank as true magnetic storms (as seen in Figures 1 and 11, the peak Dst for our events is about 50γ). For extreme levels of geomagnetic activity, the injection is likely to occur in other sectors in addition to the postmidnight-dawn sector (because of the equatorward and hence earthward expansion of the auroral oval). We leave this question to future work.

The simplest attempt to fit our data into the existing framework of magnetospheric models is to compare our observations with a model of a Stern-Volland electric field convecting particles from a source in the magnetotail earthward toward a dipole magnetic field. This type of model has been and continues to be analyzed by many authors [e.g., Chen, 1970; Ejiri, 1978; Ejiri *et al.*, 1980; Kivelson *et al.*, 1979; and many others]. As mentioned in the introduction, the steady-state ion Alfvén layers that result therefrom have at dawn (as well as at all other local times) intermediate (~ 10 -keV) energy ions penetrating closer to the earth than higher-energy ions; hence, they have the reverse sense of dispersion as seen by the DMSP satellites. Of course, the events we are investigating are obviously not steady state. We are thus

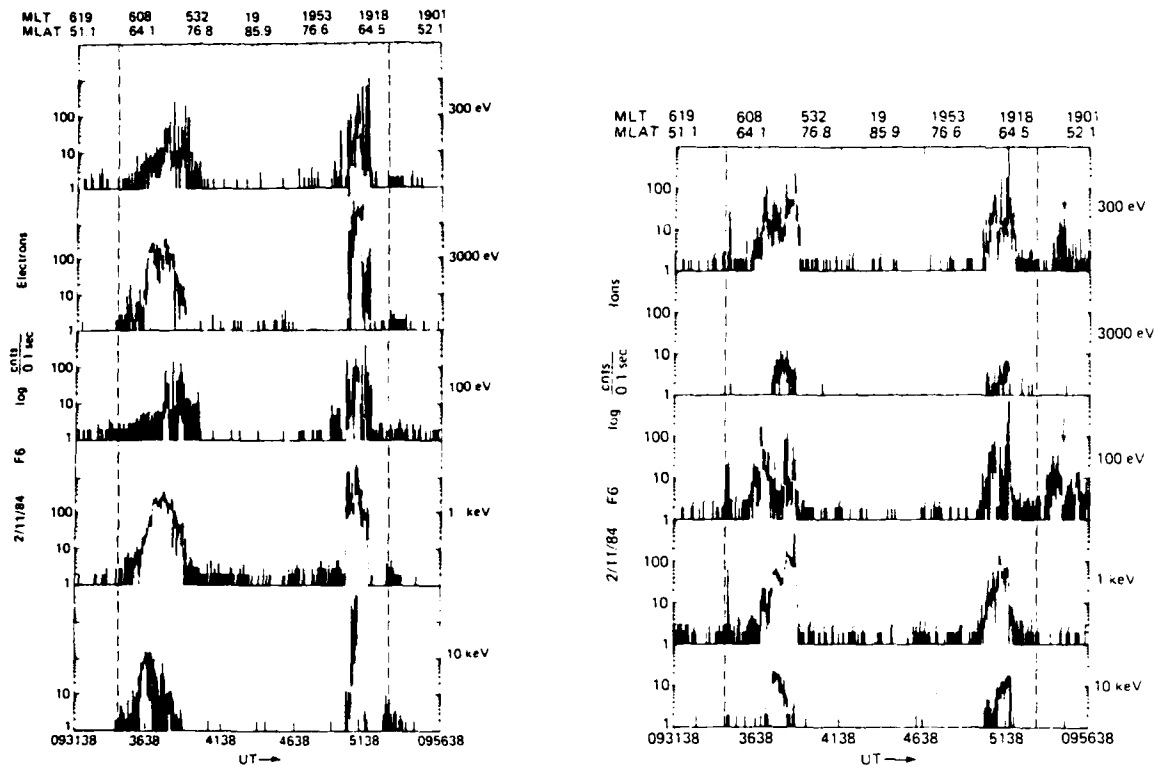


Fig. 8. Example of low-latitude ion precipitations with no corresponding electron precipitations. Left: electrons; right: ions. The dashed lines show 60° MLAT. There is no clear cutoff in the low-latitude soft ion precipitation.

led to examine the calculations presented by *Ejiri et al.* [1980] in which they model a "substorm injection" by a sudden enhancement or turning on of the cross-tail field (which convects an initially dispersionless source at $10 R_E$ in the tail earthward). The calculations by *Ejiri et al.* do indeed show that low-energy ions reach farther earthward than do higher-energy ions for the first few hours following "injection" onset. However, the amount of predicted dispersion is miniscule compared to that which we observe in such events. For example, *Ejiri et al.* [1980] calculate (using a very strong cross-tail field that gives a stagnation point at dusk at $5 R_E$ at the equator) that the difference in earthward cutoffs between a few-hundred-eV ions (essentially zero-energy ions) and 3-keV ions would be only a few tenths of an L value at dawn 1.5 hr after "injection" onset. At later times, the dispersion becomes even smaller (until eventually the steady-state Alfvén layers with the inverted dispersion are reached). Obviously such a model is not going to be able to explain the very large dispersion we observe, such as the approximately 14° MLAT in Figure 5. Whether competing and more sophisticated models, such as the E3H and M2 electric and magnetic field model of *McIlwain* [1974], are more successful is a question outside the scope of the present work. We will discuss below whistler-based observations of low-energy convection patterns that agree very well with our data.

Shelley et al. [1972] and *Sharp et al.* [1974] have made observations of what may be a related phenomenon. They report that during magnetic storms (Dst peaking between -130 and -240γ for the events they consider, as opposed to about -50γ peak for the events we consider), energetic oxygen ions can precipitate at latitudes down to $L = 3.9$ to 5.7 [*Sharp et al.*, 1974] or even $L = 2.5$ [*Shelley et al.*, 1972]. These low-latitude heavy ion

precipitations can persist for about a day, with a systematic steepening of the spectrum with increasing latitude [*Sharp et al.*, 1976]. The energy spectrum published by *Shelley et al.* [1972] for the lowest latitudes shows the flux rising rapidly with decreasing energy down to the lowest energies available with the detectors used, about 700 eV. The peak flux at 700 eV was, a few times, 10^4 ions/cm² sr eV, a value about 10 times larger than the peak flux we observe at this energy (a flux of this size would give us excellent counting statistics). The difference may possibly be due to the different pitch angles observed: the DMSP data are taken well within the loss cone, whereas the data reported by *Shelley et al.* are from near the edge of the loss cone. It may also be that the more intense activity in a magnetic storm leads to much more intense particle fluxes. Finally, we may simply be observing a different phenomenon.

Strangeway and Johnson [1984] reported that during the magnetic storm of February 21 (Dst minimum of -100γ) the inner L value at which the lowest-energy particles covered by the S3-3 mass spectrometer (~ 500 eV) had a sharp drop-off moved to lower L values with time. They concluded that this could be accounted for by earthward convection of a preexisting magnetospheric population, and on the basis of certain signatures they inferred that the injection occurred in the dawn sector. The phenomenology *Strangeway and Johnson* deduced for this particular storm thus appears to resemble the initial stages of the events we regularly observe with DMSP data. It is of interest that *Strangeway and Johnson* [1984] report that the injected particles were primarily oxygen.

A related set of observations is that of the inner edge of the ring current by equatorial satellites. *Lennartsson and Sharp* [1982], using ISEE 1 plasma composition data, conclude that

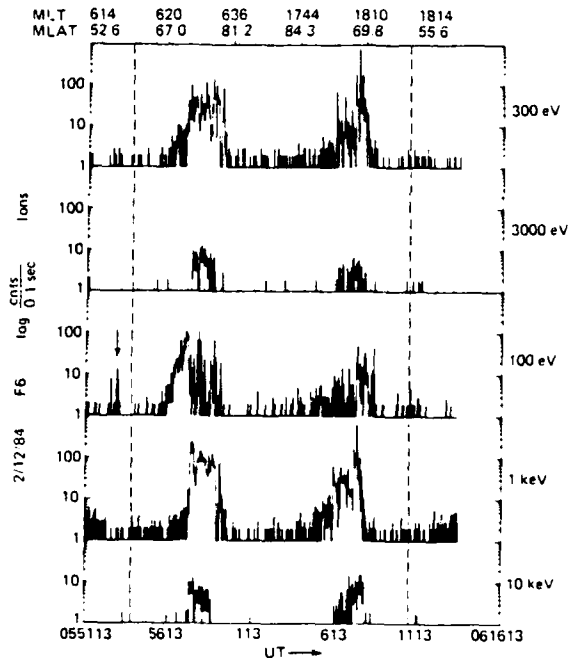


Fig. 9. The last observations of low-latitude soft ion precipitations. The enhanced flux is in the 100-eV channel at dawn. Dashed lines show 60° MLAT. The upward arrow shows the soft ion cutoff: 55.5°.

at the inner edge of the ring current ($L \sim 2-3$ during disturbed conditions and $L \sim 3-4$ during quiet conditions) oxygen can often be the dominant species. Moreover, they find that the phase space density at these lowest L values (around 3.5) is dominated by low-energy (100–1000 eV) oxygen ions. Although the observations of *Lennartsson and Sharp* [1982] are of the trapped population and ours of the precipitating ions, it appears likely that the same phenomenon is being observed. *Balsiger et al.* [1980] have also reported equatorial observations (GEOS 1) showing that the inner edge of the ring current can be dominated by oxygen.

Whether or not these observations are of the same phenomenon as the present work, we are herein concerned with more than simply confirming that low-latitude ion precipitations can occur

in intense substorm activity. We have documented here the detailed evolutionary history of such precipitation, having observed directly the sector in which the injection occurs, the initial presence and rapid loss of accompanying electron precipitation, the subsequent development into isolated precipitation regions, and that the fact that this is not an occasional but rather a pervasive feature of intense prolonged substorm activity. Because of the lower energies covered by the DMSF detector (down to 30 eV), we are able to show that the low-latitude energetic ion flux typically has a peak at about 68 eV (Figure 10).

Our physical interpretation of the dawnside soft ion introduction into low latitudes is that, following the substorm injection of fresh plasma into the roughly equatorial magnetosphere (either because the existing plasma sheet was convected earthward as some authors, for example *Kivelson et al.*, [1980], believe or because newly energized plasma reconstitutes the plasma sheet further earthward as some authors suggest), the low-energy portion of the plasma is at dawn during prolonged intense substorm activity convected earthward to very low latitudes (at least $L = 2.4$). This picture of low-energy plasma convecting earthward at dawn is in complete agreement with the results of *Carpenter et al.* [1979], in which the cross- L motion of the plasma at $L = 4$ during substorm activity was deduced from whistler paths. Figure 13 shows their results for the average flow in the magnetospheric equatorial plane during many substorms. They observe in the postmidnight to about 0800 MLT region that the plasma is convected earthward, whereas in all other sectors the substorm convection at $L = 4$ is antiearthward. It is evident that our observations of soft ion injections at dawn fit together nicely with the convection patterns determined from whistlers. Of course the whistler observations could be expected to fit most closely with the lower-energy plasma in our observations, as they in fact do. In passing, we note that the observation by *Lennartsson and Sharp* [1982] that the increase in oxygen content of the magnetospheric plasma during substorm activity beyond $L > 5$ is least in the 0100 to 0600 MLT region is not at all inconsistent with the convection patterns reported by *Carpenter et al.* [1979] and observed here. The low-energy plasma is being convected inward in this local time region.

The question arises as to why the ion precipitation is often confined to a narrow latitudinal range in the aftermath of the injection (for example, Figure 7). The cutoff at the equatorward extent can be interpreted as the limit of earthward penetration

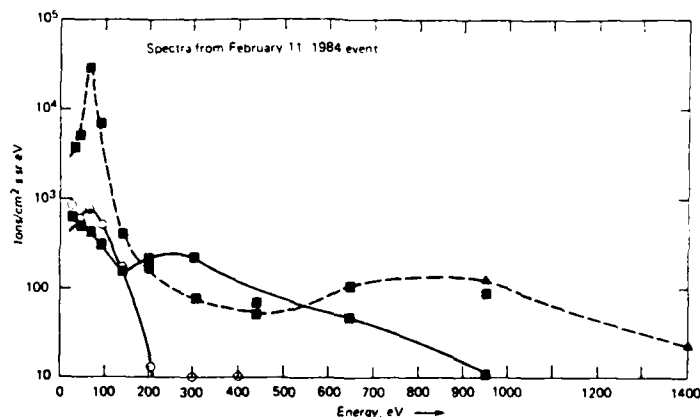


Fig. 10. Three-sample spectra of the soft ions injected, February 10–11, 1984. Dashed line is from 2013 UT February 10, 51.4° MLAT (start of injection, see Figure 5 (left)); the solid line with boxes is from 0222 UT February 11, 57° MLAT (developing injection); the solid line with circles is from 0634 UT, 52.3° MLAT (aftermath of injection, see Figure 7 (left)).

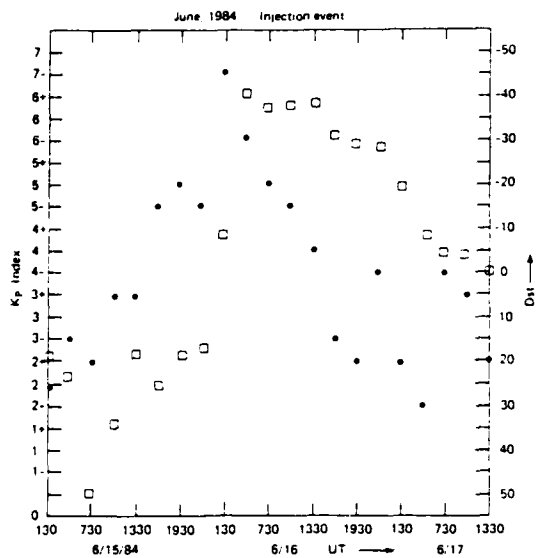


Fig. 11. Circles: 3-hr K_p indices for the June 15-16, 1984, injection. Squares: D_{st} equatorial indices (provisional) during the same time period.

because of the convection electric fields. The poleward cutoff quite likely represents the boundary of corotation, that is, the plasmapause. Although the high-latitude cutoff is typically $\sim 55^\circ$ MLAT, this is not an unreasonable value for the plasmapause latitude immediately following prolonged substorm activity. The mechanism we hypothesize is that the ions remaining in the midnight-dawn sector are eventually convected back anti-earthward. Such reversals of the convection electric field in the 0200- to 0500-MLT sector have in fact been observed by *Carpenter et al.* [1979]. Thus, narrow strips of soft ion precipitation are formed with a high-latitude boundary determined by the limit of (at least partial) corotation and with the equatorward boundary the limit of earthward convection.

The ions that DMSP is able to measure at these latitudes are all within the loss cone. Since precipitation is observed to continue for a time span of about a day following an injection, we can very roughly estimate the total number of ions involved. For example, during about 6 hr local time in 24 hr, there are $\sim 10^4$ ions/cm² sr over a 1.5° MLAT strip, centered around, say,

53° MLAT. If this is integrated over the loss cone (2.7 sr) around the earth, one concludes that $\sim 2 \times 10^{25}$ ions must have been originally injected over a period of several hours for the precipitations to last as long as they do. By comparison, it has been estimated that the circulation of ions through the entire magnetospheric convection system is about 10^{26} ions/s [*Hultqvist*, 1983].

For auroral electron and ion precipitation it is widely believed that pitch-angle scattering into the loss cone occurs through various wave-particle interactions (to cite two examples, *Ashour-Abdalla and Thorne* [1978] for ions and *Davidson* [1986] for morningside electrons). At the low L shells of interest here, the relative paucity of wave activity makes the issue more unclear. As a limiting estimate, it is of interest to compare a rough estimate of the loss time through coulomb collisions of energetic particles injected into a thermal plasma with our observations. It is much easier for collisions with ambients to scatter the superthermal particles into the loss cone than it is for them to absorb their energy directly. The dominant mechanism for this is multiple coulomb collisions with ambient ions (not ambient electrons, because of momentum considerations). The cross section for scattering through 90° by multiple collisions, each causing a deflection by a small angle, is [*Krall and Trivelpiece*, 1973]

$$\sigma_{90} = 8\pi \left(\frac{e^4}{2E} \right)^2 \ln \lambda$$

where E is the energy of the particle, $\ln \lambda$ is the coulomb collision parameter (which for the conditions in the plasmasphere is about 20), and e is the particle charge. The scattering time is

$$\tau = 1/(n\sigma_{90}v)$$

Taking a 100-eV electron in a $1000/\text{cm}^3$ plasma, we find $\tau = 6 \times 10^3/\text{s}$ or about 1.7 hr. This lifetime for electrons, which of course only represents an upper limit to the electron survival time, is in agreement with our observations. For a 100-eV ion, τ is larger by a factor of $\sqrt{m_i/m_e}$; hence, for say a proton, $\tau = 73$ hr, which is about two or three times longer than observed (if the ions are taken to be oxygen, this calculation would give a lifetime longer yet by another factor of four). However, for both protons and oxygen in the plasmasphere in this energy

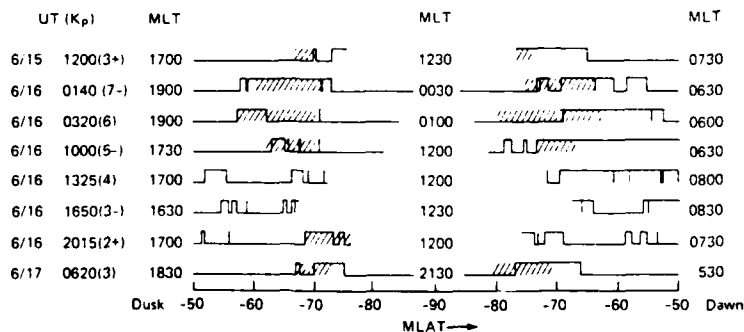


Fig. 12. A capsule view of the June 15-17, 1984, event. Each row represents one pass over the southern hemisphere for DMSP F6. The magnetic local time on the left (right) side refers to the time when the satellite moved above (below) 50° MLAT; the magnetic local time in the center corresponds to the highest latitude reached by the satellite. The hatched area is the region of 3-keV ion precipitation and is taken herein to be the region of auroral ion precipitation. The heavy solid line is high (low) for a region where the 4-s average count rate of the 100-eV ion channel was above 5 counts/0.1 s. Depending on the particular polar pass, the satellite reaches varying maximum magnetic latitudes.

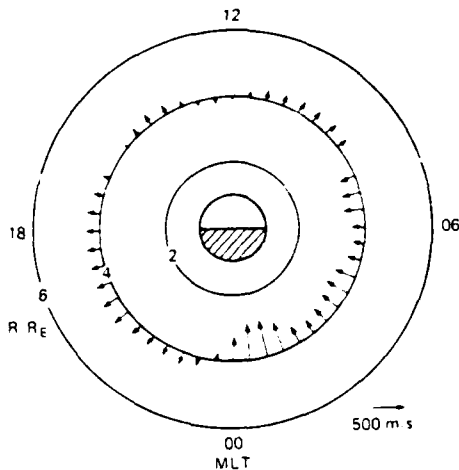


Fig. 13. Cross- L shell convection patterns during substorm activity at $L = 4$ [from Carpenter *et al.*, 1979].

range there is a faster loss mechanism, namely, charge exchange with the hydrogen geocorona. Williams [1983] has concluded that for ring current ions at these L shells the primary decay mechanism is charge exchange, although precipitation through ion cyclotron wave generation can be a significant secondary effect. On the basis of the data presented by Tinsley [1976], the lifetime of a 100-eV H^+ ion at $L = 3$ with a 45° pitch angle at the magnetic equator would be about 12 hr. Also extrapolating from Tinsley [1976], the same energy O^+ ion would have an 84-hr lifetime against charge exchange. Thus the lifetime suggested by our observations (the ions last about a day) is more consistent with the injected ions being hydrogen, although the uncertainties are such that this result is scarcely conclusive.

Because the plasmasphere is reduced to lower L shells following substorm activity, there might be some question as to whether any of the ions that we observe actually are within the plasmasphere. We have available no direct observations of our own on the plasmopause location, so we must compare with observations of others. The radial location of the plasmopause varies with local time; it reaches a minimum at dawn. Carpenter [1967] investigated the radial dependence of the plasmopause at dawn during substorm activity. His data, which include 10 points in which the peak Kp during the preceding 24 hr was 5 or greater (thus comparable to the conditions we consider), show that in none of these events was the plasmopause at the dawn minimum less than $-2.8 R_E$. Thus it seems extremely likely that the ion precipitation we observe at 50° MLAT ($L = 2.42$ in a dipole field) is indeed within the plasmasphere.

5. SUMMARY

The DMSP satellites F6 and F7 allow us to illustrate in detail a process whereby prolonged magnetospheric substorms can inject ions of up to 1 keV from near the earthward edge of the plasma sheet to deep (at least $L = 2.4$) into the plasmasphere. Such injections occur from somewhere postmidnight until about 0830 MLT (the lack of postmidnight coverage is not because of the particular substorms chosen but rather because of the limitations of the DMSP trajectories). This agrees well with the cross- L shell convection patterns of low-energy plasma deduced by Carpenter *et al.* [1979] based on storm time observations of whistlers. Subsequently, these ions begin to corotate, and latitudinally narrow well-isolated structures of ion precipitation are

formed that can persist at low latitudes for about a day. The total number of injected ions can be very roughly estimated to be $\sim 2 \times 10^{25}$. Because of similarities to the earlier observations of Shelley *et al.* [1972] and Strangeway and Johnson [1984], it is possible that the precipitating ions observed may be oxygen rather than protons or may at least contain an enhanced oxygen content [Sauvaud *et al.*, 1985]. These earlier reports discussed far more severe magnetic storm disturbances than we examine here; the events we discuss (with more detailed observations) occur several times a month. Observations by Lennartsson and Sharp [1982] showing trapped 100- to 1000-eV oxygen ions at the inner edge of the ring current are strongly reminiscent of the later stages of the events we discuss here. Our observations indicate that the lifetime of the injected ions is about a day. The present observations may be an example of a general process in which substorm activity mixes cold plasma from the plasmasphere with warm magnetosphere plasma.

Acknowledgments. This work was supported by the Atmospheric Sciences Division, National Science Foundation grant ATM-8315041, and by the Air Force Office of Scientific Research grant 84-0049. We thank the referees for their helpful comments.

The Editor thanks W. Lennartsson and C. E. McIlwain for their assistance in evaluating this paper.

REFERENCES

- Ashour-Abdalla, M., and R. M. Thorne, Toward a unified view of diffuse auroral precipitation, *J. Geophys. Res.*, **83**, 4755-4766, 1978.
- Balsiger, H., P. Eberhardt, J. Geiss, and D. T. Young, Magnetic storm injection of 0.9- to 16-keV/e solar and terrestrial ions into the high-altitude magnetosphere, *J. Geophys. Res.*, **85**, 1645-1662, 1980.
- Carpenter, D. L., Whistler studies of the plasmopause in the magnetosphere. 1. Temporal variations in the position of the knee and some evidence on plasma motions near the knee, *J. Geophys. Res.*, **71** (3), 693-709, 1966.
- Carpenter, D. L., Relations between the dawn minimum in the equatorial radius of the plasmopause and Dst , Kp , and local K at Byrd Station, *J. Geophys. Res.*, **72**, 2969-2971, 1967.
- Carpenter, D. L., C. G. Park, and T. R. Miller, A model of substorm electric fields in the plasmasphere based on whistler data, *J. Geophys. Res.*, **84**, 6559-6563, 1979.
- Chappell, C., Cold plasma distribution above a few thousand kilometers at high latitudes, in *High-Latitude Space Plasma Physics*, edited by B. Hultqvist and T. Hagfors, Plenum, New York, 1982.
- Chappell, C., C. R. Baugher, and J. L. Horwitz, New advances in thermal plasma research, *Rev. Geophys.*, **18**, 853-861, 1980.
- Chen, A. J., Penetration of low-energy protons deep into the magnetosphere, *J. Geophys. Res.*, **75**, 2458-2467, 1970.
- Davidson, G. T., Pitch angle diffusion in morningside aurorae: 1. The role of the loss cone in the formation of impulsive bursts of precipitation, *J. Geophys. Res.*, **91**, 4413-4427, 1986.
- DeForest, S. E., Spacecraft charging at synchronous orbit, *J. Geophys. Res.*, **77**, 651-659, 1972.
- Ejiri, M., Trajectory traces of charged particles in the magnetosphere, *J. Geophys. Res.*, **83**, 4798-4810, 1978.
- Ejiri, M., R. A. Hoffman, and P. Smith, Energetic particle penetrations into the inner magnetosphere, *J. Geophys. Res.*, **85**, 653-663, 1980.
- Fairfield, D. H., and A. F. Vinas, The inner edge of the plasma sheet and the diffuse aurora, *J. Geophys. Res.*, **89**, 841-854, 1984.
- Feldstein, Y. I., and Yu. I. Galperin, The auroral luminosity structure in the high-latitude upper atmosphere: Its dynamics and relationship to the large-scale structure of the earth's magnetosphere, *Rev. Geophys.*, **23**, 217-275, 1985.
- Frank, L. A., and K. L. Ackerson, Observations of charged particle precipitation into the auroral zone, *J. Geophys. Res.*, **76**, 3612-3643, 1971.
- Gussenhoven, M. S., D. A. Hardy, F. Rich, W. J. Burke, and H.-C. Yeh, High-level spacecraft charging in the low-altitude polar auroral environment, *J. Geophys. Res.*, **90**, 11009-11023, 1985.
- Gustafsson, G., A revised corrected geomagnetic coordinate system, *Ark. Geofys.*, **5**, 595, 1970.
- Hardy, D. A., L. K. Schmitt, M. S. Gussenhoven, F. J. Marshall, H.-

- C. Yeh, T. L. Schumaker, A. Huber, and J. Pantazis, Precipitating electron and ion detectors (SSJ/4) for the block 5D/flights 6-10 DMSP satellites: Calibration and data presentation, *Rep. AFGL-TR-84-0317*, Air Force Geophys. Lab., Hanscom Air Force Base, Mass., 1984.
- Hardy, D. A., M. S. Gussenhoven, and E. Holeman, A statistical model of auroral electron precipitation, *J. Geophys. Res.*, **90**, 4229-4248, 1985.
- Hultqvist, B., The hot ion component of the magnetospheric plasma and some relations to the electron component - Observations and physical implications, *Space Sci. Rev.*, **23**, 581-675, 1979.
- Hultqvist, B., On the origin of the hot ions in the disturbed dayside magnetosphere, *Planet. Space Sci.*, **13**, 173-184, 1983.
- Kivelson, M. G., S. M. Kaye, and D. J. Southwood, The physics of plasma injection events, in *Dynamics of the Magnetosphere*, edited by S.-I. Akasofu, pp. 385-394, D. Reidel, Hingham, Mass., 1980.
- Krall, N. A., and A. W. Trivelpiece, *Principles of Plasma Physics*, p. 294, McGraw-Hill, New York, 1973.
- Lennarsson, W., and R. D. Sharp, A comparison of the 0.1-17 keV/e ion composition in the near equatorial magnetosphere between quiet and disturbed conditions, *J. Geophys. Res.*, **87**, 6109-6120, 1982.
- Mauk, B. H., and C.-I. Meng, Characterization of geostationary particle signatures based on the "injection boundary" model, *J. Geophys. Res.*, **88**, 3055-3071, 1983.
- McIlwain, C. E., Direct measurement of particles producing visible auroras, *J. Geophys. Res.*, **65**, 2727-2747, 1960.
- McIlwain, C. E., Substorm injection boundaries, in *Magnetospheric Physics*, edited by B. M. McCormac, pp. 143-154, D. Reidel, Hingham, Mass., 1974.
- Meng, C.-I., Electron precipitations and polar auroras, *Space Sci. Rev.*, **22**, 223-300, 1978.
- Meng, C.-I., B. Mauk, and C. E. McIlwain, Electron precipitation of evening diffuse aurora and its conjugate electron fluxes near the magnetospheric equator, *J. Geophys. Res.*, **84**, 2545-2558, 1979.
- Sauvaud, J. A., J. Crasnier, K. Moulala, R. A. Kovrazhkin, and N. V. Jorjio, Morning sector ion precipitation following substorm injections, *J. Geophys. Res.*, **86**, 3430-3458, 1981.
- Sauvaud, J. A., J. M. Bosqued, R. A. Kovrazhkin, D. Delcourt, J. J. Berthelier, F. Lefeuvre, J. L. Rauch, Yu. I. Galperin, M. M. Mogilevsky, and E. E. Titova, Positive ion distributions in the morning auroral zone: Local acceleration and drift effects, *Adv. Space Res.*, **5**, 73-77, 1985.
- Sharp, R. D., R. G. Johnson, E. G. Shelley, and K. K. Harris, Energetic O⁺ ions in the magnetosphere, *J. Geophys. Res.*, **79**, 1844-1850, 1974.
- Sharp, R. D., R. G. Johnson, and E. G. Shelley, The morphology of energetic O⁺ ions during two magnetic storms: Latitudinal variations, *J. Geophys. Res.*, **81**, 3292-3298, 1976.
- Shelley, E. G., R. G. Johnson, and R. D. Sharp, Satellite observations of energetic heavy ions during a geomagnetic storm, *J. Geophys. Res.*, **77**, 6104-6110, 1972.
- Smith, P. H., and R. A. Hoffman, Direct observations in the dusk hours of the characteristics of the storm time ring current particles during the beginning of magnetic storms, *J. Geophys. Res.*, **79**, 966-971, 1974.
- Strangeway, R. J., and R. G. Johnson, Energetic ion mass composition as observed at near-geosynchronous and low altitudes during the storm period of February 21 and 22, 1979, *J. Geophys. Res.*, **89**, 8919-8939, 1984.
- Tinsley, B. A., Evidence that the recovery phase ring current consists of helium ions, *J. Geophys. Res.*, **81**, 6193-6196, 1976.
- Vallance-Jones, A., F. Creutzberg, R. L. Gattinger, and F. R. Harris, Auroral studies with a chain of meridian-scanning photometers. I. Observations of proton and electron aurora in magnetospheric substorms, *J. Geophys. Res.*, **87**, 4489-4503, 1982.
- Varga, L., D. Venkatesan, and C.-I. Meng, Low altitude observations of the energetic electrons in the outer radiation belt during isolated substorms, *Planet. Space Sci.*, **33**, 1259-1266, 1985.
- Vasyliunas, V. M., A survey of low-energy electrons in the evening sector of the magnetosphere with OGO 1 and OGO 3, *J. Geophys. Res.*, **73**, 2839, 1968.
- Williams, D. J., The earth's ring current: causes, generation, and decay, *Space Sci. Rev.*, **34**, 223-234, 1983.
- Young, D. T., Near-equatorial magnetospheric particles from ~1 eV to ~1 MeV, *Rev. Geophys.*, **21**, 402-418, 1983.

C.-I. Meng and P. T. Newell, The Johns Hopkins University Applied Physics Laboratory, Johns Hopkins Road, Laurel, MD 20707.

(Received February 24, 1986;
revised June 3, 1986;
accepted June 18, 1986.)

Auroral Morphology of the Midday Oval

C.-I. MENG and R. LUNDIN¹

The Johns Hopkins University Applied Physics Laboratory, Laurel, Maryland

Auroral displays in the noon sector were examined by using hundreds of Defense Meteorological Satellite Program auroral images, taken over the southern polar region in austral winters, in order to determine the morphology. The auroral displays in the midday part of the auroral oval can be grouped into five characteristic types, depending on the geomagnetic activity and the B_z component of the interplanetary magnetic field. An important characteristic is the clear disconnection in appearance between the noonside and the nightside discrete auroras. Also, there is the lack of correlation between the concurrent nightside substorm activity and midday discrete auroral activity. Thus, the occurrence of bright, discrete auroras in the midday oval may be caused by the local injection of the magnetosheath plasma into the dayside boundary layer. The observed discontinuity of discrete auroras between the dayside and the nightside ovals is consistent with the existence of two separated major injection regions along the auroral oval: the dayside cusp and the nightside plasma sheet.

INTRODUCTION

The electrodynamic coupling between the solar wind and the magnetosphere has been the key topic in the study of solar-terrestrial interaction and space plasma physics. The polar cusp is the region where the solar wind gains direct entry to the magnetosphere, regardless of the physical processes in the interaction between the solar wind and the geomagnetic field. The existence of polar cusp regions was identified in 1971 [Heikkila and Winningham, 1971; Frank, 1971]. The intersection region of the cusp with the polar ionosphere and atmosphere is normally located between 75° and 79° geomagnetic latitude near the noon meridian, the midday sector of the auroral oval. The general association between the cusp and the midday auroral oval is well accepted [Heikkila et al., 1972; Eather and Mende, 1972; Shepherd and Thirkettle, 1973; Sivjee and Hultqvist, 1975; Shepherd et al., 1976a, b; Cogger et al., 1977; Meng, 1981b; Murphree et al., 1981]. However, particle and field observations of the dayside magnetosphere near the magnetopause and the polar cusp region reveal more detailed and complex structures. The entry layer is the major injection (entry) region for magnetosheath plasma where the energy and mass transfers take place [Haerendel et al., 1978].

The low-latitude boundary layer with a strong plasma drift is proposed as the region of viscous interaction between the magnetosheath and the magnetosphere [Eastman et al., 1976]. On the other hand, field line merging has been suggested as the main energy and momentum transfer process; the boundary layer is thought to be merely a transport region for magnetospheric plasma on open geomagnetic field lines [Russell and Elphic, 1979; Cowley et al., 1983]. Recent measurements from the ISEE and Prognoz 7 satellites indicate that the interface region between the magnetosheath and the magnetosphere is highly structured and variable [Sckopke et al., 1981; Lundin, 1984]. Therefore, the ionospheric projection of these regions cannot be a simple one [Vasyliunas, 1979], and the auroral display in the midday part of the auroral oval may reveal clues to the complicated structuring of the magnetopause and the polar cusp region.

Optical observations of the midday sector of the auroral oval are rather difficult to obtain because sunlight hinders the optical measurement of auroras in visible wavelengths near noon. Midday auroras can only be seen in a very limited part of the polar region where the geographic latitude is very high and the magnetic latitude is $\approx 75^\circ$ and then only in a very limited season near the local winter solstice (such as Spitzbergen in December and the south pole in July for ground-based observations). Measurements made using the space-borne auroral imaging instrument are more flexible but are still severely limited by the observational season; ISIS 2 and the Defense Meteorological Satellite Program (DMSP) spacecraft made many observations of auroral displays in the noon sector during the local winter season [Snyder et al., 1975; Dandekar and Pike, 1978; Dandekar, 1979; Cogger et al., 1977; Meng, 1981b; Murphree et al., 1981]. The most unusual feature of the midday auroras is a permanent gap in the distribution of discrete auroral arcs; it has a width of about 15° in longitude centered at about 1130 magnetic local time (MLT). There also exist isolated discrete auroras in the early afternoon sector of the auroral oval. Additionally, diffuse and discrete auroras occur along the auroral oval [Murphree et al., 1981] with the mantle aurora at lower latitude ($\approx 70^\circ$ geomagnetic latitude) during active times [Meng and Akasofu, 1983].

Murphree et al. [1981] investigated the characteristics of the auroral display in the 1200 to 1800 MLT sector from 66 optical images at 3914 Å from the ISIS 2 auroral scanner. Only diffuse auroras were observed along the afternoon and early evening parts of the auroral oval when the B_z component of the interplanetary magnetic field (IMF) was positive and when there was no magnetospheric substorm activity. Isolated discrete auroras were observed in the afternoon oval when the IMF B_z was negative, regardless of substorm activity, and the long extended discrete auroral arcs along the oval were characteristic during a moderately intense substorm. Several DMSP satellites made detailed images of the auroral display in the noon sector over the southern polar region.

In this paper, the auroral displays in the noon sector were examined to determine the morphology; their relationships with dayside magnetospheric structures are discussed. It is found that the auroral displays can be grouped into five categories, depending on the geomagnetic activity and the B_z component of the IMF. The occurrence of bright, discrete dayside auroras is likely to be caused by the local injection of magnetosheath plasma

¹ R. Lundin is on leave from Kiruna Geophysical Institute, Kiruna, Sweden.

Copyright 1986 by the American Geophysical Union.

Paper number 5A8758.
0148-0227/86/005A-8758\$05.00

into the dayside boundary layer. An important characteristic of types 2 and 3 is the clear discontinuity between the dayside and the nightside discrete auroras. Also, there is the lack of a connection between nightside substorm activity and midday discrete auroral activity. These phenomena are consistent with the existence of two major separated "injection regions" along the auroral oval: the dayside cusp and the nightside plasma sheet.

DATA BASIS

In the DMSP, two spacecraft are maintained in sun-synchronous polar circular orbits with an inclination of 98.75° , a period of 101.5 min, and an altitude of 830 km. One orbit is in near-dawn-dusk orientation, the other in a near-noon-midnight meridian. The trajectory of the dawn-dusk orbit is nearly tangent to the midday part of the southern auroral oval between about 0900 and 1300 UT every day, and the optical imagery covering the dayside auroral oval is generally obtainable during the austral winter. Detailed auroral displays over the noon and dayside portion of the auroral oval are clearly imaged with excellent spatial resolution (≈ 2 to 3 km) and have been shown previously [Snyder and Akasofu, 1976; Akasofu, 1976; Dandekar and Pike, 1978; Meng, 1981b].

Extensive data from at least 134 images were obtained in 1975 by the DMSP 33 satellite and from 173 images in the 1978 season by the DMSP F2 and F3 satellites. The DMSP imagery covers only a 3000-km-wide swath along the satellite trajectory; thus, there are only partial views of the auroral oval and those are limited to the dayside of the late morning and afternoon. No simultaneous nightside auroral display was recorded. The approximately 310 auroral images from the dawn-dusk DMSP satellites obtained from late June to early August provide a database for an auroral morphology investigation of the noon sector of the southern auroral oval. The DMSP auroral imagery is recorded by a broadband optical line-scanning system that is sensitive to atmospheric emissions and earth albedo from ≈ 4000 to $11,000 \text{ \AA}$ with a peak response near $\approx 8000 \text{ \AA}$ [Eather, 1979]. There is no quantitative information from the DMSP imagery [Eather, 1979], in contrast to the quantitative images from the ISIS 2 narrow passband at 3914 and 5577 \AA . However, the advantages of using the DMSP data are (1) a higher spatial resolution from the low-altitude (≈ 830 km) circular orbit, (2) a large amount of data, and (3) a possible higher sensitivity (≈ 25 to 50 Rayleigh of 4278 N_2^+ emission [Eather, 1979]) for auroral monitoring.

OBSERVATIONS

It is well known that the auroral display is always variable and very complex and that no two displays are identical. However, the complicated auroral activity can usually be synthesized systematically such as in the concept of the auroral substorm [Akasofu, 1964]. The noon sector DMSP auroral observations can be categorized into five major groups, based on the auroral display characteristics. It is found that auroral features are well ordered with geomagnetic activity and interplanetary magnetic conditions. They are described below in the order of complexity of auroral displays.

Type 1: Quiet Expanded Noon Oval

The basic configuration of the midday auroral display is characterized by many extremely faint discrete arcs that are barely detectable above the background of atmospheric scattered light. The configuration is generally parallel to the dayside auroral oval in the equatorial part and gradually becomes ap-

proximately sun-earth aligned in the higher latitudes, with an indication of converging toward the polar cusp region as illustrated in Figure 1.

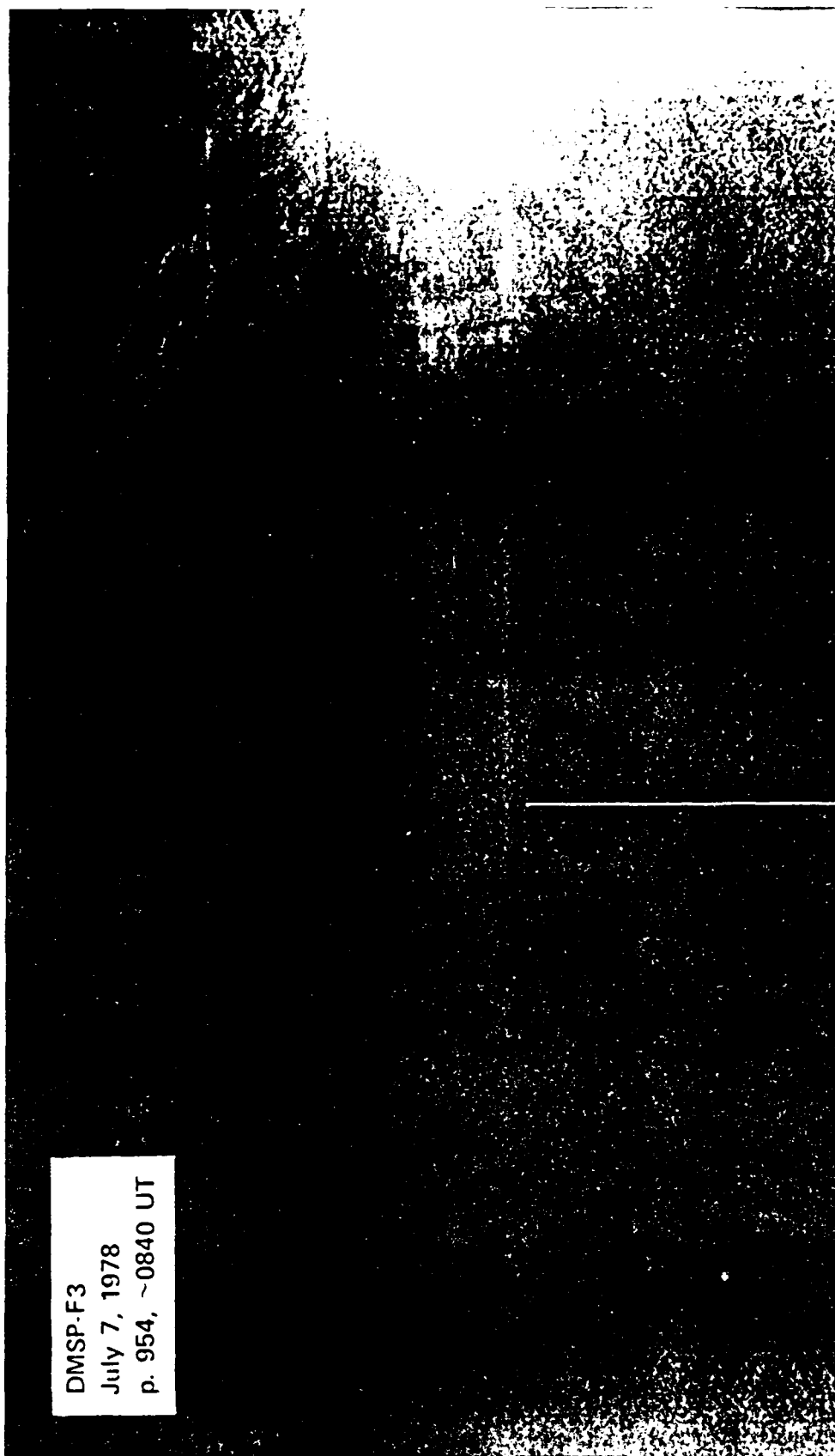
In the southern polar region auroral picture, the local time orientation is reversed from that of the familiar northern polar region configuration; dusk (dawn) is now on the right-hand (left-hand) side of the diagram. Note that the central part of the noon auroral oval is a region of no discrete auroras, a fact that is consistent with the existence of a gap in the discrete auroral oval [Dandekar and Pike, 1978]. Usually, there are many extremely faint discrete arcs parallel to one another and sometimes with a hint of an observable weak diffuse aurora background from the equatorial edge of the auroral oval to the higher latitude. These faint and long discrete arcs extend over 1000 km and gradually change orientation from a direction parallel to the equatorial edge of the late morning or afternoon part of the oval to a nearly sun-earth (i.e., noon-midnight) alignment on the poleward part (i.e., a fan-shaped configuration). These arcs are frequently distributed throughout the late morning to early evening parts of the oval and also over the so-called "polar cap region" without any clear indication of a polar cap that is void of discrete auroras. Their distribution and configuration do not give a familiar oval display and may provide a strong indication of a widened auroral oval expanding to very high geomagnetic latitudes from both the dawnside and the duskside, similar to suggestions of Meng [1981a] and Murphree *et al.* [1982].

If these faint discrete arcs are indeed part of the poleward widening of the quiet time auroral oval, many DMSP observations may indicate the disappearance of the polar cap (defined as the high latitude region poleward of the instantaneous oval) over the dayside half of the polar region. In some other events, these very faint, long, noon-midnight-oriented discrete arcs occupy only either morning or evening parts of the high latitude polar region, with a void region at higher latitudes and a narrower region of multiple faint arcs on the opposite side. The observations may also indicate the poleward widening of only a partial auroral oval and the skewness of the polar cap distribution.

Type 2: Appearance of Small Discrete Patches

The very mundane display of extremely faint and long multiple discrete auroral arcs of type 1 is rather unique among the five types of midday auroral features. In the other four types, the auroral displays have some generally common characteristics; type 2 is the fundamental pattern of the four more-active conditions. It is different from type 1 in several ways. A region of the polar cap, defined as the void of any detectable auroral discrete feature, clearly exists in the DMSP auroral imagery. Discrete auroras are distributed more or less in the familiar auroral oval configuration, often with a faint background of diffused glows.

The width of the late morning and afternoon portions of the auroral oval is generally from a few hundred to a thousand kilometers. The most distinct feature of this type of auroral display is the appearance of bright, small-scale, irregular, discrete features in the early afternoon part of the auroral oval as shown in Figure 2. The fine structures of these discrete auroras are clearly depicted with a scale size of about a few hundred kilometers or less and are closely packed. They may be described as patch-type aurora on a very small scale; they have not been seen in any other part of the auroral oval in the high resolution DMSP auroral imagery examined thus far. The significance of detecting the small, discrete auroras will be discussed later, as



DMSP-F3
 July 7, 1978
 p. 954, ~0840 UT

Fig. 1. Dayside auroral display during a very quiet condition, as recorded by DMSP F3 on July 7, 1978, at about 0840 UT over the southern polar region. The picture is in reverse and dark sections are auroras. The local time orientation is reversed from the familiar northern hemisphere situation. The right (left) side of the picture corresponds to the afternoon (late morning) part of the auroral oval, and the sunlit hemisphere is on the top. The bright diffused spot at the noon part of the auroral oval is not real, having been produced by solar reflection into the imager. Note the appearance of many long (> 1000-km) faint sun-earth-aligned auroral arcs over the entire polar region with a diffuse background. There was no indication of the polar cap proper during the pass. The poleward intensity of the morning and/or afternoon auroral oval is the typical dayside auroral display in a true quiescent (type 1) condition.

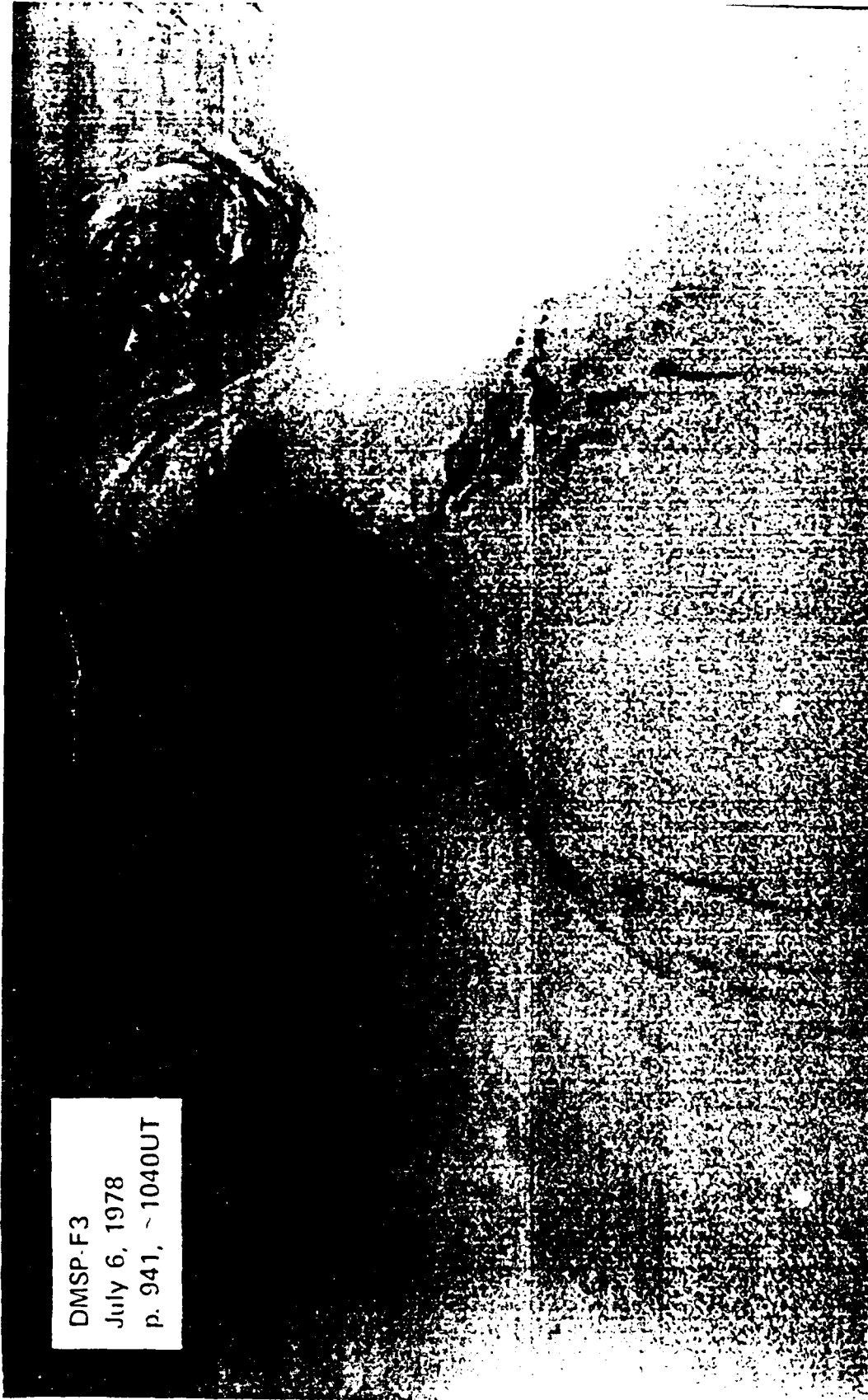


Fig. 2. Type 2 dayside auroral display. With a slight increase of solar-terrestrial interaction, many bright, small-scale (\approx few hundred kilometers), isolated, irregular, discrete auroral features (patchlike) appear in the early afternoon part of the auroral oval. The long sun-earth-aligned auroral arcs disappear, and the auroral oval configuration forms. The polar cap is clearly discernible in the imagery. No long, extended, discrete auroral arcs are seen in the dayside half of the auroral oval. There is a gap of discrete auroras near noon as previously reported.

they are believed to be related to the fine structures of the day-side magnetopause, the boundary layer, and the polar cusp.

In the late morning part of the auroral oval, the auroral display characteristics are somewhat similar to those of type 1. However, the discrete arcs parallel to the auroral oval orientation are brighter (no quantitative information is available from DMSP observations), are more closely spaced, and are generally shorter in length (< 1000 km). The midday gap of the discrete auroras is persistently located in the noon sector of the dayside auroral oval. Occasionally, there is some hint of a funnel configuration of these discrete auroras (i.e., a convergence of the auroral rays).

Another prominent auroral distribution feature of type 2 is a clear isolation of discrete auroras from the nightside of the auroral oval. The bright, irregular auroras in the early afternoon portion of the oval do not extend into the later local time sector, and there is a clear truncation in the late afternoon. The morning multiple arcs are limited in length and do not form continuous arcs extending into the nightside of the oval, in contrast to those of type 1. However, the diffused auroral emission background does provide an apparent configuration of "continuous" auroral oval.

Type 3: Bright, Isolated, Afternoon Arcs

This type of auroral display can be considered as the evolution from type 2 with higher auroral activity. Characteristic of this type is the occurrence of bright, isolated, discrete arcs in the afternoon sector of the oval. Instead of small-scale, irregular, patchlike discrete auroras, long, discrete, bright arcs are formed in the afternoon oval. They are aligned along the auroral oval orientation with an occasional kinky structure and extend for hundreds of kilometers; see Figure 3.

The number of generally parallel discrete arcs decreases toward the noon sector, indicating a merging of those arcs. They vary in each event from more than ten to only one or two and are also brighter in the early afternoon part of the oval. They fade away into the dusk sector and are definitely disconnected (i.e., isolated) from the discrete arcs extending from the nightside evening auroral oval. Also, in all of the observations, there is always a midday gap in the late morning part of the auroral oval. A gradual decrease of the latitudinal width of the oval from dusk toward noon is clearly seen; it is about 1000 km wide in the dawn-dusk direction. In the late morning sector, multiple, narrow, discrete arcs are always detected; their features are similar to those of type 2. Usually, a diffuse glow, detected on the equatorial part of the wide auroral oval, extends continuously into the early morning hours and forms a part of the auroral oval.

Type 4: Extended Bright Afternoon and Evening Arc

The afternoon auroral oval structure of this group is rather simple compared to those of the previous three types. Extremely bright, discrete auroras, generally in the form of a single strain from the nightside evening sector, extend into the noon region as a continuous, bright, poleward edge of the afternoon and evening oval; see Figure 4. A detailed examination of the original DMSP auroral imagery on 9-in. film reveals that there is sometimes an apparent "intertwine" of two narrow extended discrete arcs with a total latitudinal width of only about 100 km. (The word "intertwine" is used to describe the apparent crossover of arcs in DMSP imagery and does not infer a physical configuration.) This bright, discrete, simple, extended auroral structure frequently has some wavy features that sug-

gest the consequence of degenerated, weak, westward-traveling surges toward the early afternoon meridian along the auroral oval. Occasionally, some indication of a diffused component of the afternoon oval is located on the equatorial side of this bright, discrete, continuous, auroral configuration.

The total latitudinal width of the late afternoon and evening oval is narrow: only a few hundred kilometers. The auroral displays in the late morning oval also reduce its complexity; the oval consists of only a few simple, discrete, short auroral arcs in the poleward region (not shown in Figure 4) with diffused auroral patches in the equatorial part. The latitudinal width of the dawn part of the auroral oval is rather wide. The discrete auroral region is only a few hundred kilometers, and the diffused patchy equatorial part is greater than several hundred kilometers. The morning patchy regions, identified as mantle auroras, are produced by the drizzling energetic electrons generated by substorm activity from the midnight sector along the constant L shells [Meng and Akasofu, 1983]. The midday gap of the auroral oval is persistent; the multiple, short, discrete arcs are only seen in the dawn sector and do not extend into the late morning hours, indicating the disappearance of the discrete part of the late morning auroral oval.

Type 5: Multiple Active Afternoon Arcs

The last type of dayside auroral morphology corresponds to very active auroral displays in the afternoon sector as illustrated in Figure 5. The simple, continuous, discrete auroral arcs along the afternoon and evening oval break up into many active auroras of various types. Sometimes these auroras are in the form of an intense westward-traveling surge, are bright, multiple, discrete, irregular auroras, or are bright, discrete, multiple wave forms. They all indicate that the turbulence and activation in the auroral display originate from the midnight sector and are associated with substorm activity as observed from the earth's surface [Akasofu and Meng, 1966]. The diffuse aurora is detected on the equatorial side of active, discrete auroras along the evening and afternoon oval. Along the morning oval, only some simple, bright, discrete arcs are seen with rather bright, diffused auroras distributed over a broad region on the equatorial side. In the midday sector, a rather wide gap of discrete auroras is always present; the auroral oval is located at lower latitudes than nominal, indicating an expanded polar cap region.

MAGNETIC ACTIVITY AND IMF EFFECTS

In order to understand the characteristics of the five types of dayside auroral displays, the DMSP auroral imagery used in this study is examined along with simultaneous geomagnetic activity and also is compared with the concurrent hourly IMF whenever possible. (Note that not all of the approximately 300 images are used in this analysis; only those with the morning, afternoon, and midday parts of the oval within the DMSP auroral imagery were used for the detailed study.) A clear trend with the auroral electrojet (AE) index and IMF B_z component may be seen in Figure 6. The type 1 auroral feature was observed during a period of northward IMF with a strong B_z component (hourly average ≈ 3 nT); the AE index was low (≤ 100 nT) for many hours or during the late recovery phase of substorm activities. Therefore, it corresponds to the very quiet magnetospheric condition, possibly when magnetospheric interaction with the solar wind is very weak. The type 2 dayside auroral display was generally associated with very low geomagnetic activity (an AE of mostly < 100 nT). The hourly IMF B_z



Fig. 3. Type 3 dayside auroral display. The occurrence of bright, discrete arcs of < 1000 km length along the oval orientation in the afternoon part of the auroral oval is the key characteristic. These bright afternoon arcs are not the extension of the evening auroral oval arcs and are distinctly isolated from the rest of the oval. Long, discrete arcs are also detected along the morning auroral oval.



DMSP-33
June 12, 1975
p. 274, ~ 1345UT

Fig. 4. Type 4 dayside auroral display. In a moderately active condition, the bright, discrete auroral arcs extend from the nightside of the oval into the early afternoon sector as shown here. The bright, isolated auroras in the afternoon part of the oval, as illustrated in Figure 3, disappeared. The discrete auroral distribution forms a continuous oval configuration. Some very small-scale, discrete, auroral features form in the so-called midday auroral gap (see text for more details).

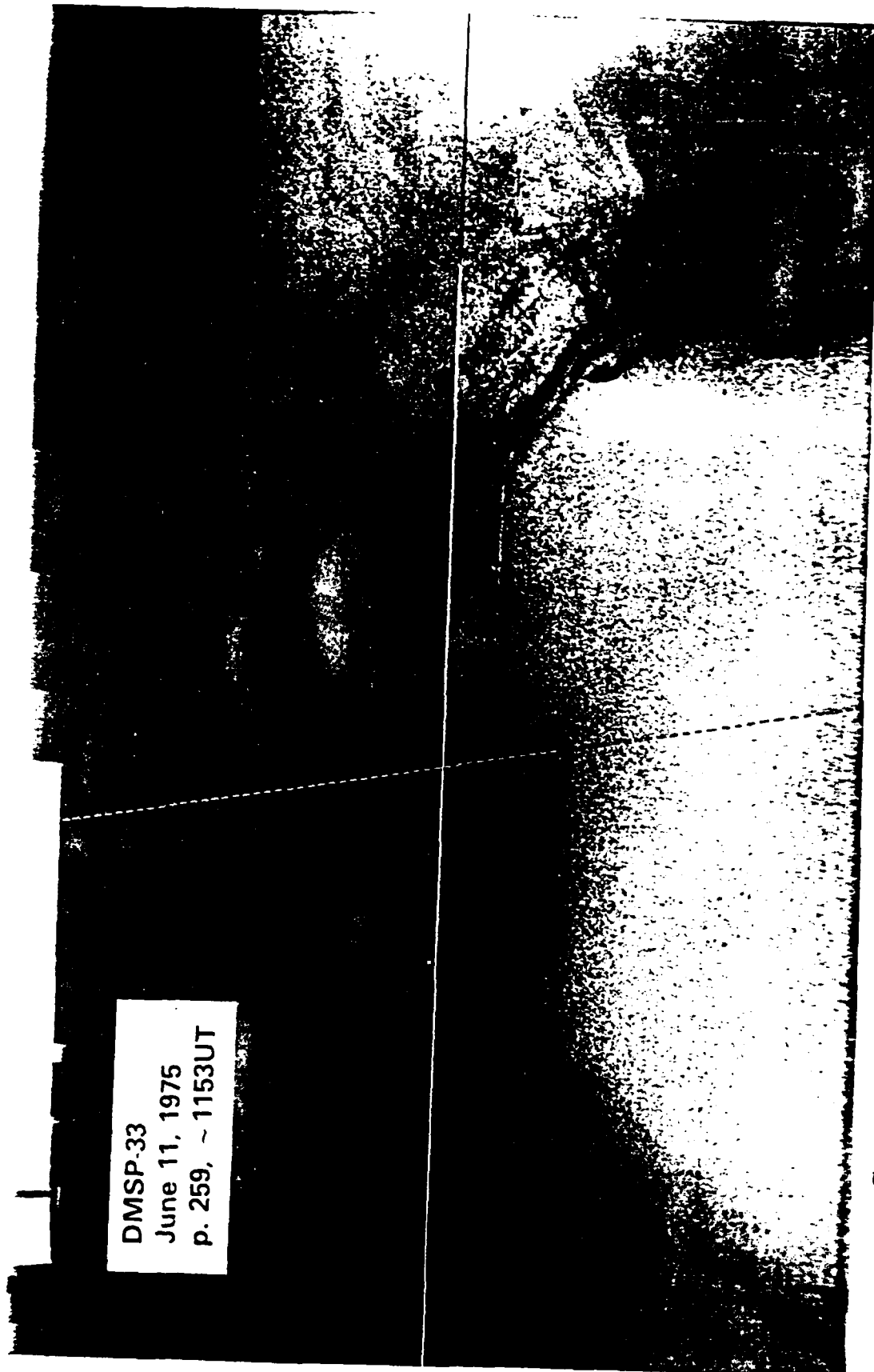


Fig. 5. Type 5 dayside auroral display. During very disturbed conditions, bright, discrete, active auroras are seen extending into both early afternoon and late morning sectors of the auroral oval. The diffuse aurora is detected on the equatorial part of the auroral oval. In the midday sector, a wide gap of discrete arcs is always present, frequently with small-scale, irregular, discrete features.

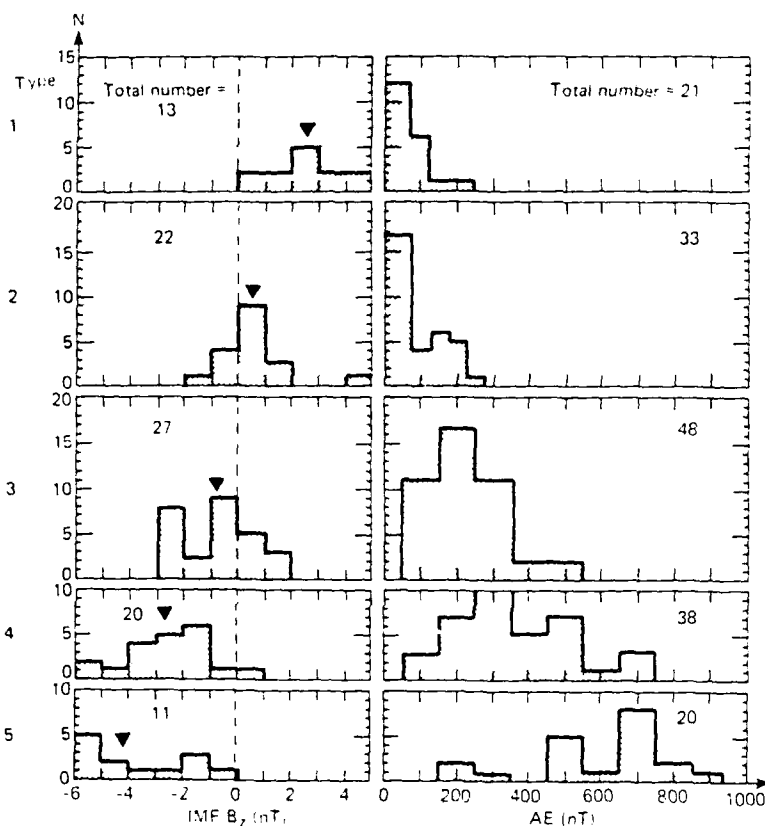


Fig. 6. Geomagnetic activity and IMF conditions of five types of dayside auroral display. Type 1 (top panel) may be called the ground state while IMF $B_z \approx +1$ nT and AE ≈ 50 nT. The geomagnetic activity increases progressively and the IMF becomes more southward as the auroral display changes from type 1 to type 5, from top to bottom panels.

component was about 1 nT, or slightly negative, with an average of ≈ 0.5 nT. This may be interpreted as a slight enhancement of the activity from the truly quiet magnetosphere with a slightly increased (weak) solar-terrestrial interaction.

The type 3 auroral condition occurred usually during weak and moderate geomagnetic activity when the AE index was about 200 nT and was associated with weak or moderate magnetospheric substorms, whereas the IMF B_z index was negative at about -1 nT. The type 4 dayside auroral characteristics appeared in more disturbed conditions. The AE index averaged about 300 to 500 nT; during the moderate substorms it averaged about -3 nT. It appeared in all phases of the auroral substorm: near onset, in the expansion, and even during the recovery. The most active dayside auroral display (type 5) was detected during very intense magnetospheric disturbances. The AE index was above 500 nT and increased to more than 1000 nT; most of the concurrent IMF B_z was very negative with an average of -4 nT.

MIDDAY AURORA AND ITS RELATION TO THE DAYSIDE BOUNDARY LAYER

Several recent reports have emphasized the connection between the dayside boundary layer and the midday auroral oval. *Iijima and Potemra* [1976] found that region 1 field-aligned currents exhibited two maxima versus local time near noon: one "upward" current maximum in the 1400 to 1600 MLT sector and one "downward" current maximum in the 0800 to 1000 MLT sector. *Bythrow et al.* [1981] concluded that the region

1 current maximum is coincident with the dayside high-latitude extension of the low-latitude boundary layer (LLBL).

A study of the midday aurora by *Akasofu and Kan* [1980] also indicated that the dayside aurora is not a natural extension of the discrete auroras from the nightside auroral oval. Thus, the dayside auroral activity should not necessarily be associated with magnetospheric substorms, which take place mainly in the nightside part of the oval. The reports by *Murphree et al.* [1981] and by *Evans* [1984] on the persistent "isolated" discrete auroras and the auroral-arc-type electron precipitation structures in the 1400 MLT sector lend further support for the separation between the dayside auroral display and the nightside auroral substorm activity. *Evans* also argued that the low temperature and relatively high density of the precipitating electrons in these "isolated" afternoon arcs suggested a plasma source with the boundary layer origin.

Lundin and Evans [1985] presented a simple model of the dayside boundary layer dynamo that can account for the observed dayside region 1 current characteristics as well as the small-scale structures of the midday aurora. Emphasizing the topological connection between the dayside auroral oval and the LLBL or the "entry layer," they proposed that the midday discrete aurora (between ≈ 0800 and 1600 MLT) results from the polarization of the dayside boundary layer associated with the temporal injection of magnetosheath plasma. According to this model, each individual arc structure is associated with an "upward" field-aligned current sheet that connects to the negatively charged side of the boundary layer injection filament. Dis-

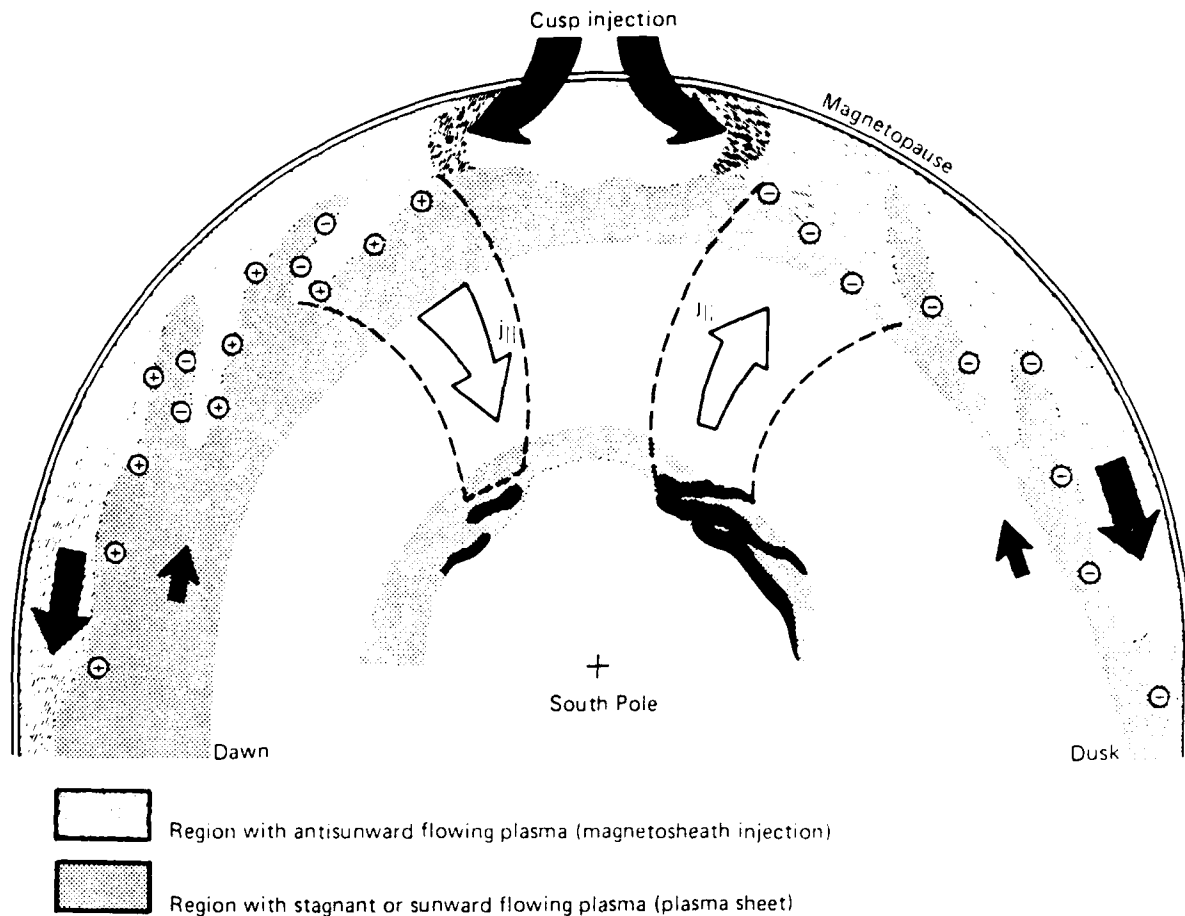


Fig. 7. Schematics to illustrate the topological connection between the dayside auroral oval and the low-latitude boundary layer (i.e., the entry layer). The midday discrete auroras are produced by the polarization of the dayside boundary layer associated with the temporal injection of magnetosheath plasma (see text for discussion).

crete arc structures are also expected to be predominantly found in the postnoon sector of the dayside auroral oval (see, for example, Figures 3 and 6 of *Lundin and Evans* [1985]).

An important implication of the boundary layer dynamo model [*Eastman et al.*, 1976; *Heikkila*, 1979; *Lundin and Dubinin*, 1984, 1985; *Lundin and Evans*, 1985] is that the directly injected magnetosheath plasma represents the source of free energy that powers the dayside region 1 current system as well as the main part of the dayside auroral activity. Thus, the discrete auroras in the midday oval are not necessarily connected to the auroral activity in the midnight sector, which is related to substorm processes in the plasma sheet of the magnetotail. We have clearly observed that types 2 and 3 of the midday auroral displays reveal a distinct isolation of midday discrete auroras from the discrete auroras in the nightside oval. Even the very elongated arcs extending into the evening/nightside sectors shown in type 4 sometimes comprise several intertwined narrow arc structures.

A pronounced feature in our observations is the "radial" configuration of the discrete aurora with fan-shaped arc structures that focus toward the cusp. This configuration is believed to result from the injection of magnetosheath plasma in the cusp/magnetosheath interface (i.e., the "entry layer"). In types 4 and 5 displays, the fan-shaped configuration degenerates, and

the discrete aurora eventually becomes more influenced by processes extending from the nightside into the dayside. Although plasma injection into the cusp is expected to be equally frequent during disturbed periods and quiet periods, it is expected that the nightside injection may overpower the dayside one during intense substorms and produce auroral displays similar to those in types 4 and 5. An important outcome of this study is that there is a disconnection between the dayside and nightside discrete auroras as the result of two different injection regions: the dayside cusp/"entry layer" and the nightside plasma sheet.

Figure 7 illustrates the topology of the dayside plasma injection into the cusp and boundary layer and the resulting dayside auroral display. Note that the mapping (not in scale for the sake of clarity) is done for the southern polar region. A similar picture viewed from the north pole was presented by *Lundin and Evans* [1985]. This updated version demonstrates more closely the projection of the discrete auroras onto the negative polarization in the boundary layer. Moreover, it emphasizes the cusp injection. Notice that the polarization induced by the plasma injection will drive preferentially "upward" currents at dusk (connecting to the discrete auroral structures) and "downward" currents at dawn. Open arrows mark the flow of the injected plasma in the late morning sector as well as the outward "counterflow" of ionospheric plasma resulting from the induced

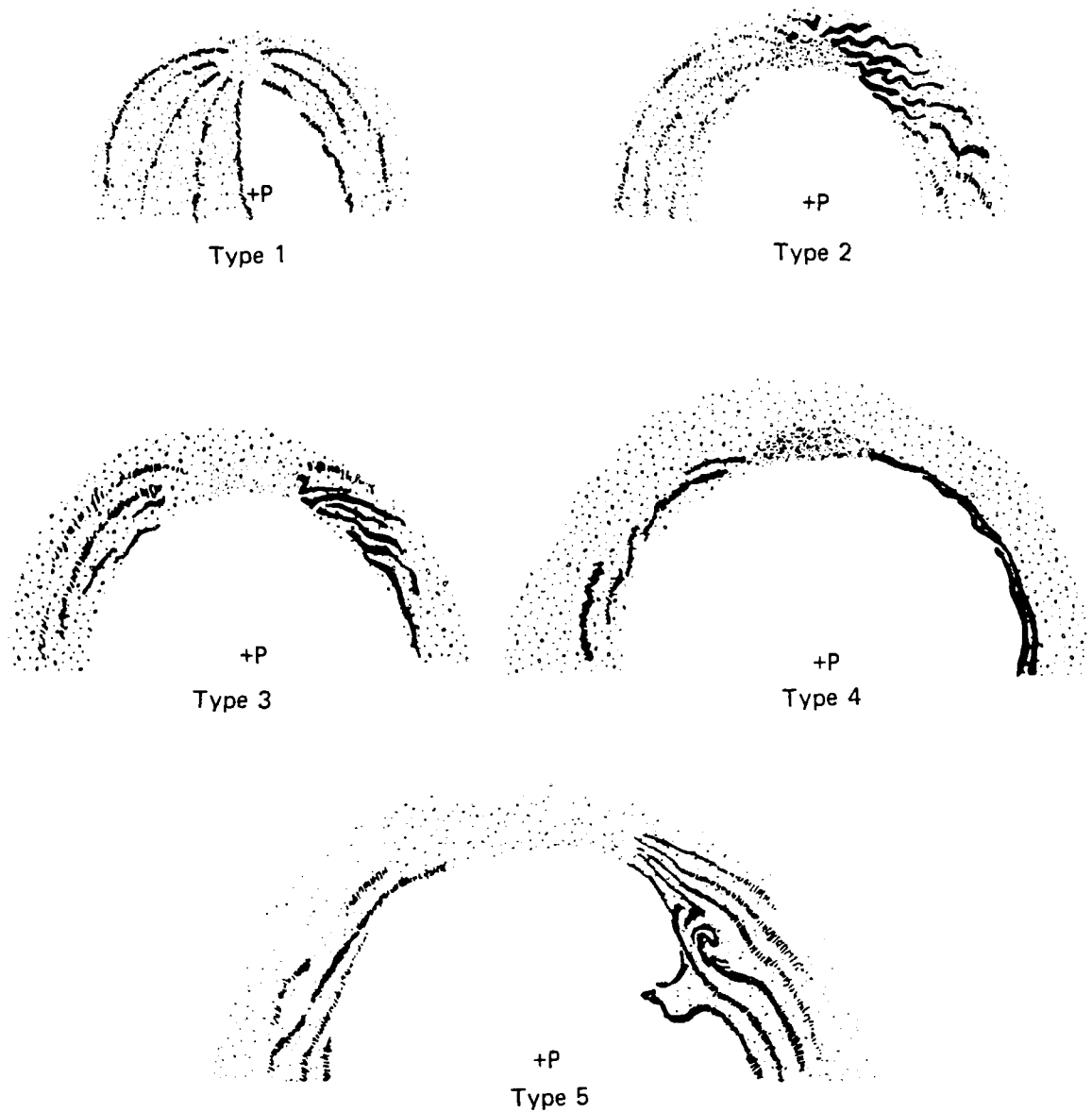


Fig. 8. Schematics summarizing the auroral display in the dayside auroral oval over the southern polar region. The midday auroral configuration can be grouped into five categories based on the common features of the characteristics. An increase of the oval size with negative IMF B_z is also indicated.

polarization in the afternoon sector. For a more comprehensive description of this model, the reader is referred to *Lundin and Evans* [1985].

CONCLUSION AND DISCUSSION

Some of the DMSP spacecraft made hundreds of images of the auroral displays near the noon meridian that are very rarely seen from the ground. Imagery of the midday part of the auroral oval was obtainable only in the local winter solstice season; the DMSP observations cover only the southern polar region. An examination of over 300 such high-resolution (≈ 2 km) dayside oval images revealed that the midday auroral display can be grouped into five categories based on the common features of the auroral characteristics. Their complexity is the con-

sequence of magnetospheric substorm activity and the interaction of the IMF with the magnetosphere. In Figure 8, we present a summary picture showing the five different types of dayside auroral displays over the southern polar region. The auroral features are subdivided into three basic groups: bright, discrete arcs (solid arcs), faint arcs (hatched arcs), and diffuse aurora (dotted regions). The cusp region, or the midday auroral gap, is marked by the heavily dotted region.

The basic display of dayside aurora (type 1) is characterized by many very faint, long, discrete arcs forming a fan-shaped configuration with an apex at the polar cusp region of no discrete auroras (i.e., the midday gap defined by *Dandekar and Pike* [1978]). These >1000 -km-long arcs are parallel to the equatorial part of the late morning or afternoon oval at lower

latitudes and gradually change to a nearly sun-earth (i.e., noon-midnight) orientation at higher latitudes. They are distributed over both the dawn and the dusk ovals and expand across very wide latitudes, indicating a very small (or sometimes no) polar cap region. It is an unusual type of auroral display, occurring during a very quiet geomagnetic condition while the IMF B_z is strongly northward.

As the geomagnetic activity increases and the IMF B_z turns southward, the discrete auroras become brighter and appear more extended in the afternoon sector, gradually extending into the evening oval. The size of the polar cap also increases, but the discrete aurora distributions in the morning and late morning sector do not change much except in the reduction of the latitudinal dimension of the oval. The discrete auroras that appear in the early afternoon (type 2) look like small-scale (≈ 100 km) patches and then appear (type 3) as multiple discrete arcs (≈ 1000 km long). They are isolated from the evening oval arcs that are connected to the midnight sector. As the activity increases further (type 4), a continuous strain of simple, discrete auroral arcs extends from the nightside evening oval into the early afternoon sector; often some small kinks imply degenerated westward-traveling surges along the evening and afternoon oval. During and after large substorms (type 5), very active, broken-up, discrete auroras extend from the nightside toward the noon sector along the evening oval.

It is important to point out that the auroral features of types 2 and 3 indicate a distinct discontinuity of discrete auroras in the dayside part of the auroral oval from those in the nightside oval. In addition to the above mentioned database, hundreds of DMSP images from the noon-midnight orbit satellites during the 1975, 1976, 1977, and 1978 summer seasons were used to examine the disconnection of discrete auroral arcs along the evening-afternoon oval. (These data were not included in the analysis because the noon-midnight orbit images very rarely cover the late morning portion of the oval.) The isolated, bright, short, discrete auroras (as in the type 2 display) and the long extended arcs (as in type 3) are the common feature along the early afternoon oval; the discontinuity between dayside afternoon arcs and nightside evening arcs is always there, except under more disturbed conditions as in types 4 and 5.

Discrete auroras in the early afternoon sector have been seen in DMSP and ISIS 2 observations for many years. However, the persistent nature of the discrete arcs with respect to location and isolation was recognized by Cogger *et al.* [1977] and Murphree *et al.* [1981], and recently from particle precipitation measurements by Evans [1984]. Murphree *et al.* [1981] investigated effects of the substorm and the IMF orientation on the auroral display in the afternoon sector. In general, the geomagnetic activity effect found in the DMSP data set reported here is very similar to the ISIS 2 observations.

During a very quiet time, DMSP observed many very faint discrete arcs embedded in extremely wide regions of diffuse glow (type 1), while ISIS 2 mainly detected the diffuse glow. This is believed to be due to the difference in the spatial resolution and/or sensitivity. A major apparent variance is in the IMF B_z dependence of the observed isolated afternoon arcs. Their occurrence over the northern polar region from ISIS 2 data was controlled by the negative B_z (13 out of 15 cases). We also investigated the IMF B_x and B_y of these arcs. For the type 2 display, the events collected in the summer of 1978 revealed a strong relationship with B_x and B_y ; 90% of the events were under negative B_x or positive B_y conditions, whereas, in the 1975 season, a completely opposite relation was seen in 80%

of the events. When combining types 2 and 3 observations with isolated discrete auroras observed over the 1975 and 1978 summers, there was no clear trend in the IMF B_x and B_y dependence. Because the present observation technique is limited to visible wavelengths, the dayside auroral observations are made during limited opportunities and for a very short time each year.

This study shows that isolated, discrete auroral features on the dayside are not associated with the substorm processes that take place in the nightside plasma sheet. Instead, their occurrence is a likely consequence of enhanced injection of magnetosheath plasma into the cusp region and an increase of solar wind energy and momentum transfer in the magnetospheric boundary layers as was first suggested by Eastman *et al.* [1976]. The radial characteristics of the discrete auroral arcs with a fan-shaped configuration converging toward the cusp support the idea that the dayside auroral oval is the plasma injection region in the dayside boundary layer [Lundin and Evans, 1985]. These injection structures act as individual dynamo elements powering the dayside region 1 current system [Iijima and Potemra, 1976] as well as generating discrete auroral features in the postnoon sector. The prevalence of upward currents in the postnoon sector and downward currents in the prenoon sector, as a result of the "viscous" interaction in the LLBL, was already pointed out by Sonnerup [1980]. What the auroral images tell us is that the region 1 currents probably are very structured, comprising many "elementary" current sheets.

As suggested by T. E. Eastman (private communication, 1985), the fan-shaped distribution of discrete auroras does not necessarily reflect a filamentation of the boundary layer to the extent indicated in Figure 7. The increased draping of the magnetic field lines toward the outer LLBL may be sufficient to explain the fan-shaped characteristics of the discrete aurora (see also Vasyliunas [1979]). However, to explain the presence of discrete aurora in the prenoon sector, a filamentation such as that proposed in Figure 7 is required. The diffuse aurora, seen as the background of the continuous auroral oval, is associated with a relatively weak particle precipitation from the preexisting plasma sheet. The shape of the continuous diffuse auroral oval is predominantly due to the gradient/curvature drift of plasma sheet electrons. However, the discrete aurora is related to intense electron precipitation, which is the result of a dynamo process of driven field-aligned currents and field-aligned acceleration potentials. This magnetospheric disturbance expands from two source regions, the polar cusp and the nightside plasma sheet, primarily because of plasma inertia and convection. An example of a limited expansion from the dayside injection region as a result of, for example, low plasma inertia is the type 2 auroral display.

An important conclusion from this study is the clear disconnection between the dayside and the nightside discrete auroras, except during very disturbed periods. This suggests that the boundary layer dynamo regions, powering the region 1 currents and producing the discrete aurora, are related to two "competing" injection sources, namely, the dayside cusp/magnetosheath and the nightside plasma sheet.

Acknowledgments. This research is supported in part by the Division of Atmospheric Sciences, National Science Foundation grant ATM-83-15041 and by the Air Force Office of Scientific Research grant AFOSR 84-0049 to The Johns Hopkins University Applied Physics Laboratory. R. Lundin, a visiting scientist, was supported by NASA task 12UOS10 under Department of the Navy contract N00024-85-C-5301 with The Johns Hopkins University Applied Physics Laboratory.

The editor thanks W. J. Heikkila and D. S. Evans for their assistance in evaluating this paper.

REFERENCES

- Akasofu, S.-I., The development of the auroral substorm, *Planet. Space Sci.*, **12**, 273, 1964.
- Akasofu, S.-I., Recent progress in studies of DMSP auroral photographs, *Space Sci. Rev.*, **19**, 169, 1976.
- Akasofu, S.-I., and J. R. Kan, Dayside and nightside auroral arc systems, *Geophys. Res. Lett.*, **7**, 753, 1980.
- Akasofu, S.-I., and C.-I. Meng, Dynamics of the aurora, IV, polar magnetic substorms and westward traveling surges, *J. Atmos. Terr. Phys.*, **28**, 489, 1966.
- Bythrow, P. F., R. A. Heelis, W. B. Hanson, R. A. Power, and R. A. Hoffman, Observational evidence for a boundary layer source of dayside region 1 field-aligned currents, *J. Geophys. Res.*, **86**, 5577, 1981.
- Cogger, L. L., J. S. Murphree, S. Ismail, and C. D. Anger, Characteristics of dayside 5577 Å and 3914 Å aurora, *Geophys. Res. Lett.*, **4**, 413, 1977.
- Cowley, S. W. H., D. J. Southwood, and M. A. Saunders, Interpretation of magnetic field perturbations in the earth's magnetopause boundary layer, *Planet. Space Sci.*, **31**, 1237, 1983.
- Dandekar, B. S., Relationship between the IMF, the midday gap, and auroral substorm activity, *J. Geophys. Res.*, **84**, 4413, 1979.
- Dandekar, B. S., and C. P. Pike, The midday, discrete auroral gap, *J. Geophys. Res.*, **83**, 4227, 1978.
- Eastman, T. E., E. W. Hones, Jr., S. J. Bame, and J. R. Asbridge, The magnetospheric boundary layer, site of plasma, momentum, and energy transfer from the magnetosheath into the magnetosphere, *Geophys. Res. Lett.*, **3**, 685, 1976.
- Eather, R. H., DMSP calibration, *J. Geophys. Res.*, **84**, 4134, 1979.
- Eather, R. H., and S. B. Mende, Systematics in auroral energy spectra, *J. Geophys. Res.*, **77**, 660, 1972.
- Evans, D. S., The characteristics of a persistent auroral arc at high latitude in the 1400 MLT sector, paper presented at Conference on the Polar Cusp Morphology and Dynamics, NATO, Lillehammer, Norway, May 7-11, 1984.
- Frank, L. A., Plasma in the earth's polar magnetosphere, *J. Geophys. Res.*, **76**, 5202, 1971.
- Haerendel, G., G. Paschmann, N. Sckopke, H. Rosenbauer, and P. C. Hedgecock, The frontside boundary layer of the magnetosphere and the problem of reconnection, *J. Geophys. Res.*, **83**, 3195, 1978.
- Heikkila, W. J., Impulsive penetration and viscous interaction, Proceedings of Magnetospheric Boundary Layer Conference, Alpbach, Austria, June 1979, *Eur. Space Agency Spec. Publ.*, **ESA SP-148**, 375, 1979.
- Heikkila, W. J., and J. D. Winningham, Penetration of magnetosheath plasma to low altitudes through the dayside magnetic cusps, *J. Geophys. Res.*, **76**, 883, 1971.
- Heikkila, W. J., J. D. Winningham, R. H. Eather, and S.-I. Akasofu, Auroral emissions and particle precipitation in the noon sector, *J. Geophys. Res.*, **77**, 4100, 1972.
- Iijima, T., and T. A. Potemra, Field-aligned currents in the dayside cusp observed by Triad, *J. Geophys. Res.*, **81**, 5971, 1976.
- Lundin, R., Solar wind energy transfer regions inside the dayside magnetopause, II, Evidence for an MHD-generator process, *Planet. Space Sci.*, **32**, 757, 1984.
- Lundin, R., and E. Dubinin, Solar wind energy transfer regions inside the dayside magnetopause, I, Evidence for magnetosheath plasma penetration, *Planet. Space Sci.*, **32**, 745, 1984.
- Lundin, R., and E. Dubinin, Solar wind energy transfer regions inside the dayside magnetopause. Accelerated heavy ions as tracers for MHD processes in the boundary layer, *Planet. Space Sci.*, **33**, 891, 1985.
- Lundin, R., and D. S. Evans, Boundary layer plasmas as a source for high-latitude, early afternoon, auroral arcs, *Planet. Space Sci.*, in press, 1985.
- Meng, C.-I., Polar cap arcs and the plasma sheet, *Geophys. Res. Lett.*, **8**, 273, 1981a.
- Meng, C.-I., Electron precipitations in the midday auroral oval, *J. Geophys. Res.*, **86**, 2149, 1981b.
- Meng, C.-I., and S.-I. Akasofu, Electron precipitation equatorward of the midday oval and the mantle aurora, *Planet. Space Sci.*, **31**, 889, 1983.
- Murphree, J. S., L. L. Cogger, and C. D. Anger, Characteristics of the instantaneous auroral oval in the 1200-1800 MLT sector, *J. Geophys. Res.*, **86**, 7657, 1981.
- Murphree, J. S., C. D. Anger, and L. L. Cogger, The instantaneous relationship between polar cap and oval auroras at times of northward interplanetary magnetic field, *Can. J. Phys.*, **60**, 349, 1982.
- Russell, C. T., and R. C. Elphic, ISEE observations of flux transfer events at the dayside magnetopause, *Geophys. Res. Lett.*, **6**, 33, 1979.
- Sckopke, N., G. Paschmann, G. Haerendel, B. U. O. Sonnerup, S. J. Bame, T. G. Forbes, E. W. Hones, and C. T. Russell, Structure of the low-latitude boundary layer, *J. Geophys. Res.*, **86**, 2099, 1981.
- Shepherd, G. G., and F. W. Thirkettle, Magnetospheric dayside cusp: A topside view of its 6300 Å atomic oxygen emission, *Science*, **180**, 737, 1973.
- Shepherd, G. G., F. W. Thirkettle, and C. D. Anger, Topside optical view of the dayside cleft aurora, *Planet. Space Sci.*, **24**, 937, 1976a.
- Shepherd, G. G., J. H. Whitteker, J. D. Winningham, J. H. Hoffman, E. J. Maier, L. H. Brace, J. R. Burrows, and L. L. Cogger, The topside magnetospheric cleft ionosphere observed from the ISIS 2 spacecraft, *J. Geophys. Res.*, **81**, 6092, 1976b.
- Sivjee, G. G., and B. Hultqvist, Particle and optical measurements in the magnetic noon sector of the auroral oval, *Planet. Space Sci.*, **23**, 1597, 1975.
- Snyder, A. L., and S.-I. Akasofu, Auroral oval photographs from the DMSP 8531 and 10533 satellites, *J. Geophys. Res.*, **81**, 1799, 1976.
- Snyder, A. L., S.-I. Akasofu, and D. S. Kimball, The continuity of the auroral oval in the afternoon sector, *Planet. Space Sci.*, **23**, 225, 1975.
- Sonnerup, B. U. O., Theory of the low-latitude boundary layer, *J. Geophys. Res.*, **85**, 2017, 1980.
- Vasyliunas, V. M., Interaction between the magnetospheric boundary layers and the ionosphere, Proceedings of a Sydney Chapman Conference on Magnetospheric Boundary Layers, *Eur. Space Agency Spec. Publ.*, **ESA SP-148**, 387, 1979.

R. Lundin, Kiruna Geophysical Institute, P.O. Box 704, 98127 Kiruna, Sweden.

C.-I. Meng, The Johns Hopkins University Applied Physics Laboratory, Johns Hopkins Road, Laurel, MD 20707.

(Received July 5, 1985;
revised October 17, 1985;
accepted October 18, 1985.)

Cusp Width and B_z : Observations and a Conceptual Model

PATRICK T. NEWELL AND CHING-I. MENG

The Johns Hopkins University Applied Physics Laboratory, Laurel, Maryland

Because a southward turning of the interplanetary magnetic field B_z enhances dayside merging, leading to an equatorward motion of the equatorward edge of the cusp, one might suppose that the cusp latitudinal width would be larger for a southward B_z condition. The Defense Meteorological Satellite Program F7 observations confirm two previous case studies showing that the cusp low-altitude latitudinal extent is actually narrower when B_z is southward than when B_z is northward. The earlier studies dealt with intense geomagnetic storms; examples presented here show that it is routine to observe a narrowing of the cusp width following a southward turning of B_z . In addition, we present a simple conceptual model that shows how enhanced tailward convection of the newly opened field lines during periods of southward B_z can account for the observed narrowness.

1. INTRODUCTION

Recent precipitating particle observations from polar orbiting satellites suggest that the low-altitude latitudinal width of the polar cusp region is narrower during times when B_z is southward (or, what is usually equivalent, during substorm activity). Meng [1982] used Defense Meteorological Satellite Program (DMSP) F2 and F4, both in approximately noon-midnight 840-km-altitude polar orbits at the time, to study the phenomenology of cusp latitudinal variation as defined by low-energy electron precipitation boundaries during a geomagnetic storm. He found that in addition to equatorward movement, the cusp width narrowed to less than a degree during the course of the storm. Meng [1984] performed an additional case study of three intense magnetic storms using the same satellites; again the cusp latitudinal extent narrowed rapidly following the onset of magnetic activity (see also *Makita and Meng* [1986]). The inverse correlation between cusp width and magnetic activity apparently does not hold only for large magnetic storms as cited above. *Carbary and Meng* [1986] and J. F. Carbary and C.-I. Meng (personal communication, 1987) performed a statistical study of the latitudinal width of the cusp as a function AE and B_z using electron data from DMSP F2 and F4 over an 11-month interval. They found that cusp width correlated best with B_z , for which the correlation coefficient was 0.59. Their studies constitute by far the largest data base for the statistical investigation of cusp latitudinal behavior.

It has recently become clear that the latitudinal width over which magnetosheathlike electrons precipitate at low altitudes is sometimes larger than the region over which both the electron and ion precipitations are exclusively magnetosheathlike. It has been proposed that the (sometimes) larger region be termed the cleft and the smaller region, which may correspond to the "gap" region of discrete arcs, be called the cusp [e.g., *Meng*, 1981; *Heikkila*, 1984; *Johnstone*, 1984]. The studies cited above, which were based solely on the precipitating electron data, would at times under this definition correspond to a region larger than the newly defined cusp (this would also apply to numerous other studies such as those of *Eather* [1985]). Nonetheless, the narrowness of the cusp, however defined, during intense magnetic activity is still clear from the above studies: For example, the observation of *Meng* [1982, 1984] that the cleft can narrow to 1° during magnetic storms rep-

resents an upper limit on the cusp width at these times, and it has been well established that the low-altitude cusp, however defined, is larger than this value most of the time.

On the other hand, one important early study of cusp phenomenology reported that the cusp width remained constant at 4° while B_z varied from slightly positive to -6γ [*Burch*, 1973]. Partly, this may be because the lowest-energy channel available for this early study, which used only electron data, was 700 eV, which is already well above the large bulk of the electron population in what is now considered the cusp proper. The same study did find that as B_z became more positive than 2γ , the cusp width increased up to 7° . The cusp as determined in this paper, in accordance with more recent opinions of what constitutes the cusp, is generally much narrower than what was found by *Burch* [1973]. An even earlier study [*Frank*, 1971, p. 5202] found that "During periods of relative magnetic disturbance the position of the polar cusp moves equatorward by several degrees in invariant latitude without a large increase in its latitudinal width, i.e., by factors ≤ 2 ." This observation is correct but greatly understated: The cusp width actually decreases during active times. In the discussions contained in several early cusp papers, it can be similarly seen that the expectation of the researchers was that the cusp should be wider during active times.

We present herein the results of a study using both electron and ion data and using a more strict definition of the cusp than some of the studies cited above. It is shown that when B_z turns from northward or near zero to southward between successive DMSP F7 polar cusp passes over the same hemisphere, the cusp is narrower for the southward B_z condition. This happens not only during major magnetic storms but also routinely with each southward turning of B_z . Two sample cases using DMSP F7 ion as well as electron data are presented to show this fairly dramatic cusp narrowing. We also present a conceptual model that can give a plausible explanation for the observed narrowing of the cusp width when B_z changes from northward (or near zero) to southward, despite the likelihood that merging is occurring at an enhanced rate for southward interplanetary magnetic field (IMF).

2. DATA PRESENTATION: TWO EXAMPLES

We have used Air Force Geophysics Laboratory (AFGL) DMSP F7 particle data to study 12 examples in which the IMF B_z turned from northward to southward during successive orbits (cusp passes). All examples are from December 1983, the first month of regular satellite operation. The DMSP F7 30-eV to 30-keV electron and ion electrostatic detectors are described in detail by *Hardy et al.* [1984]. DMSP F7 is a sun synchronous polar-orbiting satel-

Copyright 1987 by the American Geophysical Union.

Paper number 7A9066.
0148-0227/87/007A-9066\$02.00

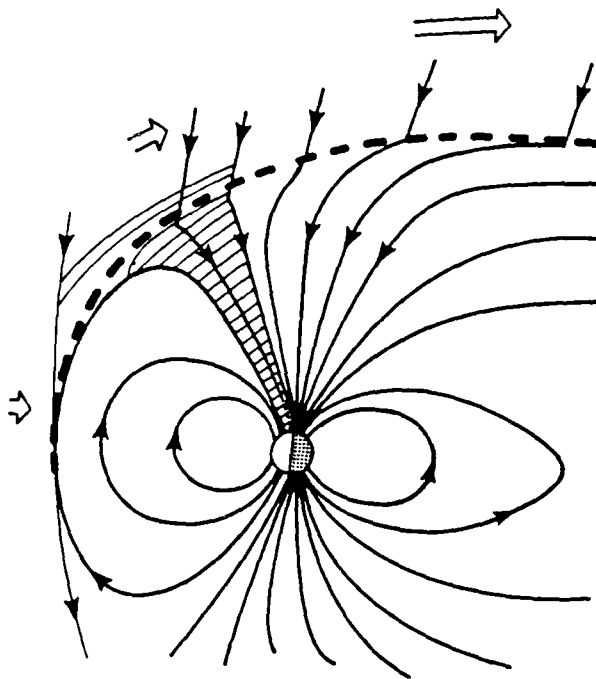


Fig. 1. Illustration of the polar cusp geometry. The shaded region contains magnetosheath plasma, but entry to low altitudes is restricted to a comparatively narrow region on the dayside where the magnetosheath tailward convection flow velocity is less than the ion thermal velocity.

lite with an approximately circular 840-km-altitude orbit in a prenoon-premidnight meridian.

The first example that we present here occurred on December 11, 1983. The hourly average of B_z (GSM) was positive for several straight hours before 1000 UT, and again from 1000 to 1100 UT, B_z (GSM) = 9.6 γ . From 1100 to 1200 UT, the hourly average B_z changed southward, to -3.7 γ . The work of *Carbury and Meng* [1986] using 10-min averages for B_z indicates that the best correlation of cusp behavior to B_z is the IMF value time delayed by 30 min. For present purposes, which is simply to illustrate that the cusp is narrower during and immediately following a period of southward B_z , these hourly averages should suffice. DMSP passes through the cusp regions in both hemispheres once every 101 min.

Plate 1a shows a DMSP F7 spectrogram of the cusp following a prolonged period of northward B_z . For the present paper, we consider the cusp region to be only that in which the electron precipitation cuts off below 1 keV and the ion-precipitated energy flux has a peak somewhere in the vicinity of ≈ 1 keV. By this conservative definition, the cusp extends, as indicated by arrows, from 74.0° to 77.5° magnetic latitude (MLAT) so that the cusp is 3.5° wide. This is a fairly average value for an interval of prolonged northward B_z . The absence of ion latitudinal energy dispersion in the cusp is most simply attributable to a wide source region with little convection.

Following an hour of negative value B_z , the cusp is as shown in Plate 1b. It extends from 74.0° to 76.0° and so is 2.0° wide. Ion energy dispersion is now present; namely, the average ion energy now falls moving poleward through the cusp. This is the signature that *Reiff et al.* [1977] cited as evidence for direct particle entry into the cusp, although one could not expect to see such dispersion in any case when the cusp is wide, as it was in Plate

1b. We again point out that the poleward low-energy ion tail results (via the mechanism pointed out by *Shelley et al.* [1976] and *Reiff et al.* [1977]) from the finite time of flight of such low-energy ions. Thus, magnetosheath plasma is not being newly introduced onto the farthest poleward lines or else the ≈ 1 -keV energy ions would also be seen there. This example shows the cusp being reduced in width from 3.5° to 2.0° promptly (within the 101-min orbital period) following a southward turning of B_z .

In the second example that we present here, the "before" picture now represents a period of weakly northward B_z , this time imbedded within intervals of generally southward B_z . The significance is that in such a situation (i.e., whenever there has not been a prolonged period of northward B_z), a very sharp equatorward boundary is usually discernible on a spectrogram. That is, it is possible to pick out what is probably the first open field line. This example is from December 25, 1983. The respective IMF B_z (GSM) hourly averages for the intervals ending 1100, 1200, 1300, and 1400 UT are -1.4, +0.7, -2.8, and -3.7 γ , respectively. Plate 2a shows the cusp during the northward IMF interval (1100-1200 UT); the cusp (conservatively defined) extends from 77.0° to 78.7° MLAT, a width of 1.7°. The "after" picture, when B_z has again turned southward, is shown in Plate 2b. The equatorward edge is fairly sharply defined at 75.8° MLAT; the poleward edge could plausibly be placed at either 76.7° MLAT (based on the electron cutoff) or at 76.5° MLAT (the latitude of the sharpest ion dropoff). Thus, the cusp has been reduced to a width of 0.7° or 0.9° (from 1.7°). Once again, it is clear that no new magnetosheath plasma is entering in the poleward low-energy ion region because otherwise more energetic ions would be entering here also. Rather, the lowest-energy ions previously injected (such ions have a transit time of the order of an hour) are finally reaching the foot of the field line.

3. THE MODEL: A PLAUSIBLE CONCEPTUAL EXPLANATION

Figure 1 shows a cartoon model of the cusp. The equatorward boundary of the cusp is usually taken to be the first open field line, although in quiet times, magnetosheath plasma can diffuse equatorward of this boundary onto closed field lines. The magnetosheath flow is antisunward, is smallest near the subsolar stagnation point, and increases at greater distances tailward, eventually reaching the solar wind velocity. Because the tailward magnetosheath flow velocity is increasingly large compared with the magnetosheath ion thermal velocity for increasing distance from the subsolar point, there is only a limited region toward the dayside (corresponding to a limited low-altitude latitudinal width) on which magnetosheath plasma can overcome the tailward convection to enter into the magnetosphere and reach low altitudes (as was suggested by *Reiff et al.* [1977]). The geometrical limitation on the cusp width due to this process applies directly only to ions since the electron thermal velocities are far above the tailward convection speeds. However, as *Burch* [1985] showed, charge quasi-neutrality is generally obeyed in the cusp so that the region of intense electron flux entry is normally limited to the ion entry region. It is possible to suppose that new merging occurs either at the subsolar point or near the cusp; Figure 1 is supposed to be arbitrary in this respect. Ground-based optical observations have found evidence for both quasi-steady-state reconnection and for flux transfer events (FTEs) (*Sandholt et al.*, 1986) associated with the cusp so that the type of merging might itself be variable.

The field lines in the cusp region, which have one foot on the Earth and one connecting, possibly through the boundary layer, into the magnetosheath, are inherently in transition. Ordinarily,

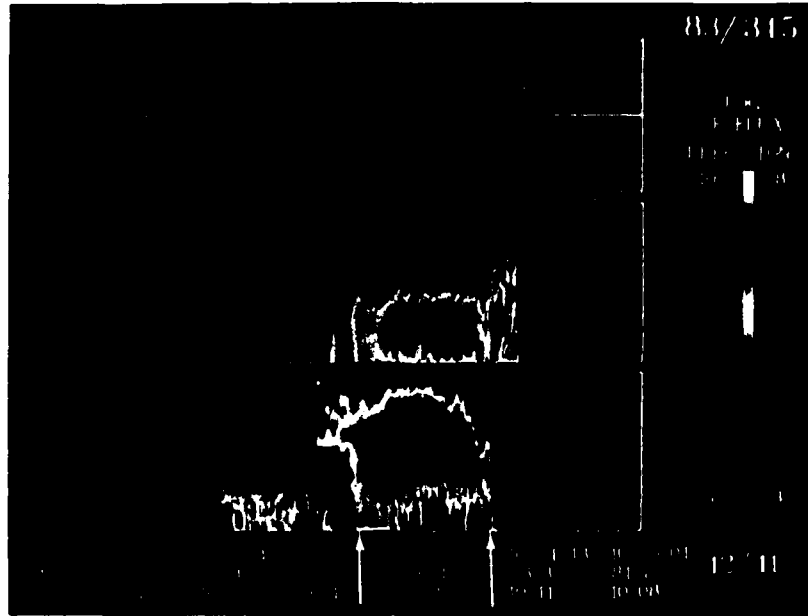


Plate 1a

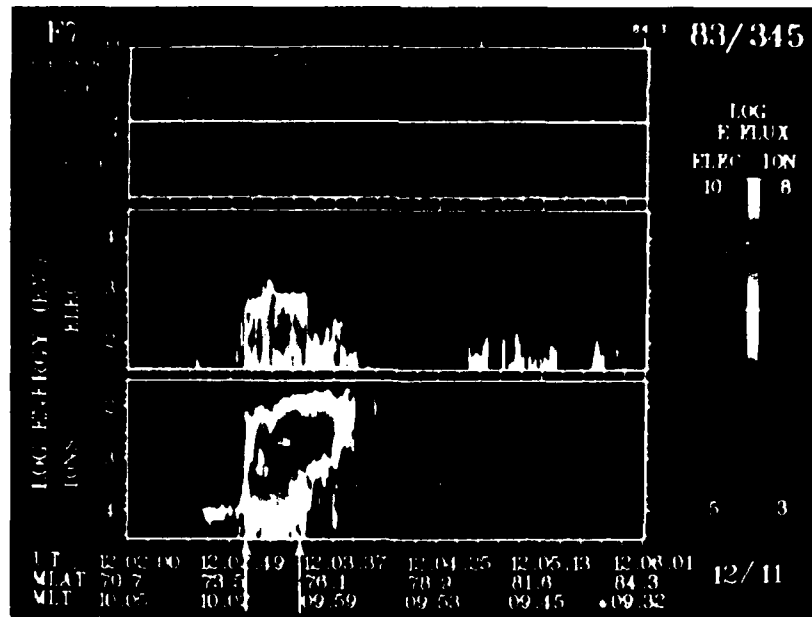


Plate 1b

Plate 1. (a) A DMSP E7 spectrogram of 32-eV to 30-keV electrons and ions in the cusp region following a long period of northward B_z . The top and following small panels give the total energy flux and average energy for electrons and ions in units of $\text{eV}/\text{cm}^2 \text{ s sr}$ and eV, respectively. The main panels show electron and ion differential energy flux in units of $\text{eV}/\text{cm}^2 \text{ s sr}$. Magnetosheath plasma is observed over a wide latitudinal region. Even a restricted definition of the cusp gives a width of 3.5° , as indicated by arrows. (b) A spectrogram of the following pass in which B_z has turned southward. The latitudinal width of the cusp (shown by arrows) has been reduced to 2.0° . Poleward convection is reflected in the ion dispersion.

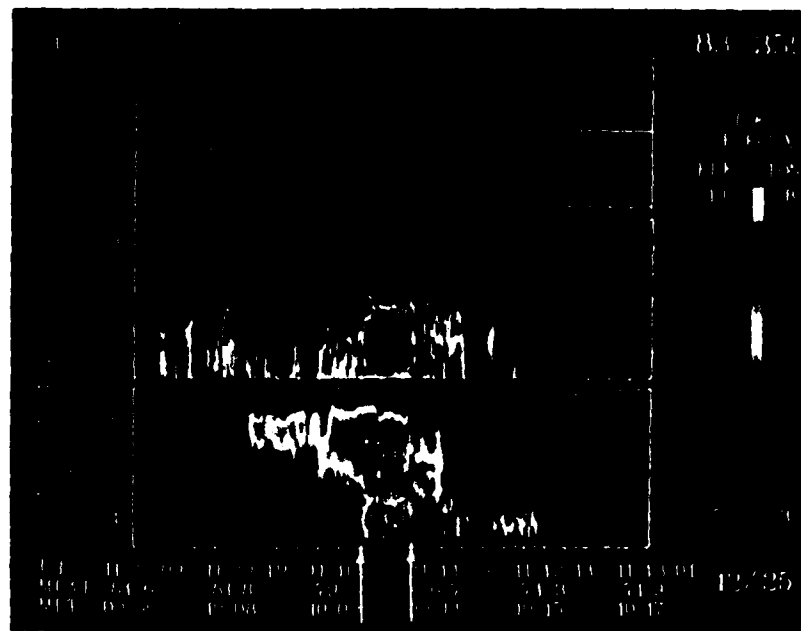


Plate 2a

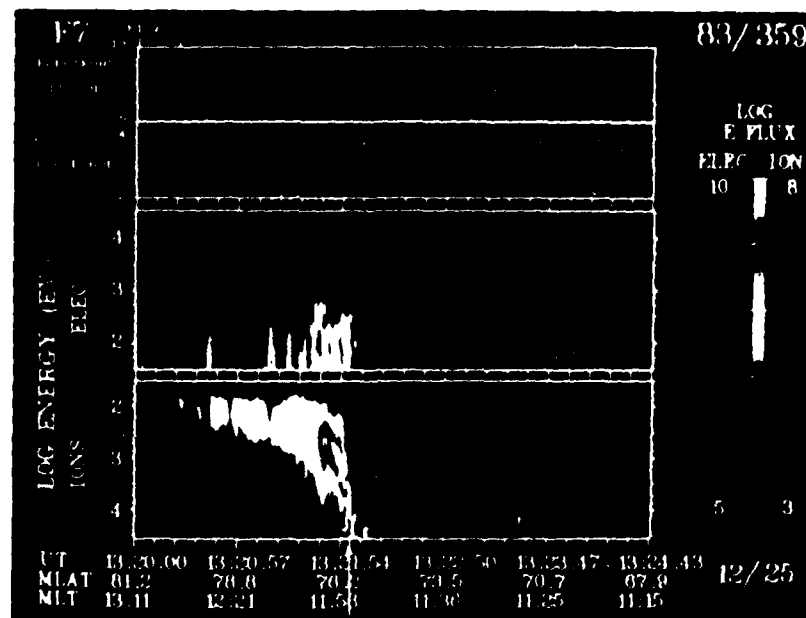
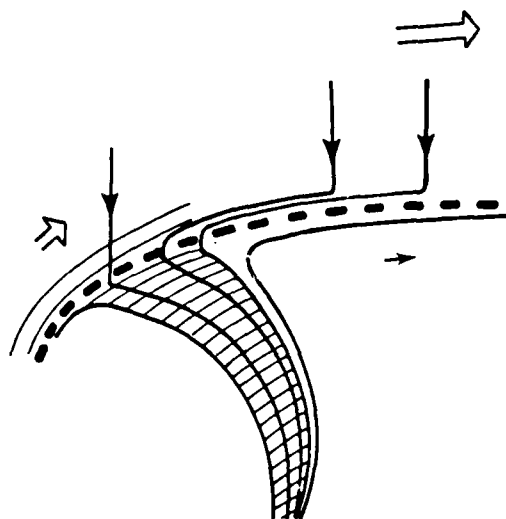
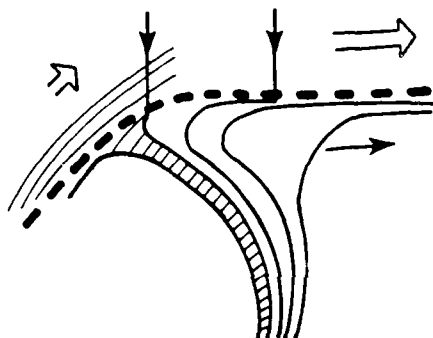


Plate 2b

Plate 2. (a) A DMSP F7 spectrogram of the cusp for weakly northward B_z , following periods of southward B_z . Poleward convection and a sharp equatorward edge are evident; the cusp width is 1.7° . (b) A spectrogram of the subsequent pass over the cusp after B_z turned southward. The cusp has been reduced to 0.7° or 0.9° width.



(a) Slow magnetospheric convection



(b) Rapid magnetospheric convection

Fig. 2. (a) The magnetic field line geometry in the cusp region when convection is slow. Most recently opened lines cross the magnetopause in the slow flow region of the magnetosheath and are thus cusp lines. Therefore, the cusp is wide. (b) Field line geometry when merged lines are rapidly convected into the magnetotail. All but the most recently opened lines have been convected downstream and cross the magnetopause at a point where the tailward magnetosheath flow is too rapid to allow plasma to reach low altitudes. Therefore, there are only a few cusp field lines, and the cusp is narrow.

they are being convected poleward (tailward) along with the boundary layer. As an approximation, the rate of magnetosheath flow immediately outside the magnetopause is taken to be time independent (but position dependent). However, the rate of plasma convection just inside the magnetopause (which is slower than magnetosheath convection) can vary considerably, as can the rate of new merging at the equatorward edge of the cusp. Depending on the relative rates of these respective processes, the cusp configuration can be quite different. When convection within the magnetopause is slow (or the rate of new merging is very high), the situation is as shown in Figure 2a. Here, many of the recently merged lines still map to the region of slow magnetosheath flow closer to the dayside. Therefore, magnetosheath plasma can reach low altitudes on these lines; thus, they are cusp lines, and the cusp is wide.

However, when the tailward convection of field lines within the magnetopause is rapid (or if it has been a long time since any new

merging occurred), all opened field lines have been convected tailward to a region of more rapid magnetosheath flow, and the situation is as shown in Figure 2b so that the cusp is narrow. Figures 2a and 2b are drawn as limiting cases for conceptual ease; a narrow cusp does not necessarily imply that no new lines are opening on the dayside. We thus propose that the cusp width is a measure of the respective dominance of new merging versus the transport of already merged lines (which depends on the convection velocities just within the magnetopause) into the tail.

During intervals of southward IMF, both the tailward convection rate and the merging rate are enhanced. Except for a brief transition time, the rate at which new flux is opened and the rate of tailward convection of the flux must balance. However, if the rate of plasma convection within the boundary layer as determined by the electric fields is fast compared with the rate at which new lines are being opened, nearly all open field lines will have been convected into the tail and will cross the magnetopause too far tailward to be a cusp line. As discussed in the introduction and as shown in the examples in section 2, observationally, the enhanced convection rate is able to dominate, and the cusp becomes narrower, when B_z turns southward.

4. DISCUSSION AND SUMMARY

It has become well established that during times of southward B_z , the rate of dayside merging increases. Therefore, one might naively expect a wider cusp during such intervals. However, observationally, this is not the case. The conceptual model proposed here shows that the enhanced rate of magnetospheric convection must also be taken into account since, as discussed in section 3, the rapid tailward convection of newly opened field lines tends to narrow the cusp. The observational result is that enhanced convection dominates over enhanced merging during intervals of southward B_z , and the cusp latitudinal width is narrower.

We should point out that the narrowing of the cusp following a southward turning of B_z is a phenomenon that seems to happen at all local times at which the cusp is observed. In the two examples presented here, the satellite was moving to later local times from pass to pass. However, in numerous other examples, the cusp narrowed following a southward turning of B_z when DMSP F7 was moving toward earlier local times from pass to pass. There does not seem to be any obvious local time effect within 2 or 3 hours around noon.

Finally, we note that like all models, particularly a simple conceptual model, the one presented herein is an oversimplification. For example, during intervals of northward B_z , there may not be simply slower tailward convection within the boundary layer but rather no tailward or even sunward convection. In Plate 2a, one can see that for northward B_z , magnetosheath plasma is diffusing equatorward of the sharp boundary that likely marks the first open field line. This implies that the poleward convection is at least slower than the cross-field diffusion rate. After a long interval of northward B_z , there is often no longer a sharp well-defined equatorward boundary of magnetosheath plasma at all. Nonetheless, in these cases also, the enhanced tailward convection associated with a southward turning of IMF B_z narrows the cusp. An enhanced tailward convection rate should inhibit the diffusion of magnetosheath plasma onto closed field lines. Thus, the essential concept presented herein, namely, that the reduced latitudinal width of the cusp for negative B_z is due to enhanced convection, is somewhat more general than the model presented in section 3.

Burch [1973] proposed an explanation for the widening of the cusp as B_z ranges from slightly positive ($< 2 \gamma$) to $+6 \gamma$. He sug-

gested that merging at the poleward edge of the cusp (i.e., with lines previously opened and convected downstream) sets in for such strongly positive B_z . This proposal seems logical, although the identification of the appropriate signatures of such merging is not yet well established (see, however, Reiff *et al.* [1980]). The signature of merging at the equatorward boundary of the cusp, namely, a sharp boundary coupled with the appropriate ion latitudinal dispersion signature, is often seen. In either case, convection velocity will play as crucial a role as the merging mechanism and rate in determining the cusp configuration.

Acknowledgments. We thank D. G. Sibeck for helpful conversations. The DMSP raw particle data were provided by AFGL through the World Data Center at Boulder, Colorado. This work was supported by the Atmospheric Sciences Division, National Science Foundation grant ATM-8315041, and by the Air Force Office of Scientific Research grant 84-0049 to The Johns Hopkins University Applied Physics Laboratory.

The Editor thanks two referees for their assistance in evaluating this paper.

REFERENCES

- Burch, J. L., Rate of erosion of dayside magnetic flux based on a quantitative study of the dependence of polar cusp latitude on the interplanetary magnetic field, *Radio Sci.*, **8**, 955-961, 1973.
- Burch, J. L., Quasi-neutrality in the polar cusp, *Geophys. Res. Lett.*, **12**, 469-472, 1985.
- Carbary, J. F., and C.-I. Meng, Correlation of cusp latitude with B_z and $AE(12)$ using nearly one year's data, *J. Geophys. Res.*, **91**, 10,047-10,054, 1986.
- Eather, R. H., Polar cusp dynamics, *J. Geophys. Res.*, **90**, 1569-1576, 1985.
- Frank, L. A., Plasma in the Earth's polar magnetosphere, *J. Geophys. Res.*, **76**, 5202-5219, 1971.
- Hardy, D. A., L. K. Schmitt, M. S. Gussenhoven, F. J. Marshall, H. C. Yeh, T. L. Shumaker, A. Hube, and J. Pantazis, Precipitating electron and ion detectors (SSJ/4) for the block 5D/flights 6-10 DMSP satellites: Calibration and data presentation, *Rep. AFGL-TR-84-0317*, Air Force Geophysics Laboratory, Hanscom Air Force Base, Mass., 1984.
- Heikkila, W. J., Definition of the cusp, in *Polar Cusp*, edited by J. A. Holtet and A. Egeland, pp. 387-395, D. Reidel, Hingham, Mass., 1984.
- Johnstone, A. D., Electron injection in the polar cusp, in *Polar Cusp*, edited by J. A. Holtet and A. Egeland, pp. 47-65, D. Reidel, Hingham, Mass., 1984.
- Makita, K., and C.-I. Meng, Polar cusp electron during quiet and disturbed period, *Mem. Natl. Inst. Polar Res. Jpn.*, **42**, 103-113, 1986.
- Meng, C.-I., Electron precipitation in the midday auroral oval, *J. Geophys. Res.*, **86**, 2149-2174, 1981.
- Meng, C.-I., Latitudinal variation of the polar cusp during a geomagnetic storm, *Geophys. Res. Lett.*, **9**, 60-63, 1982.
- Meng, C.-I., Dynamic variation of the auroral oval during intense magnetic storms, *J. Geophys. Res.*, **89**, 227-235, 1984.
- Reiff, P. H., T. W. Hill, and J. L. Burch, Solar wind plasma injection at the dayside magnetospheric cusp, *J. Geophys. Res.*, **82**, 479-491, 1977.
- Reiff, P. H., J. L. Burch, and R. W. Spiro, Cusp proton signatures and the interplanetary magnetic field, *J. Geophys. Res.*, **85**, 5997-6005, 1980.
- Sandholt, P. E., C. S. Deehr, A. Egeland, B. Lybekk, R. Viereck, and G. J. Romick, Signatures in the dayside aurora of plasma transfer from the magnetosheath, *J. Geophys. Res.*, **91**, 10,063-10,079, 1986.
- Shelley, E. G., R. D. Sharp, and R. G. Johnson, He^{++} and H^+ flux measurements in the dayside cusp: Estimates of convection electric field, *J. Geophys. Res.*, **81**, 2363-2370, 1976.

C.-I. Meng and P. T. Newell, The Johns Hopkins University Applied Physics Laboratory, Laurel, MD 20707.

(Received April 13, 1987;
revised September 28, 1987;
accepted September 21, 1987.)

Approved for public release;
distribution unlimited.

UNCLASSIFIED

RECEIVED

(CS)

**DAT
ILM**